



Arnold Schwarzenegger
Governor

INTEGRATED FORECAST AND RESERVOIR MANAGEMENT (INFORM) FOR NORTHERN CALIFORNIA: SYSTEM DEVELOPMENT AND INITIAL DEMONSTRATION

Prepared For:

California Energy Commission
Public Interest Energy Research Program

Prepared By:

**Hydrologic Research Center and
Georgia Water Resources Institute**



PIER FINAL PROJECT REPORT

March 2007
CEC-500-2006-109



Prepared By:

Hydrologic Research Center and
Georgia Water Resources Institute
Konstantine P. Georgakakos, Nicholas E. Graham,
and Aris P. Georgakakos
San Diego, California and Atlanta, Georgia
Contract No. 500-02-008

Prepared For:

California Energy Commission
Energy-Related Environmental Research

Joseph O' Hagan
Contract Manager

Joseph O' Hagan
Project Manager

Kelly Birkinshaw
Program Area Manager
ENERGY-RELATED ENVIRONMENTAL RESEARCH

Martha Krebs, Ph.D.
Deputy Director
ENERGY RESEARCH & DEVELOPMENT DIVISION

B.B Blevins
Executive Director

DISCLAIMER

This report was prepared as the result of work sponsored by the California Energy Commission. It does not necessarily represent the views of the Energy Commission, its employees or the State of California. The Energy Commission, the State of California, its employees, contractors and subcontractors make no warrant, express or implied, and assume no legal liability for the information in this report; nor does any party represent that the uses of this information will not infringe upon privately owned rights. This report has not been approved or disapproved by the California Energy Commission nor has the California Energy Commission passed upon the accuracy or adequacy of the information in this report.

Acknowledgments

The work reported in this document was co-sponsored by the following federal and state programs: Ecosystem Restoration Program of the California Bay-Delta Authority (prior CALFED), the Public Interest Energy Research (PIER) Program of the California Energy Commission, and the Climate Program Office (CPO) of the National Oceanic and Atmospheric Administration (NOAA). Supplemental support for scientific research using components of the INFORM system was provided by the California Applications Project of the Scripps Institution of Oceanography; that program is funded by the NOAA Climate Program Office. Administrative support was provided by the Hydrologic Research Center. The work is a joint effort between the Hydrologic Research Center (HRC) of San Diego, California, and the Georgia Water Resources Institute (GWRI) at the Georgia Institute of Technology in Atlanta, Georgia; the former with primary contributions in the areas of climate and hydrologic forecasting and the latter with primary contributions in the area of decision support for reservoir planning and management.

The authors wish to thank the members of the Oversight and Implementation Committee (OIC) of INFORM for their guidance and support during the first three years of this demonstration project. Their names are listed below. The work was performed in close collaboration with the staff of the National Weather Service (NWS) California-Nevada River Forecast Center (CNRFC), the California Department of Water Resources (DWR), and the Bureau of Reclamation Central Valley Operations (CVO). The agency contributions in data gathering, modeling system design, and reciprocal technology transfer process between modelers and users were numerous and essential for the development of a useful INFORM system. In particular, we wish to thank Rob Hartman of CNRFC, Paul Fujitani of CVO, and Gary Bardini of DWR for their continuing encouragement and guidance throughout the project period. Many thanks are also extended to the staff of the Environmental Modeling Center (EMC) of the U. S. National Weather Service National Centers for Environmental Prediction (NCEP) and to Louis Uccellini (NCEP Director), Steve Lord (EMC Director), and Gary Carter (Director of the NWS Office of Hydrologic Development) for their efforts to accommodate INFORM project data requirements. The climate and weather forecast information they provide is directly incorporated in the INFORM forecast and decision system, critically enhancing its value and utility for water resources forecast and management operations.

The co-principal investigators of this report also wish to thank the program managers of the funding agencies for their willingness, effort, and skill to accommodate the many idiosyncrasies of this prototype, multidisciplinary, inter-institutional, demonstration project within the institutional constraints of their organizations. Their vision and support is largely responsible for the realization of the INFORM system and the contributions it will make toward more coordinated forecast and management operations. We are grateful for such support to Claudia Nierenberg of NOAA CPO, Joe

O'Hagan of the California Energy Commission, and Rebecca Fris of the California Bay-Delta Authority (CBDA).

The INFORM system and this report are the products of contributions made by several individuals from HRC and GWRI. In alphabetical order, they are: Theresa M. Carpenter (HRC, hydrologic modeling), Aris P. Georgakakos (GWRI, decision modeling and project Co-PI), K. P. Georgakakos (HRC, hydrometeorological modeling and project PI), Nicholas E. Graham (HRC, climate modeling and project Co-PI), Martin Kistenmacher (GWRI, river and reservoir modeling), Eylon Shamir (HRC, hydrologic modeling), Jason Sperflage (HRC, systems programming), Stephen R. Taylor (HRC, hydrometeorological modeling), Jianzhong Wang (HRC, mesoscale atmospheric modeling), and Huaming Yao (GWRI, decision support and software development).

Key operational agencies for the implementation of the demonstration project were the U.S. National Weather Service (NWS) California-Nevada River Forecast Center (CNRFC), the California Department of Water Resources (DWR), the U.S. Bureau of Reclamation Central Valley Operations (USBR CVO), and the Sacramento District of the U.S. Army Corps of Engineers (USACE). Other agencies and regional stakeholders contributed through active participation in project workshops and, indirectly, through comments and suggestions conveyed to the INFORM Oversight and Implementation Committee (OIC).

Oversight and Implementation Committee of INFORM

Fris, Rebecca – California Bay-Delta Authority Ecosystem Restoration Program

Fujitani, Paul – US Bureau of Reclamation Central Valley Operations

Hartman, Robert – NOAA NWS-California Nevada River Forecast Center

Bardini, Gary – California Department of Water Resources

Johnson, Borden – U.S. Army Corps of Engineers (USACE), Sacramento District

Nierenberg, Claudia – NOAA Office of Global Programs

O'Hagan, Joe – California Energy Commission, PIER

Georgakakos, Konstantine – HRC INFORM PI

Georgakakos, Aris – Georgia Tech INFORM Co-PI

Graham, Nicholas – HRC INFORM Co-PI

Agency Alternates

Bond, Marcia – USACE Sacramento District

Collins, Robert – USACE Sacramento District

Hinojosa Jr., Arthur – California Department of Water Resources

Morstein-Marx, Tom – U.S. Bureau of Reclamation Central Valley Operations

Reed, Brendan – California Bay-Delta Authority Ecosystem Restoration Program

Strem, Eric – NOAA NWS-California Nevada River Forecast Center

Disclaimer

This report does not necessarily represent the views of the Funding Agencies, their employees, or the State of California. The Agencies, their employees and contractors and subcontractors make no warranty, expressed or implied, and assume no legal liability for the information in this report; nor does any party represent that the use of this information will not infringe upon privately owned rights. This report has not been approved or disapproved by the Agencies nor have the Funding Agencies passed judgment upon the accuracy or adequacy of the information in this report.

Please cite this report as follows:

HRC-GWRI. 2007. *Integrated Forecast and Reservoir Management (INFORM) for Northern California: System Development and Initial Demonstration*. California Energy Commission, PIER Energy-Related Environmental Research. CEC-500-2006-109.

Preface

The Public Interest Energy Research (PIER) Program supports public interest energy research and development that will help improve the quality of life in California by bringing environmentally safe, affordable, and reliable energy services and products to the marketplace.

The PIER Program, managed by the California Energy Commission (Energy Commission), conducts public interest research, development, and demonstration (RD&D) projects to benefit electricity and natural gas customers.

The PIER program strives to conduct the most promising public interest energy research by partnering with RD&D entities, including individuals, businesses, utilities, and public or private research institutions.

PIER funding efforts are focused on the following RD&D program areas:

- Buildings End-Use Energy Efficiency
- Energy-Related Environmental Research
- Energy Systems Integration
- Environmentally Preferred Advanced Generation
- Industrial/Agricultural/Water End-Use Energy Efficiency
- Renewable Energy Technologies
- Transportation

Integrated Forecast and Reservoir Management (INFORM) for Northern California: System Development and Initial Demonstration is the final report for the INFORM project (contract number 500-02-008) conducted by the Hydrologic Research Center and the Georgia Water Resources Institute. The information from this project contributes to PIER's Energy-Related Environmental Research Program.

For more information about the PIER Program, please visit the Energy Commission's website at www.energy.ca.gov/pier/ or contact the Energy Commission at 916-654-5164.

Table of Contents

Preface.....	iv
Abstract.....	xvii
Executive Summary	1
1.0 Introduction.....	4
1.1. Background and Overview	4
1.2. Project Objectives.....	5
1.3. Feasibility Studies.....	7
1.4. Report Organization.....	11
2.0 Integrated System Design and Implementation.....	12
2.1. Overview of INFORM System.....	12
2.2. Processing of Available Operational NCEP Data	14
2.3. GFS-based Ensemble Forecasts.....	16
2.4. CFS-based Ensemble Forecasts.....	20
2.5. INFORM DSS Reservoir System.....	23
2.6. INFORM DSS Overview	25
2.7. INFORM DSS Implementation Aspects	27
2.7.1. Database.....	27
2.7.2. Data Processing and Utility Tools.....	27
2.7.3. Interface Functions	28
3.0 Weather and Climate Downscaling Models	29
3.1. Introduction.....	29
3.2. Formulation of Orographic Rainfall Enhancement Model.....	30
3.2.1. Potential Theory Updrafts.....	30
3.3. Evaluation of Orographic Rainfall Enhancement Model with Data	36
3.3.1. American River Watershed.....	36
3.3.2. Other INFORM Watersheds	37
3.4. Formulation of Surface Air Temperature Model	47
3.4.1. Model Equations.....	47
3.4.2. Model Domain and Input.....	53
3.5. Evaluation of Surface Air Temperature Model with Data.....	54
3.6. Formulation of Probabilistic Climate Forecast Downscaling.....	57
3.7. Evaluation of Probabilistic Climate Forecast Downscaling.....	58

3.7.1.	Unconditional ESP.....	58
3.7.2.	ESP Conditional on CFS Forecasts	68
4.0	Hydrologic Models	83
4.1.	Introduction.....	83
4.2.	Formulation of Hydrologic Model Components	83
4.2.1.	Snow Accumulation and Ablation Model	84
4.2.2.	Sacramento Soil Moisture Accounting Model (SAC-SMA).....	86
4.2.3.	Unit Hydrograph and Channel Routing Procedures	87
4.2.4.	Stand-Alone Distributed Hydrologic Model.....	87
4.3.	Hydrologic Model Application Basins	88
4.3.1.	Basin Representations for CNRFC Operational Hydrologic Models.....	89
4.3.2.	Basin Representations for the Stand-Alone Distributed Hydrologic Models..	91
4.4.	INFORM Hydrometeorological Database.....	99
4.5.	Snow Model Sensitivities.....	100
4.5.1.	Sensitivity to Temperature Data.....	100
4.5.2.	Sensitivity to Model Parameters.....	103
4.6.	Evaluation of Hydrologic Models	106
4.6.1.	Performance Measures	107
4.6.2.	Evaluation of CNRFC Operational Models	108
4.6.3.	Evaluation of the Stand-Alone Hydrologic Model.....	118
5.0	Decision Support System	129
5.1.	Background and Overview	129
5.2.	Near-Real-Time Operations: Turbine Load Dispatching Model	129
5.3.	Short-Range Reservoir Management	133
5.4.	Mid-Range Reservoir Management	138
5.5.	Long-range Planning.....	140
5.5.1.	System Simulation Model	145
5.5.2.	Simulation Model Validation.....	153
5.5.3.	System Optimization Model.....	158
5.6.	Scenario and Policy Assessment Models.....	172
5.6.1.	Mid-range Scenario and Policy Assessment Examples.....	175
5.6.2.	Long-range Scenario and Policy Assessment Examples.....	181
6.0	Assessments.....	192
6.1.	Introduction.....	192
6.2.	Reservoir Inflow Simulations.....	193
6.3.	Precipitation and Temperature Forecasts for INFORM Catchments.....	194

6.3.1.	MAP Ensemble Forecasts	200
6.3.2.	MAT Ensemble Forecasts	206
6.4.	Reservoir Inflow Forecasts	211
6.5.	Overall Assessment of INFORM Real-Time Short-Range Forecasts	215
6.6.	Integrated Forecast-Decision Assessments	219
7.0	Conclusions and Recommendations	228
7.1.	Overarching Conclusions	228
7.2.	Specific Conclusions	229
7.2.1.	Forecast Component	229
7.2.2.	Decision Component.....	231
7.3.	Overarching Recommendations	234
7.4.	Specific Recommendations.....	234
7.4.1.	Forecast Component	234
7.4.2.	Decision Component.....	235
7.5.	Benefits to California	236
8.0	References	237
9.0	Glossary.....	242

Appendices

- A: Summary of Proceedings for the INFORM Oversight and Implementation Committee Meetings
- B: Validation Figures for the Application of the Downscaling Precipitation Model to the Folsom Lake Drainage
- C: Reliability-Diagram Tables for CFS-Conditioned and Unconditioned ESP for INFORM Reservoir Inflows
- D: INFORM Project Hydrometeorological Database
- E: Plots from the Evaluation of the CNRFC Operational Hydrologic Model
- F: Plots from the Evaluation of the INFORM Stand-Alone Distributed Hydrologic Model
- G: Selected Reservoir, Hydropower Facility, and Demand Data
- H: Historical Analog Streamflow Forecasting Model
- I: River Index Calculation and Water Year Characterization

List of Figures

Figure 1. Study area in Northern California and major reservoirs used to manage water resources for conservation, energy production, and flood damage mitigation 6

Figure 2. Reliability diagram of the unconditional (ESP) and conditional (ECHAM3-5) prediction frequencies that Folsom Lake inflow is in the lower tercile of its distribution. Vertical bars indicate 95% bounds due to sampling uncertainty. The period of record is 1970–1992, with ensemble forecasts issued every five days. 9

Figure 3. Values of Folsom Lake multiple objectives for various forecast scenarios and using the decision model of the integrated forecast-control system. Results for ECHAM3-5 are similar to those for ECHAM3-10..... 10

Figure 4. Schematic diagram of the distributed INFORM system configuration with data links indicated. Black arrows signify real-time data links, while grey arrows signify off-line data links..... 13

Figure 5. Schematic of INFORM forecast component processing 16

Figure 6. Schematic of processing flow associated with ingesting GFS ensemble forecasts and other information into the INFORM forecast component 18

Figure 7. Real-time spatial depiction of INFORM major reservoir inflow watersheds on a Google Earth display..... 21

Figure 8. Real-time ensemble-average 24-hr precipitation forecast over the INFORM domain superimposed on Google Earth displays. The precipitation scale is in inches/day..... 21

Figure 9. Real-time INFORM short- and long-term ensemble forecasts for Folsom Lake inflows and for a forecast preparation time of 3/1/06 00Z..... 24

Figure 10. A schematic of the INFORM reservoir and river system 24

Figure 11. INFORM DSS modeling framework 25

Figure 12. Mean areal updraft for Folsom Lake watershed as a function of direction angle from North (shown in degrees) for a unit 700-mbar wind inflow. The arrows indicate the direction from where the 700-mbar wind is blowing, and the magnitude of the mean areal updraft as a fraction of the incoming wind magnitude (contours of equal mean areal updraft are shown as concentric circles with indicated magnitude). Terrain slope is averaged over 10 km intervals..... 33

Figure 13. Linear regression equations between six-hourly downscaled (predictor) and observed estimates (predictant) of mean areal precipitation for the Folsom Lake sub-basins 38

Figure 14. As in Figure 13, but for daily data 39

Figure 15. Map of INFORM sub-basins. The sub-basins with the CNRFC code name are used for the evaluation of the orographic precipitation component.	40
Figure 16. Scatter grams of observed and simulated precipitation and associated regression lines and parameter values for INFORM region basins	42
Figure 17. Cumulative distribution functions of six-hourly mean areal precipitation amounts (observed in blue and simulated in red) for several basins of the INFORM region.....	44
Figure 18. Interpolated field (no model used) and downscaled field (using the temperature downscaling model) for the Northern California region for a specific 6-hour period in April 1992 (during the melting period). Both fields have a resolution of 10 km and are produced using the same 100 km-scale forcing information.....	55
Figure 19. Six-hourly observed (red line and symbols) and simulated (red line and symbols) temperature for the Chester and Weed (WED) sites and for the wet season 1997–1998.....	56
Figure 20. Theory of ensemble precipitation forecast downscaling from CFS precipitation forecasts	59
Figure 21. Distribution of N-day inflow volume anomalies for Oroville Reservoir.....	61
Figure 22. Reliability diagram for Folsom Reservoir 30-day inflow volumes in the lower tercile (left-hand column) and upper tercile (right-hand column) of the observed distribution.....	62
Figure 23. Reliability diagram, as in Figure 22, but for Trinity Reservoir 30-day inflow volumes.....	62
Figure 24. Reliability diagram, as in Figure 22, but for Shasta Reservoir 30-day inflow volumes.....	63
Figure 25. Reliability diagram, as in Figure 22, but for Oroville Reservoir 30-day inflow volumes.....	63
Figure 26. Cumulative probability distribution functions of rain-plus-melt values segregated according to high (red solid line) and low (dashed blue line) CFS monthly precipitation forecasts for Trinity and for each month of the year	73
Figure 27. As in Figure 26, but for New Bullards Bar Reservoir drainage on the Yuba River	75
Figure 28. As in Figure 26, but for the Folsom Reservoir drainage on the American River	76
Figure 29. As in Figure 26, but for the Oroville Reservoir drainage on the Feather River	77
Figure 30. As in Figure 26, but for the Shasta Reservoir drainage on the Sacramento and Pit Rivers.....	78

Figure 31. Reliability diagram for Folsom Reservoir 60-day inflow volumes in the lower tercile (left-hand column) and upper tercile (right-hand column) of the observed distribution. ESP conditioned on CFS. 79

Figure 32. Reliability diagram, as in Figure 31, but for New Bullards Bar reservoir inflows..... 79

Figure 33. Reliability diagram, as in Figure 31, but for Oroville reservoir inflows 80

Figure 34. Reliability diagram, as in Figure 31, but for Shasta reservoir inflows..... 80

Figure 35. Reliability diagram, as in Figure 31, but for unconditional ESP with 15 ensemble members. Folsom reservoir inflows. 81

Figure 36. Reliability diagram, as in Figure 35, but for New Bullards Bar reservoir inflows..... 81

Figure 37. Reliability diagram, as in Figure 35, but for Oroville reservoir inflows 82

Figure 38. Reliability diagram, as in Figure 35, but for Shasta reservoir inflows..... 82

Figure 39. Location of four major Sierra Nevada reservoir watersheds within Northern California 88

Figure 40. Schematic structure of the simulation model of the American River drainage into Folsom Reservoir for the CNRFC operational hydrologic model 90

Figure 41. As in Figure 40, except representing the operational hydrologic model for the Trinity River drainage into Trinity Lake..... 90

Figure 42. As in Figure 40 except representing the operational hydrologic model for the Sacramento River drainage into Shasta Reservoir 91

Figure 43. As in Figure 40, except representing the operational hydrologic model for the Feather River drainage into Oroville Reservoir 92

Figure 44. (a) Representation of the stand-alone distributed model of the American River drainage to Folsom Reservoir. (b) Schematic structure of routing network in this representation..... 95

Figure 45. As in Figure 44, except representing the distributed model for the Trinity Lake watershed 96

Figure 46. As in Figure 44, except representing the distributed model for the Shasta Reservoir watershed..... 97

Figure 47. As in Figure 44, except representing the distributed model for the Oroville Reservoir watershed..... 98

Figure 48. Schematic of the temperature (abscissa) relation to elevation (ordinate) by the moist adiabatic lapse rate 101

Figure 49. Snow water equivalent (SWE) in the Upper South Fork American River for water year 1980 as a function of systematic perturbation in the MAT: (a) 8

simulations in elevation zones with MAT that ranges from -5 to +3 °C; (b) areal weighted average of the perturbed simulation. The nominal simulation that uses the observed (unperturbed) MAT values is shown in red.....	102
Figure 50. Snow water equivalent (SWE) in the Upper South Fork American River for water year 1980 as a function of random perturbation of the MAT. The unperturbed MAT simulation is provided in red.	102
Figure 51. Two-parameter snow depletion curve. Parameters a and b are the angles with respect to the x- and y-axis, respectively, as shown.	104
Figure 52. The nominal simulation of SWE (blue) compared to SWE corresponding to a 50% overestimation (red) and 50% underestimation (black) of the parameter value	105
Figure 53. Example of the observed (blue) and simulated (red) flows in cubic meters per second (m ³ /s) for Water Year 1971 for the total flow at Folsom Dam and the outlet of the sub-watersheds of the South, Middle, and North Forks of the American River	109
Figure 54. Daily flow simulated by the operational hydrologic model versus observed flow in m ³ /s for the American River catchments	111
Figure 55. Cumulative distribution of the observed (blue) and simulated (red) flows over the length of the simulation for the American River catchments and for the operational hydrologic model	112
Figure 56. Observed (blue) and simulated (red) duration curves of Box-Cox transformed flow for the American River and for the operational hydrologic model.....	113
Figure 57. Scatter plots of the simulated versus observed flows at a monthly scale for the American River catchments	114
Figure 58. Observed and simulated monthly mean flows (+/- 1 standard deviation shown by "x") expressed as a fraction of the annual flow volume for the American River catchments	115
Figure 59. (a) Observed (black) and simulated (red) time trace of the spring pulse. (b) Annual differences between the observed and simulated spring pulse timing (given in days).....	116
Figure 60. Daily snow water equivalent from snow sensors (dots) compared with simulated snow water equivalent from the operational model (solid line) for four different Water Years (1988–1991) and for the South Fork of the American River sub-watershed.....	117
Figure 61. Comparison of observed (FNF, in blue) and simulated (red) inflows to Folsom Reservoir for the INFORM stand-alone distributed hydrologic model.....	125
Figure 62. Mean daily observed (FNF) versus simulated inflows to Folsom Reservoir for the stand-alone distributed hydrologic model.....	125

Figure 63. Observed (FNF, blue) and simulated (red) cumulative inflows to Folsom Reservoir for Water Years 1961–1999	126
Figure 64. Monthly scatter plots of simulated inflows versus FNF flow for Folsom Reservoir in Box Cox transformed units for the stand-alone distributed hydrologic model.....	128
Figure 65. Observed (FNF) and simulated monthly mean inflows (+/- 1 standard deviation for Folsom Reservoir, expressed as a fraction of annual flow volume. Presented is the simulation with the stand-alone distributed hydrologic model. ..	128
Figure 66. Plant power generation as function of hourly discharge and reservoir level for a) Trinity, b) Shasta, c) Oroville, and d) Folsom	132
Figure 67. Plant daily generation as function of daily release and reservoir level for a) Trinity, b) Shasta, c) Oroville, and d) Folsom.....	136
Figure 68. Typical hourly power generation schedules for a) Trinity, b) Shasta, c) Oroville, and d) Folsom.....	137
Figure 69. Mid-range model example run for Trinity. A 3-month forecast horizon from 1/1/1981.	141
Figure 70. Mid-range model example run for Shasta. A 3-month forecast horizon from 1/1/1981.	142
Figure 71. Mid-range model example run for Oroville. A 3-month forecast horizon from 4/1/1981.	143
Figure 72. Mid-range model example run for Folsom. A 3-month forecast horizon from 1/1/1965.	144
Figure 73. American River spatial aggregation.....	154
Figure 74. Delta outflow comparisons.....	155
Figure 75. X2 Location comparisons	155
Figure 76. Reservoir Storage Comparisons: (a) Trinity, (b) Shasta, (c) Oroville, (d) Folsom, and (e) New Melones	158
Figure 77. Long-range inflow forecasts from March 1, 2006	167
Figure 78. Long-range inflow forecast vs. historical means	168
Figure 79. Planning tradeoffs: a) Carry-over storage vs. demand; b) Energy generation vs. demand	169
Figure 80. Reservoir storage and release sequences associated with tradeoff point 3 ..	170
Figure 81. Energy generation sequences associated with tradeoff point 3	171
Figure 82. X2 location sequences associated with tradeoff points 3 and 5.....	172

Figure 83. Delta outflow associated with tradeoff point 3.....	173
Figure 84. Scenario and policy assessment models	174
Figure 85. Mid-range assessments: Trinity elevation and release sequences	176
Figure 86. Mid-range assessments: Shasta elevation and release sequences	177
Figure 87. Mid-range assessments: Oroville elevation and release sequences	178
Figure 88. Mid-range assessments: Folsom elevation and release sequences.....	179
Figure 89. Long-range assessments: Reservoir elevation sequences.....	184
Figure 90. Long-range assessments: Reservoir release sequences.....	185
Figure 91. Long-range assessments: Energy generation sequences	186
Figure 92. South export and deficit sequences	187
Figure 93. X2 location sequences	188
Figure 94. Delta outflow sequences	189
Figure 95. INFORM hydrologic model 6-hour simulations of Folsom reservoir inflow using CNRFC-estimated MAP and MAT time series for the period 10/5/2005– 3/15/2006 (blue dashed line). The red line signifies the corresponding CNRFC full natural flow (FNF) estimates (observations).	195
Figure 96. As in Figure 95, but for the New Bullards Bar reservoir inflow on the Yuba River	196
Figure 97. As in Figure 95, but for the Oroville reservoir inflow	197
Figure 98. As in Figure 95, but for the Shasta reservoir inflow.....	198
Figure 99. As in Figure 95, but for the Trinity reservoir inflow	199
Figure 100. Highest and lowest averages of ensemble members over the indicated forecast lead time period at each valid time (blue dashed lines). The INFORM downscaling component produced these forecasts in real time for the upper modeling area of the American River North Fork. The panels also show the corresponding observed averages estimated by CNRFC (red lines). Forecast lead times range from 12 hours to 5 days.....	202
Figure 101. As in Figure 100, but for the Middle Fork of the American River	203
Figure 102. (Upper six panels) As in Figure 100, but for the upper area of the Pit River catchment within the Shasta reservoir drainage area. (Lower six panels) as in Figure 100, but for the lower area of the Pit River catchment.	204
Figure 103. As in Figure 100, but for the upper area of the Sacramento River catchment with outlet at Delta, California	205

Figure 104. (Upper six panels) As in Figure 100, but for MAT over the upper area of the Pit River catchment within the Shasta reservoir drainage area. (Lower six panels) as in Figure 100, but for MAT over the lower area of the Pit River catchment. 207

Figure 105. As in Figure 104, but for the upper and lower areas of the Sacramento River with outlet at Delta, California 208

Figure 106. As in Figure 104, but for the North Fork Feather River with outlet at Pulga in the Oroville reservoir drainage 209

Figure 107. As in Figure 104, but for the Indian Creek in the Oroville reservoir drainage 210

Figure 108. Folsom highest and lowest ensemble member average reservoir inflow forecasts (blue dashed lines) for forecast lead times from 1 day (upper panel) to 5 days (lower panel). Corresponding CNRFC FNF estimates are shown in each case (red line). 212

Figure 109. As in Figure 108, but for the New Bullards Bar reservoir inflow on the Yuba River and for a forecast lead time of 12 hours 213

Figure 110. As in Figure 108, but for the Oroville reservoir inflow 214

Figure 111. As in Figure 108, but for the Shasta reservoir inflow 216

Figure 112. As in Figure 108, but for the Trinity reservoir inflow 217

Figure 113. As in Figure 109, but for Shasta reservoir inflows (upper panel) and for Folsom reservoir inflows (lower panel) and for a 2-day forecast lead time. Input of bias adjusted MAPs through a single factor. 223

Figure 114. Integrated, mid-range assessments: Trinity elevation and release sequences 224

Figure 115. Integrated, mid-range assessments: Shasta elevation and release sequences 225

Figure 116. Integrated, mid-range assessments: Oroville elevation and release sequences 226

Figure 117. Integrated, mid-range assessments: Folsom elevation and release sequences 227

List of Tables

Table 1. Reliability scores of forecasting Folsom Lake inflow volumes	9
Table 2. GFS Forecast Data for INFORM	17
Table 3. Statistical performance of simplified orographic model in wet season (1969–1992).....	36
Table 4. Names and code numbers of drainage basins used in the evaluation of downscaled precipitation	40
Table 5. Frequency of occurrence of zero and low precipitation.....	41
Table 6. Second moment statistics of mean areal precipitation observations and simulations for basins of the INFORM region	46
Table 7. Second moment properties of simulates and observed mean areal precipitation for southwesterly and northwesterly wind events.....	47
Table 8. CFS grid points and watershed centroids (degrees).....	69
Table 9. Tercile values for CFS-forecast monthly precipitation.....	69
Table 10. Validation results for Trinity	72
Table 11. Validation results for New Bullards Bar	72
Table 12. Validation results for Folsom.....	72
Table 13. Validation results for Oroville.....	74
Table 14. Validation results for Shasta	74
Table 15. Hydrologic Model Parameters.....	85
Table 16. Drainage areas of CNRFC major catchments	93
Table 17. Properties of stand-alone distributed model catchments	94
Table 18. Daily values of evapotranspiration demand for the Folsom Reservoir Drainage Area	99
Table 19. Nominal values of snow model parameters	103
Table 20. Performance statistics for the historical simulation of the operational hydrologic model.....	110
Table 21. Parameters of the snow and soil model components used for the Folsom Reservoir stand-alone distributed model simulation.....	120
Table 22. As in Table 21, except for the Trinity Lake inflow simulation	121
Table 23. As in Table 21, except for the Shasta Reservoir inflow simulation.....	122

Table 24. As in Table 21, except for the Oroville Reservoir inflow simulation.....	123
Table 25. Performance statistics for the historical simulation of the INFORM distributed hydrologic model.....	124
Table 26. Mid-range assessment statistics.....	180
Table 27. Long-range assessment: Reservoir statistics	190
Table 28. Long-range assessment: Hydropower and spillage statistics	190
Table 29. Long-range assessment: Water supply statistics.....	191
Table 30. Long-range assessment: Maximum X2 location statistics.....	191
Table 31. Integrated, mid-range assessments statistics	222

Abstract

This report describes the first three-year phase of the Integrated Forecast and Reservoir Management (INFORM) project. The primary INFORM objective is to demonstrate the utility of present-day meteorological/climate and hydrologic forecasts for the Northern California river and reservoir system, including all major reservoirs on the Trinity, Sacramento, Feather, American, and San Joaquin rivers, and the Sacramento-San Joaquin Delta. In close collaboration with water forecast and management agencies of the region, a software system was designed and implemented in a distributed manner, with components that ran at various agency and research centers. The system contains real-time, short-range forecast components; off-line longer-range forecast components; and off-line decision components that span forecast and decision time scales from hours to seasons. In all cases, forecast uncertainty was explicitly characterized and used for risk-based decision support. Extensive tests with historical data and an initial five-month period of operational “dry run” testing for the wet season of 2005–2006 showed that system components perform well and clearly demonstrated the value of the system in advancing the current state of forecast, management, and planning operations in the region. The main recommendation is to continue the demonstration of the INFORM system for two to three more years to reliably quantify real-time performance and utility for planning and management and to explore more fully the various applications to which the system is suited.

Keywords: Ensemble precipitation forecasting; ensemble temperature forecasting; ensemble flow forecasting; risk-based decision support; adaptive reservoir management; INFORM

Executive Summary

Introduction

Considerable investments have been made toward improving the quality and applicability of climate, synoptic, and hydrologic forecast information, and earlier retrospective studies have demonstrated clearly that the management of water resource systems with large reservoirs can potentially benefit from such information. However, before this project no focused program has ever aimed to quantify and demonstrate these benefits in an operational environment. There are three main reasons why this has not been previously accomplished:

1. Synoptic and climate forecasts include substantial uncertainty, and their effective use in management requires procedures that explicitly account for that uncertainty both in flow forecast and decision models/processes.
2. Existing reservoir management procedures depend on presently available information and operate under set institutional constraints, so that nontrivial technical and institutional changes are required to use information of a different type (i.e., improved hydrologic, synoptic, or climate timescale forecasts).
3. The development and application of such systems requires that the technical teams maintain a close relationship with the operational users and have a clear understanding of their operational environment.

As a result, up to this point few reservoir managers have been able or willing to dedicate the considerable effort required to use new approaches and realize the benefits of improved forecast information.

Purpose

The purpose of the Integrated Forecast and Reservoir Management (INFORM) Project was to demonstrate increased water-use efficiency in Northern California water resources operations through the innovative application of meteorological/climate, hydrologic, and decision science.

Project Objectives

In accordance with its purpose, the particular objectives of INFORM are to:

1. Implement a prototype integrated forecast-management system for the primary Northern California reservoirs, both for individual reservoirs as well as system-wide.
2. Demonstrate the utility of meteorological/climate and hydrologic forecasts through near-real-time tests of the integrated system with actual data and management input by comparing its economic and other benefits to those accruing from current management practices for the same hydrologic events.

Project Outcomes

To achieve the general objectives of the INFORM project, the authors performed the following technical tasks:

- Created the Oversight and Implementation Committee for project oversight and assistance with system implementation and tests.
- Developed, implemented, and performed validation of climate and weather INFORM components for Northern California with historical data and real-time data.
- Developed, implemented, and performed validation of hydrologic INFORM reservoir-inflow forecasts with historical and real-time data for all major reservoirs of Northern California.
- Developed, implemented, and performed validation of decision INFORM components with historical and real-time data for the Northern California water resources management system.
- Integrated INFORM system climate, hydrology, and decision components and performed initial operational tests producing real-time ensemble forecasts out to lead times of 16 days four times daily for the 2005–2006 wet season.
- Performed assessments of the integrated forecast-decision system value via retrospective simulation experiments.
- Held INFORM design, assessment, and training meetings with operational forecast and management agency staff.

Conclusions

There are several technical and specific conclusions that have been drawn from the outcomes of the project in the areas of meteorology/climate, hydrology, and decision science. These conclusions are detailed in the report (Chapter 7). The most important conclusion of the report is that, with available real-time availability of forecast information from the National Centers for Environmental Prediction and with real-time observed precipitation and temperature (as well as hydrologic model state values from the California Nevada River Forecast Center), integrated forecast-management systems are realizable as effective operational decision-support tools for management and planning of California water resources. Such systems assist water managers in translating forecasts and their uncertainty into a range of effective risk-based policies. In addition, these systems can advance current operational practices by (1) incorporating forecast uncertainty in decisions on a range of time scales, and (2) allowing for regional coordination of management decisions.

Recommendations

Perhaps the most important recommendation arising from this work is to continue the INFORM demonstration experiments for two or (more usefully) three additional

operational seasons beyond the system “dry run” wet season of 2005–2006 in continued close collaboration with the forecast and management partner agencies in Northern California. These additional operational seasons are necessary for the reliable evaluation of the INFORM system performance and utility in specific situations, for the application of any system corrections and adjustments that appear necessary from system evaluation, for the establishment of a protocol for its operational use by the collaborating agencies, and for exploring alternative applications for the system that have been suggested by sponsor agencies.

A second overarching recommendation pertains to the use of the INFORM system in a stand-alone mode for climate change simulations. The INFORM system closely emulates several of the actual forecast and management procedures used in routine operations in Northern California. As such, it constitutes a realistic simulation system for impact analysis in this region using the output of state-of-the-science global climate models that predict climatic variability and change. Such impacts include potential future climatic influences on precipitation, temperature, and snowmelt and runoff patterns in the Sierra Nevada resolved on the scale of INFORM catchments (from hundreds to thousands of square kilometers); the effects of increased demand scenarios; and the effectiveness of alternative management scenarios for improved water-use efficiency.

Benefits to California

A significant benefit of this first phase of INFORM for Northern California is its contribution toward integrating operational water supply forecast and management activities by federal and state agencies toward increased water use efficiency. The mutual technology transfer and science cooperation between research centers and operational agencies is another. Lastly, even in its current prototype form, the INFORM system provides a unique resource for operational and management agencies in Northern California. These agencies may benefit by using this system to evaluate potential decision policies pertaining to the use of Northern California’s water supply during real-time operations and for seasonal planning, both for present and future years.

1.0 Introduction

1.1. Background and Overview

Managed water resources affect regional economies and the environment. In turn, they are influenced by climate variability and trends, increasing demands, and changing water markets. As pressures to provide reliable water supplies at low cost increase, the need to optimize water use efficiency becomes imperative. Although considerable investments have been made to improve the quality and applicability of synoptic- and climate-scale forecast information, and water resources systems can clearly benefit from such information (e.g., NRC 2001; NRC 2004), no focused program exists aiming to quantify and demonstrate these benefits. Two main reasons are: (1) synoptic and climate forecasts include substantial uncertainty, and their effective use in management requires procedures that explicitly account for that uncertainty both in forecast and decision models/processes; and (2) existing reservoir management procedures depend on presently available information and operate under set institutional constraints, so that nontrivial technical and institutional changes are required to use information of a different type (i.e., improved synoptic or climate timescale forecasts). As a result, few reservoir managers are able to commit the considerable effort required to use new approaches and realize the benefits of improved climate information.

The fundamental premise of the INFORM project (see also Georgakakos et al. 2005) is that the use of short- and long-term operational forecasts in water resources management can be adopted only through the establishment of demonstration and assessment sites at which the following conditions have been met:

- A quantitative numerical system is developed that translates climate information to reliable forecasts of system response under dynamic operational decision policies.
- Modelers, forecasters, and managers have established a set of mutually agreed-upon performance criteria to measure the effectiveness of decision policies.
- A baseline quantitative system version is developed that reflects present management practice and operational models, together with an alternate system version that includes climate and hydrology forecasts in an integrated forecast-decision framework.
- Rigorous intercomparison of quantitative and other benefits is performed by implementing management decisions for the alternate systems using retrospective analysis of historical data and forecasts, or in real time.
- There is continuing participation of management staff in the demonstration activities and in user/modeler workshops for the mutual benefit of modelers, forecasters, and managers.

To fully realize the forecast benefits within a management process of multiple decision makers, objectives, and spatio-temporal scales, a hierarchy of interlinked decision models is necessary to address long-range, mid-range, and short-range objectives

(Georgakakos 2004). The Integrated Forecast and Reservoir Management (INFORM) Demonstration Project was conceived to *demonstrate increased water-use efficiency in Northern California water resources operations* through (1) the innovative application of climate, hydrologic, and decision science; and (2) reciprocal technology transfer activities between the INFORM scientists and the staff of federal and state agencies with an operational forecast and management mandate in Northern California. The first three years of project activities were funded by the National Oceanic and Atmospheric Administration (NOAA), the California Energy Commission (Energy Commission), and the CALFED Bay-Delta Authority (CBDA). These are the subject matter of this report.

Key operational agencies for the implementation of the demonstration project were the U.S. National Weather Service (NWS) California Nevada River Forecast Center (CNRFC), the California Department of Water Resources (DWR), the U.S. Bureau of Reclamation Central Valley Operations (USBR CVO), and the Sacramento District of the U.S. Army Corps of Engineers (USACE). Other agencies and regional stakeholders contributed through active participation in project workshops and, indirectly, through comments and suggestions conveyed to the INFORM Oversight and Implementation Committee (OIC). The OIC provided independent review of the development and demonstration activities and facilitated implementation of the integrated system components in a near-operational environment. Appendix A provides a record of the OIC meeting proceedings during the first three-year phase of the INFORM Project.

1.2. Project Objectives

The general objectives of INFORM are:

1. To implement a prototype integrated forecast-management system for primary Northern California reservoirs, individually and for the system of reservoirs.
2. To demonstrate the utility of climate and hydrologic forecasts for water resources management in Northern California through near-real-time tests of the integrated system with actual data and with management input, and by comparing its economic and other benefits to those of existing water management systems for the same events.

The primary application and demonstration system is the Northern California system of large reservoirs, consisting of the Folsom, Oroville, Shasta, and Trinity reservoirs and associated water resources (Figure 1). During the first three years of INFORM activities documented in this report, only initial assessment of the real-time system performance was possible using data from California's 2005–2006 wet season after the implementation of the integrated software system. It is anticipated that using data from at least three more seasons would be necessary to produce a reliable assessment with the implemented system.

Major Reservoirs in Northern California

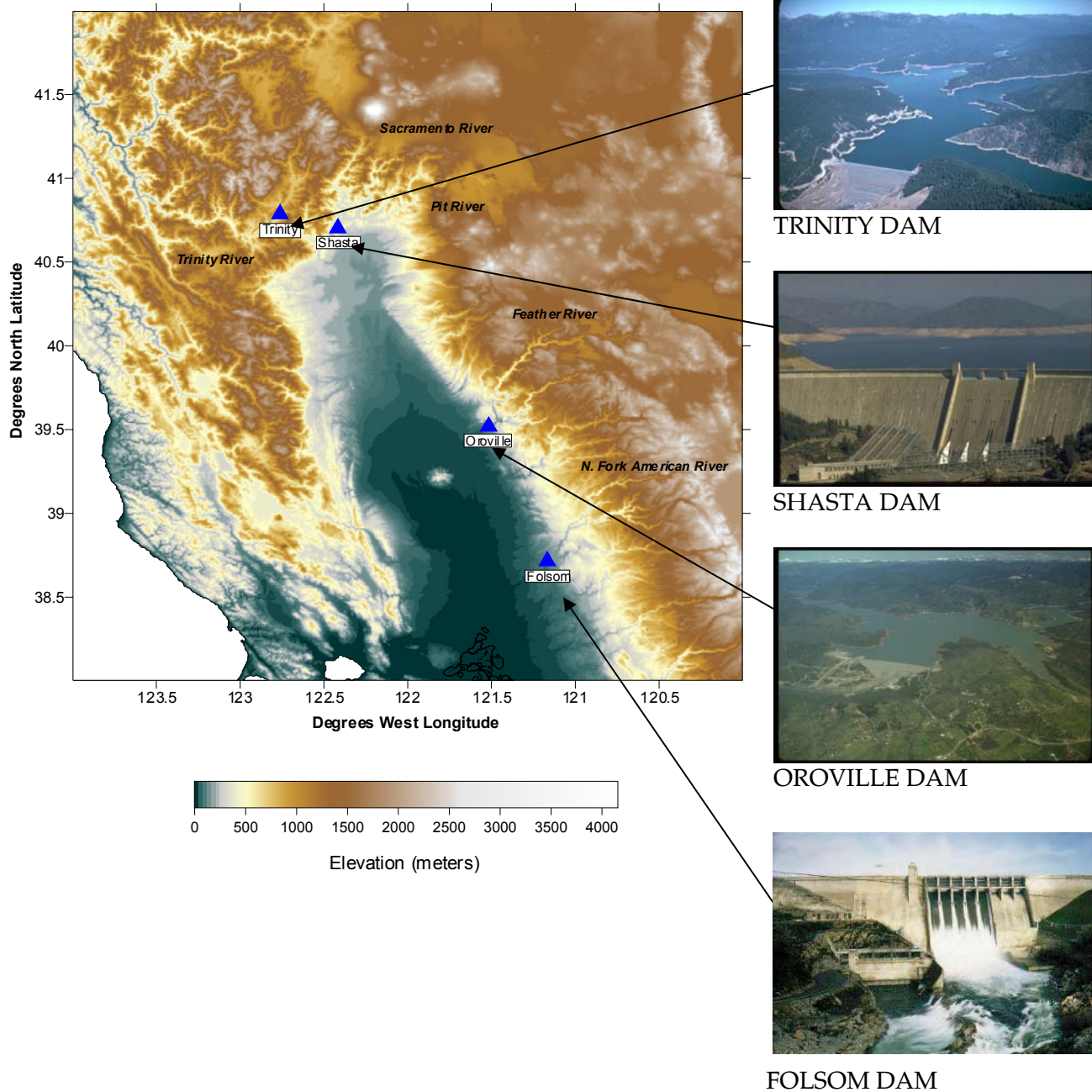


Figure 1. Study area in Northern California and major reservoirs used to manage water resources for conservation, energy production, and flood damage mitigation

To achieve the general objectives of the INFORM project, the authors performed the following technical tasks:

- Created the OIC for project oversight and assistance with system implementation and tests.
- Developed, implemented, and performed validation of climate and weather INFORM components for Northern California with historical data and real time data.
- Developed, implemented, and performed validation of hydrologic INFORM reservoir-inflow forecasts with historical and real-time data for all major reservoirs of Northern California.
- Developed, implemented, and performed validation of decision INFORM components with historical and real-time data for the Northern California water resources management system.
- Integrated INFORM system climate, hydrology, and decision components and tested with real-time data.
- Held INFORM design, assessment, and training meetings with operational forecast and management agency staff.

1.3. Feasibility Studies

Feasibility was established through retrospective studies of the Folsom reservoir (part of the INFORM system). The studies involved the application of a numerical integrated forecast-decision system designed to accommodate the considerable uncertainty of the climate information within the Folsom multi-objective decision process (Carpenter and Georgakakos 2001; Yao and Georgakakos 2001). This integrated system (used first in the Des Moines River study of Georgakakos et al. 1998) includes components for:

- Adjusting global climate model (GCM) simulations/forecasts to account for known regional biases and for biases and random errors arising from the difference between the spatial and temporal scales of the GCM and that of the reservoir catchment.
- Generating hydrologic forecasts and forecast uncertainty estimates through ensemble forecasting, either independent of, or conditional on, adjusted GCM information.
- Generating dynamic decision policies that explicitly use forecast information;
- Quantifying operational, risk-based trade-offs among competing water uses including flood protection, water supply, energy generation, and low-flow augmentation.
- Interacting with stakeholder agencies to select a shared vision tradeoff position and policy option.

- Simulating system response to quantify the benefits and risks associated with the decisions made.

The retrospective studies focused on intercomparing: (1) a system approximating current operational practices, (2) a system using an ensemble streamflow prediction (ESP) approach using historical observations only, (3) a system using the full integrated forecast-decision system using GCM monthly estimates of precipitation and temperature from two climate models and for both GCM simulations and forecasts, and (4) a system using perfect inflow foresight. The study used the Canadian Centre for Climate Modeling and Analysis coupled GCM (1 simulation, CGCM-1) and the Max Planck Institute for Meteorology ECHAM3 GCM (10-ensemble simulations, ECHAM3-10, and 5-ensemble forecasts, ECHAM3-5). The historical study extended from October 1, 1964 through December 31, 1992 for GCM simulations and from October 1, 1970 through December 31, 1992 for GCM forecasts. Reservoir inflow forecasts and management decisions were generated every five days. Researchers used an adaptation of the National Weather Service operational hydrologic forecast model, calibrated with historical data for the basin of interest. In all cases, the same number of forecast traces was generated. Forecast and decision horizons were 60 days long with daily resolution. Performance with respect to both forecast and economic indices was evaluated, and the assessment is outlined in the following. It is noted in the outset that the performance assessment comments are basin and reservoir system specific.

Researchers used several indices to quantify the performance of the ensemble inflow forecasts, including reliability diagrams and a reliability score based on each decile of the forecast ensemble distribution. The reliability score compounds the results for all probability decile ranges to provide a scalar skill score. A zero reliability score indicates perfect performance (as in the perfect foresight scenario), while higher scores reflect decreasing forecast skill. Events of particular interest to reservoir management are events associated with reservoir inflow volumes (e.g., over the forthcoming two months) being in the upper (flood) or lower (drought) terciles of their distribution.

On the basis of the reliability score, Table 1 shows that using GCM ensemble information in real-time significantly improves the reliability score of ensemble inflow forecasts as compared to using the ESP inflow forecasts that depend on climatology. This is especially so for the low tercile volumes associated with drought conditions.

The reliability diagram of Figure 2 indicates that the performance of the ECHAM3-5 ensemble flow forecasts is superior to that of the ESP forecasts for low tercile inflows mainly at the higher deciles of forecast frequency.

Reservoir management performance does not only depend on forecast performance but also on the way ensemble forecast information is used by the decision model and process. This is the compelling reason for integrating the forecasts with the reservoir management procedures. Reservoir management performance was measured by annual spillage, annual and maximum flood damage, annual hydro electric energy value, and risk of falling below minimum instream flows.

Table 1. Reliability scores of forecasting Folsom Lake inflow volumes

$$\text{Reliability Score: } \sum N_{f_i} (P_{f_i} - P_{o_i})^2 / \sum N_{f_i} \quad (*)$$

Event Forecast: Inflow Volume in Upper Tercile of its Distribution

<i>Interval(days)</i>	<i>ESP</i>	<i>CGCM-1</i>	<i>ECHAM3-10</i>	<i>ECHAM3-5</i>
30	0.004	0.004	0.002	0.002
60	0.008	0.005	0.003	0.003

Event Forecast: Inflow Volume in Lower Tercile of its Distribution

<i>Interval(days)</i>	<i>ESP</i>	<i>CGCM-1</i>	<i>ECHAM3-10</i>	<i>ECHAM3-5</i>
30	0.011	0.014	0.006	0.002
60	0.015	0.012	0.005	0.003

(*) P_{f_i} and P_{o_i} are the observed and forecast frequencies for the i^{th} decile of the event distribution, and N_{f_i} is the number of forecasts for the i^{th} decile.

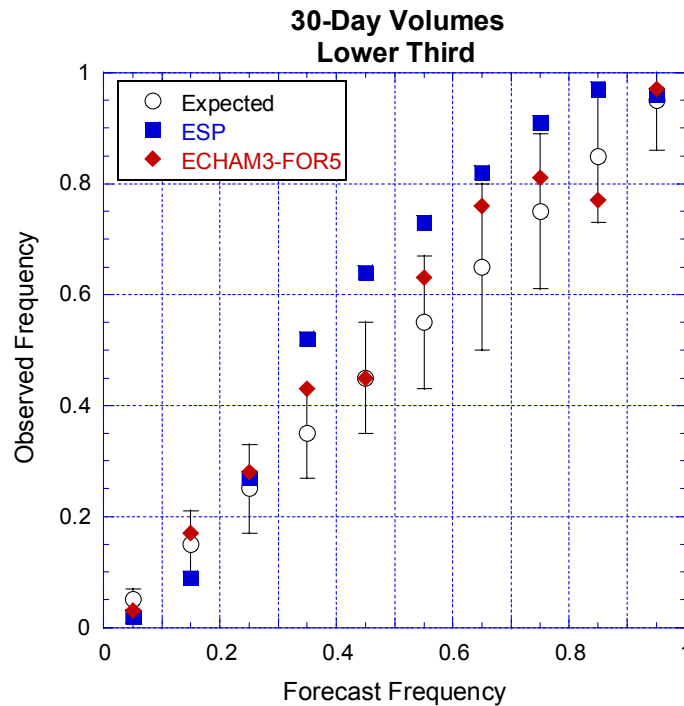


Figure 2. Reliability diagram of the unconditional (ESP) and conditional (ECHAM3-5) prediction frequencies that Folsom Lake inflow is in the lower tercile of its distribution. Vertical bars indicate 95% bounds due to sampling uncertainty. The period of record is 1970–1992, with ensemble forecasts issued every five days.

Approximate dependence of costs and benefits on the reservoir levels and releases was specified for the decision model, and decision preferences were set based on discussions with Folsom Lake operations staff. The decisions pertain to reservoir releases, power generation (turbine loads and operation hours), and spillage volumes and are updated adaptively as new inflow forecasts or other information on the condition of the system becomes available.

Comparison of simulated results using current management practices versus the integrated forecast-decision system showed that increases up to 15%–18% in annual average energy and decreases of up to 50% in unnecessary spillage are possible without increasing flood damage and with increased water supply made available for agricultural, municipal, and environmental uses. Figure 3 shows results of intercomparison of the various forecast procedures using the same decision model of the integrated system. The current operational procedure and the perfect forecast scenario produce single forecast time series, while the rest produce ensemble inflow forecast time series. The figure shows that benefits for all Folsom management objectives are associated with the use of ensemble forecasts.

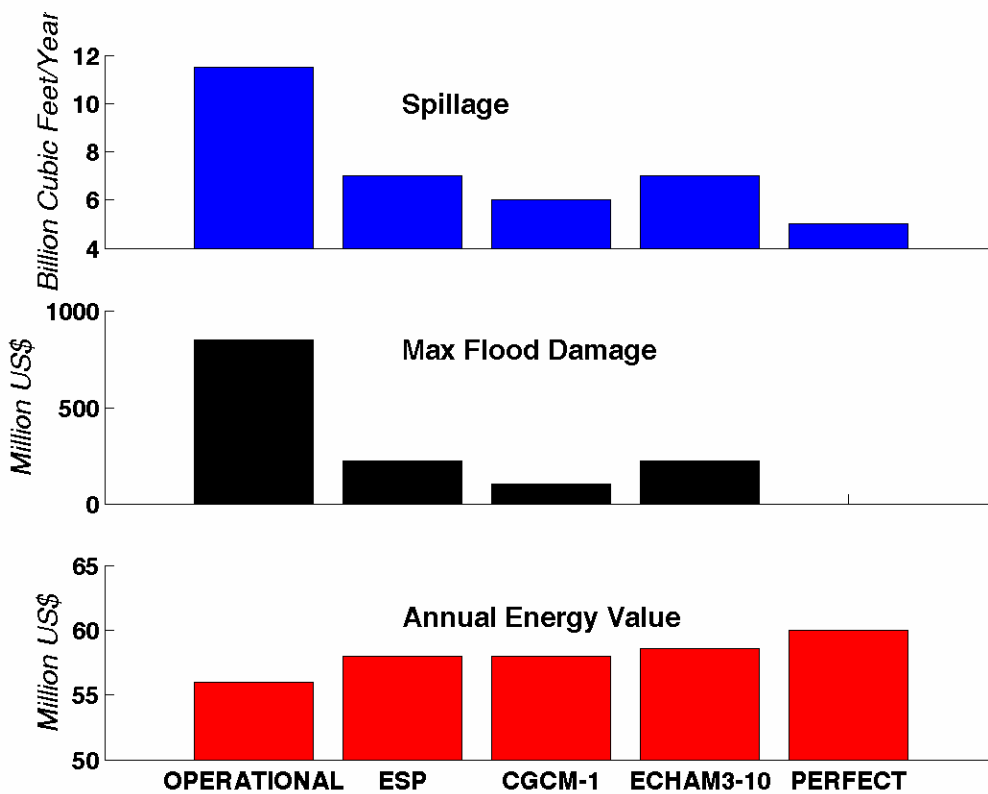


Figure 3. Values of Folsom Lake multiple objectives for various forecast scenarios and using the decision model of the integrated forecast-control system. Results for ECHAM3-5 are similar to those for ECHAM3-10.

Furthermore, these forecasts yield management benefits near those obtained from the perfect-forecast scenario. It is also shown that for this case study, the ESP and GCM-conditioned ensemble inflow forecasts produce comparable results. Additional results (Yao and Georgakakos 2001) indicate that full management benefits can only be realized by the use of reliable ensemble forecast schemes *combined with* dynamic decision rules. Namely, using GCM-conditioned forecasts in association with static management rules, or neglecting to incorporate forecast uncertainty in the decision process, are not expected to improve reservoir management. In fact, contrary to widely held views, such practices may increase the risk of costly failures.

1.4. Report Organization

The report is organized to follow the specific tasks listed in Section 1.2 (Project Objectives). Chapter 2 presents the integrated system implemented for real-time operation using information from operational forecast and management agencies. Chapters 3, 4, and 5 discuss development and validations associated with climate and weather forecast information, hydrologic forecasts, and decision models, respectively. Chapter 6 presents the assessments made from real-time tests during the wet season 2005–2006 in Northern California and from retrospective studies for the region. Chapter 7 contains conclusions and recommendations on the basis of the main findings from the assessments. References are listed in Chapter 8, while specialized technical information is reserved for the Appendices.

2.0 Integrated System Design and Implementation

2.1. Overview of INFORM System

The INFORM software system consists of a number of diverse components for data handling, model runs, and output archiving and presentation. At its current state of development and input data availability, it is a distributed system with online and off-line components. The system routinely captures real-time National Center for Environmental Predictions (NCEP) ensemble forecasts. It uses both ensemble synoptic forecasts from NCEP's Global Forecast System (GFS) and ensemble climate forecasts from NCEP's Climate Forecast System (CFS). The former are used for producing real-time, short-term forecasts, and the latter are used off-line for producing longer-term forecasts as needed. Section 2.2 summarizes the reasons for the difference between the GFS and CFS processing.

The INFORM ensemble forecast output feeds an off-line decision model component for producing risk-based short- and long-term decision alternatives for a nine-month decision horizon. The INFORM forecast component is implemented at the Hydrologic Research Center (HRC) for real-time use and with data links to the California Nevada River Forecast Center (CNRFC) databases. In addition, the ensemble reservoir inflow forecasts and maps of the ensemble surface precipitation forecasts of INFORM out to several days are posted on a secure Internet site for INFORM-developing institutions and collaborating forecast and management agencies. The INFORM decision component is implemented at the Georgia Water Resources Institute (GWRI), the U. S. Bureau of Reclamation (USBR), and DWR for off-line use. Figure 4 shows a schematic of the system distributed configuration, indicating the data links. The arrows point to the site of the database from which the organization initiating the link receives and deposits data.

Global Forecast System ensemble forecasts of three-dimensional atmospheric fields are captured, archived, ingested, and quality controlled in real time for further use. Downscaling components that use the ingested ensemble fields produce corresponding ensemble gridded forecasts of surface precipitation and temperature over the INFORM application area of Northern California. A Geographic Information System (GIS) locates the gridded forecasts over the Northern California terrain in geodetic coordinates and estimates mean areal precipitation and surface air temperature for all ensembles and forecast lead times and for the hydrologic catchments that comprise the drainage areas of interest. Hydrologic models use the downscaled ensemble forecast mean areal quantities as input to produce ensemble forecasts of snow depth and snowmelt during the cold season and of surface and subsurface runoff and streamflow (including reservoir-site inflow) throughout the year.

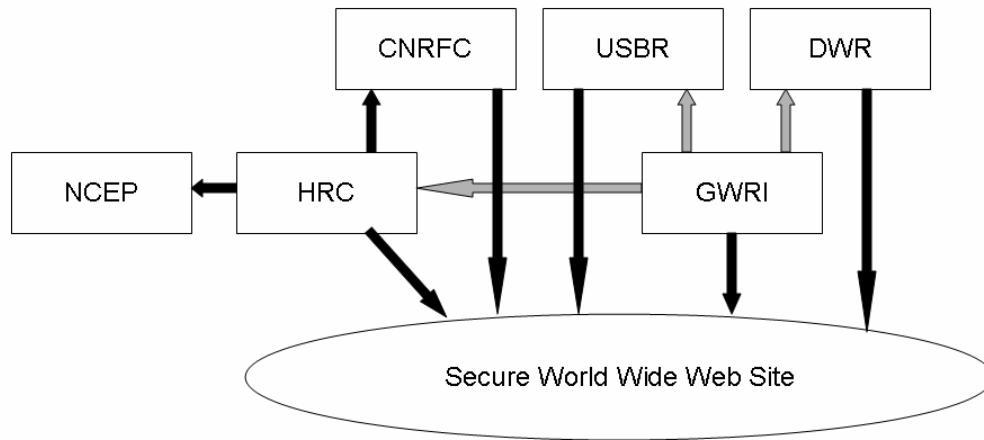


Figure 4. Schematic diagram of the distributed INFORM system configuration with data links indicated. Black arrows signify real-time data links, while grey arrows signify off-line data links.

Climate Forecast System ensemble forecasts of surface air temperature and precipitation with monthly resolution and with a nine-month maximum forecast lead time are also captured in real time by the INFORM data ingest system at HRC. At a user-specified time, a probabilistic downscaling component uses the ensemble CFS forecasts and produces high spatial and temporal resolution surface precipitation and temperature estimates for each hydrologic catchment in the INFORM region. The hydrologic component of INFORM is then engaged to produce ensemble reservoir inflow estimates for the primary reservoir sites of interest. Downscaling and hydrologic forecasting are done off-line (typically once per month) in this case of CFS processing. The short-term (GFS-based) and long-term (CFS-based) ensemble reservoir inflow forecasts of INFORM are blended to produce a consistent series of input to the decision component.

The INFORM Decision Support System (DSS) is designed to support the decision-making process, which is characterized by multiple decision makers, multiple objectives, and multiple temporal scales. Toward this goal, the INFORM DSS includes a suite of interlinked models that address reservoir planning and management at hourly, daily, seasonal, and over-year time scales. The DSS includes models for each major reservoir in the INFORM region, simulation components for downstream river reaches as necessary to incorporate downstream decision objectives, optimization components suitable for use with ensemble forecasts, and a versatile user interface. The decision

software runs off-line, as forecasts become available, to derive and assess planning and management strategies for all key system reservoirs. The DSS is embedded within a user-friendly graphical interface that links the models with the database and helps visualize and manage results. A policy assessment model has also been developed and is part of the DSS. The DSS modeling framework is described in Sections 2.5, 2.6, and 2.7.

Training and collaboration with staff of CNRFC, USBR, and DWR has produced an efficient distributed INFORM system for risk-based management and planning.

2.2. Processing of Available Operational NCEP Data

The California Nevada River Forecast Center is the primary agency for collaborative activities pertaining to ingesting and downscaling climate and weather data for INFORM. To use operational products and for sustainability reasons, the INFORM forecast team decided to use operational ensemble forecasts from NCEP to drive the downscaling procedures. The initial plan was to use ensemble forecasts of three-dimensional fields from GFS and CFS with a common statistical-dynamical downscaling procedure for consistency in blending short-term with long-term ensemble forecasts. There have been several meetings and communications between INFORM Project representatives and NCEP representatives during the project period (documented in various progress reports) to facilitate the real-time acquisition of the aforementioned ensemble forecasts from NCEP. Because a significant change in the original implementation plan resulted from these communications, a short summary of these and of the final outcomes is given below.

INFORM representatives from HRC met with the director and other members of the Environmental Modeling Center (EMC) of NCEP on December 16, 2003, in Washington to establish a collaboration plan regarding the availability of needed climate and weather forecast and retrospective analysis data for the implementation of the integrated forecast-management system for Northern California. In a subsequent meeting during January 2004, CNRFC management was briefed concerning the discussions between HRC and NCEP in December 2003. The briefing passed on to CNRFC the information from NCEP concerning weather and climate forecast systems, data availability, and acquisition. In turn, HRC personnel were briefed on communications methods available to CNRFC for acquiring data from NCEP (principally in terms of bandwidth), and CNRFC's perspective on data needs for the INFORM project. In January 2004 HRC personnel met again with NCEP EMC staff. These discussions covered in detail the retrospective climate model forecast system and data availability, the design, operational implementation and data availability for both short-range (GFS) and seasonal (CFS) forecast systems. These discussions also focused on the data required for the INFORM to produce probabilistic precipitation and snowmelt forecasts and the means of acquiring those data. This latter point was an important practical matter, as ensemble forecast systems generate large volumes of data.

In recognition of the fact that users were often required to download very large volumes of data to obtain the small fraction that they desired, NCEP has implemented a server/client system called NOMADS (NOAA Operational Model Archive Distribution System). The NOMADS system allows users to issue a request for specific model output data (for example, specific time, level, latitude, longitude, and variable). The actual preparation of this subset is carried out at NCEP on dedicated servers, and the subset is transmitted directly to the user or is placed in a defined location for user retrieval. NCEP scientists briefed HRC personnel on the use of the NOMADS system. HRC personnel met again with CNRFC staff in April 2004 to brief them concerning the January meeting with NCEP EMC and to familiarize them with the NOMADS system's capabilities. These meetings have been essential to the design of the INFORM ingest component for climate and weather data and have paved the way for a longer-term fruitful collaboration among operational global centers (NCEP), regional hydrologic forecast centers (CNRFC), and INFORM developers. HRC personnel familiarized themselves with the process of retrieving data from the NOMADS system and wrote and tested software necessary to automatically download and ingest GFS ensemble forecasts of three-dimensional fields from NCEP into the INFORM forecast component for further processing.

Although the INFORM team was successful in receiving ensemble GFS forecasts of three-dimensional fields from NCEP, the request for analogous data from the seasonal CFS forecast system was not met due to processing and staff limitations at NCEP. The original plan was to receive ensemble CFS forecasts of three-dimensional fields in real time with 12-hourly resolution for further processing by the INFORM system forecast component. In this way, short-term and long-term forecasts would be generated seamlessly by the INFORM system. After considerable dialogue with NCEP staff, monthly resolution surface precipitation and air temperature two-dimensional fields became available from the CFS system so that each month an ensemble of such forecasts could be downloaded and used by the INFORM system. Compared to the real-time dynamical downscaling used for GFS data, a purely probabilistic downscaling procedure was developed for CFS using historical time series of surface mean areal precipitation and air temperature data from each hydrologic catchment in the area of interest. The probabilistic downscaling procedure is used off-line (typically once per month) for generating long-term ensemble reservoir inflow forecasts. A schematic of the final INFORM forecast component processing may be seen in Figure 5. Elements of the schematic in Figure 5 will be discussed in Sections 2.3 and 2.4. The difference between the type of short-term and longer-term (seasonal) input ensemble forecast data and their downscaling procedures led to deviations from the initial INFORM implementation plan. It also generated the need for appropriate blending of the downscaling procedures for the times when the GFS data ends. The blending approach used is discussed in Section 2.4 in the context of the Decision Component.

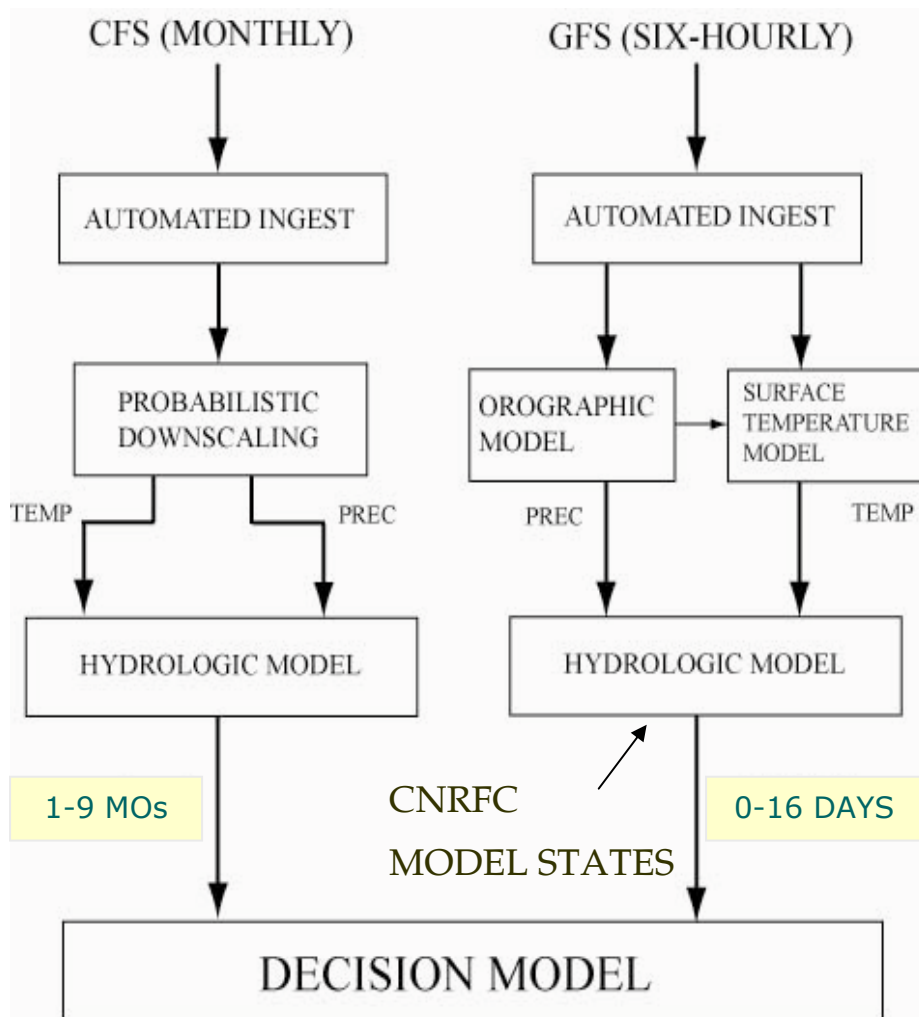


Figure 5. Schematic of INFORM forecast component processing

2.3. GFS-based Ensemble Forecasts

The real-time (Kanamitsu et al. 1991) processing elements of the INFORM system associated with the use of GFS data are shown on the right path of Figure 5. After the ensemble GFS forecasts of three-dimensional fields are downloaded in an automated fashion onto INFORM servers, the system performs dynamical downscaling using tailored orographic precipitation and surface air temperature models for the region of interest. Processing continues by using the resultant gridded downscaled ensemble surface precipitation and air temperature fields to produce mean areal input for the hydrologic catchments in the INFORM region. The INFORM system then activates the hydrologic models to process this input and to produce ensemble forecasts of reservoir inflow and of other hydrologic model output. Table 2 shows the GFS data processed by the INFORM system.

Table 2. GFS Forecast Data for INFORM

<u>At surface</u>
Precipitation
Snow accumulation
2 m air temperature (T)
2 m relative humidity (Q)
10 m wind vector components (U and V)
Net solar radiation
Net long-wave outgoing radiation
Sensible heat
Latent heat
<u>At available upper levels (at least at standard pressure levels)</u>
Wind vector components (U and V)
Air temperature (T)
Relative humidity (Q)
Geopotential height

The data consists of 8 ensembles of the forecast variables shown in Table 2, each with a 16-day (384-hour) maximum lead time. The spatial resolution of the GFS data fields in longitude – latitude coordinates for the development and testing period (up to the end of May 2006) is $1^\circ \times 1^\circ$ out to 96 hours and it is $2.5^\circ \times 2.5^\circ$ for greater forecast lead times. The temporal resolution is 6 hours for lead times up to 96 hours, and it is 12 hours for longer lead times. Due to the current limitations in the computing power of the INFORM servers and for a four-time daily forecast generation (GFS forecasts at 00UTC,¹ 06UTC, 12UTC, and 18UTC), the INFORM system uses 8 out of the available 14 ensemble members of the GFS fields. In addition, INFORM uses GFS forecast fields from 23 vertical layers. Figure 6 shows a more detailed depiction of the INFORM forecast component processing flow associated with GFS data. A short description of the processing elements is given next. Chapters 3 and 4 discuss the individual numerical models used.

¹ Coordinated Universal Time (UTC)

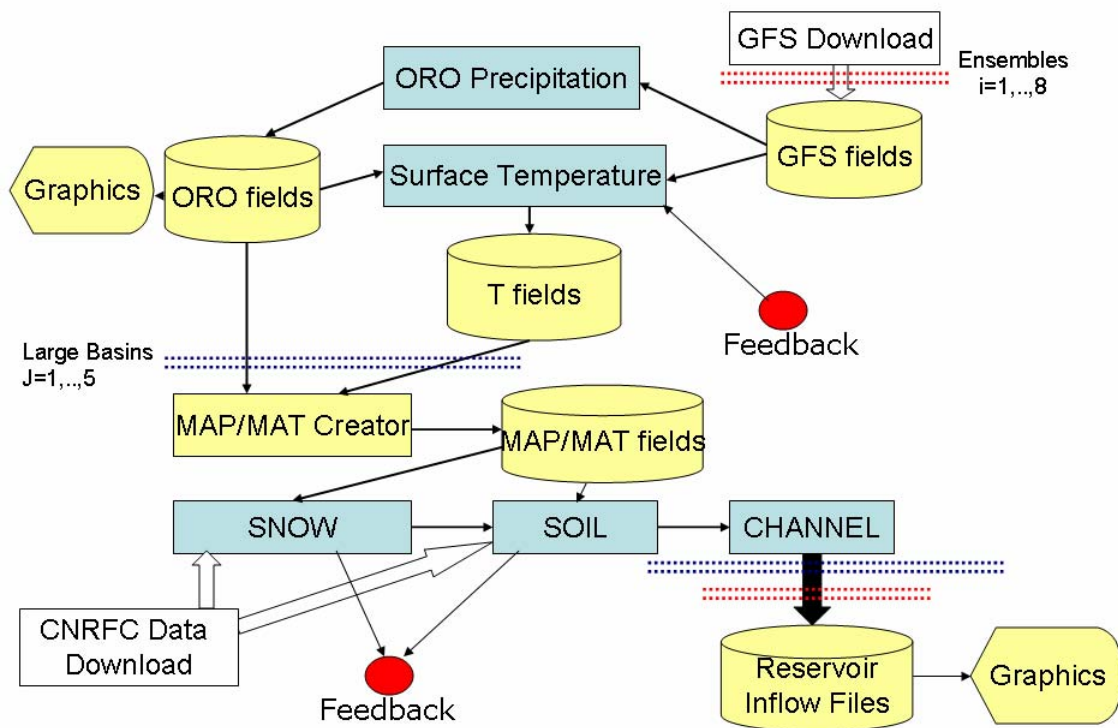


Figure 6. Schematic of processing flow associated with ingesting GFS ensemble forecasts and other information into the INFORM forecast component

At each forecast preparation time and after each download is complete, a computer processing unit (CPU) of the ROCKETCALC Multicomputer at HRC processes each GFS ensemble forecast time series. For this GFS processing, the multicomputer uses eight CPUs to process eight GFS ensemble members and to produce ensemble forecasts quickly. Once downloaded from the NOMADS system, the three-dimensional fields of each ensemble member are used to produce initial and boundary conditions for the orographic precipitation and surface air temperature models of INFORM (see Chapter 3 for model description and evaluation). Processing is through the orographic precipitation model first to produce downscaled gridded precipitation fields with a 10 x 10 square kilometer (km²) resolution. The surface air temperature model is based on surface energy balance computations and uses the downscaled precipitation fields in conjunction with GFS forecast fields to produce concurrent, consistent surface air temperature gridded fields with the same resolution. The temperature model computations also use snow cover and soil water estimates produced by the hydrologic component of INFORM to allow the computation of reflected energy and the separation of latent and sensible heat at the land surface.

Five large hydrologic drainage areas comprise the INFORM region upstream of the large reservoir sites of interest: Folsom (American River), New Bullards Bar and Englebright (Yuba River), Oroville (Feather River), Shasta (Sacramento, McCloud, and Pit Rivers), and Trinity or Clair Engle (Trinity River). For modeling purposes, each of these drainage areas has been subdivided into smaller catchments. These catchments correspond largely to the catchments used by the CNRFC in their operational hydrologic forecast system so that the INFORM system can duplicate as much as feasible the CNRFC hydrologic modeling component. Efforts to improve the timing of the simulated flows resulted in a few deviations from CNRFC delineations. The CNRFC (and consequently the INFORM) hydrologic models require mean areal precipitation and surface temperature input for each of these catchments (see hydrologic model description in Chapter 4). A processing component of the INFORM system (see MAP/MAT Creator in Figure 6) uses the downscaled gridded surface precipitation and temperature fields for each ensemble member (ORO and T fields in Figure 6) and GIS geodetic mapping information to produce mean areal precipitation (MAP) and mean areal surface air temperature (MAT) fields for each subcatchment, forecast time step, and ensemble member.

Once the MAP and MAT fields are available for all the catchments in the domain of interest for a particular forecast lead time, the hydrologic models (snow accumulation and ablation model, soil water accounting model, and channel routing model) of INFORM use these fields to produce reservoir inflow forecasts for each of the five large reservoirs of interest. The snow model produces snow cover and snow depth as well as snowmelt estimates during the cold part of the year. The snowmelt and any bare-ground rainfall feed the soil water model, which produces soil water estimates for each catchment as well as surface and sub-surface channel inflows. Lastly, the channel routing component receives the inflows from the soil water component and routes these through the stream network to produce channel outflows for all the tributary streams of each large drainage basin. The hydrologic models produce forecasts given a set of initial conditions. For the 00UTC, 06UTC, and 18UTC forecast preparation time, initial conditions are provided by the previous cycle of INFORM processing. For the 12UTC forecast preparation time, the INFORM system acquires the values of the model current state variables for all the catchments in the domain of interest from the operational CNRFC simulation runs (using observed MAP and MAT). This download is performed in real time (daily), and it is shown in the lower left corner of Figure 6. In this way, at initial forecast time 12UTC the INFORM hydrologic models are aligned with the CNRFC operational models. There is only one forecast preparation time for which alignment occurs because under all but exceptional conditions the CNRFC simulations occur once daily, for 12UTC. Although some deviation is expected between INFORM and CNRFC simulations after three additional forecast lead times for the smaller catchments, the INFORM team felt that the once-daily alignment should not produce significant deviations for the forecast inflows of the INFORM domain large reservoirs.

For each forecast lead time, the processing system stores the latest estimates of snow cover and soil water content for use by the surface air temperature downscaling component during the next forecast lead time cycle. For each GFS ensemble forecast member, each forecast preparation time and each forecast lead time, the INFORM system goes through the processing sequence depicted in Figure 6 for all delineated catchments in the INFORM domain before initiating the processing of the next forecast lead time fields. This is necessary to realize the feedback described from the snow and soil models to the surface air temperature downscaling model (see feedback link in Figure 6).

To allow easy access and feedback from the members of the INFORM forecast team (including CNRFC staff) and for the winter 2005–2006, HRC created a website with real-time INFORM forecast information (www.hrc-lab.org/INFORM/realtime). The INFORM system updated the website every six hours with new INFORM forecast products generated on the basis of GFS ensemble input. The website contained ensemble reservoir inflow forecasts (in the form of line plots of hydrographs) for all five large reservoir sites, ensemble statistics of spatial maps of forecast cumulative precipitation fields for a given forecast period, and estimates of the probability of precipitation exceeding given thresholds over a given time period. The displays allowed the use of Google Earth for the precipitation fields. Figures 7 and 8 present examples of real-time displays.

2.4. CFS-based Ensemble Forecasts

As mentioned earlier, the original plan for INFORM was to use a single downscaling procedure for both the GFS and the CFS ensemble forecast input. This requires the availability of three-dimensional CFS ensemble forecast fields, as in the case of GFS (see previous section). In lieu of such detailed forecast output, the INFORM team decided to use ensemble surface precipitation and air temperature fields with monthly resolution as input to INFORM. The ensemble members are formed by long-term CFS integrations (at least out to nine months) performed twice daily with corresponding initial conditions. The left processing path of Figure 5 shows that, even though the INFORM system downloads the ensemble members of the CFS forecasts in real time, it processes CFS forecast information off-line using a probabilistic downscaling procedure. Chapter 3 includes a detailed discussion of the mathematical formulation and its evaluation with retrospective forecasts and observations. The following discussion serves to outline the computational INFORM components of the downscaling procedure for CFS data.

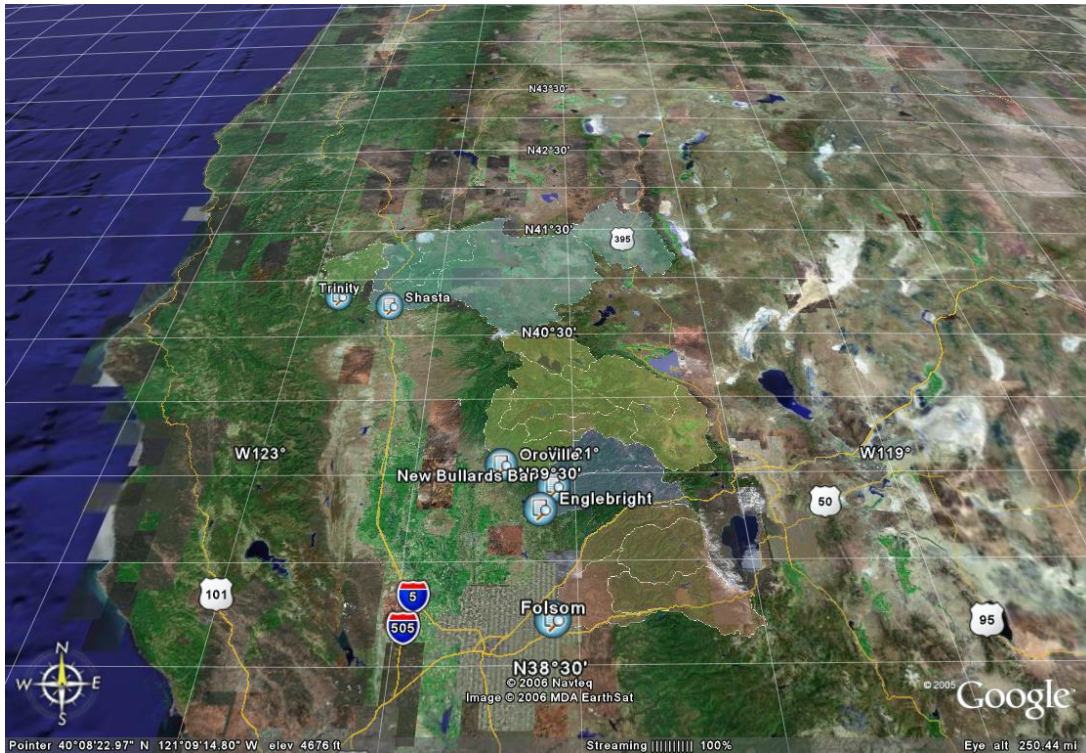


Figure 7. Real-time spatial depiction of INFORM major reservoir inflow watersheds on a Google Earth display

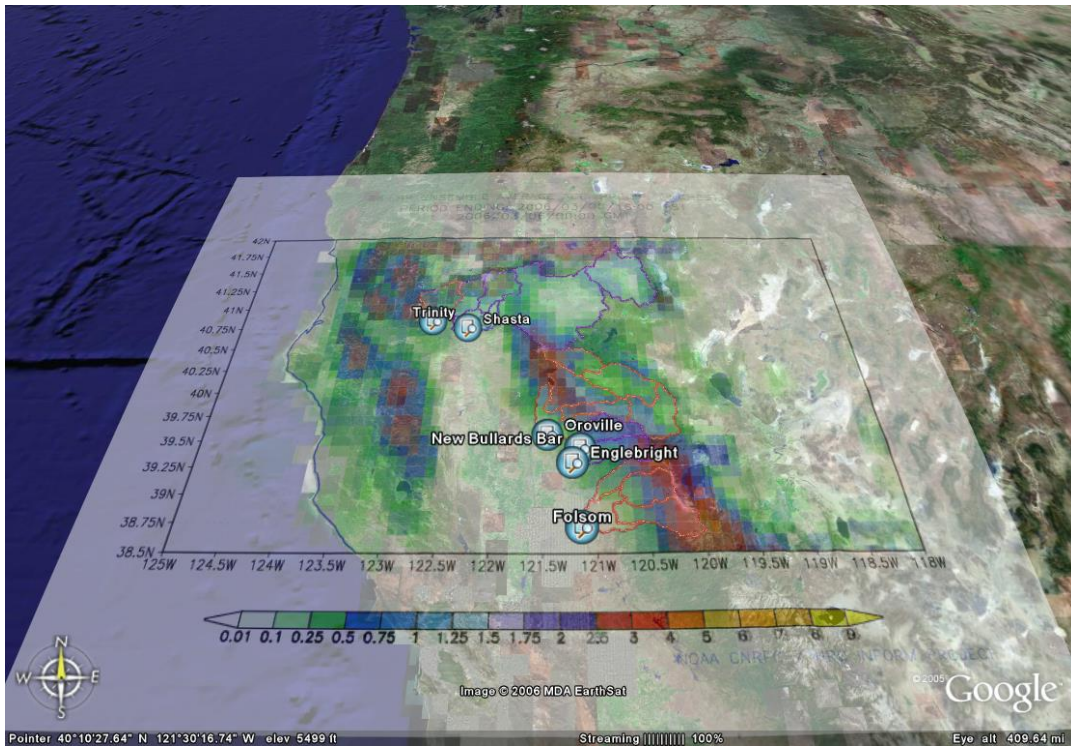


Figure 8. Real-time ensemble-average 24-hr precipitation forecast over the INFORM domain superimposed on Google Earth displays. The precipitation scale is in inches/day.

In contrast to the real-time utilization of GFS forecasts, the INFORM system uses downloaded CFS forecasts off-line once per month or as required by the forecast and management agencies in Northern California. The off-line processing involves two procedures that yield two sets of ensemble reservoir inflow time series with maximum lead time of nine months and six-hourly temporal resolution. The first procedure, called ensemble streamflow prediction (ESP), was developed by the NWS (Smith et al. 1991) and uses solely historical mean areal surface precipitation and air temperature data of a six-hour resolution for all the catchments in the INFORM region. For a given date of forecast preparation time and for a given initial condition of hydrologic model states, the ESP procedure feeds into the hydrologic models historical time series of concurrent observed mean areal precipitation and temperature from all the previous historical years, extending to the duration of the maximum forecast lead time (nine months). For the river location of interest, including reservoir inflow points, the generated output flow time series forms the flow forecast ensemble. The ESP procedure serves as the climate baseline for the CFS-driven downscaling procedure.

The second downscaling procedure uses the CFS ensemble forecasts to condition the ESP procedure to include only historical years for which CFS forecasts had similar behavior to that predicted by the CFS for the current forecast period. Similar behavior in this context means that a certain quantity computed from CFS forecasts falls in the upper, lower, or middle tercile (third) of its distribution. Preliminary analysis showed that the total precipitation in the first month of the forecast can serve as a good index for judging similar behavior of CFS forecasts in the current and archived forecast periods with the same month, day, and hour of forecast preparation time. As in the case of the unconditional ESP procedure, an ensemble of reservoir inflow forecasts is the result of the CFS processing described.

At the present stage of development and as described above, there are two different processing paths that produce GFS-based short-term (out to 16 days) and CFS-based long-term (out to nine months) ensemble reservoir inflow forecasts. For reliable estimation of risk by the INFORM decision component (see Section 2.5), appropriate blending of downscaling procedures must be done at times near the maximum forecast lead time of the short-term ensemble forecasts. The authors tested a number of alternatives with the final selection involving the use of the ensemble of estimated hydrologic model states at the end of the 16-day period of GFS-driven forecasts to provide an ensemble of initial conditions for the unconditioned and CFS-conditioned ESP runs. Thus, the initial month of INFORM system output involved the first 16 days with eight ensemble forecasts from the GFS-driven processing and a larger number of ensemble forecast members for the rest of the days of the forecast horizon (out to nine months) from the unconditional and CFS-conditioned ESP runs. The decision models were structured to use eight ensembles with six-hourly resolution out to 16 days and a larger number of ensembles with monthly resolution out to nine months (see discussion in the next section).

For illustration, Figure 9 shows an example of the resulting ensemble reservoir inflow into Folsom Lake with a March 1, 2006, forecast preparation time that combines short- and long-term forecasts. The x-axis in the Figure is in six-hourly time steps and the transition from GFS-driven forecasts to ESP forecasts is evident at forecast lead time (time step) 64 (384 hours or 16 days). The ESP ensemble inflow forecasts are generated using initial conditions from each of the ensemble members of the GFS-forced hydrologic forecasts at the end of the 16 days. A total of 14 members are selected randomly from the total of 40 possible for each of the eight ensembles to contribute to the climate forecast ensemble.

2.5. INFORM DSS Reservoir System

The scope of the originally proposed INFORM DSS included four reservoirs: Trinity, Shasta, Oroville, and Folsom. However, the operational planning and management of these reservoirs is dependant upon the downstream facilities and water uses including the Sacramento-San Joaquin Delta, and the export system to Southern California. Thus, based on extensive discussions with the INFORM Oversight Committee, DWR, USBR, and the USACE, it was decided to expand the scope of the original four reservoir system to include most downstream elements that have a bearing on planning decisions. More specifically, the original project scope was expanded to include the elements shown on Figure 10. This system encompasses the Trinity River system, the Sacramento River system, the Feather River system, the American River system, the San Joaquin River system, and the Sacramento-San Joaquin Delta. Major regulation and hydropower projects on this system include the Clair Eagle Lake (Trinity Dam) and the Whiskeytown Lake on the Trinity River, the Shasta-Keswick Lake complex on the upper Sacramento River, the Oroville-Thermalito complex on the Feather River, the Folsom-Nimbus complex on the American River, and several storage projects along the tributaries of the San Joaquin River, including New Melones. The Sacramento River and the San Joaquin River join to form an extensive Delta region and eventually flow out into the Pacific Ocean. The Oroville-Thermalito complex comprises the State Water Project (SWP), while the rest of the system facilities are federal and comprise the Central Valley Project (CVP).

The Northern California river and reservoir system serves many vital water uses, including providing two-thirds of the state's drinking water, irrigating seven million acres of the world's most productive farmland, and being home to hundreds of species of fish, birds, and plants. In addition, the system protects Sacramento and other major cities from flood disasters and contributes significantly to the production of hydroelectric energy. The Sacramento-San Joaquin Delta provides a unique environment and is California's most important fishery habitat. Water from the Delta is pumped and transported through canals and aqueducts south and west, serving the water needs of many more urban, agricultural, and industrial users.

A 1986 agreement between the U.S. Department of the Interior, USBR, and DWR provides for the coordinated operation of the SWP and CVP facilities (Agreement of Coordinated Operation, COA). The agreement aims to ensure that each project obtains

its share of water from the Delta and protects other beneficial uses in the Delta and the Sacramento Valley. The coordination is structured around the necessity to meet the in-basin use requirements in the Sacramento Valley and the Delta, including Delta outflow and water quality requirements.

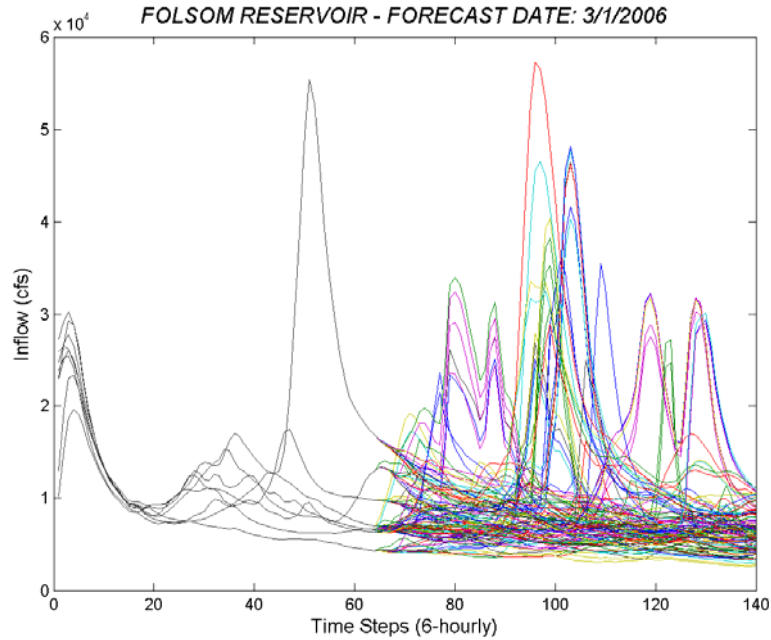


Figure 9. Real-time INFORM short- and long-term ensemble forecasts for Folsom Lake inflows and for a forecast preparation time of 3/1/06 00Z

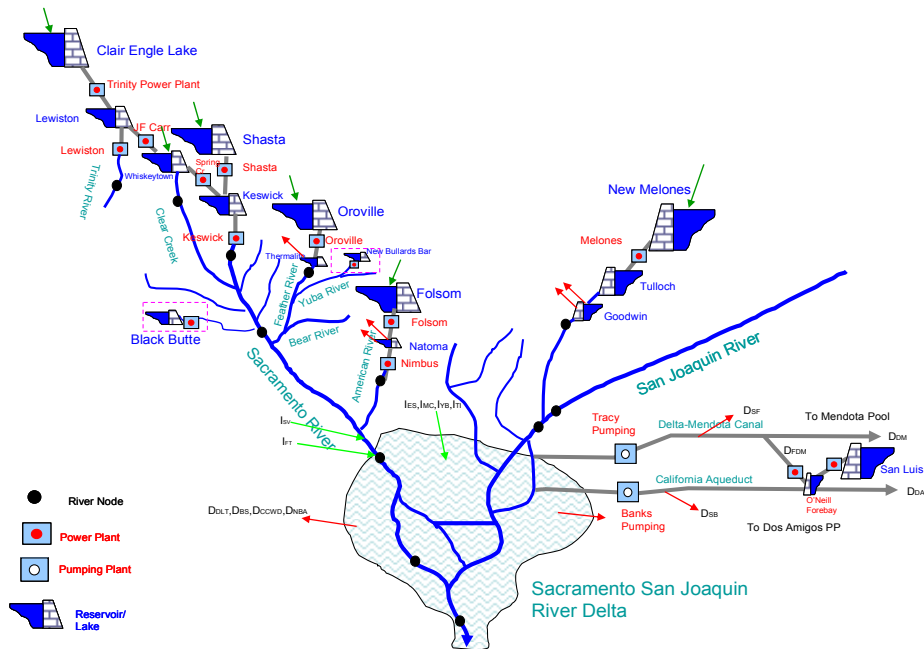


Figure 10. A schematic of the INFORM reservoir and river system

The expanded INFORM system is intended to “drive” the decision making process at the long-range (planning) level. An overview of the INFORM DSS is provided next to better clarify the role of the expanded system.

At present, a number of tools are being used by the federal and state agencies responsible for the management of the northern California water resources system. Such tools include spreadsheet models (USBR), hydropower scheduling models (USBR), simulation models (DWR, USACE), and forecasting models (CNRFC). However, these tools are not fully integrated, either vertically (planning to management to operations) nor horizontally (agency-wise). Perhaps, the most significant contribution of the INFORM project is that it provides an integration framework and a common set of tools that facilitate agency communication, cooperation, and coordination.

2.6. INFORM DSS Overview

The INFORM DSS modeling framework is illustrated in Figure 11.

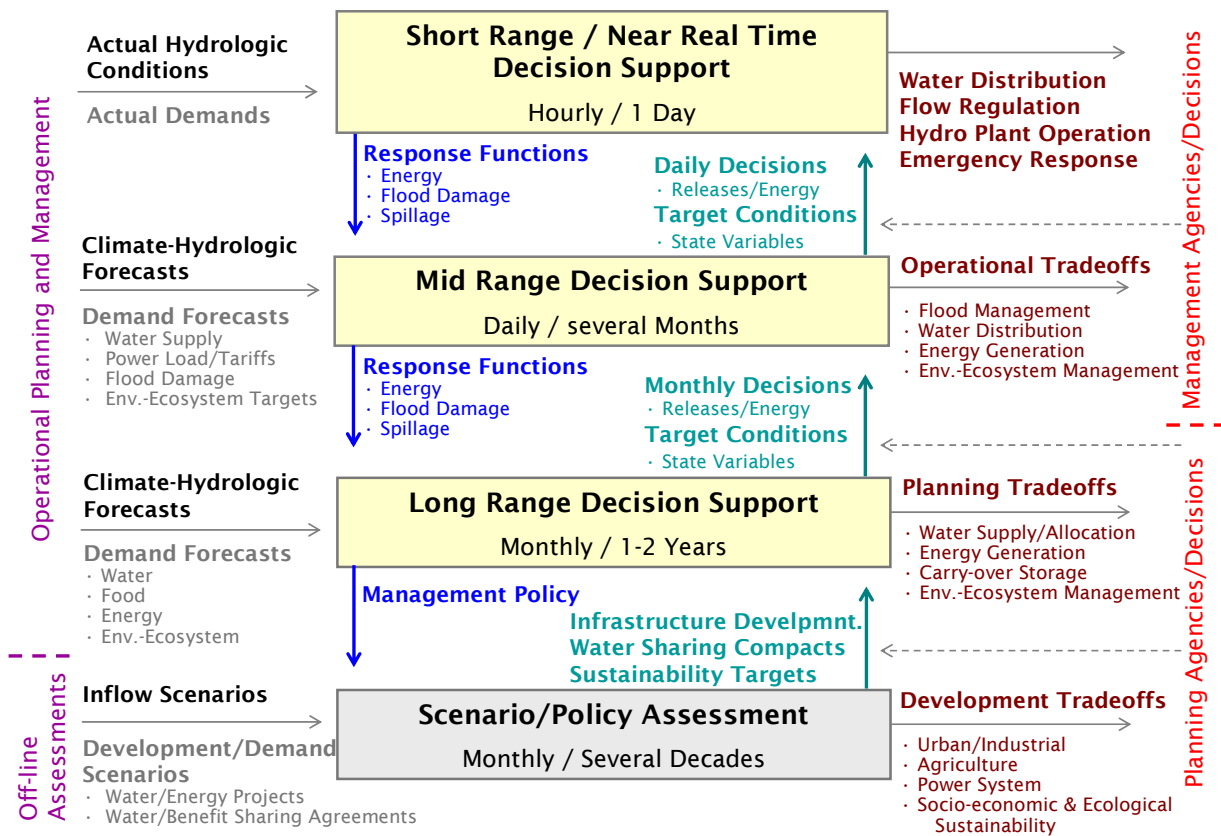


Figure 11. INFORM DSS modeling framework

The DSS includes multiple modeling layers designed to support decisions pertaining to various temporal scales and objectives (Georgakakos 2006). The three modeling layers shown in the figure include: (1) short range and near-real-time operations decision support (which has hourly resolution and a horizon of one day), (2) mid-range reservoir management (which has a daily resolution and a horizon of several months), and (3) long-range planning (which has a monthly resolution and a horizon of one or two years). The INFORM DSS also includes an assessment model which replicates the system response under various inflow scenarios, system configurations, and policy options.

The INFORM DSS is designed to operate sequentially. In a typical application, the long-range planning model is activated first to consider long-range issues such as water conservation strategies for the upcoming year in view of the climate and hydrologic forecasts. As part of these considerations, the DSS quantifies several tradeoffs of possible interest to the planning and management agencies and system stakeholders. These include, among others, assessments regarding relative water allocations to water users throughout the system (including ecosystem demands), reservoir carry over storage, reservoir coordination strategies and target levels, water quality constraints, and energy generation targets. This information is provided to the planning and management agencies to use as part of their decision process together with other information. After completing these deliberations, key decisions are made on monthly water supply contracts, reservoir releases, energy generation, and reservoir coordination strategies. The INFORM DSS planning level is linked to the INFORM forecast component through the use of the long-range forecasts (nine-month forecast ensemble) described in Section 2.4.

The mid-range management model is activated next to consider system operation at finer time scales. The objectives addressed here are more operational than planning and include flood management, water supply, and power plant scheduling. This model uses mid-range forecast ensembles with a daily resolution (described in Sections 2.3 and 2.4) and is intended to quantify the relative importance of, say, upstream versus downstream flooding risks, energy generation versus flood control, and other applicable tradeoffs. Such information is again provided to the management agencies (the operational departments) to use it within their decision processes to select the most preferable operational policy. Such policies are revised as new information on reservoir levels and flow forecasts is acquired. The model is constrained by the long-range decisions, unless current conditions indicate that a departure is warranted.

Lastly, the short-range and near-real-time operations models are activated to determine the turbine and spillway operations that realize the hourly release decisions made by the mid-range decision process. The results of this model can be used for near-real-time operations.

In developing the INFORM DSS, particular attention has been placed on ensuring consistency across modeling layers, both with respect to physical system

approximations as well as with respect to the flow of decisions. For example, the mid-range management model utilizes aggregate power plant functions that determine power generation based on reservoir level and total plant discharge. These functions are derived by the short-range and turbine load dispatching models which determine the optimal turbine loads for each plant corresponding to the particular reservoir level and total discharge. Thus, the mid-range model “knows” how much power generation will actually result from a particular daily release decision. Furthermore, the mid-range model generates similar energy functions to be used by the long-range planning model. In this manner, each model has a consistent representation of the benefits and implications of its decisions.

The three modeling layers discussed earlier address planning and management decisions. The scenario/policy assessment model addresses longer term planning issues such as the implications of increasing demands, inflow changes, storage reallocation, basin development options, and mitigation measures. The approach taken here is to simulate and compare the system response under various inflow, demand, development, and management conditions.

Altogether, the purpose of the INFORM DSS is to provide a modeling framework responsive to the information needs of the decision making process at all relevant time scales and water uses.

2.7. INFORM DSS Implementation Aspects

The INFORM DSS runs on personal computers under the Windows operating system. The software includes a graphical interface that provides access to data, activates model runs, and visualizes/manages model results.

2.7.1. Database

The DSS database uses the Microsoft (MS) Access engine. All system data and model inputs and outputs are organized in MS Access relational tables. The data in the database are accessible from the DSS interface and can be easily visualized and updated through Excel and graphical menu screens. The interface is written in MS Visual Basic. Interface implementation for the database has been completed, and the available data have been incorporated into the database.

2.7.2. Data Processing and Utility Tools

Use of the original data by the various DSS models requires processing. For example, the reservoir management models require analytic forms of the reservoir elevation-storage and elevation surface curves. Such curves can be derived via regression analysis. To automate this process, a regression utility tool has been developed allowing the user to generate the analytic relationships interactively. Other utility tools are also developed to derive optimal power plant functions and daily energy functions.

2.7.3. Interface Functions

As explained earlier, the DSS includes a suite of reservoir management models to support decisions pertinent to long-range planning, as well as short-range scheduling. The management models have a hierarchical structure according to their time resolution. In a typical run, the interface enables the user to select (or generate) the forecast ensemble first, followed by the long-range planning model (monthly resolution), the short-range management model (hourly resolution), and the turbine load dispatching model. In this execution order, the results of the upper level models are automatically passed onto the lower level models. In addition, the DSS interface also allows the user to run all applications independently. The user can start with any of the models without previously running any of the upper level models. In this case, however, one would have to prepare the required input data externally. The DSS interface also provides Excel templates to help the user prepare input data externally for all models.

The INFORM DSS was provided to the operational management agencies participating in the INFORM project. Training and demonstration workshops have been conducted to ensure that agency personnel have the necessary knowledge and experience to correctly use and interpret the results of the software.

3.0 Weather and Climate Downscaling Models

3.1. Introduction

It is typical that the resolution of present day operational weather and climate prediction models is much coarser than that required for hydrologic and water resources applications. Downscaling is the process of deriving finer-resolution information from larger-scale weather and climate model output for use in applications (e.g., hydrologic modeling and water resources management). There are primarily two kinds of downscaling methods: statistical/probabilistic methods and dynamical downscaling methods.

Statistical/probabilistic downscaling methods use historical data and archived forecasts to produce downscaled information from large-scale forecasts. These methods may be based on parametric regressions (e.g., Georgakakos and Smith 2001) or on non-parametric probabilistic formulations (e.g., Georgakakos 2003; Dettinger et al. 2004). Their advantages are that they are simple to implement and use and, for regions with large datasets, they produce unbiased and reliable estimates for periods similar to those used for their calibration. Their disadvantages are that they require large historical datasets for calibration and that their ability to reproduce the relationships between large and small scales diminishes as the future weather and climate conditions change with respect to those used for calibration

Dynamical downscaling methods involve dynamical models of the atmosphere nested within the grids of the large-scale forecast models. Typically, one-way nested limited area weather or regional climate models are implemented to produce finer resolution gridded information for applications, with coarse-resolution models providing initial and lateral boundary conditions. The advantage of using dynamic downscaling is that the physics of the models provide justification for their application under a variety of weather and climate conditions in a changing climate, especially for situations with strong boundary forcing (e.g., mountainous terrain, land-sea interfaces). Their disadvantages are that they are expensive in terms of computational time and data requirements, they require three-dimensional boundary and initial conditions, and in most cases they require output bias adjustment procedures for good reproduction of conditions at the higher resolution.

The INFORM system contains simplified dynamical models for downscaling numerical weather prediction (NWP) from the GFS, which runs routinely at NCEP. This approach is feasible for INFORM because of the availability of three dimensional boundary and initial conditions as discussed in Chapter 2. The INFORM models allow reproduction of orographic enhancement of surface precipitation, and of the influences of precipitation, snow cover and soil water on surface air temperature. Model simplification allows for the production of ensemble downscaled fields with feasible computational time requirements for INFORM project goals. In addition, and given the limitations in data availability discussed in Chapter 2, the INFORM system uses probabilistic methods for downscaling the seasonal ensemble forecasts of the NCEP CFS. The present chapter

presents the mathematical formulation of the precipitation (Section 3.2) and air temperature (Section 3.4) downscaling models and evaluates their performance (Sections 3.3 and 3.5, respectively) with historical data from the INFORM region. The authors present the probabilistic downscaling formulation and performance evaluation with historical data in Sections 3.6 and 3.7 respectively.

3.2. Formulation of Orographic Rainfall Enhancement Model

In the INFORM system, a newly developed simplified orographic precipitation model is the means for dynamical downscaling of ensemble GFS NWP forecasts to ensemble precipitation forecasts on scales of $10 \times 10 \text{ km}^2$ over the mountainous terrain of Northern California. The simplified orographic precipitation model decouples the momentum from the moisture conservation equations in the atmosphere. An analytical potential theory flow solution provides estimates of three-dimensional air velocities (e.g., Georgakakos et al. 1999) over complex terrain. The solution uses 700 millibar (mbar) wind velocities from the GFS model fields. Global forecast system forecast fields also provide the boundary conditions for a three-dimensional moisture conservation model based on Kessler (1969), which uses the orographic model flow velocities to produce precipitation rates over complex terrain. The formulation differs from earlier simplified approaches (e.g., Pandey et al. 2000; Rhea 1978) in that it produces consistent three-dimensional velocity fields over complex terrain, and in that it has explicit microphysical parameterizations for the generation of cloud and precipitation. Compared to full non-hydrostatic mesoscale models, its computational efficiency allows the generation of ensemble downscaled forecasts relatively fast while preserving the deterministic signal in orographic rainfall (see earlier examples in Georgakakos et al. 1999 for the tropics and in Tateya et al. 1991 for the mid latitudes). The model has been used in a recent HRC study funded by USACE for reconstructing the deterministic signal in Sierra Nevada rainfall from historical radiosonde observations and analysis fields.

3.2.1. Potential Theory Updrafts

Fundamental assumptions for applicability are:

- The atmosphere is near saturation.
- The free atmosphere has a steady uniform flow for the time interval of interest.
- The spatial scale of the atmospheric flow fluctuations is longer than the topographic fluctuations considered.
- The Coriolis effect is assumed negligible for the spatial scales of interest.

With those conditions and for incompressible and irrotational flow without momentum sources or sinks, the following holds true:

$$\nabla \times U = 0 \quad (1)$$

and

$$\nabla \cdot U = 0 \quad (2)$$

In the previous two equations, ∇ represents the gradient vector and U represents the three-dimensional velocity vector. Equation 1 shows the vector (or cross) product and Equation 2 shows the scalar (or inner) product of the two vectors. The first condition of zero curl implies that there exist a scalar single-valued velocity potential ϕ so that the velocity field is given by:

$$U = \nabla \phi \quad (3)$$

This, when substituted in the incompressible condition (2) of zero divergence (absence of momentum sources and sinks), yields:

$$\nabla \cdot \nabla \phi = 0 \quad (4)$$

or

$$\nabla^2 \phi = 0 \quad (5)$$

Equation 5 is Laplace's equation and its solutions are called *harmonic functions*. This equation constitutes the basis for the potential theory flow estimation of three-dimensional air velocities over complex terrain. The expanded constitutive equation and boundary conditions are written in the following for a rectangular domain ($LxKxH$) whose lower boundary is the complex terrain, whose upper boundary is located in the upper troposphere, and with the free air stream velocity (700 mbar upstream velocity u_0) aligned with the x-axis.

Solutions of the velocity potential $\phi(x,y,z)$ are sought for the following boundary value problem:

$$\frac{\partial^2 \phi}{\partial x^2} + \frac{\partial^2 \phi}{\partial y^2} + \frac{\partial^2 \phi}{\partial z^2} = 0 \quad (6)$$

with the Neumann boundary conditions specified:

$$\frac{\partial \phi}{\partial y} = u_o \quad \text{at} \quad y = 0 \quad (7)$$

$$\frac{\partial \phi}{\partial y} = u_o \quad \text{at} \quad y = L \quad (8)$$

$$\frac{\partial \phi}{\partial x} = 0 \quad \text{at} \quad x = 0 \quad (9)$$

$$\frac{\partial \phi}{\partial x} = 0 \quad \text{at} \quad x = K \quad (10)$$

$$\frac{\partial \phi}{\partial z} = 0 \quad \text{at} \quad z = 0 \quad (11)$$

$$\frac{\partial \phi}{\partial z} = u_o \frac{\partial s}{\partial y} \quad \text{at} \quad z = -H \quad (12)$$

It is noted that dependence of ϕ on the spatially independent variables is not shown for notational convenience. The boundary conditions represent conditions on the velocity field, such that the free stream velocity u_o is specified at the boundaries ($y=0$ and $y=L$) in the y -direction under the assumption of flat terrain there; zero velocity is specified in the x -direction at the boundaries ($x=0$ and $x=L$); and zero velocity is specified at the upper boundary ($z=0$) in the z -direction, while the lower boundary vertical velocity is forced by the boundary topographic gradient function ($\partial s / \partial y$) along the direction of u_o . By definition, the velocity components are:

$$\text{(along } x\text{-axis)} \quad v = \frac{\partial \phi}{\partial x} \quad (13)$$

$$\text{(along } y\text{-axis)} \quad u = \frac{\partial \phi}{\partial y} \quad (14)$$

$$\text{(along } z\text{-axis)} \quad w = \frac{\partial \phi}{\partial z} \quad (15)$$

The solutions of Georgakakos et al. (1999) were used in this work to obtain analytical expressions for the three-dimensional velocity vector at each point in the three-dimensional rectangular domain. The horizontal resolution is set to 10 kilometers (km) for both x and y .

The authors used existing HRC software (e.g., Sperflage et al. 1999) to produce the numerical solution of the potential theory flow equations (Equations 6 through 15) for terrain aligned with the 700-mbar wind velocity. Rotated terrain coordinates are produced from original Northings and Eastings of 1 km resolution for Northern California to accommodate incoming wind from different directions. A resolution of $\pi/8$ in the interval $(0 - 2\pi]$ was used, with 0 and 2π signifying wind from the North and with a clockwise convention for the angles in between (e.g., $\pi/2$ signifies wind from the east, while $3\pi/2$ signifies wind from the west). The solutions for each of 16 angles in the interval $(0, 2\pi]$ and for unit upstream 700 mbar wind were produced in rotated coordinates and were used to provide the three dimensional wind vectors to the atmospheric moisture conservation component described in the next subsection. There is strong dependence of the watershed-averaged updraft strength on the 700-mbar wind direction for the Folsom Lake watershed. The compass plot in Figure 12 shows this dependence for a unit 700-mbar wind with direction that spans the interval $(0,2\pi]$ clockwise with resolution of $\pi/8$. For real-time application, solutions were pre-computed and tabulated for a unit 700 mbar wind speed and for 16 directions spanning 360 degrees with a 22.5 degree resolution. This tabulation shortens computational time significantly, and it is possible because the potential theory flow velocity solutions are linear in 700-mbar wind speed.

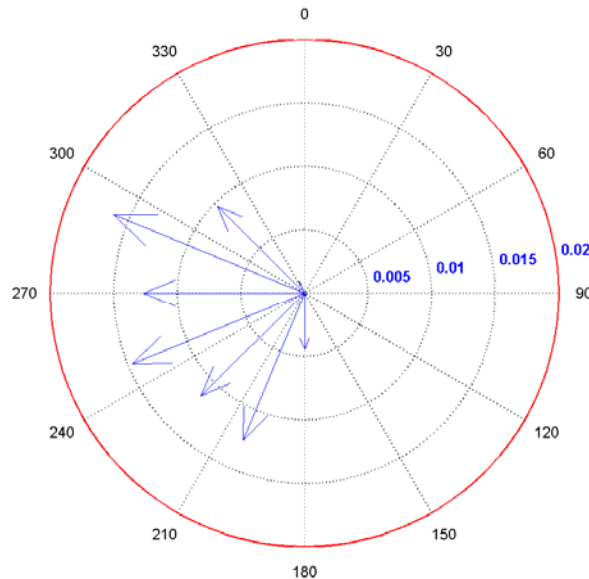


Figure 12. Mean areal updraft for Folsom Lake watershed as a function of direction angle from North (shown in degrees) for a unit 700-mbar wind inflow. The arrows indicate the direction from where the 700-mbar wind is blowing, and the magnitude of the mean areal updraft as a fraction of the incoming wind magnitude (contours of equal mean areal updraft are shown as concentric circles with indicated magnitude). Terrain slope is averaged over 10 km intervals.

Figure 12 clearly shows that the Folsom watershed terrain generates updrafts for winds with angles of approach in the interval 180 to 337.5 degrees [π , $7\pi/4$] or for S to NNW winds. It also shows that the mean areal updraft strength depends non-linearly on the direction angle due to the terrain morphology (local slopes and Coastal and Sierra Nevada mountain alignment along the 700 mbar wind direction). Most significant mean areal updrafts are generated for SSW to WNW winds with magnitudes of about 1.5% of the 700-mbar wind speeds (e.g., 0.45 meters per second (m/s) averaged over the Folsom watershed for a 30 m/s 700-mbar wind). These updrafts are responsible for the generation of orographic precipitation even in the absence of convection in the region. The next section describes the model for computing surface precipitation on the basis of the derived three-dimensional air velocities and of microphysical parameterizations.

3.2.2 Precipitation Modeling

The atmospheric moisture model for cloud and precipitation first proposed by Kessler (1969) is the basis of the orographic precipitation computations (see also microphysical formulation in Tsintikidis and Georgakakos 1999). The model equations describe the response of the water content of air to the air motions and microphysical processes:

$$\frac{\partial M}{\partial t} = -v \frac{\partial M}{\partial x} - u \frac{\partial M}{\partial y} - (V + w) \frac{\partial M}{\partial z} - M \frac{\partial V}{\partial z} + Mw \frac{\partial \ln \rho}{\partial z} + k_1(m - a) + k_2 E N_0^{1/8} m M^{7/8} \exp(kz/2) + k_3 N_0^{7/20} m M^{13/20} \quad (16)$$

$$\frac{\partial m}{\partial t} = -v \frac{\partial m}{\partial x} - u \frac{\partial m}{\partial y} - w \frac{\partial m}{\partial z} + wG + mw \frac{\partial \ln \rho}{\partial z} - k_1(m - a) - k_2 E N_0^{1/8} m M^{7/8} \exp(kz/2) - k_3 N_0^{7/20} m M^{13/20} \quad (17)$$

The model states are m and M , with the first being the cloud content if positive and the amount of moisture required to saturate the air if negative, and the second being the precipitation content (both in units [grams per cubic meter, gm m^{-3}]). The velocities u , v , and w are as defined earlier for y , x , and z directions, and ρ represents the air density. The derivatives dM/dt and dm/dt are in [grams per cubic meter per second, $\text{gm m}^{-3} \text{s}^{-1}$], $k = 10^{-4} [\text{m}^{-1}]$ if compressibility of air is taken into account, otherwise zero; $k_1 = \text{constant}$ (usually $10^{-3} [\text{s}^{-1}]$) when $m > a$, otherwise, $k_1 = 0$; $k_2 = 6.96 \times 10^{-4}$ when $m > 0$, otherwise, $k_2 = 0$; $k_3 = 1.93 \times 10^{-6}$ when $m < 0$, otherwise, $k_3 = 0$; $V = -38.3 N_0^{1/8} M^{9/8} \exp(kz/2) [\text{m s}^{-1}]$; G is treated as a constant at a given altitude; and a , E , and N_0 are parameters (Kessler used the values of $0.5 [\text{gm m}^{-3}]$, 1 , and $10^7 [\text{m}^{-4}]$, respectively).

The main assumptions implicit in this system are (adopted from Kessler 1969):

- Cloud is condensed water that fully shares the air motion.

- Cloud forms in saturated rising air and evaporates in saturated descending air at the rate $wG = -w\rho(dQ'_s/dz)$ where Q'_s is the saturation mixing ratio of water in air computed from radiosonde or embedding model information. Cloud-containing air is always saturated, and unsaturated air never contains cloud.
- Cloud changes to raindrops that are distributed in size according to an inverse exponential distribution at the rate $k_1(m - a)$, where the magnitude of k_1 and a may be selected to simulate various processes and rates.
- Precipitation particles once formed are assumed to be distributed in size according to an inverse exponential law and to collect cloud particles or evaporate in sub-saturated air according to approximations of the natural accretion and evaporation processes.
- Precipitation shares the horizontal motion of the air, but the vertical mass transport of precipitation is based on the fall speed of the median-diameter precipitation particle. The formulation omits change of shape of a distribution by virtue of differing fall speeds within it, and by evaporation, condensation and accretion processes.

As part of the downscaling procedure, the numerical code simulates the system of Equations 16 and 17 using vertical profiles of temperature, pressure, and humidity as boundary conditions, and utilizing the potential theory flow solutions of the previous subsection for a given speed and direction of the boundary 700-mbar wind. The code uses a non-diffusive spline-interpolation method for the computation of three-dimensional advection (see Pielke 1984; cf. Mahrer and Pielke 1978) and a fourth order Runge–Kutta integration method for the computation of the source and sink contributions of Equations (16) and (17) due to microphysical terms. A series of numerical sensitivity studies was conducted to determine appropriate temporal discretization intervals for advection (Δt_a) and for source/sink term integration (Δt_s). The ranges of the intervals examined in each case were: $56 \text{ s} \leq \Delta t_a \leq 900 \text{ s}$; $1 \text{ s} \leq \Delta t_s \leq 300 \text{ s}$. It was found that $\Delta t_a=112 \text{ s}$ and $\Delta t_s=11 \text{ s}$ are adequate to reproduce the surface precipitation magnitude and pattern obtained by a very accurate integration ($\Delta t_a=56 \text{ s}$; $\Delta t_s=1 \text{ s}$). The sensitivity studies were conducted with boundary conditions taken from the NCEP operational Eta regional model analysis data obtained for the significant Northern California storm of the November 7 and 8, 2002. Once the three-dimensional wind computations of the previous subsection are completed, it takes approximately 2.5 minutes of CPU time on a 1 GHz PC to produce a three-hourly surface precipitation field for Northern California (from 37°N to 42°N and from 118°W to 125°W) with a 10 km resolution in rotated coordinates. This is a small fraction of the time it takes a full mesoscale numerical weather prediction model to complete the same integration. The following subsection discusses the evaluation of the simplified orographic precipitation (SIMOROP) model.

3.3. Evaluation of Orographic Rainfall Enhancement Model with Data

3.3.1. American River Watershed

The California Nevada River Forecast Center made available six-hourly MAP data for the period 1969–1992. CNRFC estimated the MAP from precipitation gauge measurements and standard NWS procedures applicable over mountainous terrain. The simplified orographic precipitation model was run for the period from 1 November to 15 May (the wet season of the year) for each of the water years from 1969 through 1992. Six-hourly NCEP reanalysis data were used as input to the model with a resolution of about $2.5^\circ \times 2.5^\circ$ (about $250 \times 250 \text{ km}^2$). In this case, the orographic model was the means for downscaling the reanalysis data. The domain of analysis covered the INFORM domain in Northern California with a resolution of $10 \times 10 \text{ km}^2$. On the basis of available digital catchment boundaries, MAP estimates over the North, Middle, and South Forks of the American River and the entire Folsom Lake drainage were computed by averaging the gridded output of the simplified orographic model within each of these catchments.

Appendix B contains plots of six hourly observed and downscaled MAP estimates for all the Folsom catchments considered and for the period 1 November through 15 May for each water year of record. Visual inspection shows that in most cases the downscaled estimates capture the variability of the observed six-hourly rainfall for the entire 3,300- km^2 Folsom Lake catchment and in each of the three sub-catchments (areas from 800 to 1,400 km^2). There is a tendency to overestimate the low six-hourly precipitation rates, especially in the Middle and the South Forks of the American River.

Table 3 shows the values of statistical performance indices for the period of record and for six-hourly and daily time intervals.

Table 3. Statistical performance of simplified orographic model in wet season (1969–1992)

	<i>Folsom Lake</i>	<i>North Fork</i>	<i>Middle Fork</i>	<i>South Fork</i>
<u>Six-Hourly Data</u>				
ρ_c	0.52	0.49	0.48	0.46
r_m	-0.46	-0.02	-0.74	-1.00
r_s	0.96	0.91	1.10	1.15
<u>Daily Data</u>				
ρ_c	0.67	0.66	0.65	0.64
r_m	-0.66	-0.11	-0.97	-1.30
r_s	0.86	0.78	1.00	1.09

The indices computed are the cross correlation coefficient between observed and downscaled mean areal precipitation estimates (ρ_c), the ratio of the residual mean to the

observations mean (r_m), and the ratio of the residual standard deviation to the observed standard deviation (r_s). Perfect performance is indicated by values of 1, 0, and 0 for these three performance measures respectively. The analysis was performed for those time steps for which the observed MAP was greater than 0.1 millimeter per six hours (mm/6 hrs) for the six-hourly time step case, or 0.5 mm/day for the daily time step case. It is apparent that the downscaled estimates exhibit high cross correlation with the observations even at the six-hour time step for all the catchments examined. The downscaled estimates have low bias and residual variability that is lower than that of the observations, especially for the North Fork and the entire Folsom Lake catchment.

These results support the use of the orographic model as the component for downscaling large-scale weather and climate information for INFORM. Prior to the use of the downscaled data for hydrologic and water resources analysis, adjustment of the downscaled estimates is necessary to account for the model bias and residual errors as indicated in Table 3. This may be done by regressing the observed MAP values on the downscaled precipitation values, and estimating the linear regression parameters from the historical data shown in Appendix B. Figures 13 and 14 show the scatter plots of observed and downscaled MAP together with the regression lines and the regression equation for six-hourly and daily data, respectively. The observations are denoted by "O" and the downscaled estimates are denoted by "D" in the regression equations of these two figures. Thus, after downscaling the weather information to the level of the catchments, these equations may be applied to the downscaled estimates to yield unbiased estimates for use by the hydrologic models. Additional analysis may be pursued to develop these regression equations by month and possibly by magnitude of downscaled precipitation.

3.3.2. Other INFORM Watersheds

The authors obtained MAP estimates for each of 15 basins throughout the INFORM application domain from the CNRFC calibration data files. These estimates constitute "ground truth" for the purposes of this validation analysis as in the previous section. The orographic precipitation component, used to downscale the GFS information to surface precipitation, ran for the period 1 November to 15 May (California's wet season) for each year from 1969 through present. The NCEP global reanalysis fields provided six-hourly forcing for the historical period. The output of the orographic model is a gridded 10 km x 10 km surface precipitation field. Gridded values were averaged within the basin domains to produce model MAP over the test basins. These model MAP values were compared to the CNRFC mean areal precipitation values and a number of statistical performance indices were evaluated to quantify model performance. It is noted that the resolution of the NCEP global reanalysis model is much coarser than that of the GFS model. Unfortunately there is no long historical record of GFS analysis data to perform the analysis with the GFS. It is expected that the results shown here are also indicative of the lower limit of model performance with GFS analysis fields. It is also noted that to facilitate the production of a long simulation series of values for the

domain, for these simulation runs, the global reanalysis data were used to produce upper air information for the Oakland site, and this information was used to force the orographic precipitation model for the entire domain. Thus, it is expected that good performance should be associated with southwesterly winds, which bring moisture to the INFORM domain. For operational application, other sites may be used as well.

Figure 15 shows a georeferenced (UTM coordinates) map of the larger sub-basins of the INFORM domain and the location of the basins for which an evaluation of downscaled mean areal precipitation was made. The latter basins have been identified by the five-digit CNRFC data code name and are on the western facing slopes of the Sierra Nevada. The performance analysis results presented below are indexed by the code name of each sub-basin. In each case, Table 4 associates the code names with the names of the draining rivers and the major reservoir drainage area.

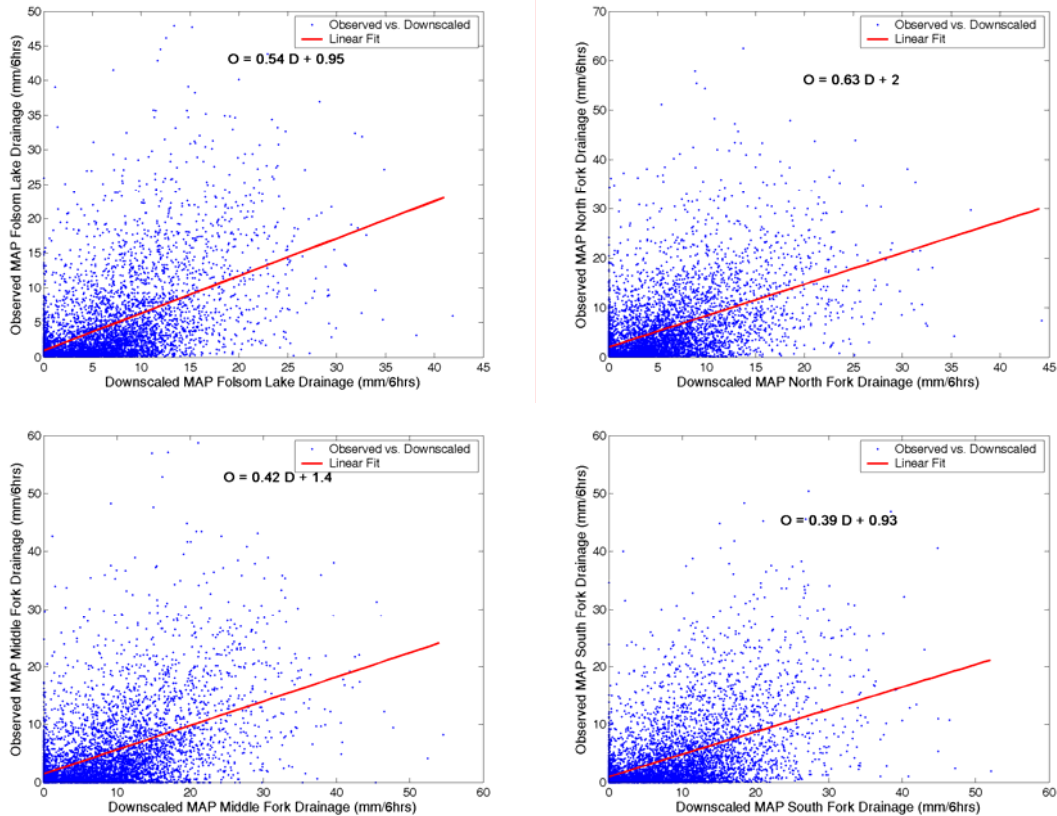


Figure 13. Linear regression equations between six-hourly downscaled (predictor) and observed estimates (predictant) of mean areal precipitation for the Folsom Lake sub-basins

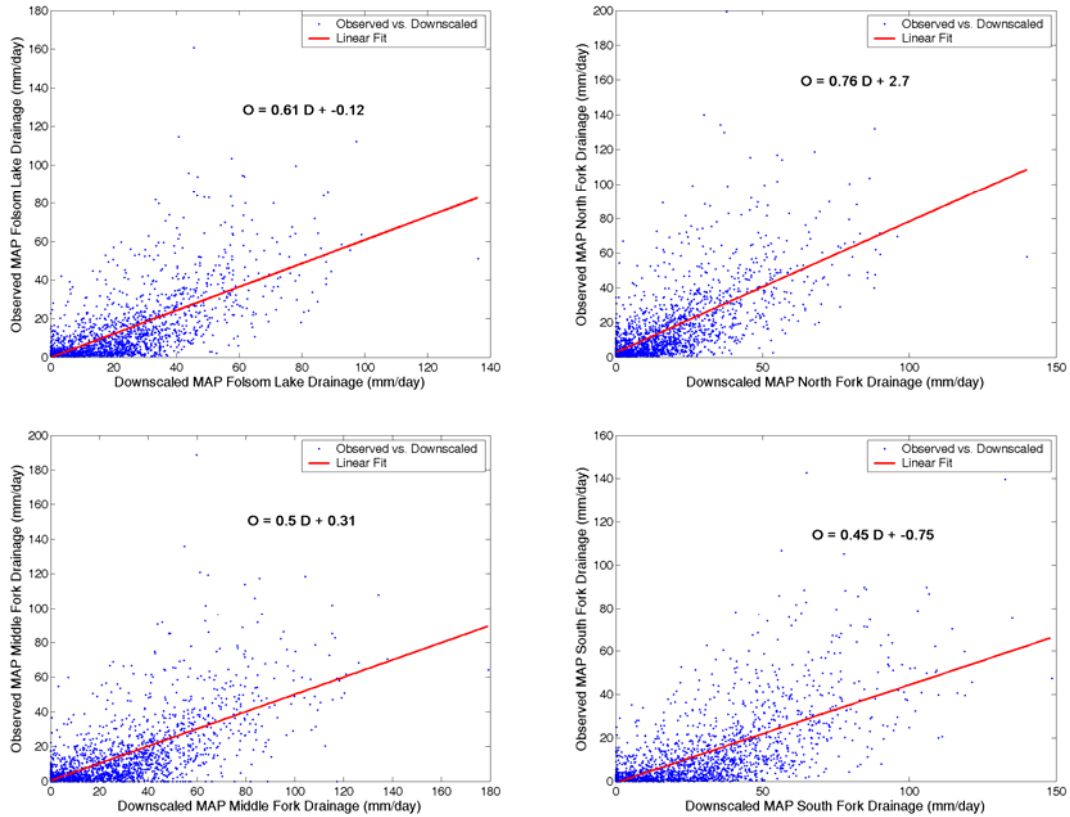


Figure 14. As in Figure 13, but for daily data

To account for the fact that precipitation is highly intermittent in the region, the authors did an analysis of the frequencies of occurrence of zero and low precipitation for both the simulated and the observed data. Table 5 shows the results for various thresholds of low precipitation (in mm/6 hrs) and for both the simulations and the observations of mean areal precipitation. It is evident that the frequency of occurrence of zero precipitation in the simulations is much lower than that of the observations, indicating that the model, when forced with reanalysis data, tends to produce significantly more low precipitation than observed. For the range of low precipitation thresholds examined in Table 5, it is clear that different catchments require different low precipitation thresholds to match the frequency of occurrence between observations (equal to zero) and simulations (less than a low precipitation threshold). The majority of the basins, however, require a 1 mm/6 hrs threshold to approximate the zero precipitation frequency of occurrence in the observations.

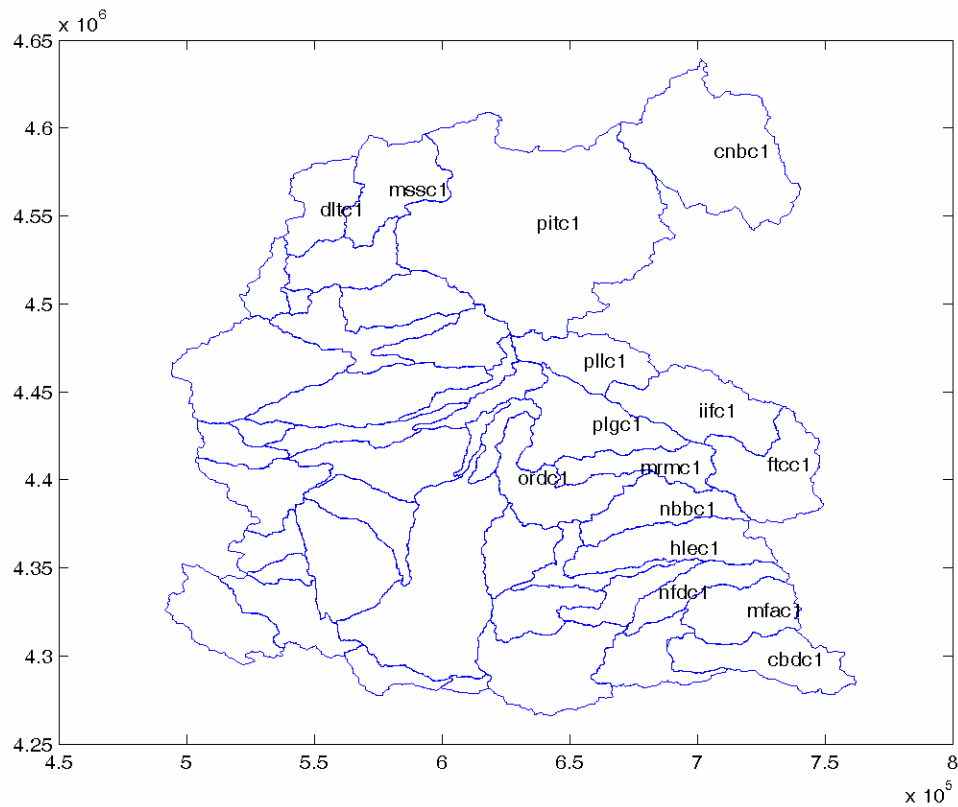


Figure 15. Map of INFORM sub-basins. The sub-basins with the CNRFC code name are used for the evaluation of the orographic precipitation component.

Table 4. Names and code numbers of drainage basins used in the evaluation of downscaled precipitation

<i>Code</i>	<i>Name</i>
cbdc1:	South Fork, American River - Folsom
cnbc1:	Pit River at Canby - Shasta
dltc1:	Sacramento River at Delta - Shasta
ftcc1:	Middle Fork feather at Clio - Oroville
hlec1:	South Yuba River
iifc1:	Indian Creek - Oroville
mfac1:	Middle Fork, American River - Folsom
mrmc1:	Middle Fork Feather River at Merrimac - Oroville
mssc1:	McCloud River - Shasta
nbbc1:	North Yuba River
nfdc1:	North Fork, American River - Folsom
ordc1:	Local Feather River at Oroville - Oroville
pitc1:	Pit River at Montgomery Creek - Shasta
plgc1:	North Fork Feather River - Oroville
pllcl:	Lake Almanor drainage - Oroville

Table 5. Frequency of occurrence of zero and low precipitation

BASIN	OBS<=0	OBS<=1	OBS<=2	SIM<=0	SIM<=.5	SIM<=1	SIM<=2	SIM<=3	SIM<=4	SIM<=5
cbdc1	0.71	0.81	0.85	0.34	0.49	0.55	0.61	0.66	0.69	0.73
cnbc1	0.74	0.90	0.93	0.38	0.63	0.72	0.85	0.93	0.97	0.99
dltc1	0.68	0.79	0.83	0.29	0.47	0.57	0.69	0.78	0.85	0.90
ftcc1	0.76	0.87	0.91	0.40	0.70	0.82	0.92	0.96	0.98	0.99
hlecl	0.67	0.78	0.82	0.41	0.60	0.65	0.72	0.77	0.81	0.84
iifc1	0.69	0.84	0.89	0.51	0.87	0.91	0.95	0.96	0.97	0.98
mfac1	0.71	0.77	0.83	0.39	0.57	0.60	0.65	0.69	0.72	0.75
mrmc1	0.68	0.78	0.82	0.43	0.63	0.71	0.78	0.82	0.86	0.89
mssc1	0.69	0.79	0.83	0.31	0.51	0.58	0.70	0.78	0.85	0.89
nbbc1	0.66	0.77	0.81	0.42	0.58	0.65	0.73	0.78	0.82	0.86
nfdc1	0.71	0.79	0.83	0.41	0.61	0.66	0.72	0.78	0.82	0.86
ordc1	0.69	0.79	0.82	0.45	0.65	0.70	0.77	0.82	0.86	0.89
pitc1	0.68	0.83	0.88	0.33	0.62	0.76	0.91	0.96	0.98	0.99
plgc1	0.69	0.80	0.84	0.43	0.65	0.72	0.80	0.86	0.91	0.94
pllc1	0.70	0.82	0.86	0.36	0.60	0.72	0.85	0.90	0.93	0.95

Figure 16 shows the scattergram of CNRFC-observed versus orographic-model simulated six-hourly precipitation for simulated amounts greater than 2 mm/6 hrs for each of the evaluation basins. The figure also includes the corresponding linear regression lines and parameter values, with the observations being regressed on the simulations. Such relationships may be used to produce bias adjusted precipitation estimates in each case. The results in Figure 16 show some relationship between observed and simulated precipitation for most basins and at the six-hourly temporal resolution. In all cases, there is considerable scatter of the data about the regression lines.

To characterize the correspondence of the distribution of precipitation amounts, the cumulative frequency distribution of six-hourly precipitation observations and simulations was computed for each basin and for the entire period of record, and it is shown in Figure 17. The results indicate that in all the cases the shape of the distribution function is very similar between observations and simulations. The sub-basins of the Oroville reservoir show overestimation of low precipitation amounts, but for those cases the observed and simulated distribution are similar for the higher amounts, while for several basins the entire distribution is reproduced well.

The correspondence of the second moment statistics of the simulated and observed MAP is examined next. Table 6 shows the mean, standard deviation, and cross-correlation coefficient between the six-hourly observations and simulations for the two cases. In Case (a), all the data is used to compute the statistics, including zeros and low rainfall amounts; in Case (b) only the six-hour time steps for which the simulated value was greater than a low threshold are used to compute the statistics. Case (a) results occupy the first five columns of the table and Case (b) results occupy the last five columns of the table.

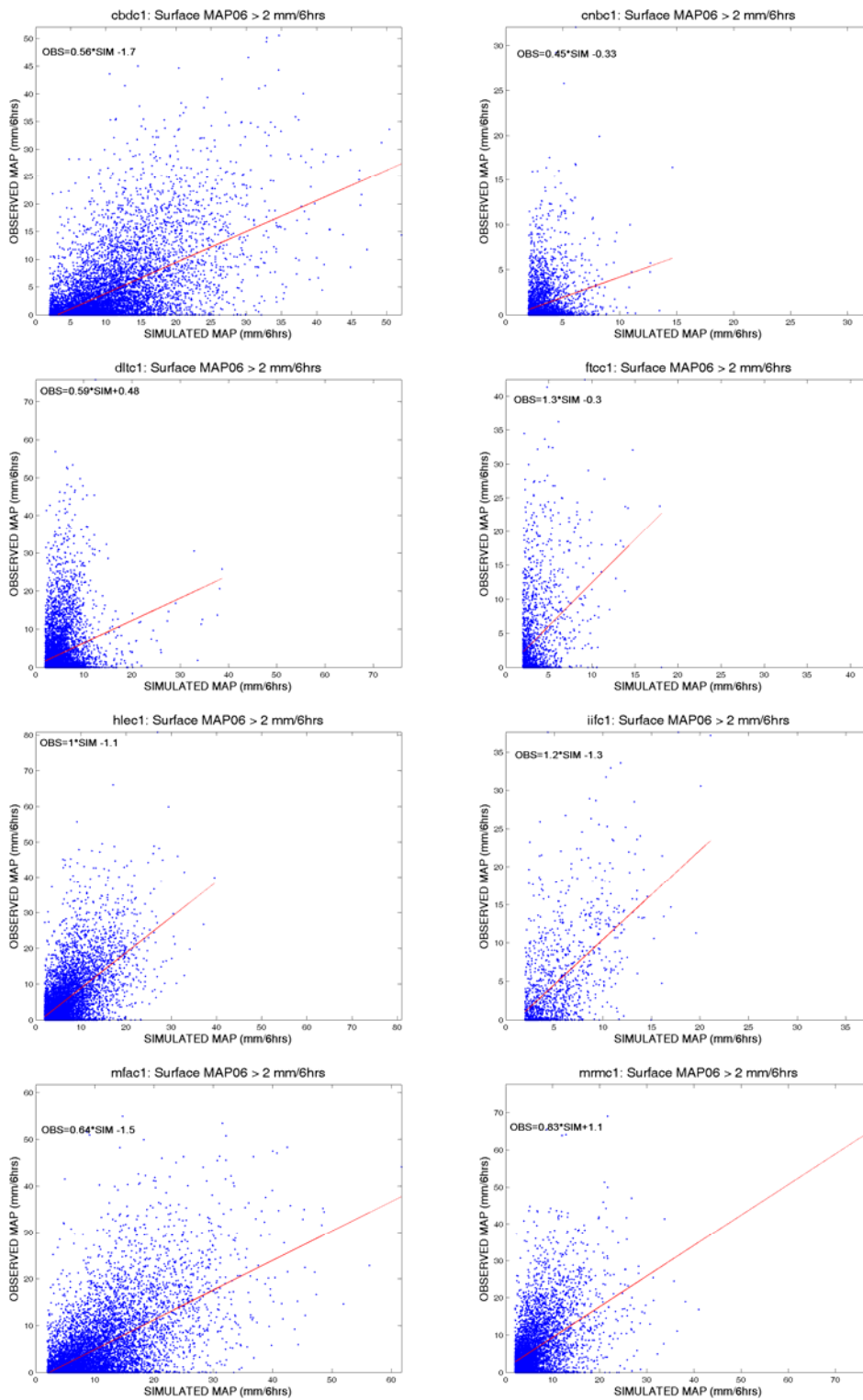


Figure 16. Scatter grams of observed and simulated precipitation and associated regression lines and parameter values for INFORM region basins

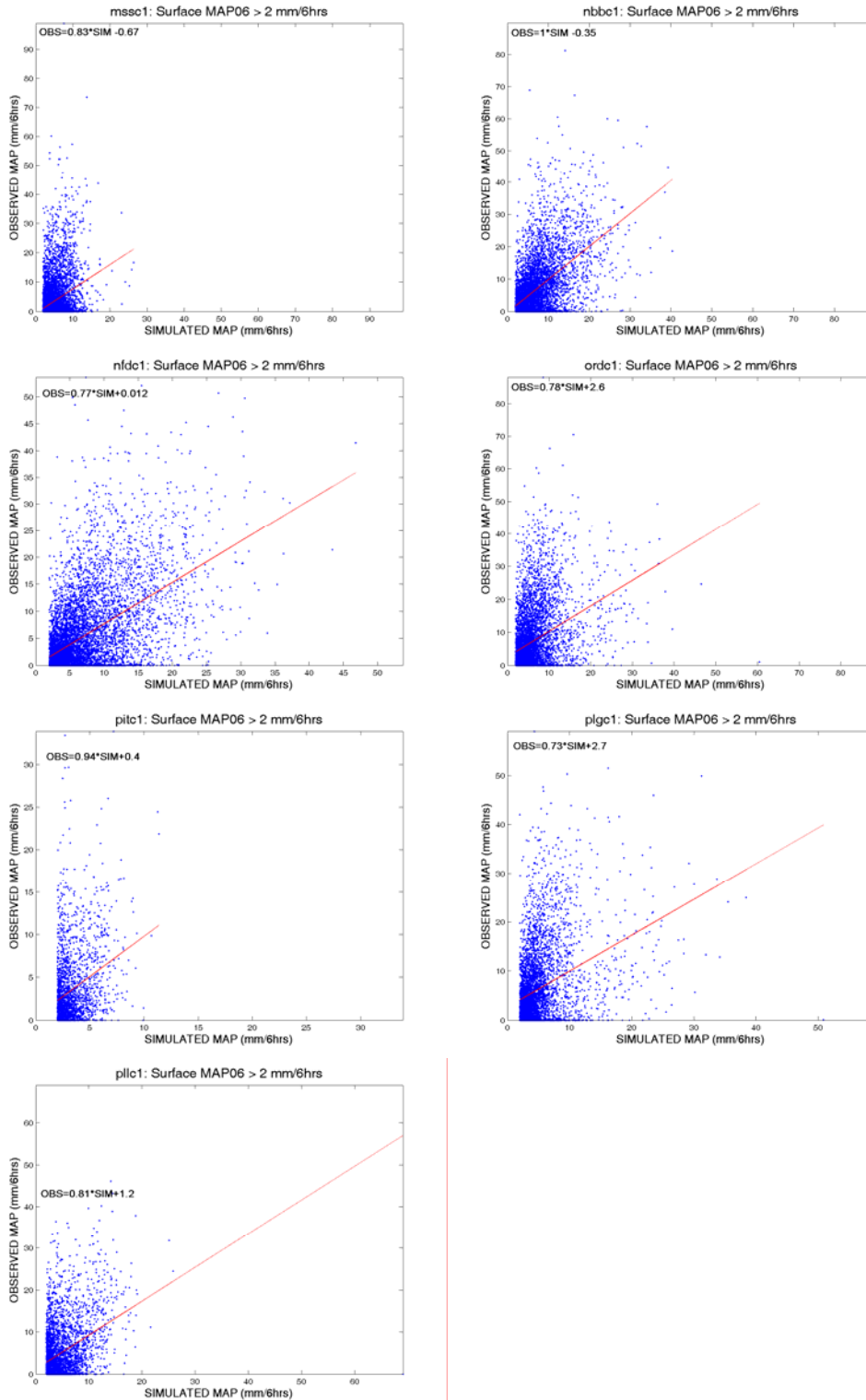


Figure 16. (cont'd) Scatter grams of observed and simulated precipitation and associated regression lines and parameter values for INFORM region basins

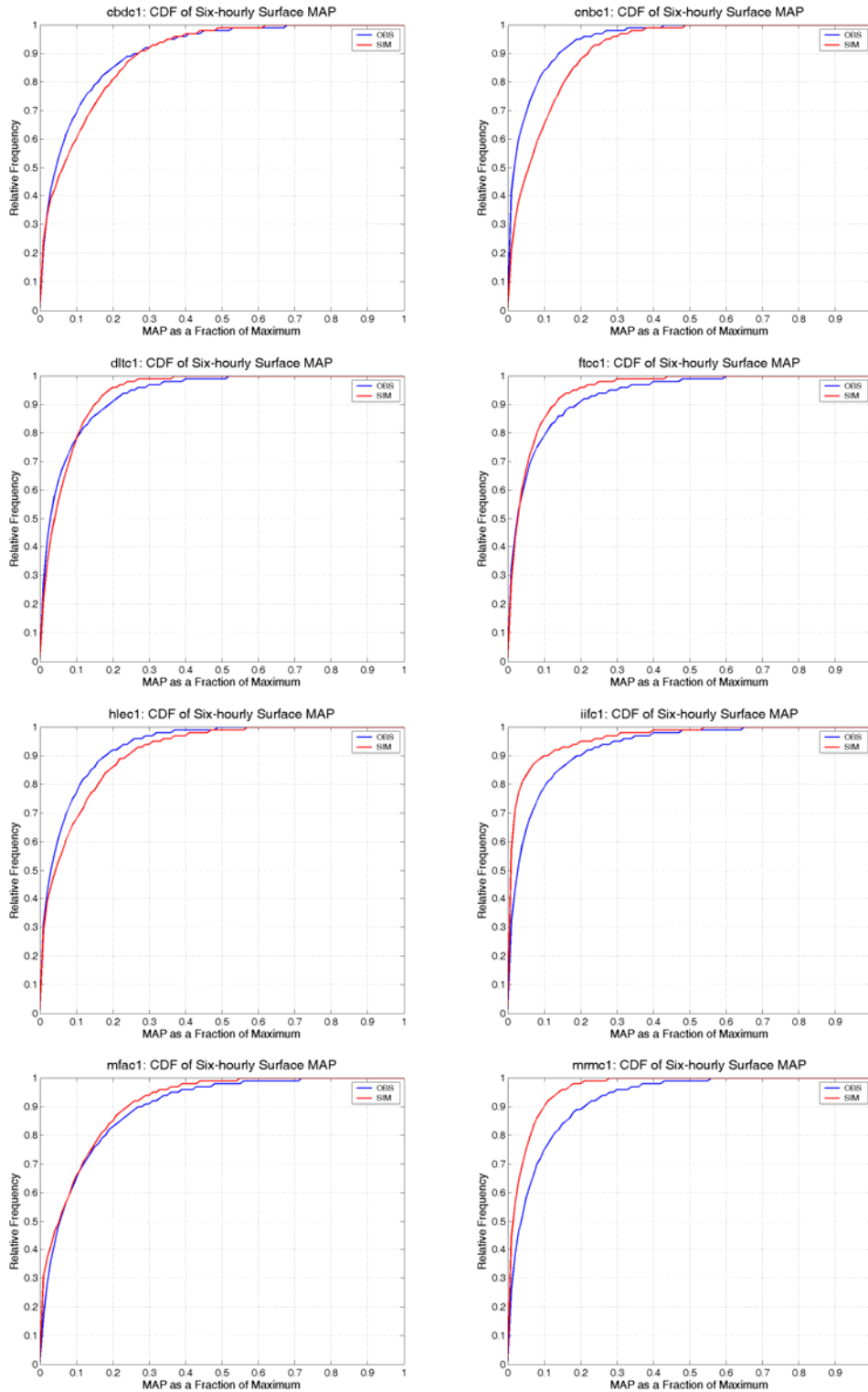


Figure 17. Cumulative distribution functions of six-hourly mean areal precipitation amounts (observed in blue and simulated in red) for several basins of the INFORM region

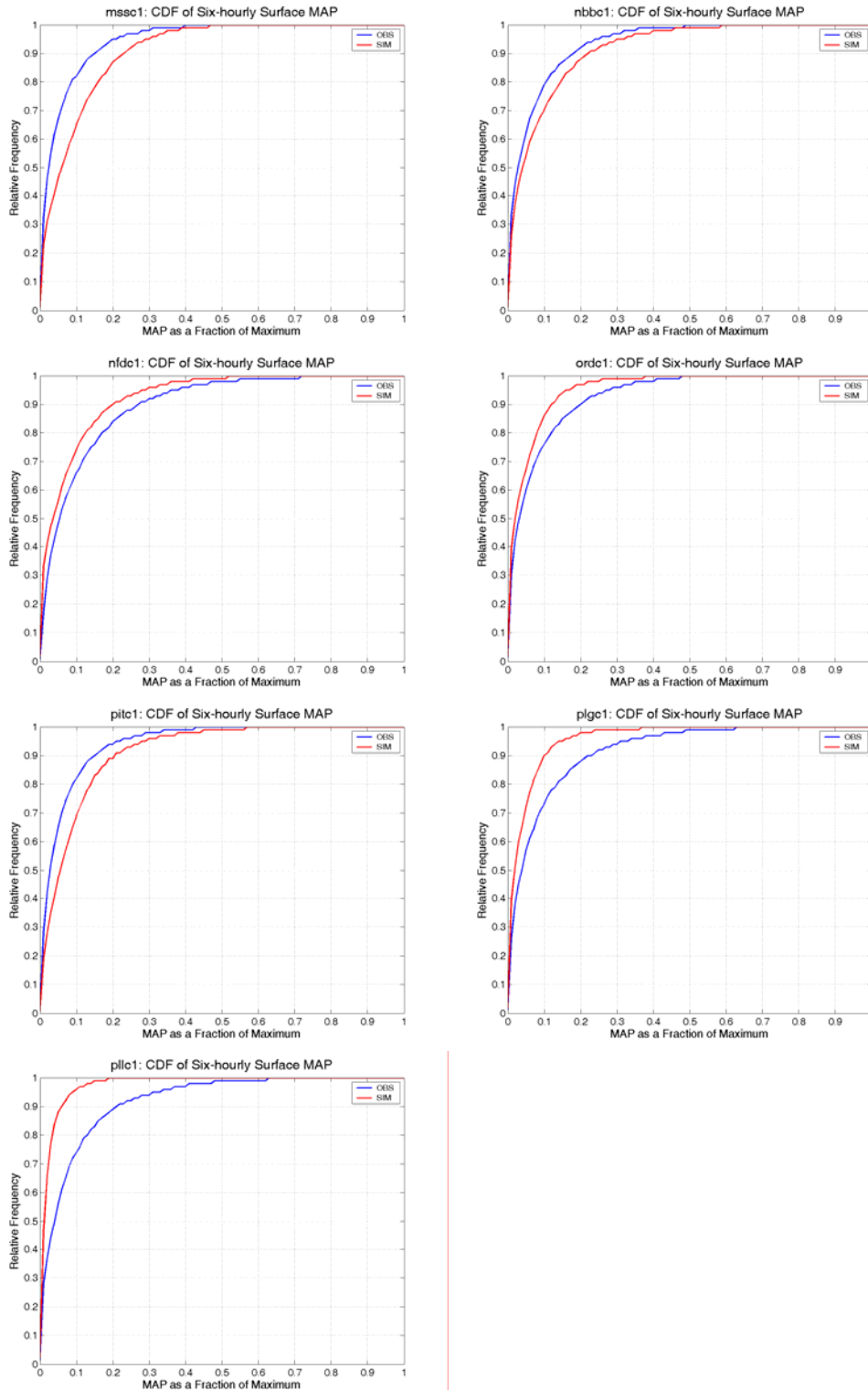


Figure 17. (cont'd) Cumulative distribution functions of six-hourly mean areal precipitation amounts (observed in blue and simulated in red) for several basins of the INFORM region

Table 6. Second moment statistics of mean areal precipitation observations and simulations for basins of the INFORM region

BASIN	<i>(a)</i>					<i>(b)</i>				
	AV-OBS	STD-OBS	AV-SIM	STD-SIM	CC-S/O	AV-O>T	STD-O>T	AV-S>T	STD-S>T	CC-S/O>T
cbdc1	1.40	3.72	4.06	5.89	0.65	4.17	10.87	6.41	6.15	0.57
cnbc1	0.42	0.81	1.44	1.28	0.27	0.86	2.47	2.05	1.33	0.27
dltc1	1.62	1.74	4.66	2.55	0.32	3.26	4.72	6.50	2.77	0.25
ftcc1	0.71	0.57	2.55	1.10	0.52	2.80	2.32	5.00	1.60	0.39
hlec1	1.77	2.08	4.87	3.86	0.70	4.79	5.82	7.28	4.65	0.62
iifc1	0.82	0.40	2.60	1.33	0.48	2.76	2.68	5.04	2.74	0.52
mfac1	1.71	3.46	4.72	6.01	0.69	5.49	11.20	7.53	6.65	0.58
mrnc1	1.70	1.61	4.72	3.36	0.66	5.20	5.18	7.42	4.50	0.53
mssc1	1.67	1.68	4.84	2.46	0.31	3.24	4.71	6.62	2.47	0.31
nbbc1	1.98	2.00	5.41	3.79	0.69	5.26	5.50	8.05	4.71	0.60
nfdc1	1.63	2.06	4.52	3.98	0.67	5.27	6.86	7.23	4.97	0.53
ordc1	1.96	1.55	5.57	3.23	0.58	5.94	4.99	8.75	4.28	0.43
pitc1	0.78	0.67	2.18	1.06	0.51	1.80	1.63	3.16	1.21	0.40
plgc1	1.53	1.19	4.40	2.53	0.59	4.85	3.94	7.07	3.50	0.43
pllc1	1.12	1.04	3.31	2.04	0.59	3.37	3.20	5.39	2.85	0.47

The results of Table 6 make clear that there is an overestimation of low amounts of precipitation by the orographic model when driven by NCEP reanalysis data, that tends to produce a high bias in the mean and standard deviation for all the basins examined (results of case *(a)*). If only the results above a low precipitation threshold are considered (case *(b)*) the bias is reduced significantly, while the cross-correlation of observed and simulated six-hourly mean areal precipitation maintains values around 0.5 for most cases. This provides confidence that the model, suitably constrained in the low precipitation amounts, may be used to estimate basin precipitation from upper air global model data with good six-hourly correspondence to observations.

The results of Table 7 further elucidate the performance of the model by separating the statistics for the case of southwesterly and northwesterly 700 mbar wind events. The first five columns of the table correspond to southwesterly events, while the last five columns correspond to northwesterly events. Clearly, using the global reanalysis data for the Oakland site favors the performance for southwesterly wind events. However, it is also important to note that for these events and for certain basins, the orographic model simulation explains more than 40% of the six-hourly precipitation variance over basin areas on the order of 1000 km². These results attest to the utility of the model as a downscaling tool.

Table 7. Second moment properties of simulates and observed mean areal precipitation for southwesterly and northwesterly wind events

BASIN	Southwesterly events					Northwesterly events				
	AV-OSW	STD-OSW	AV-SSW	STD-SSW	CC-S/OSW	AV-ONW	STD-ONW	AV-SNW	STD-SNW	CC-S/ONW
cbdc1	2.70	6.36	5.86	7.87	0.66	1.20	3.84	3.31	4.83	0.58
cnbc1	0.59	1.24	1.84	1.72	0.36	0.49	0.88	1.44	1.09	0.11
dltc1	3.94	1.85	7.25	3.11	0.38	0.91	2.33	2.69	2.36	0.26
ftcc1	1.53	0.90	3.97	1.61	0.59	0.50	0.54	1.72	0.77	0.27
hlecl	3.58	4.39	7.16	5.58	0.69	1.45	1.63	3.74	2.47	0.65
iifc1	1.85	1.10	4.12	2.24	0.48	0.53	0.11	1.54	0.25	0.05
mfac1	3.22	6.46	6.71	8.27	0.68	1.53	3.24	3.95	4.63	0.64
mrnc1	3.64	3.87	7.15	5.10	0.62	1.27	0.94	3.27	1.58	0.67
mssc1	4.05	1.74	7.56	2.97	0.40	0.95	2.37	2.76	2.39	0.19
nbbc1	4.11	4.35	8.08	5.61	0.66	1.54	1.48	3.94	2.19	0.66
nfdc1	3.09	4.55	6.43	5.92	0.67	1.45	1.47	3.77	2.16	0.65
ordc1	4.34	3.58	8.49	4.92	0.53	1.34	1.01	3.72	1.63	0.57
pitc1	1.56	1.15	3.30	1.53	0.48	0.63	0.66	1.56	0.75	0.45
plgc1	3.40	2.75	6.80	3.90	0.54	1.05	0.78	2.81	1.23	0.60
pllc1	2.43	2.32	5.13	3.15	0.56	0.80	0.64	2.14	0.93	0.52

3.4. Formulation of Surface Air Temperature Model

3.4.1. Model Equations

The surface air temperature downscaling model is an adaptation of the Advanced Regional Prediction System (ARPS) mesoscale modeling system developed by Xue et al. (2000). It couples a column atmospheric radiation model with a two-soil-layer land surface model. This two-layer model (i.e., surface and deep soil layers) is designed to simulate the essential processes involved in interactions between the surface air and the underlying ground with the minimal amount of computation time and the fewest parameters and complexities. The model is based on the following prognostic equations:

$$\frac{\partial T_s}{\partial t} = C_T (R_n - H - LE) - \frac{2\pi}{\tau} (T_s - T_2) \quad (18)$$

$$\frac{\partial T_2}{\partial t} = \frac{1}{\tau} (T_s - T_2) \quad (19)$$

$$\frac{\partial T_a}{\partial t} = \frac{H}{C_p} \quad (20)$$

$$\frac{\partial W_g}{\partial t} = \frac{C_1}{\rho_w d_1} (P - E_g) - \frac{C_2}{\tau} (W_{gs} - W_{geq}) \quad (21)$$

$$\frac{\partial W_2}{\partial t} = \frac{C_1}{\rho_w d_2} (P - E_g - E_{tr}) \quad (22)$$

$$\frac{\partial W_r}{\partial t} = vegP - E_r \quad (23)$$

The meaning of each of the symbols used in this section is given in the following:

T_s : Ground surface temperature

T_2 : Deep ground temperature

T_a : Surface air temperature

W_g : Surface soil moisture

W_{geq} : Surface moisture when gravity and the capillary forces are balanced

W_2 : Deep soil moisture

W_r : Canopy moisture

P : Precipitation rate

R_n : Net radiation

E_g : Evaporation from ground

E_{tr} : Transpiration of the dry portion of leaves

E_r : Direct evaporation from the fraction of foliage

C_T : Land surface heat capacity

C_p : Specific heat of dry air at constant pressure

C_1 : Coefficient of the net precipitation

C_2 : Coefficient of the perturbed near surface moisture

τ : Length of the day

veg : vegetation fraction

d_1 : Top layer depth of soil column, 0.01 m

d_2 : Deep layer depth of soil column, 1 m

ρ_w : Density of water

Equation 18 expresses that the time rate of change in surface soil temperature is the residual of the surface energy balance between net radiation R_n , surface sensible heat flux H , latent heat flux LE and the soil heat transfer. Equation 21 shows that the time rate of change in volumetric soil moisture near the soil surface results from the residual of the precipitation rate at the ground, the evaporation rate from the ground, and the transfer of surface soil moisture to the deep soil layer. Equations 19 and 22 describe the heat and moisture budget in deep soil. Equation 23 predicts the time rate of change of water W_r in the canopy. Lastly, Equation 20 indicates that in this model the change of surface air temperature is induced only by the sensible heat H . The functional forms of various terms in the above set of equations are discussed next.

Thermal coefficients

The thermal coefficient C_T in Equation 18 can be written as

$$C_T = \frac{1}{\frac{1-veg}{C_G} + \frac{veg}{C_v}} \quad (24)$$

in which veg is the fractional coverage of vegetation, the thermal coefficient of vegetation is

$$C_v = 10^{-3} Km^2 J^{-1} \quad (25)$$

and the thermal coefficient of bare soil is

$$C_G = C_{Gsat} \left(\frac{W_{sat}}{W_2} \right)^{b/(2 \ln 10)} \quad (26)$$

where b stands for slope of the retention curve and C_{Gsat} is the thermal coefficient for bare ground at saturation.

Radiation flux

The net radiative flux in Equation 18 is given by

$$R_n = R_{sw}(1-\alpha) - \varepsilon_g \sigma T_s^4 + \varepsilon_a \sigma T_a^4 \quad (27)$$

in which ε_g is the emissivity of the earth's surface, $\varepsilon_a = 0.725$ is the emissivity of the air, $\sigma = 5.67 \cdot 10^{-8} \text{ Wm}^{-2}\text{K}^{-4}$ is the Stefan-Boltzmann constant, and T_a is the air temperature at an atmospheric level. The total albedo is $\alpha = \alpha_s + \alpha_z$, where α_s is the albedo at polar zenith and α_z the zenith angle adjustment to α . The zenith angle adjustment is given by

$$\alpha_z = 0.01[\exp(0.003286Z^{1.5}) - 1] \quad (28)$$

where Z is the solar zenith angle in radians and the minimum albedo α_s with $Z = 0$ is dependent on the type of land cover /land use.

Sensible heat flux

The sensible heat flux is given by

$$H = \rho_a C_p C_{dh} V_a (T_s - T_a) \quad (29)$$

where ρ_a and V_a are, respectively, the air density and wind speed at an atmospheric level; C_{dh} is the exchange coefficient depending upon the thermal stability and roughness.

Latent heat flux

The latent heat flux is the sum of the evaporation from the soil surface E_g , transpiration E_{tr} , and evaporation from wet parts of the canopy E_r

$$LE = L(E_g + E_{tr} + E_r) \quad (30)$$

in which L is the latent heat of vaporization and

$$E_g = (1 - veg) \rho_a C_{dq} V_a [h_u q_{vsat}(T_s) - q_{va}] \quad (31)$$

where the relative humidity at the ground surface is

$$h_u = \begin{cases} 0.5[1 - \cos(\pi W_g / W_{ft})]; & W_g < W_{ft} \\ 1; & W_g \geq W_{ft} \end{cases} \quad (32)$$

with field capacity $W_{ft} = 0.75W_{sat}$.

$$E_r = veg \rho_a \frac{F_w}{R_a} [q_{vsat}(T_s) - q_{va}] \quad (33)$$

$$E_{tr} = veg \rho_a \frac{1 - F_w}{R_a + R_s} [q_{vsat}(T_s) - q_{va}] \quad (34)$$

in which the wet fraction of the canopy, F_w , is defined as

$$F_w = \left(\frac{W_r}{W_{rmax}} \right)^{2/3} \quad (35)$$

$$W_{rmax} = 0.2 veg LAI (mm) \quad (36)$$

Here LAI is the leaf area index of vegetation and it depends on the vegetation type. The aerodynamic resistance is parameterized by

$$R_a = \frac{1}{C_{dq} V_a} \quad (37)$$

The surface resistance for evapotranspiration is computed as

$$R_s = \frac{R_{smin}}{LAI F_1 F_2 F_3 F_4} \quad (38)$$

in which

$$F_1 = \frac{f + R_{s\min} / R_{s\max}}{1 + f} \quad (39)$$

with

$$f = 0.55 \frac{R_G}{R_{GL}} \frac{2}{LAI} \quad (40)$$

where $R_{s\max} = 5,000 \text{ s/m}$, $R_G = R_{sw}$, and R_{GL} depends on the vegetation type.

□

$$F_2 = \begin{cases} 1, & W_2 > W_{fl} \\ (W_2 - W_{wilt}) / (W_{fl} - W_{wilt}), & W_{wilt} \leq W_2 \leq W_{fl} \\ 0, & W_2 < W_{wilt} \end{cases} \quad (41)$$

$$F_3 = \begin{cases} 1 - 0.06(q_{vsat}(T_a) - q_{va}), & q_{vsat}(T_a) - q_{va} \leq 12.5 \text{ g/kg} \\ 0.25, & \text{otherwise} \end{cases} \quad (42)$$

$$F_4 = 1 - 0.0016(298.0 - T_a)^2 \quad (43)$$

Surface soil moisture

In Equation 21, the surface volumetric moisture W_{geq} when gravity balances the capillary force is computed according to

$$\frac{W_{geq}}{W_{sat}} = x - ax^p(1 - x^{8p}) \quad (44)$$

in which

$$x = \frac{W_2}{W_{sat}} \quad (45)$$

In Equation 21, the coefficients are given by

$$C_1 = C_{1sat} \left[\frac{W_{sat}}{W_g} \right]^{\frac{b}{2}+1} \quad (46)$$

$$C_2 = C_{2ref} \frac{W_2}{W_{sat} - W_2 + W_l} \quad (47)$$

where W_l is a small numerical value that limits C_2 at saturation. The parameters C_{1sat} , C_{2ref} , b , and p are soil-texture dependent.

3.4.2. Model Domain and Input

The area of interest covers Northern California and part of northwestern Nevada and Southern Oregon, with the Sierra Nevada ranges occupying most of the domain. There are two categories of input datasets. One is composed of parameters such as terrain height, land-use/land-cover type, leaf area index, vegetation fraction, and others. Another group of necessary input data is for the radiation transfer computations. Required variables for the downscaling model are the three-dimensional mixing ratio of water vapor, cloud and precipitation particles, and three-dimensional air temperature, including surface air temperature. Also required are incoming radiation, soil surface temperature and moisture, deep soil temperature and moisture, canopy moisture, and snow cover information. Since current large scale models have embedded land surface models of some complexity, these variables may be obtained from the coarse resolution GFS model.

Important real-time inputs to the temperature downscaling model are cloud and precipitation estimates. Because the GFS can only provide very coarse resolution estimates, it underestimates significantly the spatial variability of cloud and precipitation. The HRC simplified orographic precipitation model downscales coarse

resolution weather forecasts onto 10 km x 10 km cloud and precipitation (see previous sections). The INFORM system uses a one-way coupling of these downscaling models to provide high resolution three-dimensional cloud fields (such as the mixing ratio of cloud water (q_c) and rain (q_r)) and two-dimensional surface precipitation fields (p) for the temperature downscaling model. In addition, the airflow model described in Section 3.2 above, estimates the three dimensional air flow (u, v, w) over complex terrain. This high-resolution surface air flow is used as an input to the temperature downscaling model to improve the calculation of the sensible heat and latent heat flux. Lastly, for real-time operation as part of the INFORM system, the surface air temperature model also receives boundary snow cover and surface soil water estimates from the hydrologic component, as described in Chapter 2.

3.5. Evaluation of Surface Air Temperature Model with Data

As a first test, the authors ran the well-known MM5 mesoscale numerical simulation model with a 100-km grid spacing, to produce products similar to those that are available from GFS during the operation of the temperature downscaling model as part of the INFORM system. Similar to the five-day forecast period of the GFS model, a five-day simulation period was used for MM5. The NCEP global reanalysis data provided model input and lateral boundary conditions. The MM5 model ran for April 1992, during the melting period. The model ran at 0000z of April 1, 5, 9, 13, 17, 21, and 25, for a five-day simulation. Therefore there is one-day overlap for these simulations. After these 100 km resolution simulations were completed, the formulated surface temperature downscaling model ran using the MM5 output for boundary and initial conditions.

At first, the authors investigated the downscaling model to see if it could reproduce the subgrid variability of surface air temperature attributable to the finer terrain and land-cover/land-use features. Figure 18 shows the surface air temperature fields before and after applying the temperature downscaling model at 0000Z on April 10, 1992. Significant improvements generated by the downscaling temperature model are evident when comparing the two panels of Figure 18. For instance, the downscaling model redistributes surface air temperature based on finer terrain elevation data so that the lowest temperature in the domain becomes -8°C in the high mountainous region with elevation greater than 3000 m. The surface air temperature over the lakes is higher than the neighboring land area at midnight after downscaling. Therefore, this test shows that after downscaling, the resulting surface air temperature bears the scaling features of terrain and land use/land cover.

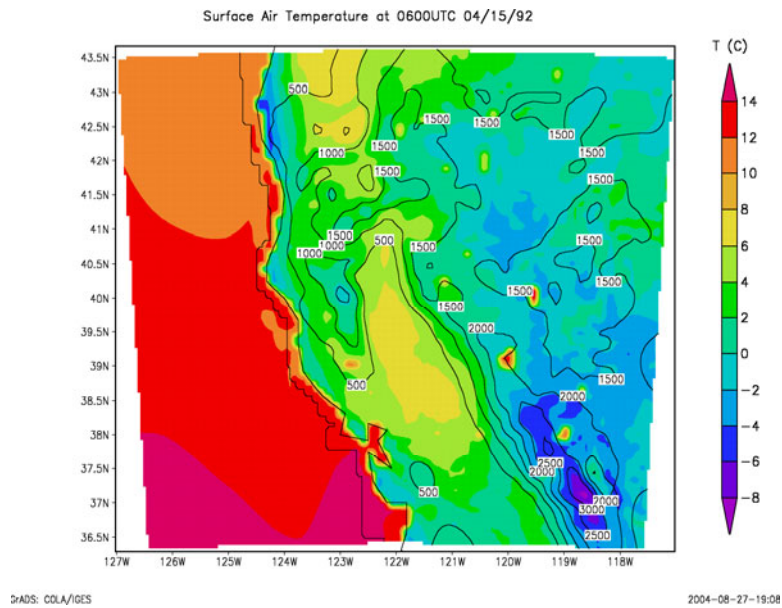
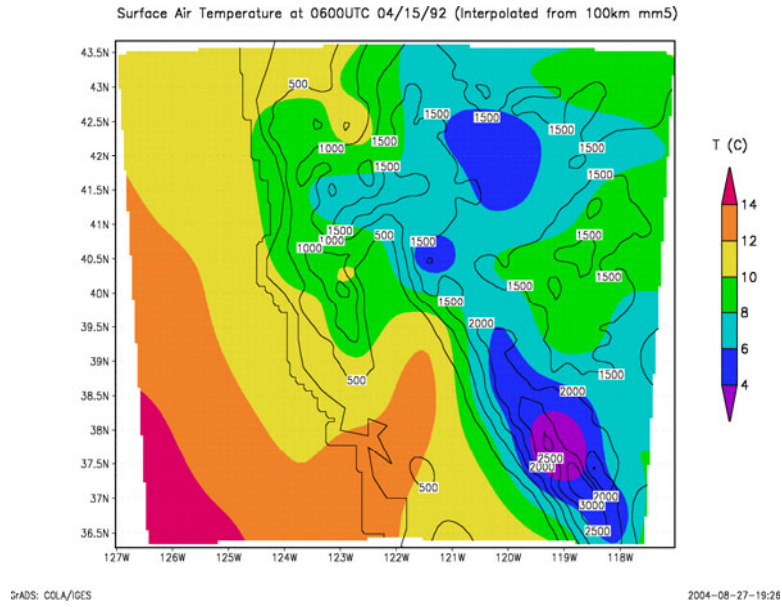


Figure 18. Interpolated field (no model used) and downscaled field (using the temperature downscaling model) for the Northern California region for a specific 6-hour period in April 1992 (during the melting period). Both fields have a resolution of 10 km and are produced using the same 100 km-scale forcing information.

A second test used: (1) six-hourly NCEP global reanalysis data for the wet season 1997–1998, and (2) derived cloud fields from the orographic precipitation model of Section 3.2. Figure 19 shows the time series of six-hourly averaged observed temperature for the Chester station within the Oroville drainage (upper panel) and the Weed station within the Shasta drainage, together with the corresponding six-hourly closest grid-point estimates from the downscaling model.

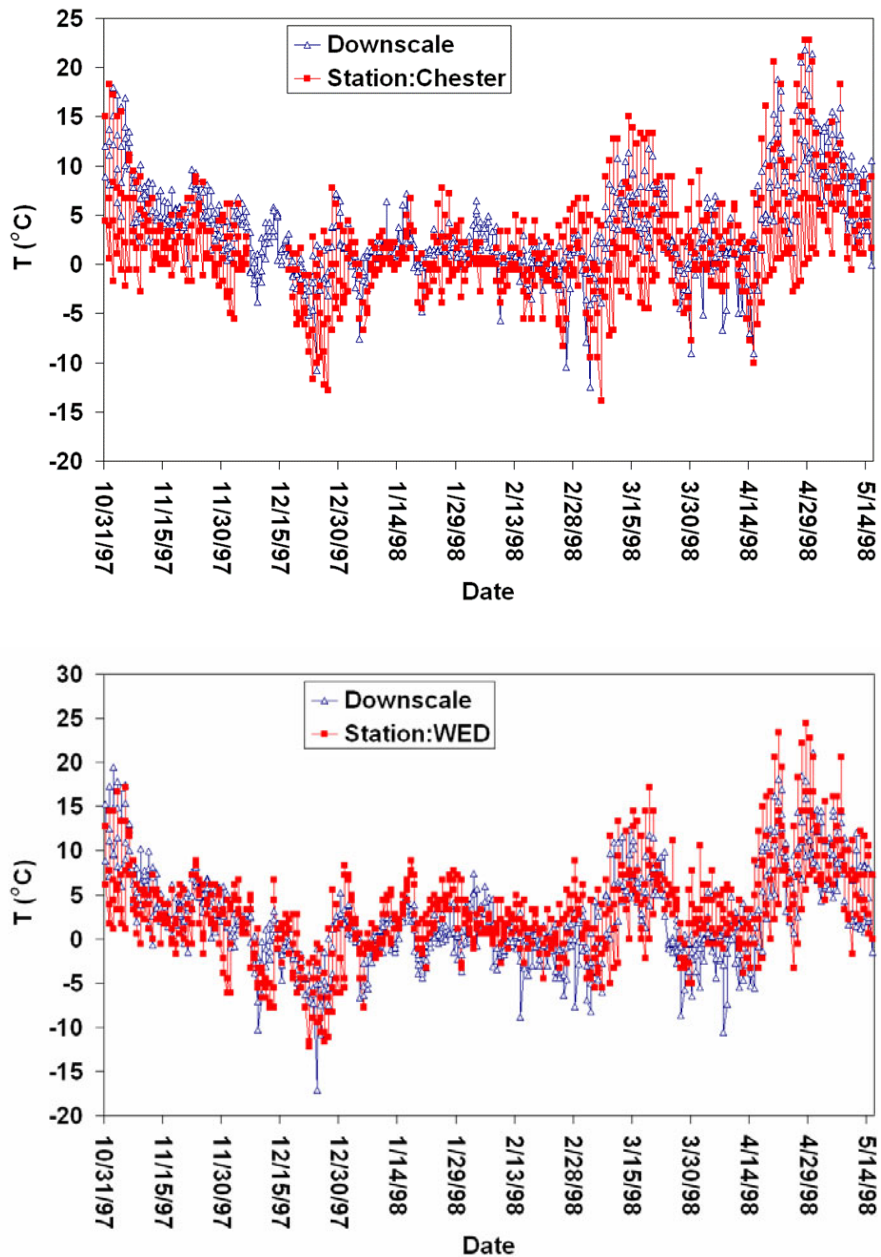


Figure 19. Six-hourly observed (red line and symbols) and simulated (red line and symbols) temperature for the Chester and Weed (WED) sites and for the wet season 1997–1998

The Chester station has coordinates (40.2830N; 121.2330W) and an elevation of 1360 m. The Weed station has coordinates (41.4790N; 122.4540W) and an elevation of 880 m. These results indicate that the model reproduces the variability of temperature well, including longer-term changes in diurnal amplitude and mean daily precipitation. For the northern station, there is a tendency for underestimation and occasional low departures of the simulated from the observed values. These errors may be due to the scale difference between station data and simulated gridded values, the use of climatological snow and soil water conditions for these off-line tests, and downscaling model errors. Overall, these tests suggest utility of the temperature downscaling model for the INFORM forecast component. Chapter 7 provides additional performance evaluation of the downscaling temperature model when run as part of the INFORM system for the wet season 2005–2006. For those tests the snow and soil water boundary conditions are updated every time step from estimates of the hydrologic model component (see schematic in Figure 6 of Chapter 2).

3.6. Formulation of Probabilistic Climate Forecast Downscaling

As discussed in Chapter 2, the INFORM processing of CFS and GFS data is split into two different paths, to accommodate the differences in operationally available data for these two models. Thus, pertaining to the CFS processing path, INFORM ingests seasonal ensemble forecasts with monthly resolution and uses probabilistic downscaling procedures to generate an ensemble of six-hourly mutually consistent precipitation and temperature data for each of the INFORM drainage basins. Both unconditional ESP (used operationally by the NWS) and conditional ESP methodologies are used. The latter methodology uses the ensemble of CFS forecasts with monthly resolution to condition the time series of precipitation and temperature that enters into the ESP procedure of the NWS. The generation of the streamflow ensembles for the INFORM reservoir sites is done off-line, typically once per month. This section discusses the formulation of the conditional ESP generation, while Sections 3.7.1 and 3.7.2 present evaluation results for both the unconditional ESP and the conditional ESP methodologies applied to historical data that include archived CFS forecasts.

Conditioning is done by identifying the tercile of monthly CFS precipitation with the highest frequency of occurrence in the current CFS ensemble forecasts. Then, the historical six-hourly precipitation and temperature observed time series of 9 months' duration that originate at the CFS forecast month are selected, to force the hydrologic model component if the years of their occurrence have monthly forecast precipitation for CFS that was in the aforementioned tercile of its distribution. The precipitation and temperature time series selected provide the input to the hydrologic model that generates ensemble reservoir inflows for each reservoir site in the INFORM region. The hydrologic model is described in Chapter 4 and contains components for snow accumulation and ablation, soil moisture accounting, and channel routing. The formulation and parameters of the model components mirror those of the operational CNRFC hydrologic forecast models. The output of the hydrologic model when forced

with the ensemble of precipitation and temperature for each basin in the INFORM domain is a set of reservoir inflow time series at the sites of the INFORM study reservoirs. These ensembles then feed the INFORM decision model.

Figure 20 shows the mathematical formulation of the probabilistic downscaling. The approach is a sample path approach that was used earlier in Carpenter and Georgakakos (2001) and Georgakakos (2003). It uses the ability of the CFS to consistently forecast monthly precipitation in the upper or lower terciles of its distribution when the observations are in the corresponding tercile of their distribution. It also considers the model errors of the hydrologic model in generating ensemble streamflow forecasts.

3.7. Evaluation of Probabilistic Climate Forecast Downscaling

3.7.1. Unconditional ESP

For each major reservoir, the ESP methodology generated ensemble inflow simulations (1) on a daily-basis, with six-hourly resolution and extending 90 days from the ensemble preparation date, and (2) on the first of each month, with monthly resolution and extending 12-months from the preparation date. The ensemble simulations spanned the historical period October 1961–September 1999. This section reports on a probabilistic evaluation of the retrospective ensemble simulations of reservoir inflow. The analysis examines the ensemble simulations capability to reliably reproduce selected “target events” with good resolution and sharpness properties, which are defined in the following sections. The “observations” of reservoir inflows were defined as the available full natural flow (FNF) estimates provided by CNRFC. Reliability diagrams are presented to summarize the analysis, as these compactly display the full frequency distribution of the ensemble simulations and are thus more informative than single scalar performance measures. The theoretical basis for ensemble forecast evaluation and development of the reliability diagram is discussed by Wilks (1995). Selected reliability diagrams are presented in this section.

3.7.1.1. Validation methodology

For analysis of the generated long-term (seasonal or longer) ensemble simulations, this study defines the “target events” on the basis of multi-month inflow volumes. Specifically, the target events considered are defined by the 30-, 60- and 90-day, and six-month inflow volumes occurring in the upper and lower terciles of the observed inflow volume distribution. Therefore, the analysis investigates the ensemble simulation of both low-flow volumes and high-flow volumes.

FORECAST THEORY

Lake Inflow Ensemble Generation:

$$Q'(t; \omega) = Q(t; \omega) + \xi(t; \omega')$$

$Q(t; \omega)$: a sample path of forecast inflows forced by an input vector sample path $\underline{u}(t; \omega)$

$\xi(t; \omega')$: representing a sample from the distribution $N(I_m, S_m)$ of hydrologic errors

t : time in the forecast interval $(t_o, t_f]$ in units of days, and in month m

I_m, S_m : mean and standard deviation of model residual errors for month m

Input Vector Generation with Monthly CFS Information:

$$\Omega_u = \{ \underline{u}(t, t \geq t_0; \omega \in \Omega_y) \}$$

$$\Omega_y = \{ \omega \in \Omega : (z_p^y \leq q_l \cap z_p \leq q_l) \cup (q_l < z_p^y \leq q_u \cap q_l < z_p \leq q_u) \cup (q_u < z_p^y \cap q_u < z_p) \}$$

$$z_p = \frac{P_1 - m}{\sigma}$$

$$z_p^y = \frac{P_1^y - m}{\sigma}$$

Ω_u : set of input forecast vectors

Ω_y : set of sample paths of input vectors

P_1 : GCM monthly precipitation forecast

P_1^y : historical GCM monthly simulations of precipitation (m -mean; σ -st dev)

q_u, q_l : upper and lower terciles of the GCM precipitation frequency distribution

Figure 20. Theory of ensemble precipitation forecast downscaling from CFS precipitation forecasts

To account for the seasonal cycle in observed streamflow, the upper and lower tercile volume limits were defined on the basis of standardized inflow volume anomalies:

$$A(i) = \frac{V_N(i) - \overline{V_{N,mo(i)}}}{S_{N,mo(i)}} \quad (48)$$

where $A(i)$ is the computed anomaly for the i^{th} preparation time, $V_N(i)$ is the observed N -day inflow volume computed on the i^{th} preparation time, $\overline{V_{N,mo(i)}}$ is the mean N -day inflow volume computed from all preparation times beginning in the month of i^{th} preparation time, and $S_{N,mo(i)}$ is the standard deviation of the N -day inflow volume for the month of i . Here N corresponds to the 30-, 60-, or 90-day volume. Due to the serial correlation of streamflow, particularly at the daily and sub-daily scale, the observed and ensemble inflow volumes and ensembles were computed every five days (specifically on the 1st, 6th, 11th, 16th, 21st, and 26th of each month). Figure 21 illustrates the distribution of the 30-, 60-, and 90-day observed inflow anomalies for the Oroville Reservoir on the Feather River. The anomaly values associated with the upper tercile and lower tercile of the observed distributions were extracted to compute the monthly-varying lower tercile and upper tercile volume thresholds used in the reliability analysis.

The longer ensemble simulations, extending one year from the ensemble preparation date, were generated only on the 1st of each month in the retrospective analysis. The upper and lower tercile six-month inflow thresholds were computed similarly to Equation 48 above; however, the mean and standard deviation were computed from seasonally pooled volumes, in contrast to the monthly statistics indicated above. Accordingly, the upper and lower tercile thresholds varied on a seasonal scale. The seasons were defined for *winter* (JFM), *spring* (AMJ), *summer* (JAS), and *fall* (OND).

For each reservoir, eight target events are defined: (a) $V_N < V_N^L$ and (b) $V_N > V_N^U$, where V_N is the N -duration volume, V_N^L is the lower tercile N -duration volume threshold and V_N^U is the upper tercile N -duration volume threshold with $N=30, 60$, and 90 days and six months. The target events represent the volumes occurring in the lower tercile and the upper tercile of the observed inflow volume distribution.

Reliability diagrams were constructed for each of these events and for each major reservoir. For example, Figures 22 through 25 contain the 30-day volume diagrams for the Folsom, Trinity, Shasta, and Oroville Reservoirs, respectively. Additionally, the analysis was repeated for the “wet season” only. The wet season analysis considered only the ensemble simulations and the observed inflow volumes occurring from October through April. The relevant figures for the wet season analysis are discussed in the following paragraphs.

In Figures 22 through 25, the reliability diagrams for the two target events of a given inflow duration are included, with inflow volumes in the lower tercile given in the left-hand panels, and inflow volumes in the upper tercile presented in the right-hand panels of each figure.

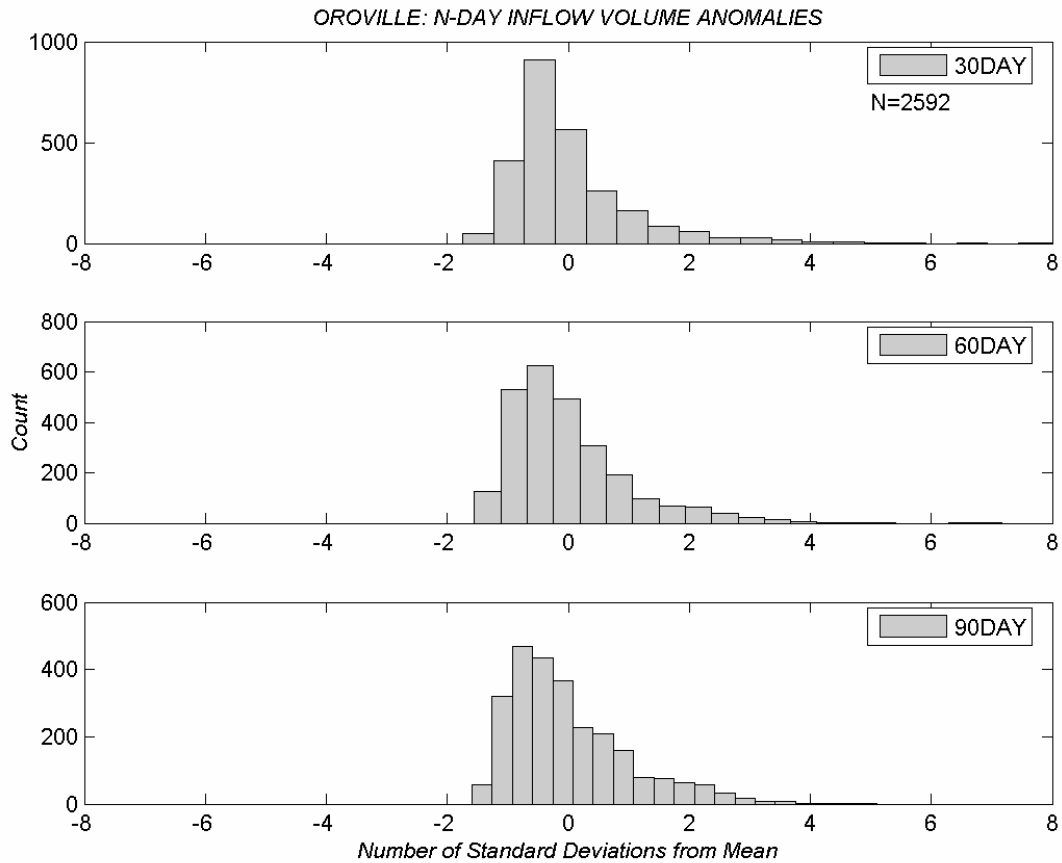


Figure 21. Distribution of N-day inflow volume anomalies for Oroville Reservoir

The reliability diagram presents the observed frequency of occurrence of a target event relative to the ensemble frequency. If F_i denotes the probability of the target event occurring at the preparation time I , as determined by the ensemble simulations, and O_i signifies the observation of the target event occurring at preparation time i , then the joint probability distribution of the simulations and observations, $p(F_i, O_i)$, fully characterizes the ensemble simulations and observations at time i , considered as stationary random processes for varying time. The joint probability may be decomposed into a conditional and a marginal distribution:

$$p(F_i, O_i) = p(O_i | F_i) p(F_i). \quad (49)$$

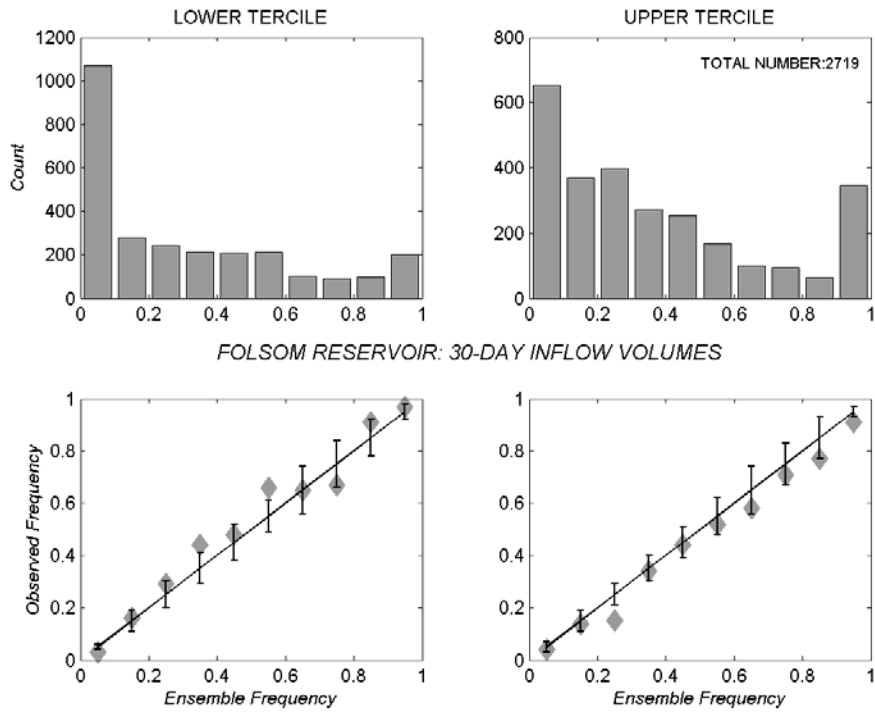


Figure 22. Reliability diagram for Folsom Reservoir 30-day inflow volumes in the lower tercile (left-hand column) and upper tercile (right-hand column) of the observed distribution

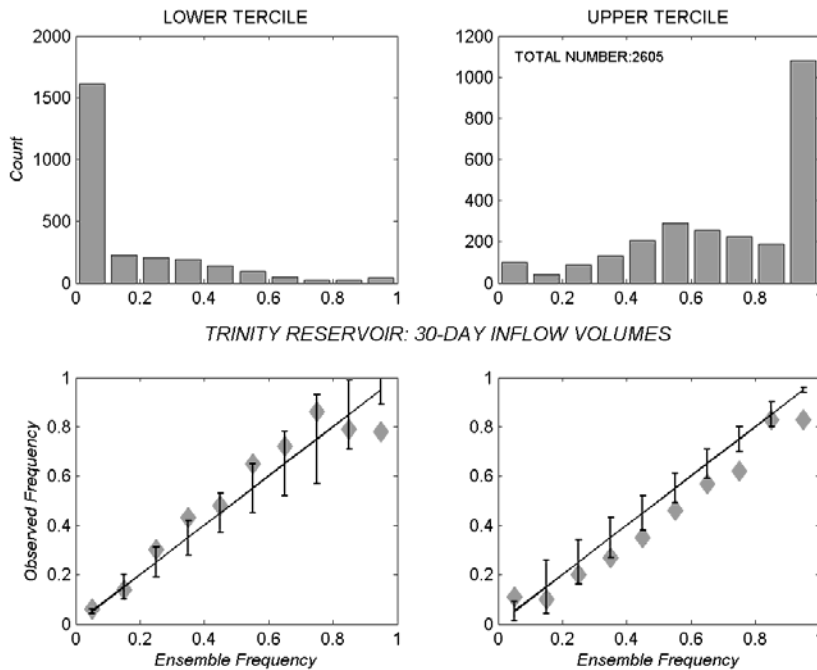


Figure 23. Reliability diagram, as in Figure 22, but for Trinity Reservoir 30-day inflow volumes

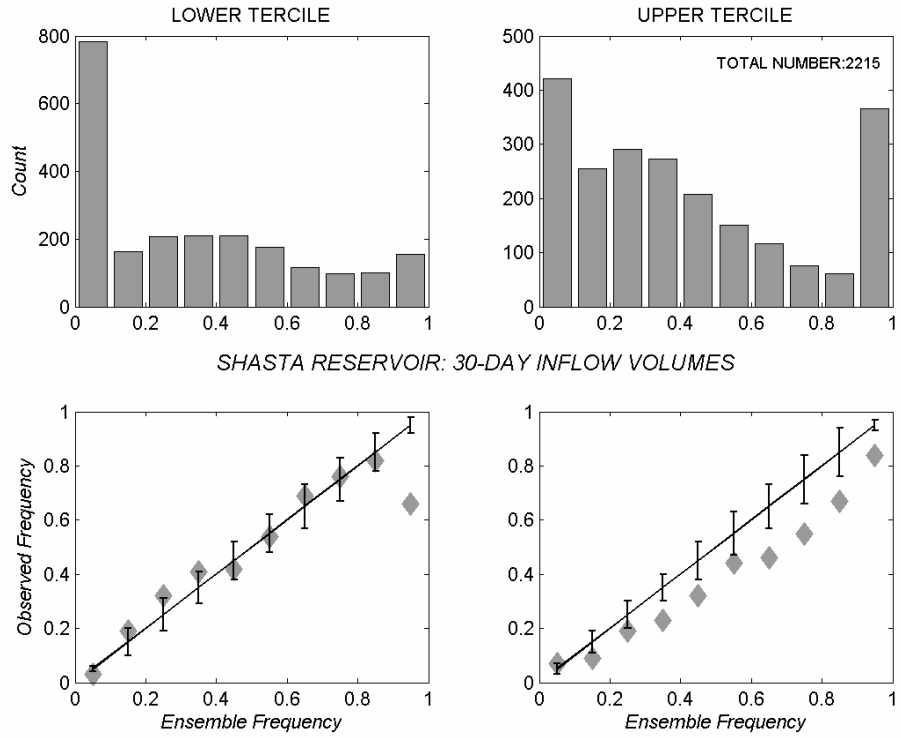


Figure 24. Reliability diagram, as in Figure 22, but for Shasta Reservoir 30-day inflow volumes

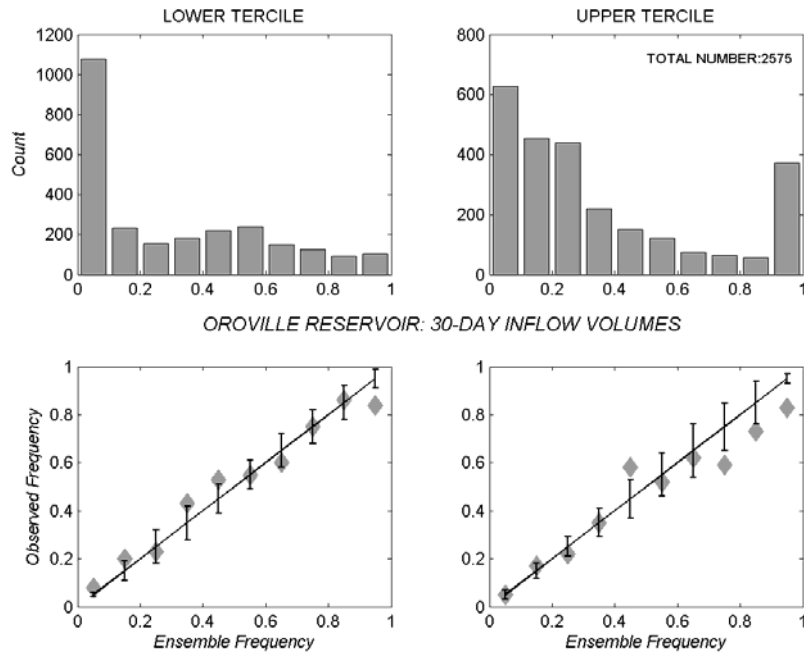


Figure 25. Reliability diagram, as in Figure 22, but for Oroville Reservoir 30-day inflow volumes

These distributions are represented in the combined “sharpness/reliability” diagram (Figures 22 through 25). The marginal distribution describes the frequency of use of various frequencies of occurrence of the target event by the ensemble simulation in the range [0,1]. The marginal distribution is shown in the bar plots of the upper half of the figures. The marginal distribution allows for the examination of the sharpness of the ensemble simulations. Low-sharpness ensemble simulations reproduce results similar to the climatological exceedance frequencies of the target event. High-sharpness (desired attribute) simulation results deviate significantly from the climatological exceedance frequencies. When the probabilities are concentrated near 0 and 1, the simulation results are described as being “extremely sharp.”

The reliability of the ensemble simulations is assessed using the conditional probability distribution. The conditional distribution describes the observed frequency of occurrence of the target event given the simulation frequency in a specified range: $f_i^L < F_i < f_i^H$, where the range of F_i is divided into subintervals (in our analysis, deciles). Reliability compares the correspondence of a given simulated frequency to the sample frequency of observations for times when the simulated frequency is within the range of interest. Thus, the reliability is a measure of whether the simulated frequencies of the target event correctly estimate the true frequency of event occurrence. This is presented in scatter plots shown in the lower portion of the included figures. The abscissa designates the range in the computed ensemble frequency, and the ordinate the conditional observed frequency. The 1:1 diagonal signifies the case of perfect reliability.

Large deviations from equality for a particular subinterval indicate unreliable simulation in the frequency subinterval for the target event. Assuming the probability of finding the observed inflow volume satisfying the target event in a given subinterval is fixed and equal to the subinterval middle value, a goodness of fit test is devised. Under this assumption, the number of observations, N_o , within a certain subinterval follows a binomial distribution with an expected value $N_s p$ and variance $N_s p (1-p)$, where N_s is the number of observed inflow volume samples in the subinterval and p is the constant probability of the subinterval (e.g., Benjamin and Cornell 1970). The standardized residual ν is defined:

$$\nu = \frac{N_o - N_s p}{\sqrt{N_s p (1-p)}} \quad (50)$$

The central limit theorem applies if $N_s p$ is not too small (i.e., > 10); then ν is approximately normally distributed with zero mean and variance of one, and ν^2 is χ^2 distributed. This residual was used to define 95% confidence error bars included in the reliability diagrams. Deviations outside of these error bounds indicate unreliable ensemble simulations. Considering Figure 22, it is evident that the error bars are narrow for the frequency ranges with the high number of samples (N_s , as indicated in the bar

plot of the upper diagram). For the 30-day volumes in the upper tercile for Folsom Reservoir, most of the observed frequencies fall within the error limits, with the exception of frequencies in the ranges [0.2, 0.3] and [0.9, 1.0]; therefore the ensemble simulations for the event “inflow volumes in the upper tercile,” are reliable across most frequency of occurrence ranges.

The conditional distribution may also be used to assess the “resolution” of the ensemble simulations. Resolution summarizes the ability of the ensembles to distinguish differences in the conditional frequency of observations for different simulated frequencies of the target event. Focusing on right-hand column of Figure 25 (30-day volumes in the upper tercile for Lake Oroville), there is a distinct increase in observed frequency over the simulation frequency range [0, 0.4]. However, over the simulated frequency range [0.4, 0.8], the conditional observed frequency maintains values near 0.55. Consequently, the ensemble simulations exhibit low resolution over this latter frequency range.

3.7.1.2. Reliability results

The results of the probabilistic analysis of the retrospective ensemble simulations are discussed in this section for each of the major reservoirs. These results are obtained from the unconditional ESP methodology of the NWS. The reader should keep in mind that the forecast skill in ESP methodology for a particular forecast preparation time is due to the long memory of snow and soil water processes represented in the hydrologic models of INFORM, rather than the skill of the atmospheric input to the ESP procedure.

Folsom Reservoir, American River

The reliability diagrams for Folsom Reservoir were constructed for the 30-, 60-, 90-day and six-month for ensemble simulations produced during all months of the retrospective analysis. The wet-season diagrams (covering ensemble simulations produced and the observed inflow distribution for the months of October through April only) were also constructed. For the 30-, 60-, and 90-day lower tercile inflow volume event, the marginal distribution shows a concentration of probability mass in the lowest [0, 0.1] simulated frequency range, indicating sharpness for this target event. There is, however, a tendency toward lower sharpness at the 90-day inflow volume case. The upper tercile inflow volume event also displays lower sharpness across the target events. For both the upper and lower tercile events, the ensemble simulations show good resolution and are reliable with only a very few deviations outside the 95% confidence bounds.

For the longer-term, six-month inflow volume events, it is first apparent that the confidence bounds are significantly wider, particular at the higher ensemble frequency range, due to the fewer number of samples (recall that the year-long ensembles were produced only on the first of each month). The marginal distribution again shows higher sharpness for the lower tercile inflow volume event when compared to the upper tercile event. The condition distribution that indicates the ensembles are reliable and exhibit

fairly good resolution throughout the simulated frequency ranges, for both inflow volumes in the lower tercile and in the upper tercile.

For the wet seasons, the reliability diagrams indicate similar results, but with lower sharpness in the marginal distribution and larger deviations from the perfect reliability. In spite of these larger deviations, most of the observed conditional frequencies remain within the confidence bounds, and are thus reliable. There is a trend toward underrepresentation of the observed frequency of the lower tercile inflow volume at higher frequency values for the 60- and 90-day inflow volume durations.

Trinity Lake, Trinity River

The reliability diagrams for Trinity Lake were constructed for the 30-, 60-, 90-day and six-month durations for all months and for the wet season. The analysis period covers May 1963 through September 1999, due to the length of the historical observation record. In contrast to the results for the Folsom Reservoir, the marginal distribution for Trinity Lake shows higher sharpness for both the lower and the upper tercile inflow volume events for the 30-, 60-, and 90-day durations. The upper tercile events indicated good resolution, albeit with a tendency to over-represent the observed frequency and to be slightly outside the reliable confidence bounds. The resolution of the lower tercile inflow event tends to be low as the simulation frequency increases.

For the six-month duration analysis, the lower tercile event demonstrates high sharpness, but at the expense of resolution at higher simulation frequency ranges. The ensembles remain reliable for both the lower and upper tercile event, although the confidence bounds are quite wide at the higher frequency ranges. For the wet season analysis, the reliability and resolution are improved for both the lower tercile volume and upper tercile volume events. However, the resolution for the lower tercile events is reduced at the higher (90-day and six-month) durations.

Shasta Reservoir, Sacramento River

The reliability diagrams for Shasta Reservoir were constructed for the 30-, 60-, 90-day and six-month inflow volume for all months and for the wet season. The historical observation record and analysis period cover the period October 1961–September 1992. The lower tercile inflow volume event exhibits good resolution and reliability in all frequency ranges except the highest decile (0.9-1.0) for each of the 30-, 60-, and 90-day durations. The marginal distribution also exhibits sharpness for the lower tercile event, although the sharpness decreases with the longer durations. The observed frequency of the upper tercile inflow event is over estimated by the ensembles and is generally outside the reliability bounds for all durations. Similar the Folsom Reservoir, the marginal distribution for Shasta Reservoir shows low sharpness for the upper tercile inflow volume events for the 30-, 60-, and 90-day durations. While within the confidence limits, the observed frequency of the upper tercile six-month inflow event, again, tends to be over estimated by the ensembles, while that of the (six-month) lower tercile event is under estimated over several frequency ranges. The wet season analysis indicates

similar conclusion as the analysis for all months in terms of reliability and resolution. However, the wet season marginal distributions indicate lower sharpness for all events.

Oroville Reservoir, Feather River

The reliability diagrams for Lake Oroville were constructed for the 30-, 60-, 90-day and six-month inflow volumes for all months and for the wet season. The historical observation record and analysis period cover the period October 1961 through September 1997. The analysis indicates good reliability and resolution for each of the 30-, 60-, and 90-day inflow events (for inflow volumes both in the upper and the lower terciles). As for Folsom and Shasta Reservoirs, the marginal distribution for the upper tercile inflow events points toward lower sharpness, particularly as the volume duration increases. The six-month upper tercile inflow volume event is reliable, with the exception of the highest frequency range (0.9–1.0), and shows reduced resolution at these higher frequency ranges. The six-month lower tercile event results again suggest good resolution with lower sharpness than the shorter duration volumes, but generally reliable ensemble simulations.

For the wet season analysis of the Oroville Reservoir, the conditional distribution indicates reliable ensembles especially for the 30-day lower tercile event, with a trend for under estimation of the observed frequency at higher frequency ranges. The ensemble simulations are also reliable with respect to inflow volumes in the upper terciles for the 30-, 60-, and 90-day durations. For the six-month duration wet season events, reliability and resolution is good in the lower frequency range (e.g., < 0.5). At higher simulation frequencies, the resolution is reduced and the confidence bounds become quite large, due to the low sample size (the criterion for $N_s * p$ to be “not too small” for the central limit theorem to apply is likely violated).

Conclusions of Reliability Analysis

In summary, the probabilistic analysis of the retrospective ensemble simulations indicates generally reliable simulations for multi-month inflow volumes occurring within the lower and the upper terciles of the observed distributions. A notable exception is the over-representation of the upper tercile observed frequency for the 30-, 60-, and 90-day inflow volumes for Shasta Reservoir. The marginal distribution of the ensemble simulations frequency consistently exhibit higher sharpness, or deviation from the climatological exceedance frequency, for the cases of low inflow volume (volumes in the lower tercile). The resolution of the ensemble simulations is usually good, in particular over the lower simulation frequency ranges. The wet season analysis yielded similar results and conclusions as the analysis for all seasons, although the confidence limits allowed for a wider range of reliable observed frequencies, due to the reduced number of simulations.

3.7.2. ESP Conditional on CFS Forecasts

3.7.2.1. Data and methodology

NCEP archived CFS monthly-resolution 15-member ensemble forecasts for the period January 1981 to December 2003. The CFS monthly-averaged surface precipitation forecasts with a one-month lead time were used to segregate the six-hourly simulations of rain plus melt from the drainage areas of Trinity (Trinity River), New Bullards Bar (NBB; Yuba River), Folsom (American River), Oroville (Feather River), and Shasta (Sacramento and Pit Rivers). The six-hourly rain plus melt values were segregated into two groups based on whether the historical month in which they fall has a first-month surface precipitation CFS forecast in the upper or the lower tercile of its distribution. The two resultant distributions of the six-hourly rain-plus-melt for each month of the year were subjected to a Kolmogorov-Smirnov (K-S) hypothesis test to determine whether they are from different populations. The cumulative histograms of the two distributions were plotted to also determine whether the segregated distributions had a direct association to the segregating CFS terciles (high with high and low with low). These histograms were also used to decide whether the first-month CFS forecast would produce adequate samples for segregating the distributions, as the K-S test is powerful for the central region of the distribution. In addition to the Kolmogorov-Smirnov test, the Wilcoxon rank sum test was performed. This is a two-sided test of the hypothesis that two independent samples come from distributions with equal medians. This test is useful in case the two segregated distributions are identical, except possibly from a locational shift. The mean, median, standard deviation, and skewness coefficient were computed for each of the two segregated rain-plus-melt distributions for each watershed and each month of the year.

Conditioning of the ensemble streamflow prediction (ESP) procedure is done during real-time operation when the following two conditions are met: (1) the segregated snow-plus-melt distributions are statistically different for the first-CFS forecast month; and (2) there is a direct association of the terciles of the segregated distributions with those of the CFS monthly precipitation forecasts (high with high and low with low). The conditioned ESP procedure generates ensemble reservoir inflows for the Northern California reservoirs of INFORM. The rank sum test was also used to find cases for which the segregated distribution medians were statistically indistinguishable, to exclude these cases from using the CFS forecasts to condition the ESP procedure. The terms p_{KS} and p_{RS} are the probabilities of observing the given result by chance if the null hypothesis is true—that is, segregated distributions are statistically indistinguishable (p_{KS}), or the medians are equal (p_{RS}). Small values of p cast doubt on the validity of the null hypothesis. In all cases, a confidence level of 1% is used to decide the validity of the null hypothesis.

The CFS forecasts are available on a grid with a $2.5^\circ \times 2.5^\circ$ resolution. For this analysis, the closest CFS grid point to the centroid of the watershed of interest is used to provide data for this analysis (see Table 8 for associations of grid points and basin centroids).

The tercile values for the two grid points of interest are shown in Table 9. The analysis is done for rain-plus-melt time series from the three watersheds of interest. The rain-plus-melt time series from the upper region of the Trinity Reservoir watershed, the upper region of the Yuba River that flows into New Bullards Bar, the upper region of the North Fork of the American River that flows into the Folsom Reservoir, the upper region of the Feather River that flows into Oroville Reservoir, and the upper region of the Shasta drainage area. The time series has a six-hourly resolution in all cases, and they are produced by simulations of the calibrated INFORM hydrologic models. The historical record for these simulations is January 1950 through December 1999 for Trinity, and October 1960 through September 1999 for the other drainage areas.

Table 8. CFS grid points and watershed centroids (degrees)

	<i>Watershed Centroid^(*)</i>		<i>CFS Closest Grid-Point</i>	
	<i>Latitude</i>	<i>Longitude</i>	<i>Latitude</i>	<i>Longitude</i>
<i>Trinity</i>	41.02	122.72	40.00	122.50
<i>NBB</i>	39.48	120.78	40.00	120.00
<i>Folsom</i>	38.95	120.55	40.00	120.00

(*) Centroid coordinates are approximate.

Table 9. Tercile values for CFS-forecast monthly precipitation

Grid Point (Lat:40.00°; Lon:122.50°)

	JAN	FEB	MAR	APR	MAY	JUN	JUL	AUG	SEP	OCT	NOV	DEC
UPPER	9.02	7.74	7.03	3.28	1.58	0.62	0.06	0.07	0.56	2.58	8.18	9.31
LOWER	5.06	4.39	4.01	1.74	0.78	0.17	0.01	0.01	0.15	1.08	4.58	5.53

Grid Point (Lat:40.00°; Lon:120.00°)

	JAN	FEB	MAR	APR	MAY	JUN	JUL	AUG	SEP	OCT	NOV	DEC
UPPER	6.32	6.16	5.70	3.52	2.71	1.63	0.36	0.31	0.88	2.29	6.43	6.85
LOWER	3.88	3.50	3.57	1.98	1.40	0.53	0.03	0.03	0.24	1.06	3.62	4.12

Lastly, the authors constructed reliability diagrams for the ESP conditioned by CFS forecasts in a similar fashion to that reported for the unconditional ESP runs. The discussion of these diagrams is included in the next section. Appendix C presents the results in table form for all cases.

3.7.2.2. Results and discussion

Trinity

Table 10 and Figure 26 show the validation results for the Trinity tests. On the basis of these results, the research team concluded that for all the months the segregated distributions of rain-plus-melt are statistically distinguishable, the high from the low, at the 1% confidence level. However, the cumulative distribution plots indicate that for September and November there is an inverse relationship between the high and low cumulative probability distributions and segregating CFS monthly precipitation forecast terciles—that is, the high tercile is associated with a distribution of smaller values. The mean values of the samples also confirm that for September and November there is an inverse relationship of central tendency values with CFS tercile rank. In all cases, the Wilcoxon rank sum test indicates distinguishable median values at the 1% confidence level. For most cases (apart from September and November) the sample standard deviation is higher for the sample conditioned with high tercile CFS forecasts. Apart from August, the skewness coefficient is higher for the low CFS tercile-generated sample. The plots in Figure 26 also indicate that for the months of May and October for considerable cumulative distribution range the distributions are very close. It is thus suggested (in a conservative sense) that CFS-conditioned ESP may be used for the Trinity basin for all months except when the first-month of monthly surface precipitation is May, September, October, or November, when unconditional ESP should be used.

New Bullards Bar

Table 11 and Figure 27 show the results for the New Bullards Bar Reservoir drainage on the Yuba River. In this case too, the distributions are distinguishable at the 1% confidence level except from May. The same is true for the Wilcoxon rank sum test. The plots of the cumulative distributions show that for September and November the relationship between the distributions and the conditioning CFS precipitation terciles is inverse (i.e., high to low and low to high). It is notable that the means for September through November also bear an inverse relationship to the high and low terciles of the conditioning CFS monthly precipitation. It is also notable that the results for October show regions of cumulative distribution (high values) that are very close among the two segregated samples. The research team concludes that CFS conditioning of ESP should be used in all months but May, September, October, and November in this case, too.

Folsom

Table 12 and Figure 28 show the results for the Folsom Reservoir drainage on the American River. Following the same reasoning as previously described, the research team concludes that for this case, conditioning of the ESP procedure may be done for all the months except for May, September, October, November, and December.

Oroville

In this case Table 13 and Figure 29 show the results for the Oroville Reservoir drainage on the Feather River. The research team concludes that conditioning of the ESP procedure may be done for all the months except for May, September, October, and November.

Shasta

Table 14 and Figure 30 show the results for the Shasta Reservoir on the Sacramento and Pit Rivers. On the basis of these results the research team concludes that conditioning of the ESP procedure may be done for all the months except for (possibly) September, November, and January.

Reliability Diagrams

Figures 31 through 34 show the reliability diagrams for 60-day reservoir inflow volumes in the upper and lower tercile for Folsom, New Bullards Bar, Oroville, and Shasta. The data is for the period 1981–1999 and for the wet season only (October through April). Because of the reduced number of samples in these diagrams and for a fair comparison, the authors also produced analogous unconditional ESP diagrams with the same number of ensemble members as in the corresponding case of CFS-conditioned ESP. These ensemble members were randomly selected from the unconditional ESP ensemble. Figures 35 through 38 show the unconditional ESP reliability diagrams mentioned. On the basis of these results the research team concludes that conditioning of the ESP procedure on CFS forecasts provided with monthly resolution offers limited improvement over the unconditional ESP results.

Table 10. Validation results for Trinity

	JAN	FEB	MAR	APR	MAY	JUN	JUL	AUG	SEP	OCT	NOV	DEC
pKS	4.442e-010	3.095e-067	1.996e-034	2.067e-027	7.660e-005	3.662e-019	9.919e-012	1.893e-014	1.121e-010	9.887e-009	2.217e-004	3.791e-031
pRS	6.699e-013	1.226e-057	3.255e-029	2.277e-029	6.129e-003	2.527e-014	4.791e-013	2.108e-021	2.774e-004	8.732e-009	6.300e-004	1.229e-013
HiMd	0.080	0.080	0.080	0.080	0.080	0.080	0.080	0.080	0.080	0.080	0.080	0.080
LoMd	0.080	0.080	0.070	0.080	0.070	0.080	0.080	0.070	0.070	0.080	0.080	0.070
HiMe	1.231	1.346	1.317	1.219	1.007	1.242	1.156	1.146	0.845	1.162	1.007	1.133
LoMe	0.951	0.913	0.727	0.861	0.870	1.048	0.951	0.815	1.050	0.982	1.196	0.753
HiSd	3.288	3.354	3.473	3.227	2.669	3.322	2.944	3.077	2.230	3.163	2.667	3.121
LoSd	2.660	2.658	2.019	2.486	2.560	2.991	2.708	2.271	3.110	2.802	3.374	2.101
HiSw	6.136	5.613	5.617	5.971	5.153	5.955	5.042	5.989	5.757	5.882	5.194	6.287
LoSw	6.832	7.307	7.200	7.386	7.718	7.420	6.741	5.868	6.674	7.247	6.571	6.512

Table 11. Validation results for New Bullards Bar

	JAN	FEB	MAR	APR	MAY	JUN	JUL	AUG	SEP	OCT	NOV	DEC
pKS	1.948e-020	1.560e-040	1.602e-015	3.568e-034	1.208e-001	5.947e-028	3.809e-006	1.292e-031	2.044e-021	3.473e-010	4.932e-018	1.487e-013
pRS	2.939e-022	2.220e-028	3.545e-018	8.243e-050	8.730e-001	2.938e-037	4.303e-008	9.823e-037	1.473e-024	1.524e-012	8.994e-017	1.042e-013
HiMd	0.080	0.120	0.080	0.140	0.080	0.150	0.080	0.170	0.080	0.080	0.080	0.080
LoMd	0.080	0.080	0.080	0.080	0.080	0.080	0.080	0.080	0.080	0.080	0.080	0.080
HiMe	1.842	2.187	2.102	2.250	1.904	2.322	2.045	2.128	1.543	1.411	1.585	1.948
LoMe	1.520	1.864	1.221	1.497	1.791	1.461	1.654	1.731	2.257	1.734	2.048	1.556
HiSd	4.749	5.154	5.625	5.843	5.052	5.718	5.286	5.283	4.324	3.922	4.103	5.346
LoSd	4.659	5.517	3.335	4.244	5.133	4.330	4.377	4.916	5.717	4.557	5.416	4.619
HiSw	6.444	5.257	5.626	7.260	6.582	5.098	6.029	6.165	7.223	6.578	5.532	8.040
LoSw	9.997	7.172	6.896	7.289	8.207	6.813	6.386	6.085	5.790	6.328	5.950	7.267

Table 12. Validation results for Folsom

	JAN	FEB	MAR	APR	MAY	JUN	JUL	AUG	SEP	OCT	NOV	DEC
pKS	3.682e-015	4.322e-022	1.954e-016	1.856e-021	9.286e-005	4.402e-037	4.591e-010	7.149e-012	4.996e-023	8.728e-006	1.832e-013	5.224e-007
pRS	3.361e-019	4.788e-017	2.522e-014	2.619e-026	5.893e-002	3.100e-031	1.168e-006	3.398e-008	9.914e-018	9.805e-008	2.297e-015	6.113e-002
HiMd	0.030	0.030	0.030	0.030	0.020	0.030	0.030	0.030	0.020	0.020	0.020	0.020
LoMd	0.020	0.020	0.020	0.020	0.020	0.020	0.020	0.020	0.030	0.020	0.030	0.020
HiMe	1.243	1.444	1.326	1.448	1.208	1.461	1.341	1.368	1.037	0.904	1.002	1.249
LoMe	0.990	1.177	0.820	0.969	1.167	1.069	1.137	1.210	1.454	1.155	1.355	1.056
HiSd	3.203	3.756	3.781	3.823	3.476	3.951	3.640	3.700	2.899	2.647	2.904	3.473
LoSd	2.949	3.529	2.351	2.853	3.343	3.453	3.218	3.457	3.943	3.200	3.764	3.099
HiSw	6.078	5.630	6.154	5.989	6.237	5.443	5.939	6.144	6.332	6.986	6.168	6.620
LoSw	7.123	6.995	7.047	6.988	6.971	7.055	6.648	6.220	5.774	6.644	5.985	6.643

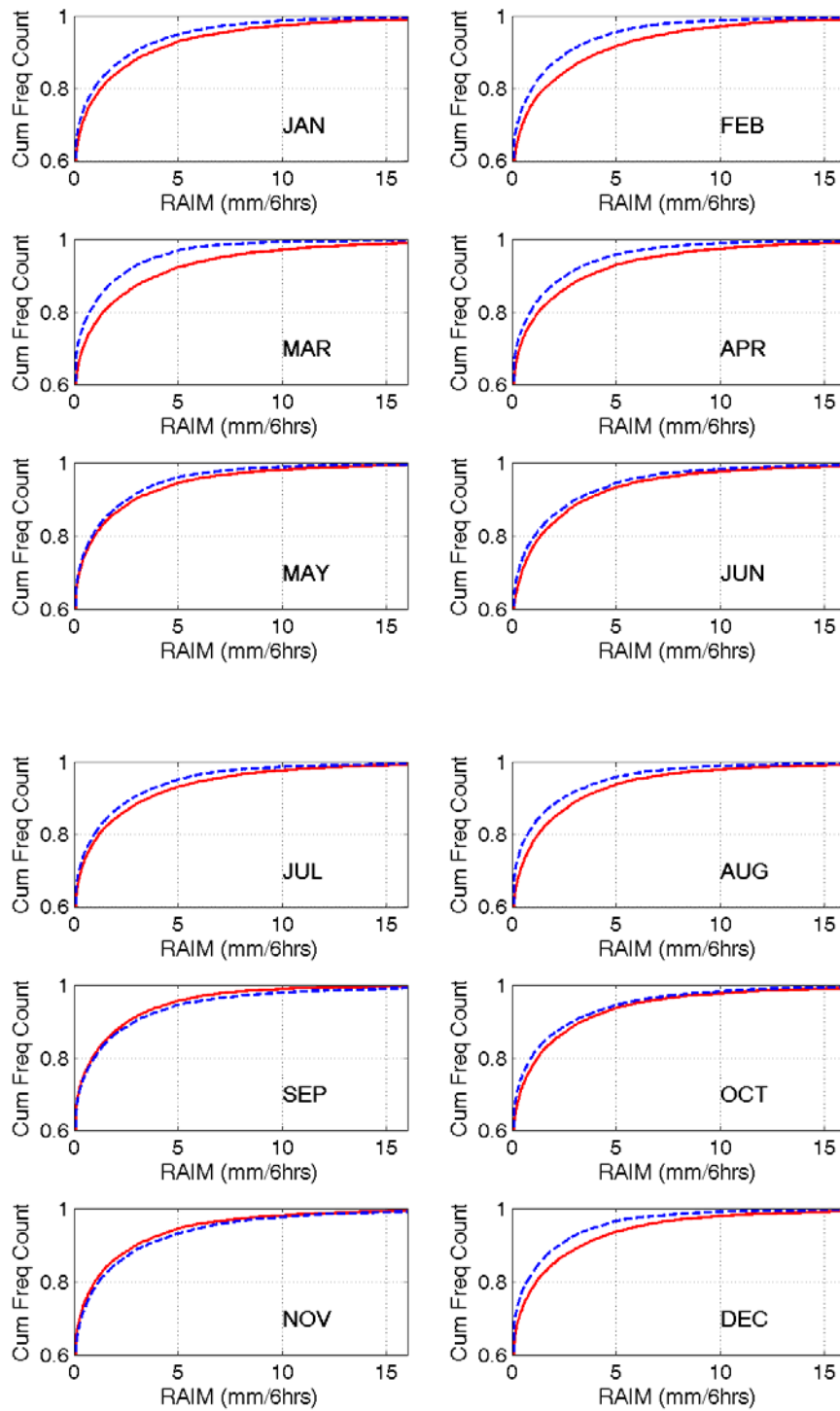


Figure 26. Cumulative probability distribution functions of rain-plus-melt values segregated according to high (red solid line) and low (dashed blue line) CFS monthly precipitation forecasts for Trinity and for each month of the year

Table 13. Validation results for Oroville

	JAN	FEB	MAR	APR	MAY	JUN	JUL	AUG	SEP	OCT	NOV	DEC
pKS	1.279e-014	5.796e-050	7.072e-010	5.089e-034	7.929e-001	2.104e-031	1.454e-002	6.957e-016	1.471e-013	4.808e-013	3.105e-007	6.532e-022
pRS	8.433e-021	6.453e-039	1.018e-009	1.364e-050	9.466e-001	1.828e-039	2.447e-001	1.922e-016	5.372e-015	5.645e-013	1.356e-007	3.185e-019
HiMd	0.080	0.080	0.080	0.080	0.080	0.110	0.080	0.080	0.080	0.070	0.080	0.080
LoMd	0.070	0.080	0.070	0.070	0.080	0.070	0.080	0.080	0.080	0.080	0.080	0.070
HiMe	1.494	1.724	1.677	1.822	1.474	1.886	1.603	1.681	1.235	1.144	1.269	1.605
LoMe	1.220	1.454	0.984	1.160	1.453	1.084	1.302	1.339	1.750	1.322	1.584	1.199
HiSd	3.395	3.721	4.423	4.204	3.777	4.540	4.011	3.898	3.100	3.015	3.187	3.980
LoSd	3.440	4.142	2.422	3.187	3.786	2.762	2.962	3.459	4.304	2.986	3.923	3.403
HiSw	5.673	4.880	6.113	5.914	6.695	6.070	5.682	5.453	6.652	7.140	6.458	6.560
LoSw	8.796	7.294	7.168	8.361	7.081	5.946	5.518	6.082	6.161	5.334	6.169	7.745

Table 14. Validation results for Shasta

	JAN	FEB	MAR	APR	MAY	JUN	JUL	AUG	SEP	OCT	NOV	DEC
pKS	9.891e-008	4.369e-077	9.293e-019	1.913e-045	1.236e-036	8.618e-043	1.500e-018	1.469e-016	5.038e-020	2.829e-045	1.189e-001	1.599e-007
pRS	2.617e-005	2.631e-065	3.129e-015	3.685e-045	9.222e-041	5.312e-027	4.423e-015	2.510e-012	2.829e-015	8.773e-043	2.712e-001	1.700e-005
HiMd	0.080	0.640	0.080	0.080	0.080	0.110	0.080	0.080	0.080	0.250	0.080	0.080
LoMd	0.080	0.080	0.070	0.080	0.070	0.080	0.080	0.070	0.070	0.080	0.080	0.070
HiMe	1.441	2.411	1.565	1.691	1.576	2.103	1.507	1.448	1.262	1.986	1.452	1.437
LoMe	1.439	1.669	0.957	1.153	1.096	1.420	1.241	1.173	1.261	1.245	1.502	1.129
HiSd	3.653	4.485	4.205	4.015	3.630	5.072	3.782	3.855	3.009	4.597	3.398	3.850
LoSd	3.625	4.467	2.448	3.241	3.509	3.799	3.544	3.107	3.879	3.114	4.083	3.174
HiSw	5.101	3.825	5.640	4.785	4.683	5.088	4.942	6.107	5.321	5.373	4.887	6.178
LoSw	6.515	6.703	5.873	7.756	8.309	5.466	7.008	5.641	6.946	5.459	6.275	6.166

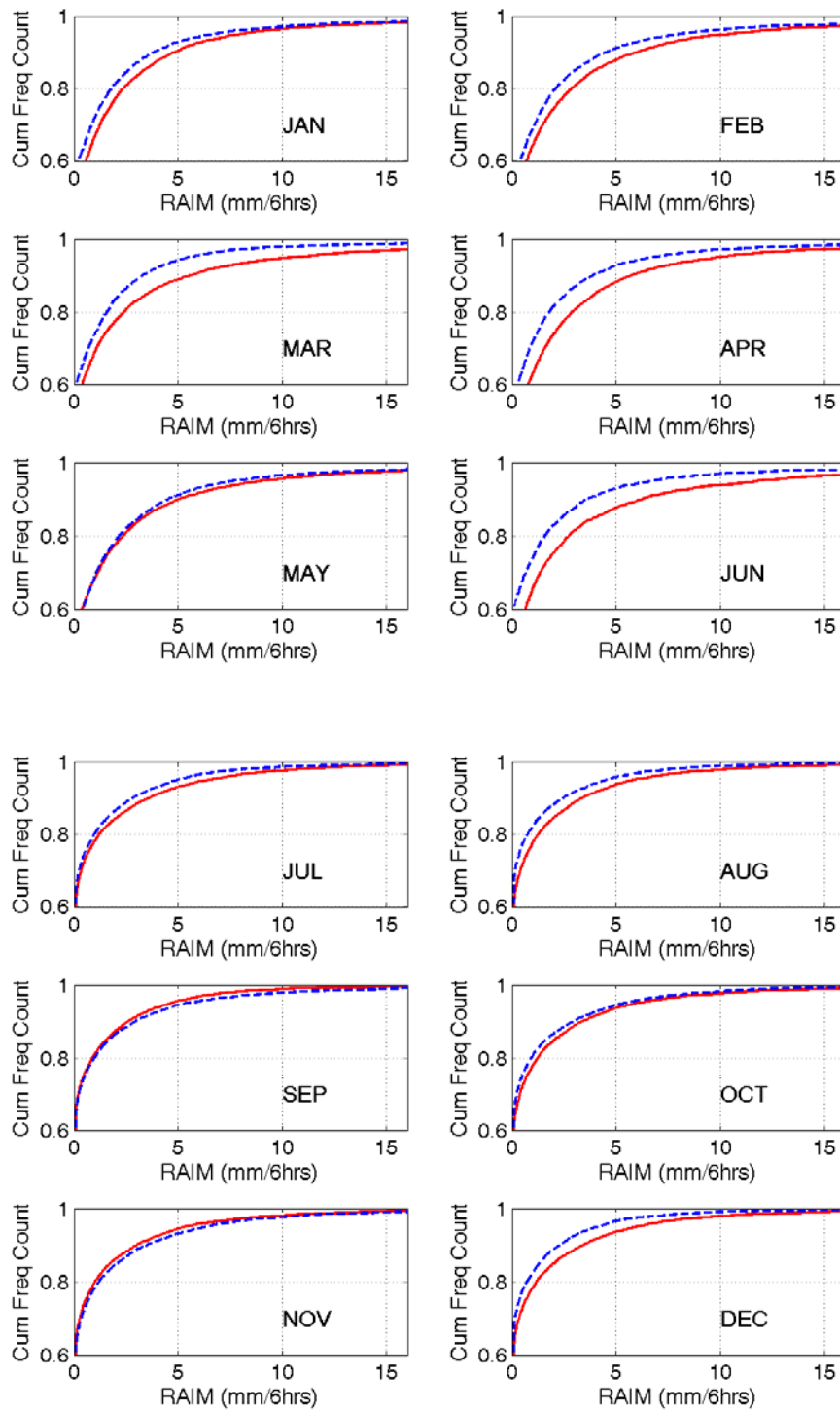


Figure 27. As in Figure 26, but for New Bullards Bar Reservoir drainage on the Yuba River

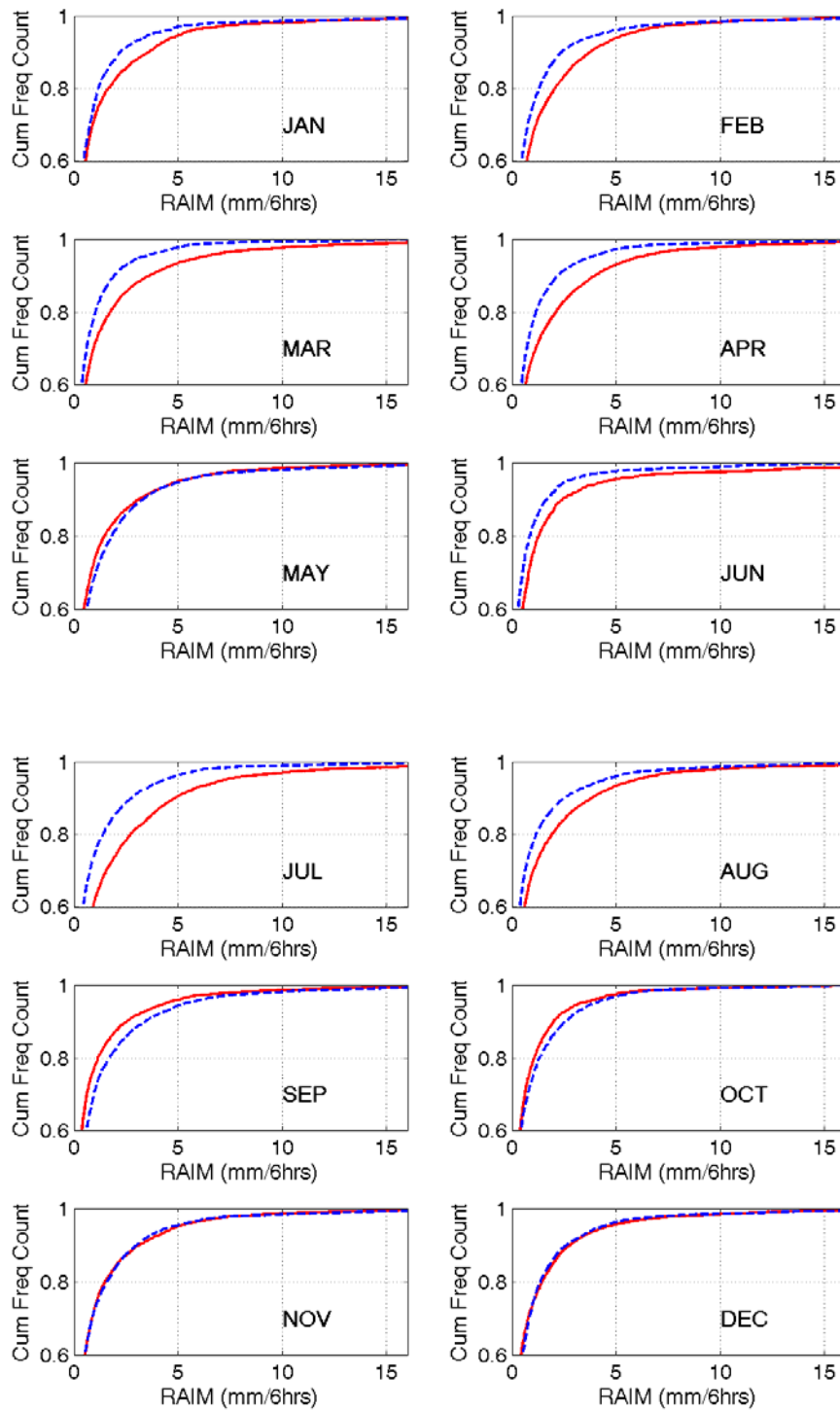


Figure 28. As in Figure 26, but for the Folsom Reservoir drainage on the American River

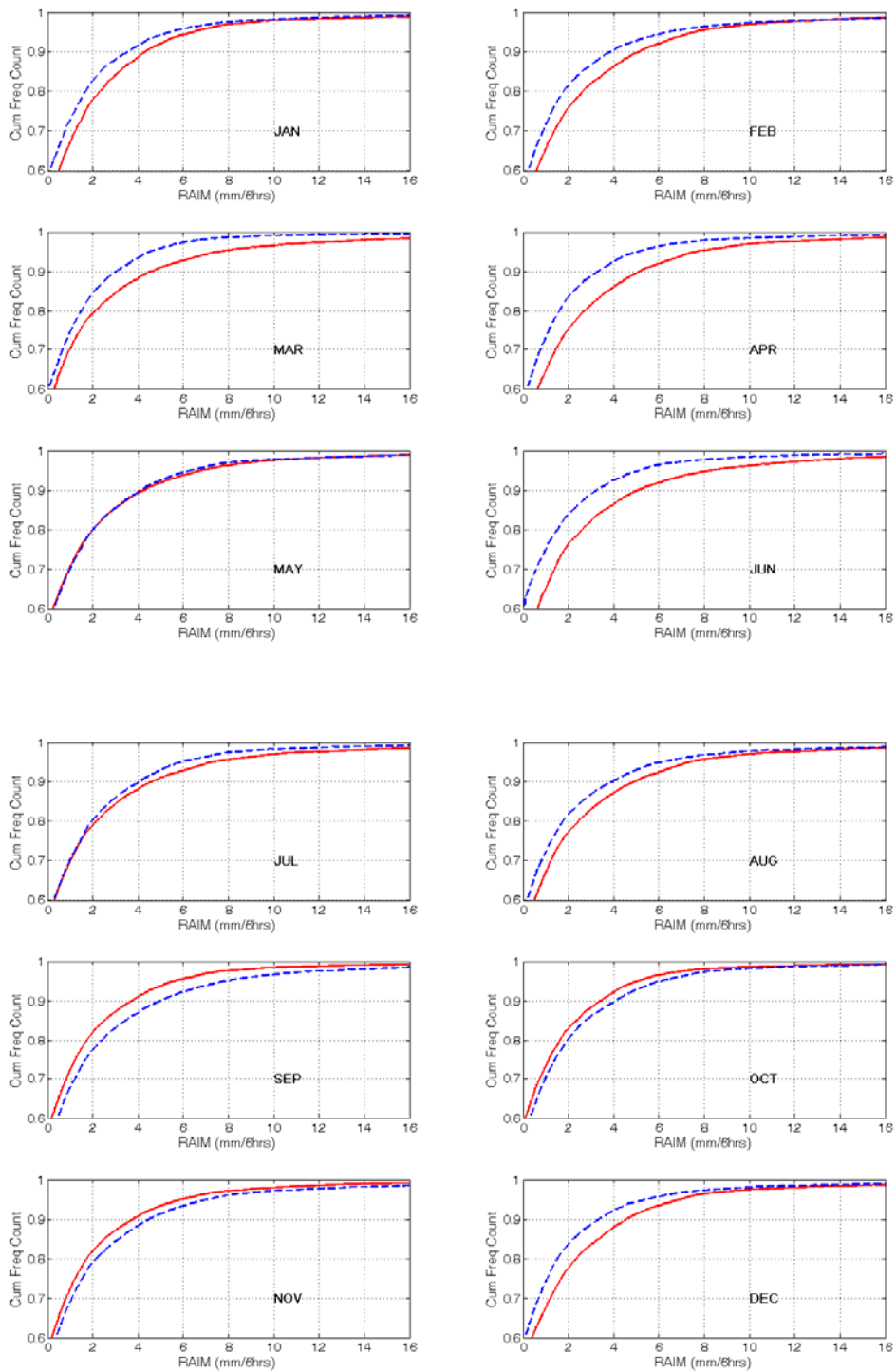


Figure 29. As in Figure 26, but for the Oroville Reservoir drainage on the Feather River

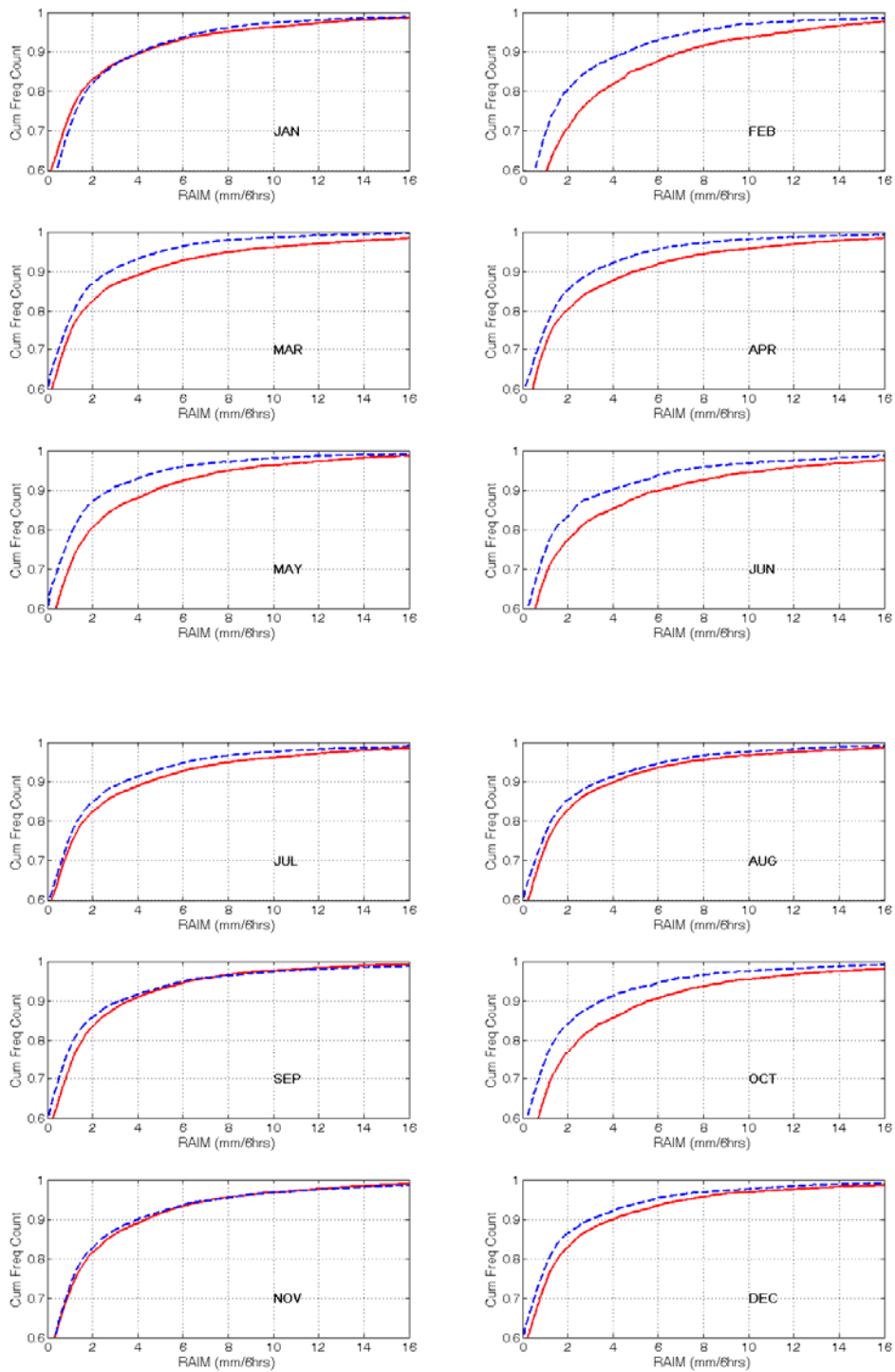


Figure 30. As in Figure 26, but for the Shasta Reservoir drainage on the Sacramento and Pit Rivers

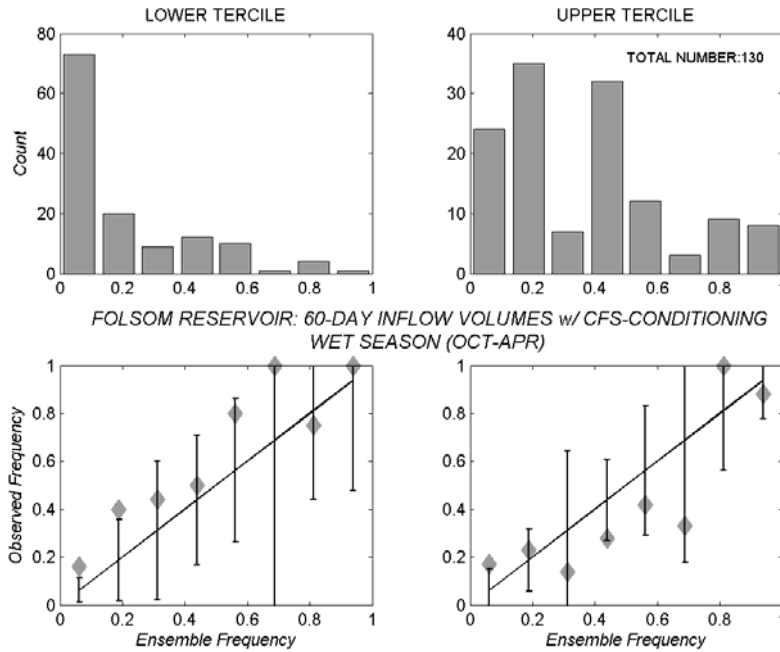


Figure 31. Reliability diagram for Folsom Reservoir 60-day inflow volumes in the lower tercile (left-hand column) and upper tercile (right-hand column) of the observed distribution. ESP conditioned on CFS.

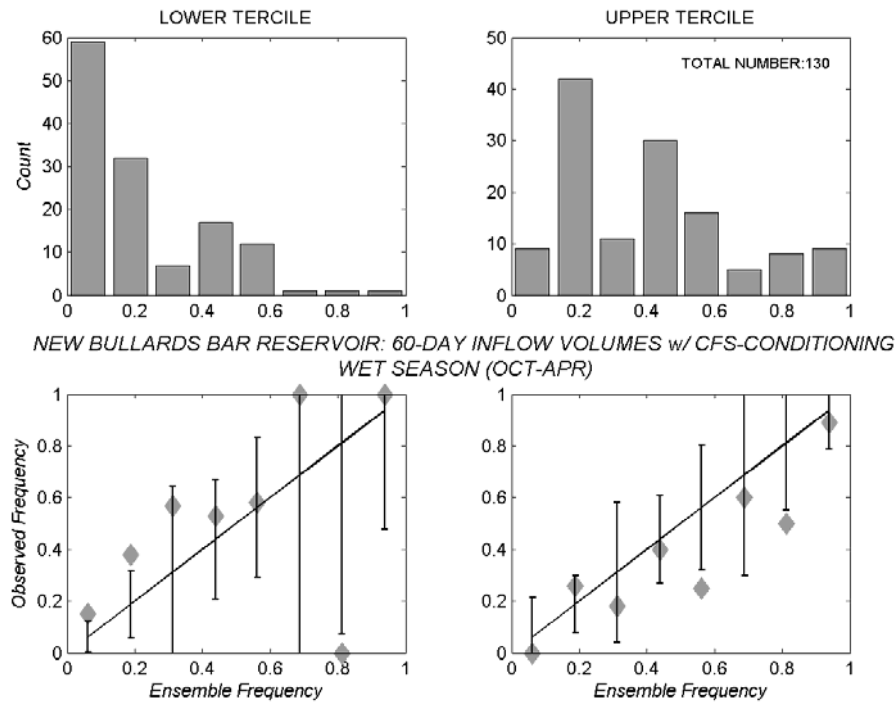


Figure 32. Reliability diagram, as in Figure 31, but for New Bullards Bar reservoir inflows

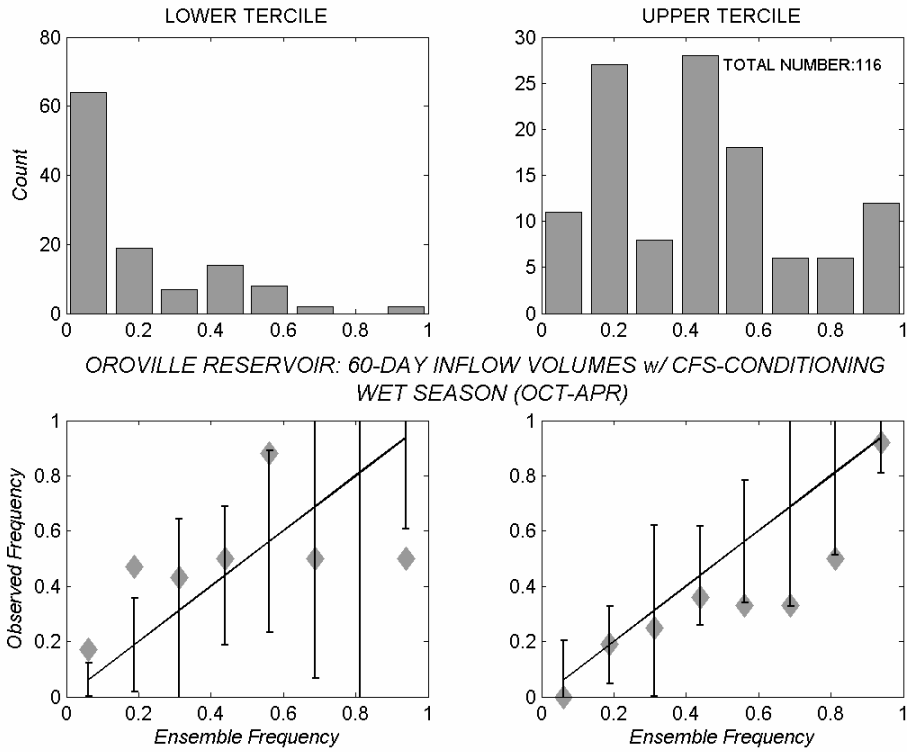


Figure 33. Reliability diagram, as in Figure 31, but for Oroville reservoir inflows

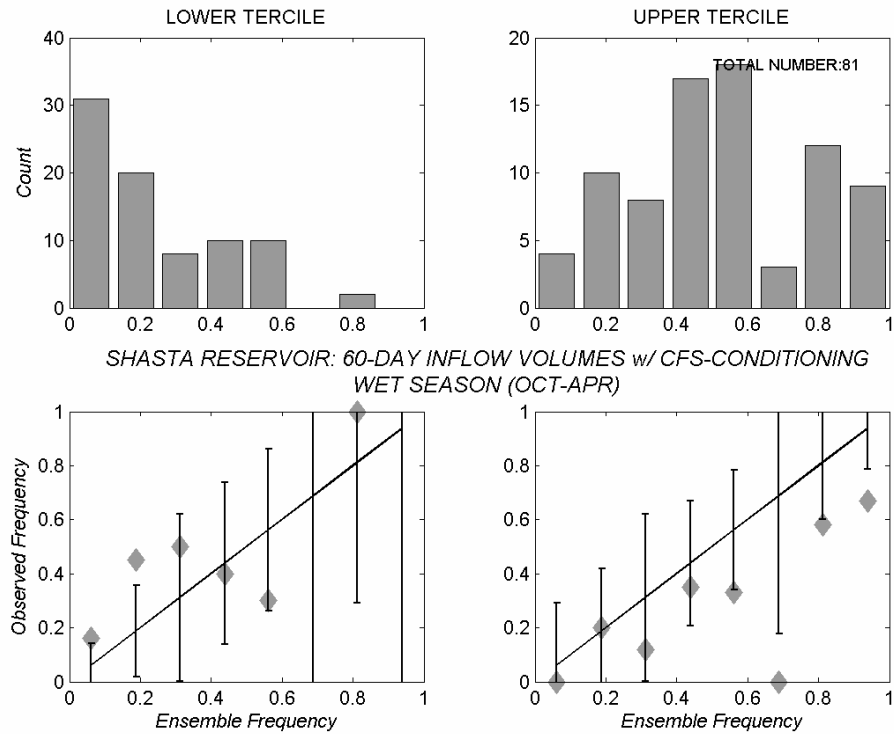


Figure 34. Reliability diagram, as in Figure 31, but for Shasta reservoir inflows

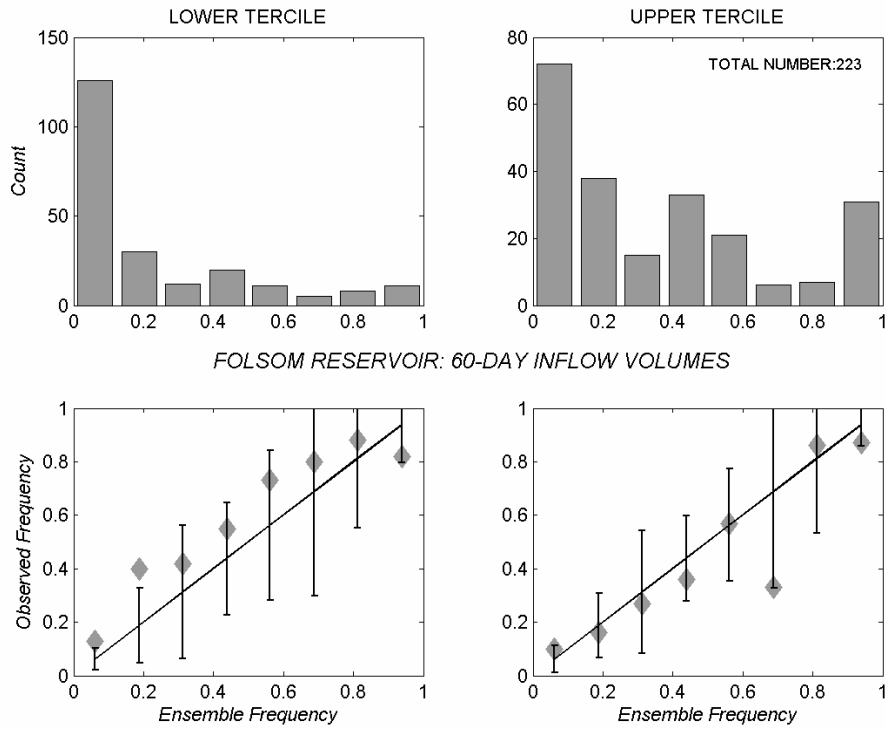


Figure 35. Reliability diagram, as in Figure 31, but for unconditional ESP with 15 ensemble members. Folsom reservoir inflows.

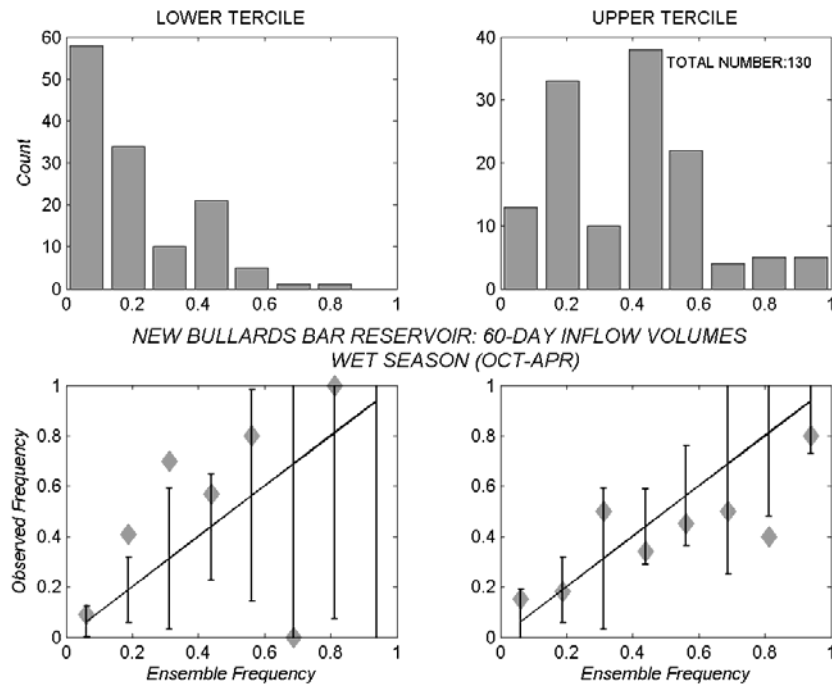


Figure 36. Reliability diagram, as in Figure 35, but for New Bullards Bar reservoir inflows

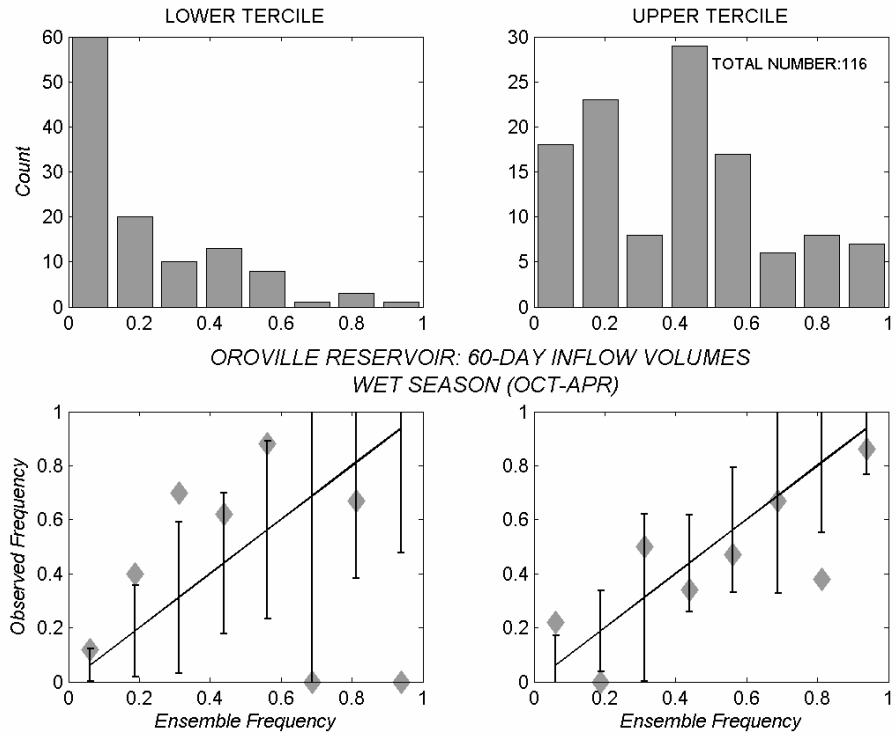


Figure 37. Reliability diagram, as in Figure 35, but for Oroville reservoir inflows

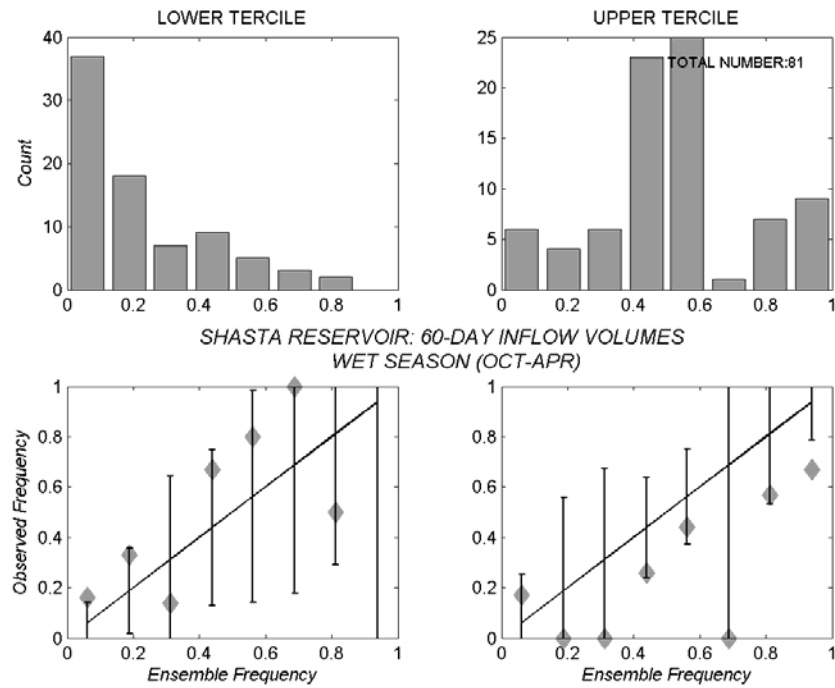


Figure 38. Reliability diagram, as in Figure 35, but for Shasta reservoir inflows

4.0 Hydrologic Models

4.1. Introduction

This chapter discusses the formulation and evaluates the performance of the land surface hydrology models of INFORM. The objective of the analysis is twofold: (1) to validate the operational hydrologic forecasts of reservoir inflow and, if necessary, refine the hydrologic model parameter values; and (2) to develop, implement and test the stand-alone hydrologic model for the entire INFORM area for use as part of the integrated INFORM system. The hydrologic component of INFORM consists of a snow accumulation and ablation model, the Sacramento soil water accounting model, and a channel routing model. These models are adaptations of the operational forecast models used at the CNRFC. The parameter sets of the INFORM snow and soil water models are drawn from those of the CNRFC models. The INFORM channel routing model differs from the operational routing model, but the parameters of these two models have a direct relationship. The analysis in this chapter uses historical data for the drainage areas of the four major Sierra Nevada reservoirs: Trinity, Shasta, Oroville, and Folsom.

The chapter first presents descriptions of the land surface hydrology model components, followed by a description of the model application drainage areas, and by a discussion of the subdivision into catchments for both the operational and stand-alone hydrologic models. Section 4.4 discusses the data collected to comprise the INFORM Project Hydrometeorological Database, with a complete listing of all data provided in Appendix D. Given the importance of snow accumulation for the Sierra Nevada water resources, the authors conducted a sensitivity analysis of the snow model with respect to parameters and input air temperature, with results presented in Section 4.5. The last section, and the bulk of this chapter, focuses on the evaluation of reservoir inflow simulations for both the operational and stand-alone models for the four major reservoirs. The assessment of the quality and utility of the real-time INFORM hydrologic forecasts is reserved for Chapter 6.

4.2. Formulation of Hydrologic Model Components

The objective of hydrologic models within INFORM is to represent the physical processes within each catchment of interest so that, when driven by atmospheric forcing (e.g., precipitation, temperature) and for known catchment physical characteristics (e.g., topography, land cover), the models generate streamflow hydrographs at the catchment outlet that reproduce the corresponding observed hydrographs. The National Weather Service River Forecast System (NWSRFS) that facilitates operations at the CNRFC contains a variety of hydrologic models and procedures for operational streamflow forecasting. Of interest in this work are the continuous-time hydrologic simulation model components, which are utilized for operational inflow modeling of the major Sierra Nevada reservoirs at CNRFC. These model components, adapted to suit the INFORM data environment, serve as the basis of the developed stand-alone INFORM hydrologic model. The model components estimate the catchment states (e.g., snowpack

liquid water equivalent, snowpack energy properties, soil water volume, and channel water volume) and outputs (e.g., rain plus snowmelt, runoff, and channel flow) at each time step on the basis of initial conditions and hydrometeorological input forcing. The three major model components include: snow accumulation and ablation (SNOW-17); basin rainfall-runoff model (Sacramento Soil Moisture Accounting (SAC-SMA)); and unit-hydrograph/channel routing procedures. A short description of the model components follows.

4.2.1. Snow Accumulation and Ablation Model

For the Sierra Nevada, special attention is given to the snow model. The Sierra Nevada intermittent seasonal snowpack contributes approximately 70% to the annual flow. The interaction of snow accumulation and melt controls seasonal flows and is responsible for the interannual flow regime. The snow model used is the NWS Hydro-17 model (often called *SNOW-17*). For a detailed description, the interested reader is referred to NOAA Technical Memorandum NWS HYDRO-17 (Anderson 1973) and NOAA Technical Report NWS 19 (Anderson 1976). This model is constructed to account for the energy and mass balance of the snowpack, and was developed to run in conjunction with a rainfall-runoff model. The model is driven by mean areal temperature (MAT) and mean areal precipitation (MAP), and computes the combined rain plus snowmelt input to the soil water model. The model requires values for 13 model parameters, as listed in Table 15. In addition, the model requires a relationship between snow water equivalent (SWE) and snow cover area (SCA), and another that relates terrain elevation to catchment area.

Mean areal temperature is used as an index for the energy exchange across the snow-air interface in the computation of snowmelt heat exchange and for the determination snowfall versus rainfall. The energy balance of the model is indexed by the pack heat deficit, which is used to refreeze available liquid water in the snowpack. Model states are the energy deficit in the snowpack, an antecedent temperature index that approximates snowpack temperature, the liquid water equivalent of the snowpack, and the volume of the liquid water of the snowpack. During periods with no precipitation but warm temperatures, a seasonally varied melt factor is used to produce the volume of melt. For rain-on-snow events, the model uses a simplified energy balance approach that considers temperature and precipitation data. The formulation also accounts for snow-soil interface flux, liquid water storage in the pack, and transmission of liquid water through the snowpack. To better understand the factors that affect the model, the authors conducted a sensitivity analysis with respect to the snow model input and parameters (Section 4.5).

Table 15. Hydrologic Model Parameters

SNOW MODEL PARAMETERS

<i>SCA</i> :	SNOW CATCH ADJUSTMENT FACTOR
<i>MFMAX</i> :	MAXIMUM MELT FACTOR (MM DEGC ⁻¹ D ⁻¹)
<i>MFMIN</i> :	MINIMUM MELT FACTOR (MM DEGC ⁻¹ D ⁻¹)
<i>NMF</i> :	MAXIMUM NEGATIVE MELT FACTOR (MME DEGC ⁻¹ D ⁻¹)
<i>PLWHC</i> :	FRACTION OF SNOW COVER FOR WATER HOLDING SNOW CAPACITY
<i>TIPM</i> :	PARAMETER FOR ANTECEDENT TEMPERATURE INDEX COMPUTATIONS
<i>MBASE</i> :	BASE TEMPERATURE FOR MELT COMPUTATIONS (DEGC)
<i>UADJ</i> :	AVERAGE DAILY WIND FUNCTION FOR RAIN-ON-SNOW PERIODS (MM MB ⁻¹ DAY ⁻¹)
<i>DAYGM</i> :	CONSTANT MELT AT SNOW-SOIL INTERFACE (MM DAY ⁻¹)
<i>PXTEMP</i> :	TEMPERATURE TO DELINEATE RAIN FROM SNOW (DEGC)
<i>SI</i> :	MAXIMUM SWE FOR 100% COVER IN SNOW DEPLETION CURVE (MM)
<i>ELV</i> :	ELEVATION OF CENTROID OF BASIN (10 ² M)
<i>PADJ</i> :	PRECIPITATION ADJUSTMENT FACTOR

SACRAMENTO MODEL PARAMETERS

<i>UZTWM</i> :	UPPER ZONE TENSION WATER CAPACITY (MM)
<i>UZFWM</i> :	UPPER ZONE FREE WATER CAPACITY (MM)
<i>LZTWM</i> :	LOWER ZONE TENSION WATER CAPACITY (MM)
<i>LZFPM</i> :	LOWER ZONE FREE PRIMARY WATER CAPACITY (MM)
<i>LZFSM</i> :	LOWER ZONE FREE SUPPLEMENTARY WATER CAPACITY (MM)
<i>DU</i> :	INTERFLOW RECESSION (6HRS ⁻¹)
<i>DLPR</i> :	RECESSION COEFFICIENT FOR LOWER ZONE FREE PRIMARY WATER ELEMENT (6HRS ⁻¹)
<i>DL DPR</i> :	RECESSION COEFFICIENT FOR LOWER ZONE FREE SUPPLEMENTARY WATER ELEMENT (6HRS ⁻¹)
<i>EPS</i> :	CONSTANT FACTOR IN PERCOLATION FUNCTION
<i>THSM</i> :	EXPONENT IN PERCOLATION FUNCTION
<i>PF</i> :	FRACTION OF PERCOLATION BYPASSING THE LOWER ZONE TENSION WATER ELEMENT
<i>XMI OU</i> :	FRACTION OF WATER LOST TO DEEP GROUNDWATER LAYERS
<i>ADIMP</i> :	ADDITIONAL IMPERVIOUS AREA MAXIMUM FRACTION
<i>PCTIM</i> :	FRACTION OF PERMANENTLY IMPERVIOUS AREA
<i>ETADJ</i> :	EVAPOTRANSPIRATION DEMAND ANNUAL ADJUSTMENT FACTOR

CHANNEL MODEL PARAMETERS

<i>n_c</i> :	NUMBER OF LINEAR RESERVOIRS REPRESENTING THE CHANNEL SEGMENT
<i>α</i> :	COMMON COEFFICIENT OF LINEAR RESERVOIRS WITH INVERSE DESCRIBING TRAVEL TIME (6HRS ⁻¹)

4.2.2. Sacramento Soil Moisture Accounting Model (SAC-SMA)

The soil water accounting component of the NWSRFS applied within the INFORM study region is the Sacramento soil moisture accounting model, SAC-SMA. It is a continuous simulation model of the wetting and drying processes in the soil and produces surface and sub-surface flows that feed the basin channel network. The discrete form of the model has been described in Burnash et al. (1973) while a continuous time form is described in Georgakakos (1986). The model is used operationally by the CNRFC to produce streamflow estimates and forecasts for basins with drainage areas of the order of a hundred to a thousand km² ($O[100-1000 \text{ km}^2]$). The model requires input in the form of MAP or rain-plus-snowmelt (as estimated by the snow model component) and evapotranspiration demand (ETD), and yields estimates of total runoff volume to the receiving channels. Model states represent the volume of soil water (depth integrated soil moisture) in each model soil water compartment for an upper and a lower soil layer, and for a time-varying impervious area. The effectiveness of the SAC-SMA model to reproduce high flow conditions under spatially lumped and spatially distributed implementations is most recently demonstrated by the results of the Distributed Modeling Intercomparison Project (DMIP) organized by the NWS Office of Hydrologic Development (Smith et al. 2004; Reed et al. 2004).

The SAC-SMA model requires estimation of a set of model parameters, as given in Table 15. The parameters describe the soil water holding capacity of various model storage zones, withdrawal rates from these storages, the characteristics of the exchange between the upper and the lower zone zones, and the nature of changes in impervious area. These parameters are typically estimated through calibration based on historical precipitation, temperature, and streamflow records. The aim of the calibration is to reproduce the observed streamflow at the outlet of the watershed of interest without persistent biases, while at the same time capturing extreme high and low flows (NOAA 1999).

The SAC-SMA model runs operationally at CNRFC for several basins within the INFORM study region. The California Nevada River Forecast Center produces streamflow estimates and forecasts at several regular forecast preparation times with a resolution of six hours. At the completion of the operational forecast run, the current estimates of the volumes in each of the model soil water compartments, valid at the particular forecast preparation time, are stored for subsequent use as initial conditions for future forecast runs of the model when new forecast or observed input (MAP, MAT, and/or ETD) becomes available. In some regions (e.g., Forks of the American River), the model has been complemented with a state estimator for the assimilation of discharge observations and for the generation of variance estimates for the real-time flow forecasts (Georgakakos 2002).

4.2.3. Unit Hydrograph and Channel Routing Procedures

To translate the volume of runoff produced by the SAC-SMA in the form of total channel inflow into streamflow rate, the CNRFC typically employs unit hydrographs (e.g., Bras 1990). These characterize the surface response of a catchment on the basis of several unit-hydrograph ordinates that must be estimated from historical data. Calibration is typically done jointly with the SAC-SMA parameters (NOAA 1999). Although well suited and successful for areas with historical databases, unit hydrographs are not easily transferable to areas with no historical data. Routing models that consist of cascades of conceptual reservoirs are more flexible because: (1) the user can estimate their parameters from channel geometry and roughness data in lieu of historical data (e.g., Georgakakos and Bras 1982), and (2) for linear conceptual reservoir response, their parameters bear a direct relationship to those of the unit hydrograph models (e.g., Singh 1992 or Sperflage and Georgakakos 1996). The unit hydrographs are used with parameters calibrated by the CNRFC. The INFORM stand-alone hydrologic system uses a linear reservoir routing model with parameters that are estimated as part of the calibration process.

4.2.4. Stand-Alone Distributed Hydrologic Model

The INFORM system stand-alone hydrologic model was designed for reservoir inflow simulation. The model components include a version of the snow accumulation and ablation model (Anderson 1973), the Sacramento soil moisture accounting model as described in Georgakakos (1986), and the linear conceptual reservoir channel routing model of Georgakakos and Bras (1982). For several of the INFORM reservoir drainage areas, the stand-alone hydrologic component offers a more refined subdivision of the upstream drainage areas than that represented in the CNRFC operational hydrologic model. The authors subdivided the reservoir drainage areas into catchments considering terrain differences, channel network topology, reservoir locations, and streamflow gauging sites. The Geographic Information System (GIS) software *GRASS* delineated these catchments by processing 90-meter digital terrain elevation data and stream network information. The authors followed this more refined distributed modeling approach for the stand-alone hydrologic model in order to improve channel routing simulations for the available six-hourly data resolution. Section 4.3 highlights differences in the hydrologic model spatial representations of the major reservoir drainage areas.

It is important to note that the stand-alone hydrologic model was designed to use the same input and similar model components as the operational hydrologic forecast model. Thus, as mentioned earlier, the parameters of the stand-alone distributed hydrologic model (listed in Table 15) bear close relationship to the parameters of the operational hydrologic model. The staff of CNRFC provided model parameter values and historical records of MAP and MAT input. For each catchment, the snow and soil water models produce rain-plus-melt and channel inflow volumes. These volumes then feed the channel routing model, which transports and attenuates the flows through the channel

network. The kinematic channel routing component of the stand-alone model is based on a series of linear reservoirs with identical parameters (Table 15). The sum of the values of the inverse of the channel routing α -parameter for all linear reservoirs representing a single channel segment approximates the travel time in the channel segment. Calibration of the routing component of the stand-alone model used available observed streamflow data to calibrate this α parameter (see Section 4.6.3). In addition to reservoir inflows for the INFORM application area, the stand-alone distributed hydrologic model produces stream outflow at each catchment outlet.

4.3. Hydrologic Model Application Basins

This section discusses the catchment representations of (1) the CNRFC operational hydrologic model, and (2) the INFORM stand-alone distributed hydrologic model, for the drainage areas of the four major reservoirs of study. The reservoir drainage areas are shown in Figure 39 and correspond to the following outlet locations:

- Trinity (Clair Engle) Lake on the Trinity River
- Shasta Reservoir on the Sacramento, McCloud, and Pit Rivers
- Oroville Reservoir on the Feather River
- Folsom Reservoir on the American River

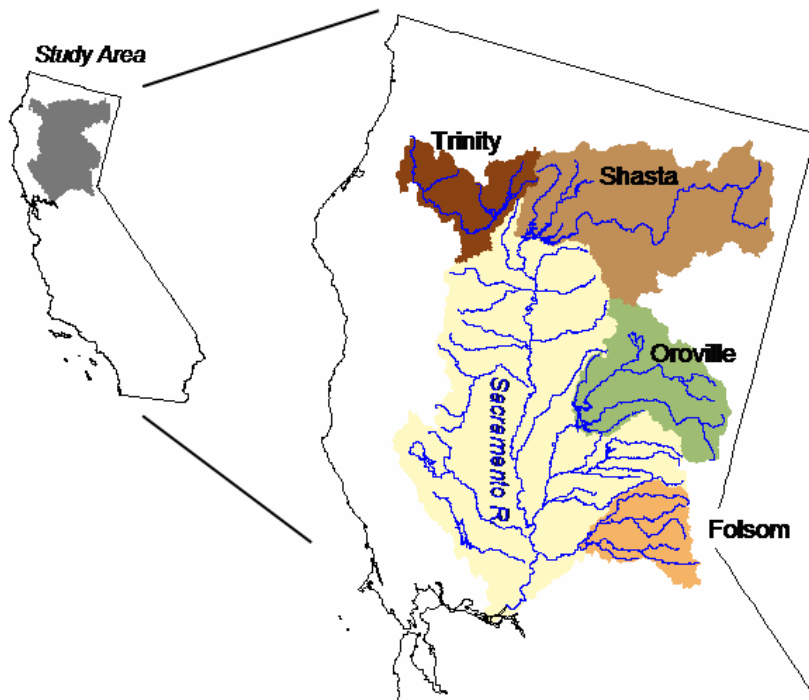


Figure 39. Location of four major Sierra Nevada reservoir watersheds within Northern California

Figures 40 to 43 are schematics of the structure of the CNRFC operational hydrologic model of each reservoir drainage area at the commencement of the INFORM Project. Figures 44 to 47 illustrate the stand-alone distributed hydrologic model representations of each reservoir drainage area. The representations as treated in INFORM are described briefly in the following sections. It is noted that since these operational and stand-alone model representations were developed for the INFORM Project, CNRFC has made changes in the operational hydrologic model area representations (particularly for the drainage area of Folsom reservoir).

4.3.1. Basin Representations for CNRFC Operational Hydrologic Models

For operational hydrologic modeling, CNRFC staff has subdivided the reservoir drainage areas into major catchments based on major drainage divides and available streamflow gauging locations. CNRFC further divided each major catchment area into upper and lower elevation reaches based on climatological estimates of the snow line elevation. Hydrometeorological input and hydrologic model components are applied at the major catchment scales. Table 16 contains a listing of the major catchments and their area for each reservoir drainage area.

Figure 40 presents the schematic of the structure of the operational hydrologic model for Folsom Reservoir. It includes four major catchments: the North, Middle, and South Forks of the American River, plus the Folsom reservoir local area drainage. The first three catchments are further subdivided into upper and lower areas using an elevation cutoff of 1,500 m (5,000 feet, ft). As noted above, further division of the Folsom reservoir drainage basin has subsequently been adopted at CNRFC for operational hydrologic forecasting to better represent the regulation in the upper reaches of the watersheds. Due to the late timing, these changes were not considered in the INFORM project analyses.

The Trinity Lake drainage area is treated as a single major catchment for operational forecast purposes, with upper and lower area subdivisions based on an elevation threshold of 1,500 m (5,000 ft). Figure 41 shows the simple schematic representation of the operational hydrologic model for Trinity.

Figure 42 presents the schematic of the operational model for the Shasta drainage area. Five major catchments comprise this drainage area, representing the Shasta reservoir local area drainage, the Sacramento River at Delta, the McCloud River, and the Pit River at Canby and at Montgomery Creek. Each catchment is further sub-divided into upper and lower areas using a 1,500 m (5000 ft) elevation for the Delta and McCloud and an elevation of 1,650 m (5,500 ft) for the two sub-watersheds of the Pit River. The Iron Canyon Diversion diverts water from the McCloud River to the Pit River. The operational model accounts for it as a conceptual basin that receives the same model forcing as the lower Pit River.

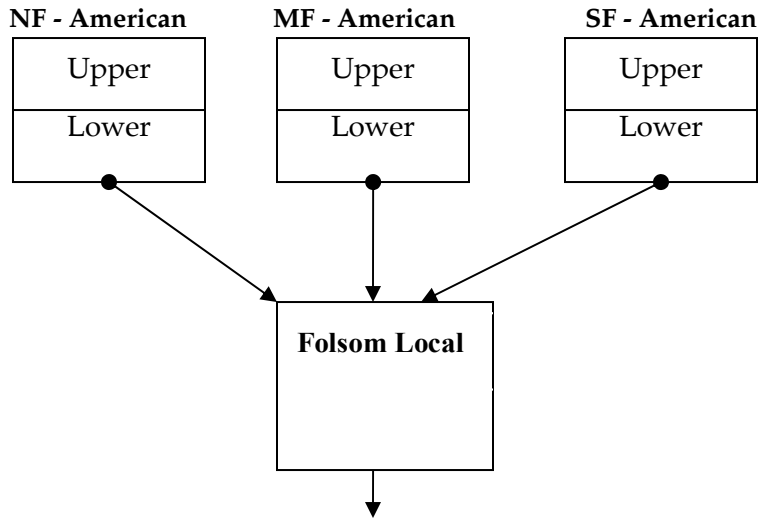


Figure 40. Schematic structure of the simulation model of the American River drainage into Folsom Reservoir for the CNRFC operational hydrologic model

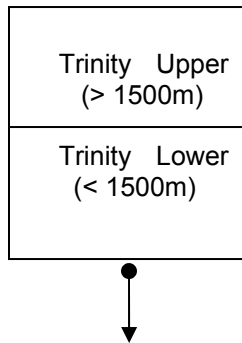


Figure 41. As in Figure 40, except representing the operational hydrologic model for the Trinity River drainage into Trinity Lake

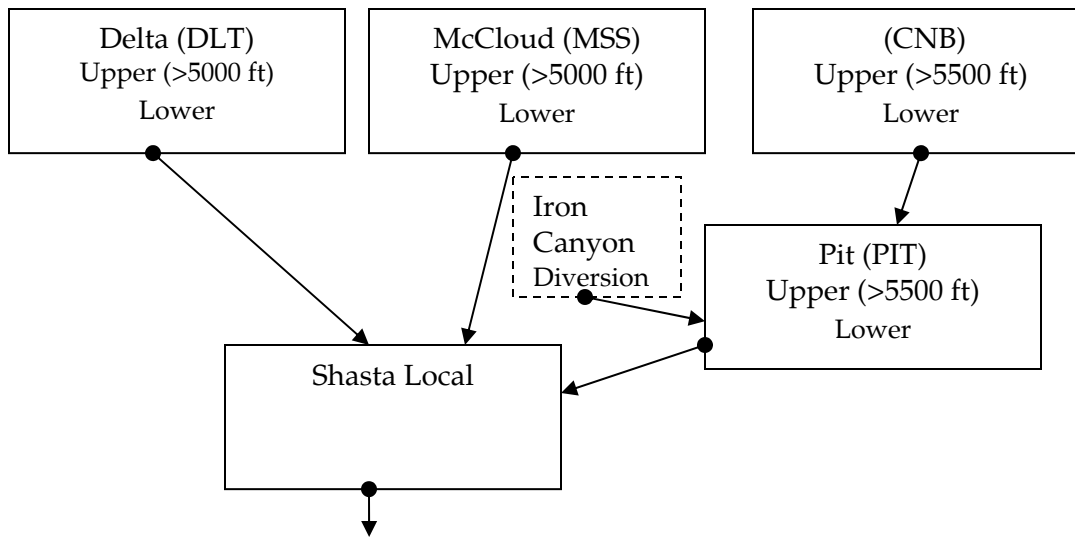


Figure 42. As in Figure 40 except representing the operational hydrologic model for the Sacramento River drainage into Shasta Reservoir

Figure 43 illustrates the operational model structure for the Oroville drainage area. This drainage area is sub-divided into six major catchments, representing the North Fork of the Feather River at Lake Almanor and at Pulga, Indian Creek, the Middle Fork of the Feather River at Clio and at Merrimac, and the Oroville reservoir local area drainage. Each major catchment is further subdivided into upper and lower areas using the 1,500 m (5,000 ft) elevation.

4.3.2. Basin Representations for the Stand-Alone Distributed Hydrologic Models

It was previously noted that the INFORM stand-alone distributed hydrologic models were designed to use the same input and similar models as the CNRFC operational hydrologic models. An important objective of the stand-alone model development was to represent the reservoir drainage basins in a distributed fashion in order to render the channel routing component response consistent with the high temporal resolution of the simulations (i.e., six hours). This distributed approach considered catchments with drainage areas of the order of a few hundred km² ($O[100 \text{ km}^2]$), considering such factors as stream topology, the climatological snow line elevation threshold, and streamflow gauging locations. Hydrometeorological forcing input and the snow and soil model components are applied for the upper and lower elevation reaches of the major catchments defined by CNRFC (see Table 16). The runoff volume generated for each distributed catchment was apportioned according to drainage area and was routed downstream in the high resolution INFORM channel network using the channel routing component based on linear conceptual reservoirs. Table 17 contains catchment characteristics for the stand-alone distributed hydrologic model.

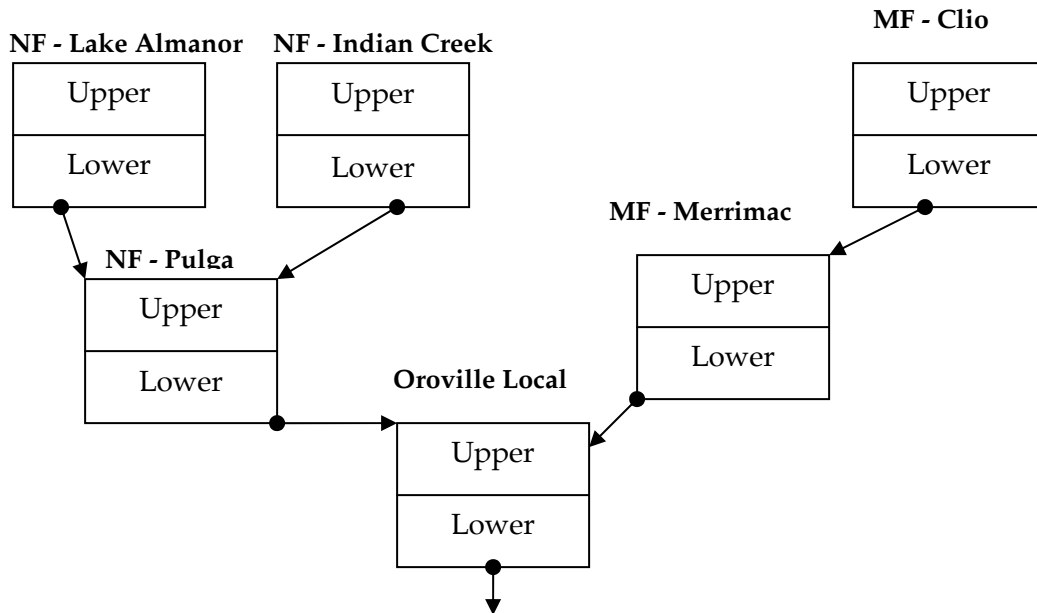


Figure 43. As in Figure 40, except representing the operational hydrologic model for the Feather River drainage into Oroville Reservoir

Figures 44 through 47 illustrate the INFORM distributed hydrologic model representations for each of the four major reservoir basins (Folsom, Trinity, Shasta, and Oroville, respectively). Part (a) of each figure shows the distributed model catchments in varying color with the stream network (in blue) and the CNRFC-defined major sub-watersheds (thick black outlines). For example, Figure 44a outlines the four major catchments of the Folsom reservoir drainage area—the North, Middle and South Forks of the American River, and the Folsom reservoir local area drainage—with the varying colors within each major catchment representing the distributed model catchments. For each reservoir, the distributed model catchments represent an area that is entirely in the upper elevation reach or in the lower elevation reach of a major catchment, such that the runoff apportionment is simplified. Part (b) of each figure presents a schematic of the routing structure for each reservoir drainage area. The complexity of the routing network varies for each reservoir drainage area, depending on the size and nature of the catchment and stream network. There are just 9 routing segments for the Folsom reservoir drainage area, while the Shasta reservoir drainage area has nearly 50 routing segments. The authors discuss the routing schematics next using the Folsom reservoir drainage area as an example.

The Folsom reservoir drainage area contains 9 routing segments, as shown in Figure 44b. The first of these represents the upper and lower elevation catchments of the North, Middle, and South Forks (e.g., NF_up, NF_lo, etc.). For each fork, runoff from an upper catchment is routed to that catchment’s outlet and it is input to the downstream lower catchment. It is then combined with lower catchment runoff, and it is then routed to the lower catchment outlet. The total channel flow from the Middle Fork lower catchment (MF_lo) is routed through a “junction catchment” (JCT1) with this catchment’s runoff, and is summed with the North Fork lower catchment outlet flow (NF_lo). Likewise, the

total channel flow from the South Fork lower catchment (SF_lo) is routed through a second junction catchment (JCT2), it is combined with the junction catchment's runoff, and it is summed with both the North Fork-Middle Fork combined channel flow and the Folsom reservoir local runoff (FOL-LOCAL). This combined channel flow (at SUM2) is then routed to the reservoir inflow point (FOLSOM DAM).

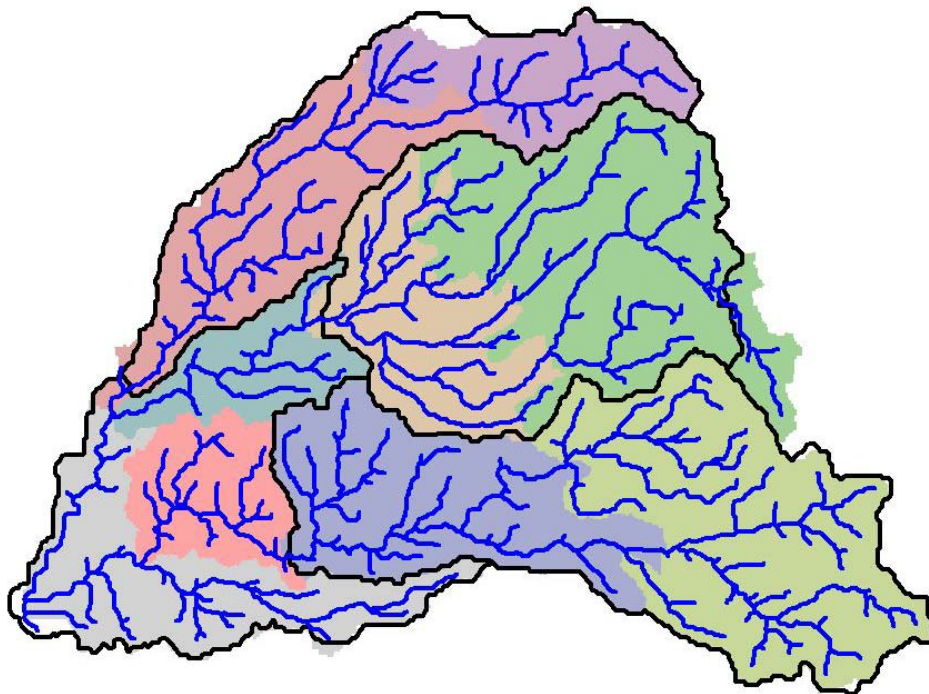
In a straightforward manner, similar routing descriptions can be derived from the schematics of Figures 45b through 47b. For brevity, such descriptions will not be presented here. It is noted that 13 routing segments were used for the Trinity Lake drainage basin to represent the main stem Trinity River and tributaries of the East Fork, Coffee Creek, Swift Creek, Covington Creek, and Stuart Creek. There are 49 routing segments within the five major catchments of the Shasta reservoir drainage and 51 segments within the six major catchments of the Oroville reservoir drainage.

Table 16. Drainage areas of CNRFC major catchments

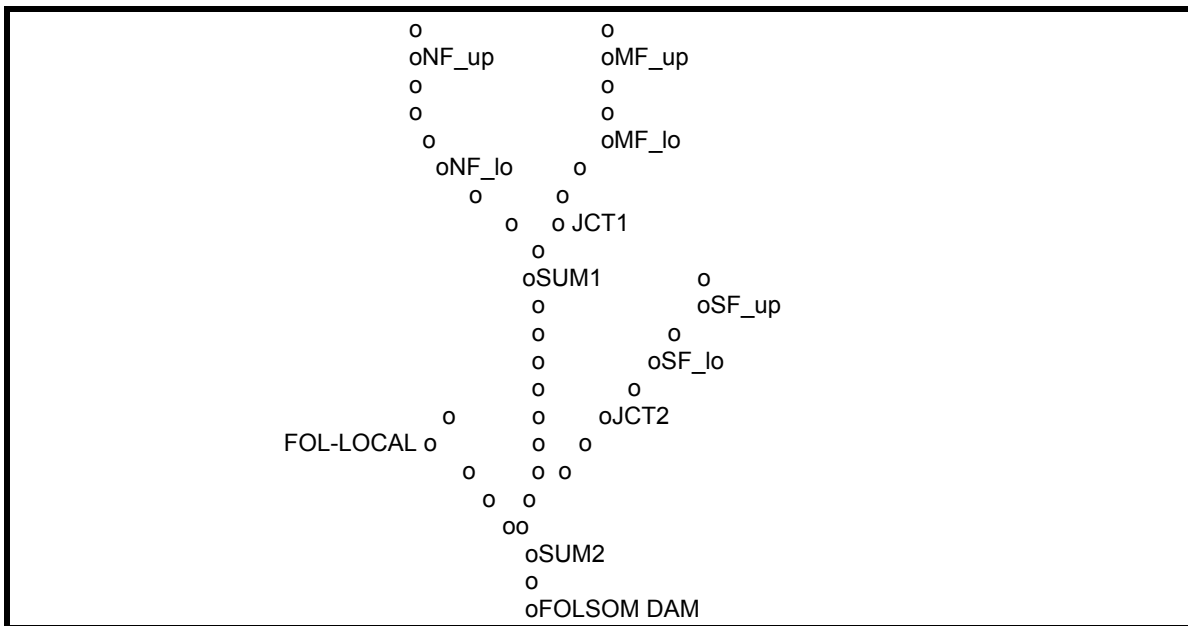
	<i>Upper Elev</i>	<i>Lower Elev</i>	<i>Total Area (km²)</i>
<u>American</u>			
North Fork	325.1	550.4	875.5
Middle Fork	713.0	533.5	1246.5
South Fork	898.6	632.3	1530.9
Folsom Local		1016.3	1016.3
<u>Trinity</u>			
	842.0	949.5	1791.5
<u>Shasta</u>			
Pit River, Canby	1148.9	2557.1	3706.0
Pit River, Mont. Creek	1914.2	7201.3	9115.5
McCloud River	437.8	1125.9	1563.7
Sacramento R, Delta	296.8	802.2	1099.0
Iron Canyon		2011.6	2011.6
Shasta Local		1165.0	1165.0
<u>Feather</u>			
North Fork, Lake Almanor	965.7	305.5	1271.2
Indian Creek	1492.2	421.0	1913.2
North Fork, Pulga	748.7	1123.1	1871.8
Middle Fork, Clio	1367.5	408.5	1776.0
Middle Fork, Merrimac	574.3	399.1	973.4
Oroville Local	245.2	1287.4	1532.6

Table 17. Properties of stand-alone distributed model catchments

	<i>Number of sub-basins in Upper Elev</i>	<i>Average Area (km²)</i>	<i>Number of sub-basins in Lower Elev</i>	<i>Average Area (km²)</i>
<u>American</u>				
North Fork	1	325.1	1	550.4
Middle Fork	1	713.0	1	533.5
South Fork	1	898.6	1	632.3
Folsom Local			3	338.8
<u>Trinity</u>	5	168.4	8	118.7
<u>Shasta</u>				
Pit River, Canby	4	287.2	4	639.3
Pit River, Mont. Creek	8	239.3	17	423.6
McCloud River	1	437.8	5	225.2
Sacramento R, Delta	1	296.8	3	267.4
Iron Canyon			1	2011.6
Shasta Local			5	233.0
<u>Feather</u>				
North Fork, Lake Almanor	3	321.9	1	305.5
Indian Creek	5	298.4	4	105.2
North Fork, Pulga	4	187.2	7	160.4
Middle Fork, Clio	6	277.9	1	408.5
Middle Fork, Merrimac	5	114.9	4	99.8
Oroville Local	3	81.7	8	160.9

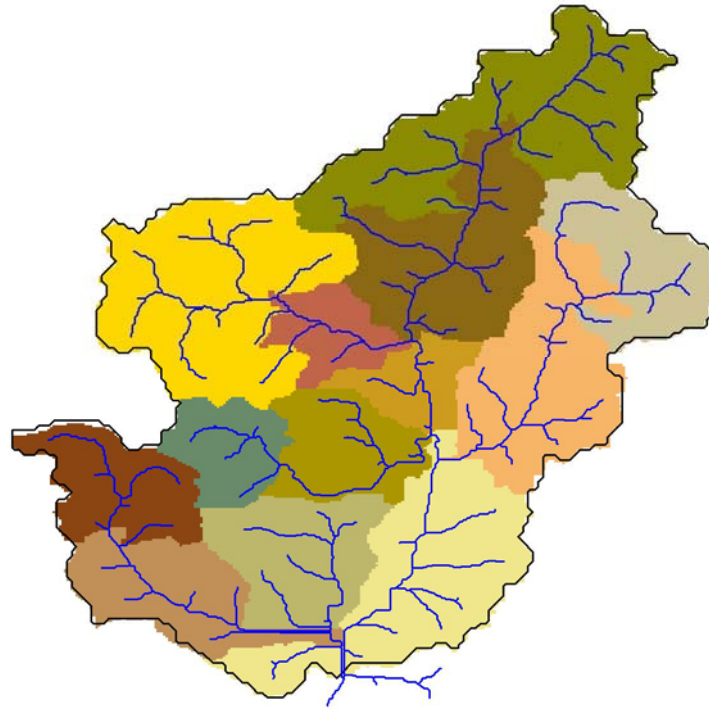


(a)

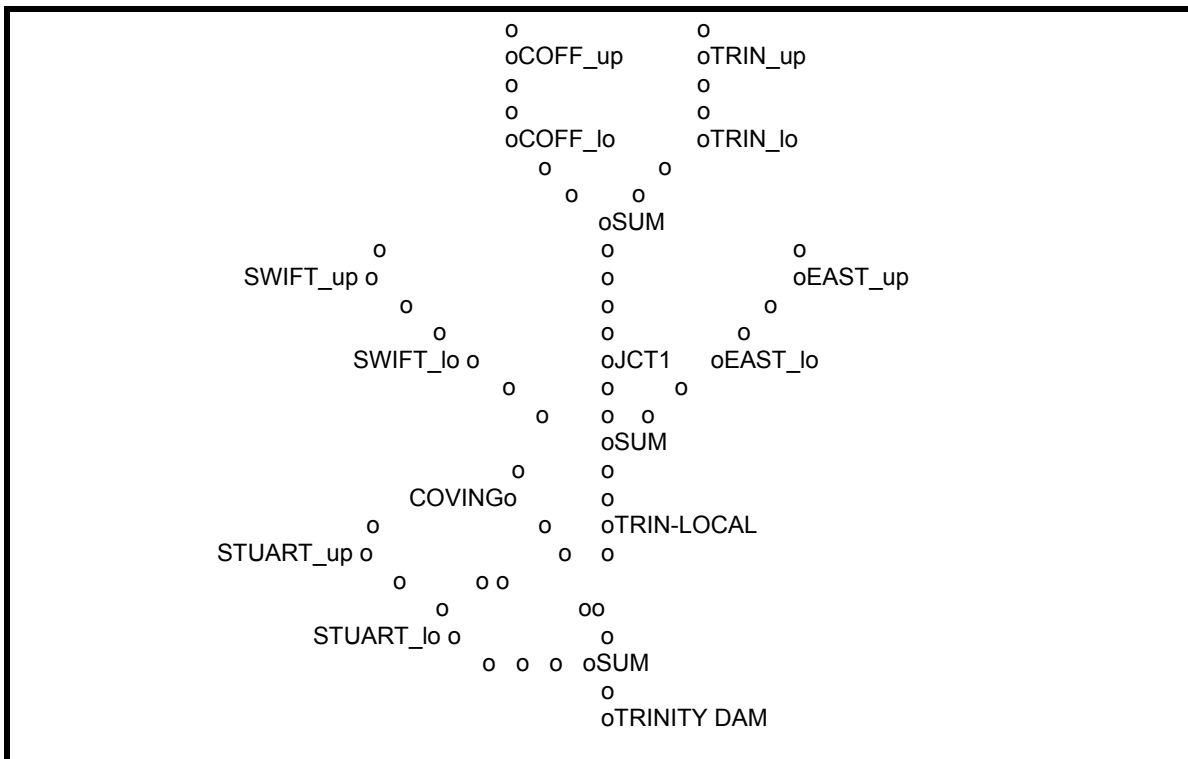


(b)

Figure 44. (a) Representation of the stand-alone distributed model of the American River drainage to Folsom Reservoir. (b) Schematic structure of routing network in this representation.

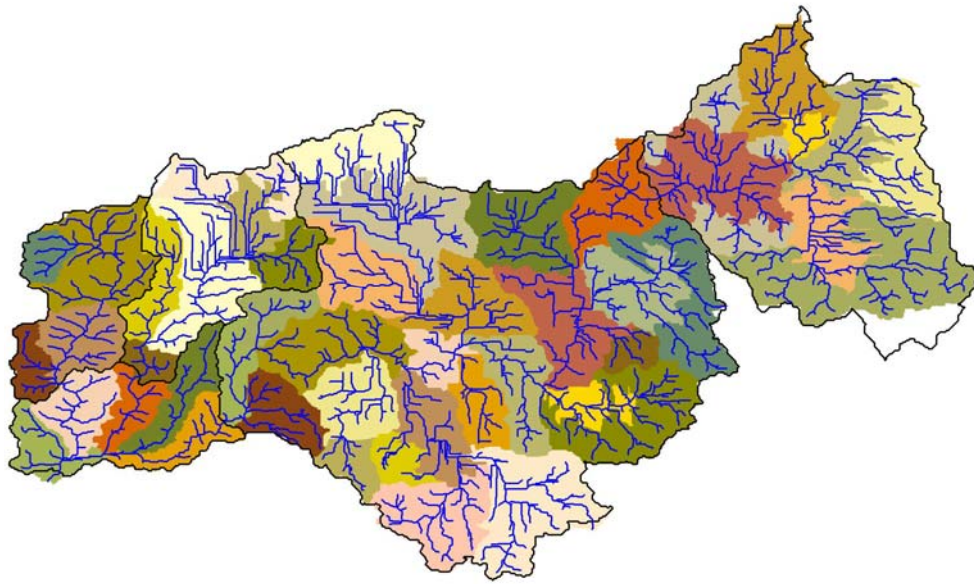


(a)

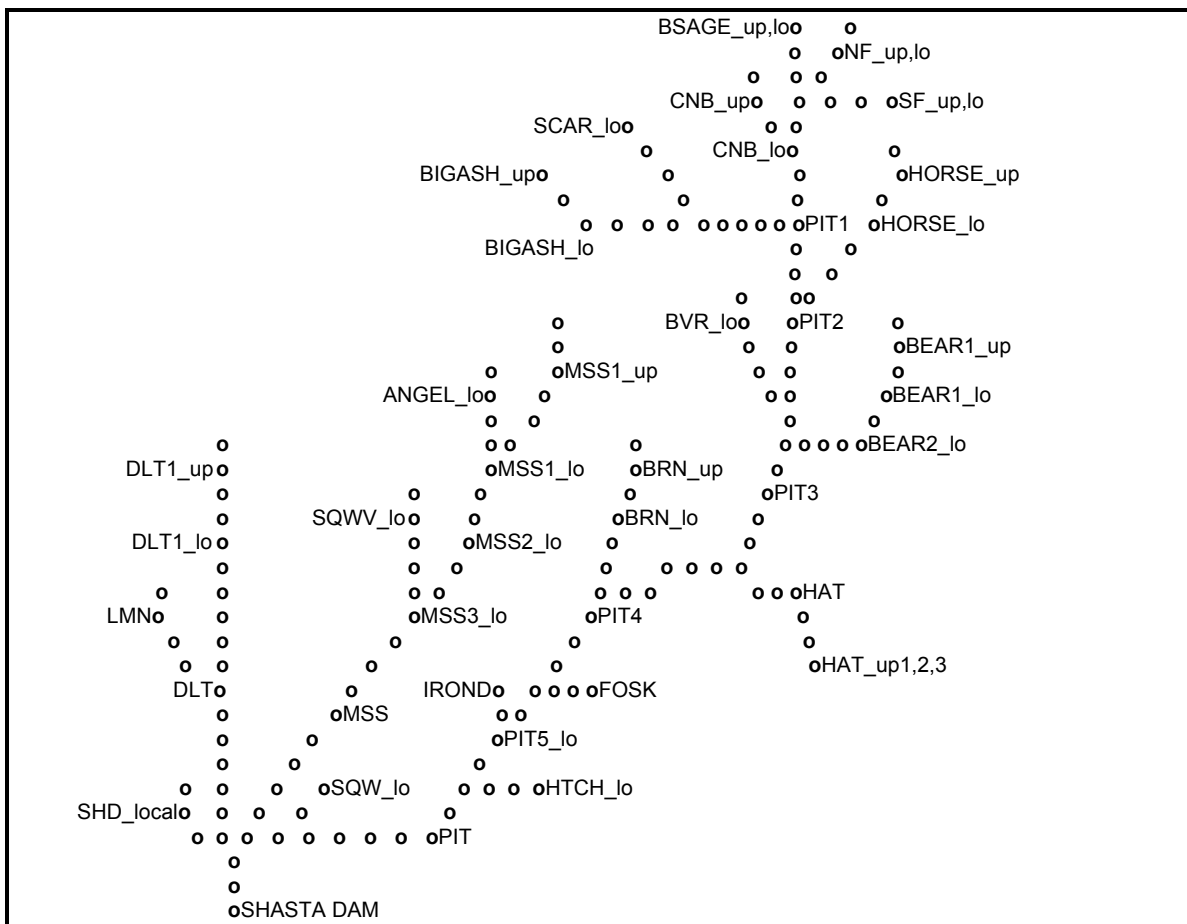


(b)

Figure 45. As in Figure 44, except representing the distributed model for the Trinity Lake watershed



(a)



(b)

Figure 46. As in Figure 44, except representing the distributed model for the Shasta Reservoir watershed

4.4. INFORM Hydrometeorological Database

Hydrologic model input for INFORM consists of MAP, MAT, and ETD for each of the major catchments defined by CNRFC (see Table 16). For historical analysis and calibration of the stand-alone distributed hydrologic models, CNRFC staff provided time series of the MAP and MAT data. These time series were consistent with the calibration parameter sets used for the CNRFC operational hydrologic models. The time period covered by the data varied somewhat among the major catchments, but generally extended from October 1960 through September 1999. In addition, long-term averaged daily values of ETD for each month were included in the CNRFC parametric files for the major sub-watersheds and were used in the hydrologic modeling. An example of the monthly mean ETD (in mm/day) is given in Table 18 for the Folsom Reservoir watershed.

Table 18. Daily values of evapotranspiration demand for the Folsom Reservoir Drainage Area

	<i>NF_up</i>	<i>NF_lo</i>	<i>MF_up</i>	<i>MF_lo</i>	<i>SF_up</i>	<i>SF_lo</i>	<i>Fol_local</i>
JAN	0.760	1.280	0.760	1.280	0.780	1.300	0.860
FEB	0.780	1.400	1.060	1.860	1.450	2.470	1.120
MAR	0.820	1.800	1.470	2.520	1.670	2.940	1.640
APR	1.030	2.290	1.950	3.110	1.800	3.200	2.480
MAY	1.800	3.640	2.550	4.110	2.280	3.850	4.150
JUN	3.040	6.040	4.320	6.330	3.580	7.390	4.560
JUL	5.260	8.220	5.400	8.650	5.760	9.160	4.640
AUG	5.570	8.250	6.150	9.730	5.840	8.760	4.100
SEP	4.100	6.550	4.770	6.950	3.270	3.790	3.220
OCT	1.940	3.100	2.690	3.120	1.810	2.300	2.200
NOV	1.140	1.690	1.190	1.440	1.360	2.050	1.230
DEC	0.910	1.400	0.940	1.250	1.080	1.800	0.880

Values for each month are given in mm/d.

The staff of CNRFC also provided reconstructed full natural flow (FNF) estimates for each major reservoir. This dataset was used in the calibration of the stand-alone distributed hydrologic model (see Section 4.6.3) and in the evaluation of both the operational hydrologic model and the stand-alone distributed hydrologic model. The FNF estimates represent unimpaired mean daily flow at the given location with the effects of upstream streamflow regulation within the reservoir drainage area taken into consideration.

For the evaluation of the hydrologic model and as part of the INFORM project objectives, additional hydrometeorological data were collected beyond the minimal requirement for model forcing. This data consists of snow sensor data, station precipitation, evaporation and temperature data, and observed streamflow records at

additional locations. This data collection forms the INFORM Project Hydrometeorological Database, with a complete listing provided in Appendix D. The dataset was used during various aspects of the project for model evaluation. Appendix D includes information on the type of data, sources, station locations, and periods of record.

4.5. Snow Model Sensitivities

Seasonal snowpack is an important water resource for the mountainous western United States and the Sierra Nevada region in particular. As stated above, intermittent seasonal snowpack contributes approximately 70% to the total annual flow in the Sierra Nevada Mountains, and is relied upon as a resource for water supply from Northern to Southern California. Thus, the snow model is an important component of the hydrologic modeling system for the INFORM study region. Snow accumulation and melt controls seasonal flows, and, consequently, the intra-annual flow regime. To better understand factors that affect the snow model, the authors conducted a sensitivity analysis of the snow model to temperature input and model parameters.

4.5.1. Sensitivity to Temperature Data

Mean area temperature input forcing affects several aspects of the snow model. It is used as an index to radiation properties, snowpack properties, and for several threshold parameters. Such model structures that rely on a single input variable for the calculation of different processes create dependency among the processes and high sensitivity to the forcing data. Thus, good quality temperature data are required to achieve good model simulations. In mountainous regions with large heterogeneity of snow cover, such as in the Sierra Nevada, there is significant temperature heterogeneity and it is difficult to produce representative MATs for certain regions or areas by interpolating point measurements.

To demonstrate the sensitivity of the model to the MAT values, the authors conducted a case study in which the MAT data was perturbed within a range of assumed reasonable uncertainty. The case study focused on the upper South Fork of the American River in the Folsom reservoir drainage area. The temperature uncertainty range reflected differences in surface elevation, which ranges from 1500 to 3150 meters for the upper South Fork American River. The air temperature was assumed to be linearly correlated to ground surface elevation by the moist adiabatic lapse rate (1°C/150 meters). This approach can be used to derive a temperature distribution from a topographic dataset such as a digital elevation model. Temperature differences due to orography in the upper South Fork American can reach about 10°C. However, it has been documented that on the Sierra Nevada western slopes the temperature gradient is occasionally larger than the moist lapse rate (Knowles 2000). Thus, the selection of the moist adiabatic rate for this study can be regarded as a conservative choice.

In this analysis the model sensitivity to temperature is realized using both systematic and non-systematic perturbation of the MAT values. The basin was divided into bands

of an elevation range of 150 meters, and the MAT was modified based on the lapse rate and the elevation at the centroid of each band. An illustration of such perturbation is shown in Figure 48, where a perturbation of $\pm 1^\circ\text{C}$ from the basin centroid MAT corresponds to a change in mean basin elevation of ± 150 m. Such delineation yields 8 temperature bands for the upper region of South Fork with an increase of up to 3°C and decrease of up to 5°C in MAT. Figure 49 presents the results of the systematic perturbation sensitivity analysis for Water Year 1980 (October 1, 1979–September 30, 1980). Figure 49a shows the snow water equivalent (SWE) computed for each elevation band (black lines) compared with the SWE simulation derived from the unperturbed MAT (red line). The differences in temperature due to the lapse rate can create a range of snowpack response with peaks that can range from about 250 to 2300 mm of SWE, as compared to the peak of 1000 mm of SWE derived from the unperturbed MAT. The area-weighted SWE from the systematic perturbation is compared to the MAT derived SWE in Figure 49b. While similar behavior is observed for much of the analysis period shown, different properties of the melting period result for the case of the run with weighted systematic error in MAT compared to the unperturbed run.

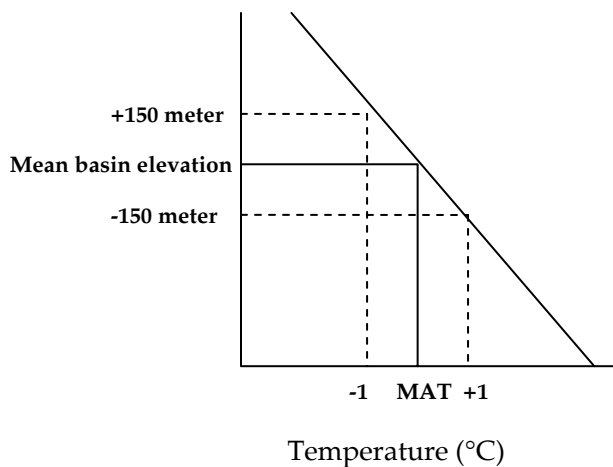


Figure 48. Schematic of the temperature (abscissa) relation to elevation (ordinate) by the moist adiabatic lapse rate

Similarly, the authors examined model sensitivity to randomly perturbed MAT. In this analysis, MAT forcing was sampled randomly from the distribution of elevations of the upper South Fork American River at each time step. Figure 50 presents the sensitivity of the SWE from an ensemble of 20 nonsystematic temperature perturbations for Water Year 1980. It can be seen that the SWE is sensitive to the temperature data and the ensemble provide SWE realizations (blue lines) that are different from the unperturbed MAT derived SWE (red line).

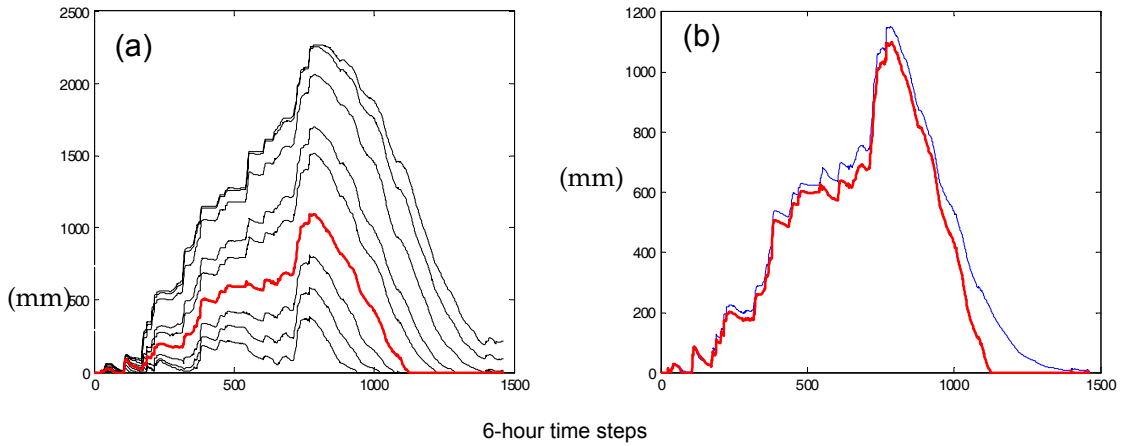


Figure 49. Snow water equivalent (SWE) in the Upper South Fork American River for water year 1980 as a function of systematic perturbation in the MAT: (a) 8 simulations in elevation zones with MAT that ranges from -5 to +3 °C; (b) areal weighted average of the perturbed simulation. The nominal simulation that uses the observed (unperturbed) MAT values is shown in red.

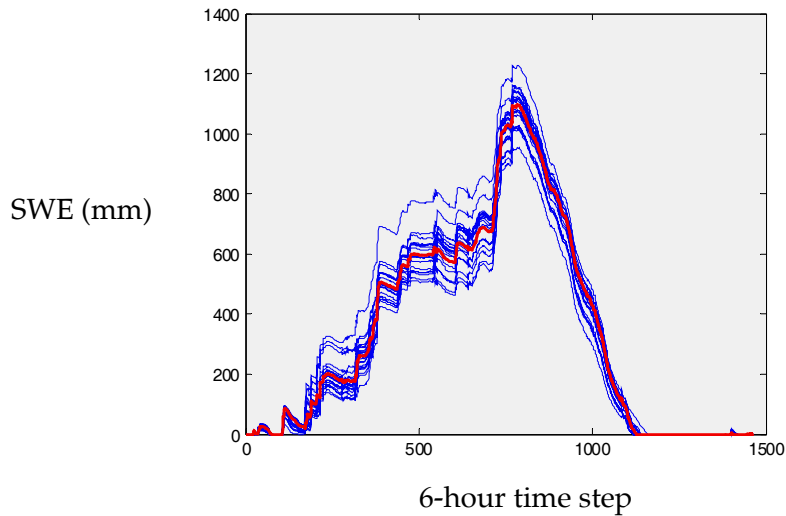


Figure 50. Snow water equivalent (SWE) in the Upper South Fork American River for water year 1980 as a function of random perturbation of the MAT. The unperturbed MAT simulation is provided in red.

4.5.2. Sensitivity to Model Parameters

A second sensitivity analysis was conducted to examine the sensitivity of snow model response to uncertainty in model parameters. The case study focused on the North Fork of the American River for two water years: 1959 and 1960. Water Year 1959 represents a relatively wet year, whereas Water Year 1960 was a relatively dry year. In these sensitivity runs, one parameter value was modified at a time, while the remaining parameters were held equal to their nominal values, as given in Table 19. The modified parameters were adjusted by +/-50% of their nominal values for the sensitivity runs, with the exception of the snow depletion curve as explained below. The nominal values presented in Table 19 are those estimated by CNRFC staff for use in their operational hydrologic model runs.

Table 19. Nominal values of snow model parameters

<i>Parameters</i>	<i>Nominal Values</i>
SCA – Snow correction adjustment factor	1.15
MFMAX – Maximum melt factor during non-rain periods (mm °C 6hr ⁻¹)	1
MFMIN – Minimum melt factor during non-rain periods (mm °C 6hr ⁻¹)	0.4
UADJ – Average wind function during rain on snow (mm/mb)	0.15
SI – Mean areal water equivalent above which there is always 100% snow cover (mm)	900
NMF – Negative melt factor (mm e °C ⁻¹)	0.15
TIPM – Antecedent weight factor	0.25
PXTEMP – determination of rain from snow (°C)	2
MBASE – base temperature °C	0
PLWHC – Percent liquid water holding capacity	0.02
DAYGM – Snow soil interface melt factor (mm day ⁻¹)	0.3

A central function of the snow model determines the SCA. This function requires the specification of an SDC that relates the ratio (R) between the current pack SWE and the minimum pack water equivalent for which the SCA is 100% (SI). In the nominal run, the SDC is a 45 degree straight line which indicates a 1:1 ratio between R and SCA. To evaluate the sensitivity of the SDC as a specified parameter in the model, the authors established an SDC function that depends on two parameters: a and b . This SDC curve consists of three straight lines, as illustrated in Figure 51. The first line for $R < 0.33$ is defined by parameter a , which is the angle of the curve with the x-axis; the second line for $R > 0.67$ is defined by parameter b , which is the angle with the right y-axis; and the third line for $0.33 < R < 0.67$ is a line that connects the end of the first two line segments at locations $R = 0.33$ and $R = 0.67$. In the sensitivity analyses, the curve was symmetrically changed, which implies that the curve is dependent on one parameter, a , or the angle of the curve with either the x- or the y-axis. For, the nominal case, this angle is set equal to 45 degrees.

2-Parameter Snow Depletion Curve

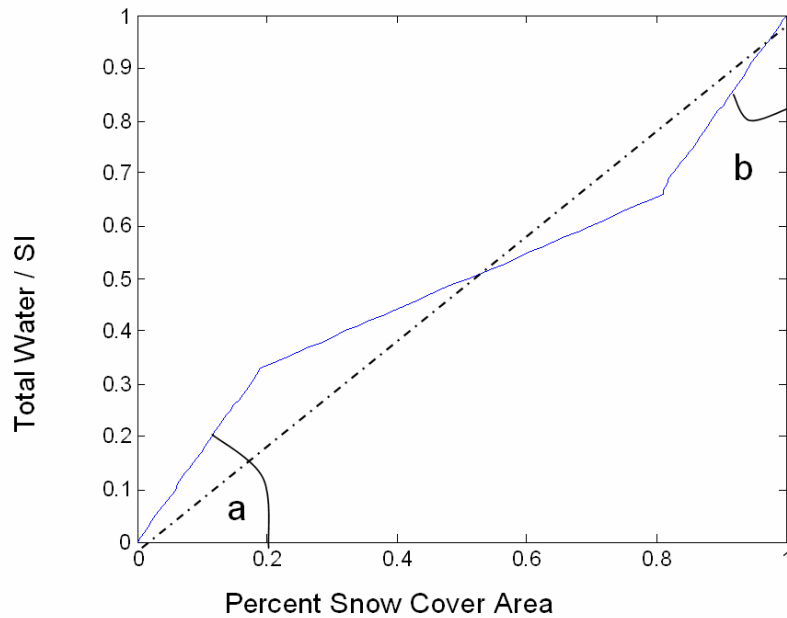


Figure 51. Two-parameter snow depletion curve. Parameters a and b are the angles with respect to the x- and y-axis, respectively, as shown.

Figure 52 presents the results of this sensitivity analysis with respect to snow model parameters in terms of the SWE derived from the sensitivity runs. In each plot, the nominal SWE is shown in blue, while the SWE corresponding to a 50% underestimation of the parameter value is shown in red and that corresponding to a 50% overestimation is shown in black. The parameters can be classified into sensitive and insensitive parameters. The sensitive parameters are SCF, MFMAX, MFMIN, SI, PXTEMP and the SDC; whereas the other parameters (UADJ, NMF, TIPM, MBASE PLWHC and DAYGM) are relatively insensitive on an annual scale. The following is a summary of the effect of each of the sensitive parameters on snow model simulations:

- SCF – This parameter has the largest effect on total snow water equivalent simulations, with an over- or underestimation of up to 70% of the nominal SWE. However, this effect seems to be symmetric and monotonic for this analysis.
- MFMAX – This parameter is involved in the calculation of the rate of melt in non-rainy periods and the calculation of heat deficit in non-melt periods. Therefore, as expected, it affects the declining limb of the SWE. The effect appears to be monotonic and uniform. The parameter also determines to a large degree the end of the melting season and the disappearing of the snowpack.
- MFMIN – Similar to the previous parameter, this parameter has an effect on the melting part of the annual SWE curve. However sensitivity to changes in this

parameter is shown to be less pronounced than to changes in MFMAX. This parameter also does not affect melt timing.

- SI – Changes in this parameter seem to have a significant effect only when they underestimate the nominal parameter value. This can be seen during the wet year when underestimation of the nominal value speeds up the pack melting processes.
- PXTEMP – Changes in this parameter have a clear effect on the overall volume of the pack. This parameter is best evaluated from single isolated events from the snow model output, rain-plus-melt.
- SDC – This parameterized curve affects significantly the shape of the SWE-graph. In the wet year, the SDC affects mainly the melting process, with an overestimation of the equal angles in Figure 51 providing a tail of melting that continues into the summer months. On the other hand, the underestimation of the equal angles yields a sharp melting process. The SDC also produces a significantly different appearance of the SWE pack in the drier year.

Snow Water Equivalent

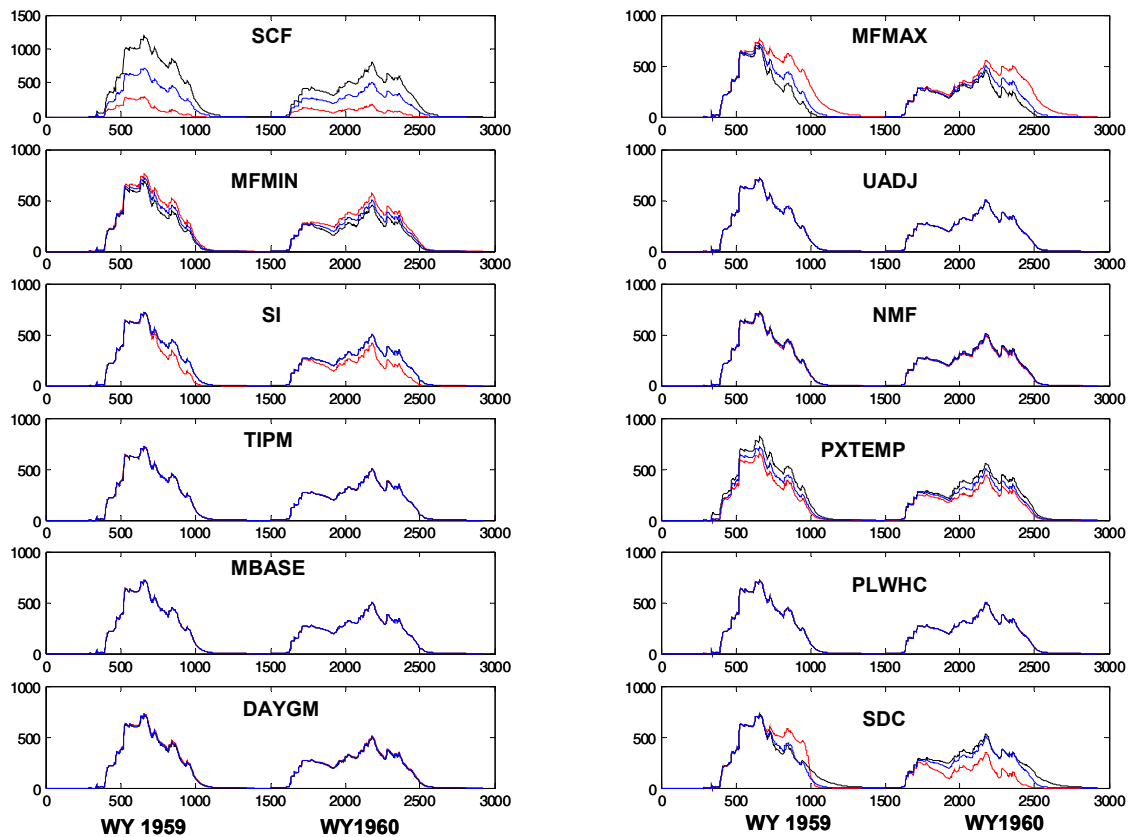


Figure 52. The nominal simulation of SWE (blue) compared to SWE corresponding to a 50% overestimation (red) and 50% underestimation (black) of the parameter value

Calibration of the model parameters using physical reasoning usually implies that the parameters have to be estimated in a sequential manner. As such, the order in which parameters are selected for the calibration is important, with the most sensitive parameters calibrated first. It is also observed that except from SDC, the other sensitive parameters have a well-identified and predicted effect on the simulation, compared to nominal. Therefore these parameters can be tuned rather easily in order to match an observed SWE time series. The SDC curve is the parameter that affects the overall shape and behavior of snow accumulation and ablation processes the most. This observation implies that this curve should be estimated first to achieve a reasonable annual evolution of the snowpack.

4.6. Evaluation of Hydrologic Models

The goal of the hydrologic modeling of the major reservoir drainage areas in the INFORM study region is to represent the physical processes that occur within each basin, influenced by both atmospheric forcing and basin physical characteristics, and to produce a streamflow hydrograph that effectively represents the total inflow into the reservoir under observed or forecast hydrometeorological forcing. While the main task of the modeling may be to predict floods, the models may also be used—or have the potential to be used—for longer hydrologic response time predictions aimed toward water resources management, ecological preservation, and assessing the effect of long-term climate variability on water resources. To meet these objectives, the model must perform well on different time scales and under a variety of forcing scenarios. The time scales are clearly manifested by the different modules that represent different processes (i.e., snow, soil water accounting with runoff production and channel routing). The three modules represent distinct processes which are closely interlinked, and in the validation processes it is not a simple task to isolate the contribution of each process to the performance and overall uncertainty in the simulation.

In this section, the authors evaluate the reservoir inflow simulations for the four major reservoirs for both the operational hydrologic models and the INFORM stand-alone distributed hydrologic models. CNRFC provided operational hydrologic model simulations for each reservoir and for the available historical record (which varied by drainage area). These simulations resulted from calibration performed at CNRFC and correspond to the model structures as presented in Section 4.3.1. Hydrologic Research Center staff generated the stand-alone distributed model simulations based on the input forcing data provided by CNRFC and parameters established through model calibration (see Section 4.6.3.1). The time periods of the stand-alone model simulations varied with the historical records provided, but generally included the period October 1960 to September 1999.

The next subsection presents a description of performance measures utilized in the model evaluations. Subsequent subsections contain the evaluations of the CNRFC operational hydrologic model simulations and the INFORM stand-alone hydrologic model simulations. Additional evaluation graphics are included in Appendix E for the

operational model simulations, and in Appendix F for the stand-alone model simulations.

4.6.1. Performance Measures

Model evaluation focuses on the ability to simulate the unimpaired reservoir inflow discharge for each reservoir drainage area. Therefore, the evaluation was based on the comparison of the model simulated inflow to the historical FNF at each reservoir. When available, the authors used additional long-term streamflow gauge records. These gauged sites generally correspond to the major catchments defined by CNRFC, and the comparison there was made based on mean daily flows.

The authors computed statistical performance indices with a daily discharge time step for the entire available record. In the following formulations, the simulations are denoted by S while the corresponding observations by O , and n is the record length. Although the different length of the available time series used in this evaluation might affect the confidence in the computed index values, all the indices account for the time series length and, hence, it is reasonable to intercompare the performance among different cases. Three statistical performance indices were used:

(1) The coefficient of determination, R^2 :

$$R^2 = [COV(S, O) / \sqrt{\text{var}(S) \text{var}(O)}]^2. \quad (51)$$

where $COV(S, O)$ denotes covariance between S and O , and $\text{var}(x)$ denotes the variance of x . The coefficient of determination measures the linear relationship between the two variables, with a score of R equal to 1 indicating a perfect linear relationship.

(2) Root Mean Square Error (RMSE):

$$RMSE = \sqrt{n^{-1} \sum (S - O)^2}. \quad (52)$$

(3) Percent of Daily Absolute Error (PDAE):

$$PDAE = \sum |S - O| / \sum O. \quad (53)$$

The PDAE is an indicator to the degree of daily correspondence, on average, between the observed and simulated discharges. The minimum possible PDAE value is equal to 0.

For the evaluation of the operational hydrologic model, the authors also compared snow model output to snow sensor data throughout the region. Daily snow water equivalent from the snow sensors was obtained from the California Data Exchange Center (<http://cdec.water.ca.gov/>) and was used in this comparison. A listing of the snow sensors is given in Appendix D, and includes 11 snow sensors in the Folsom drainage, 7 sensors within the Trinity drainage, and 8 sensors each within the Shasta and Oroville

drainage areas. Such analysis was not repeated for the stand-alone distributed snow-model component output, given the nearly identical simulations.

It must be noted that in this evaluation study, the authors assumed good observed data quality, and the errors and uncertainties in this analysis are solely attributed to the model. It is expected that the observation sensors which are operated by multiple agencies possess differences with respect to data quality. However, there is not enough information to account for these differences at present.

4.6.2. Evaluation of CNRFC Operational Models

Table 20 presents the results of the statistical evaluation of simulated mean daily flows for the CNRFC operational hydrologic model. This table provides a means for an intercomparison of performance among different catchments. Based on these statistical measures, the operational model performs well for most catchments examined, with daily R^2 values that are above 0.83, with the majority of catchments exceeding 0.90. There are clearly some catchments for which the model exhibits superior performance (North Fork of the American River, McCloud River, Sacramento River at Delta, and Indian Creek), with R^2 values well into the upper 0.90s.

With respect to the other two statistical measures for which near-zero values represent optimal performance, catchments with better RMSE performance generally have worse PDAE performance. The converse also applies (catchments with better performance in PDAE showed poorer performance with respect to RMSE scores). For example the Shasta Lake inflow has a low value of PDAE, but a fairly poor performance for RMSE. Similarly the Middle Fork Feather River near Clio has a low RMSE, but a relatively high value of PDAE. These results indicate that the measures used represent specific aspects of the hydrologic response and further evaluation is necessary to clarify performance.

A comprehensive evaluation was conducted by comparing the streamflow and the SWE simulations to observations. Different types of plots were used that highlight various aspects of hydrologic response and model performance. Selected figures from the American River (Folsom drainage) are presented as examples and to aid discussion within this chapter. Analogous evaluation figures are included in Appendix E for the other reservoirs.

4.6.2.1. Streamflow evaluation

Starting with the evaluation of streamflow, Figure 53 presents an example of the observed and simulated hydrographs of the four major catchments of the American River for Water Year 1971. Such plots are utilized to visually assess the simulated flow response, in terms of overall flow magnitude, peak timing and number of event responses. The model simulation generally reproduces the observations, with the largest deviations occurring for medium to low flows (i.e., the South Fork of the American River). Such deviations are attributed to unaccounted regulation in upstream reservoirs that alters the downstream natural flow. Complete sets of such plots have

been included in a previous INFORM project progress report and are not repeated here (see Georgakakos et al. 2004). The plots corroborate the results of Table 20, indicating that the model reproduces the observed hydrograph well.

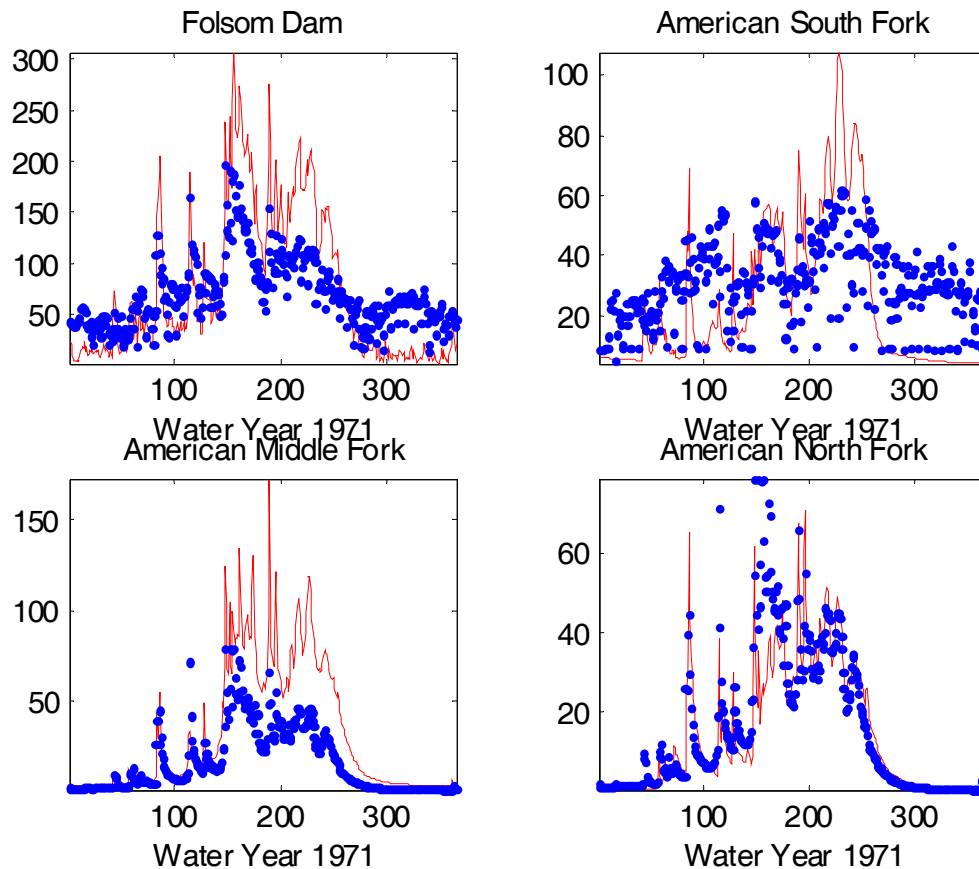


Figure 53. Example of the observed (blue) and simulated (red) flows in cubic meters per second (m^3/s) for Water Year 1971 for the total flow at Folsom Dam and the outlet of the sub-watersheds of the South, Middle, and North Forks of the American River

Figure 54 presents scatter plots of the simulated flow as a function of the observed flow at each time step for the American River major catchments. These scatter plots display the overall functional relationship and the performance with respect to exceptional events which are distinct from the crowded cloud of points. The line of perfect correspondence is shown in Figure 54 for reference, as significant deviation from this line indicates poor performance. Such plots can also indicate consistent bias in the flow simulations, where overestimation bias results in the cloud of points above the 45° line of perfect correspondence and underestimation bias results in the points being mostly below the line. Figure 54 indicates an overestimation bias for the Folsom reservoir inflow (Folsom Dam). Again, however, the performance for all sub-basins is quite good, as evidenced from similar plots included in Appendix E for Trinity, Shasta, and Oroville.

Table 20. Performance statistics for the historical simulation of the operational hydrologic model

	R^2	RMSE	PDAE	USGS id	Water Years
<u>American</u>					
North Fork	0.95	14.1	0.24	11427000	10/54–9/93 (39)
Middle Fork	0.94	34.2	0.78	11433300	10/58–9/99 (41)
South Fork	0.86	27.6	0.44	11444500	10/64–9/93 (39)
Folsom Dam	0.98	78.9	0.38	FNF	10/64–9/89 (25)
<u>Trinity</u>					
	0.96	30.14	0.32	FNF	10/63–9/99
<u>Shasta</u>					
Canby				FNF	
Pit	0.94	45.54	0.27	FNF	10/65–9/89
McCloud	0.97	17.27	0.35	NF	10/60–9/99
Delta	0.97	20.31	0.25	FNF	10/60–9/99
Shasta Lake	0.98	65.24	0.11	FNF	10/50–9/89
<u>Feather</u>					
Lake Almanor	0.93	12.2	0.32	11399000	10/81–9/97 (18)
Indian Creek	0.95	10.6	0.29	11401500	10/77–9/92 (15)
North Fork nr. Pulga	0.85	49.0	1.46	11404500	10/80–9/92 (12)
Middle Fork nr. Clio	0.83	9.8	0.48	11392500	10/60–9/79 (19)
Middle Fork nr. Merrimac	0.92	25.9	0.31	11394500	10/60–9/79 (19)
Oroville Local	0.94	36.1	0.40	11406800	10/69–9/87 (18)

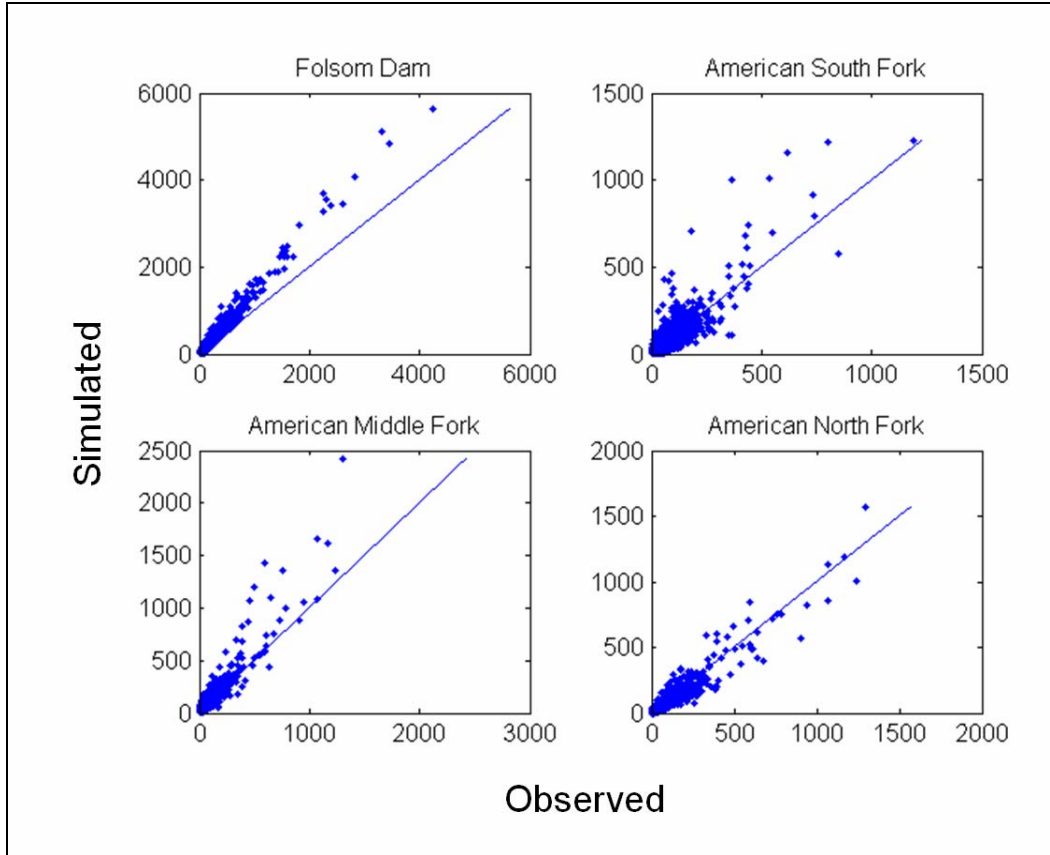


Figure 54. Daily flow simulated by the operational hydrologic model versus observed flow in m³/s for the American River catchments

Figure 55 shows cumulative flow curves for the American River. Deviation of the simulation curve from the observed curve suggests errors in the long-term water yield of the model. The importance of model long-term biases and the significance of monthly water balance are emphasized in such plots. In cases when the model runs in a semi-distributed mode but the model calibration is done with performance measures pertaining to downstream aggregate response, it may be that due to compensation of errors, downstream points show overall good model performance even though upstream points exhibit persistent over- or underestimation of the observed flow.

Flow duration curves are other consistency plots which provide insight on the overall systematic errors. The example for the American River is shown in Figure 56.

The flow discharges in this case are transformed using the Box-Cox transformation. The Box-Cox transformation is used for visualization purposes as this transformation maps the independent discharge values into a homoscedastic time series with an approximately normal distribution. The transformation is given by:

$$q_{t,transform} = \frac{(q_t + 1)^\lambda - 1}{\lambda}, \quad (54)$$

where λ is set to 0.3 and the units of discharge are cubic meters per second (m^3/s). The duration curves are used to highlight consistent behavior of the simulations in a variety of flow magnitudes.

Streamflows along the western face of the Sierra Nevada undergo rapid transitions from late summer low flow, to winter mid flow, to spring peak flows. It is important to capture the annual dynamics and the timing of these transitions in the operational model simulations. Thus, a comparison on a monthly timescale was explored.

Figure 57 presents scatter plots of the daily simulated versus observed flows in Box-Cox transformed units for the American River separated by each month of the year.

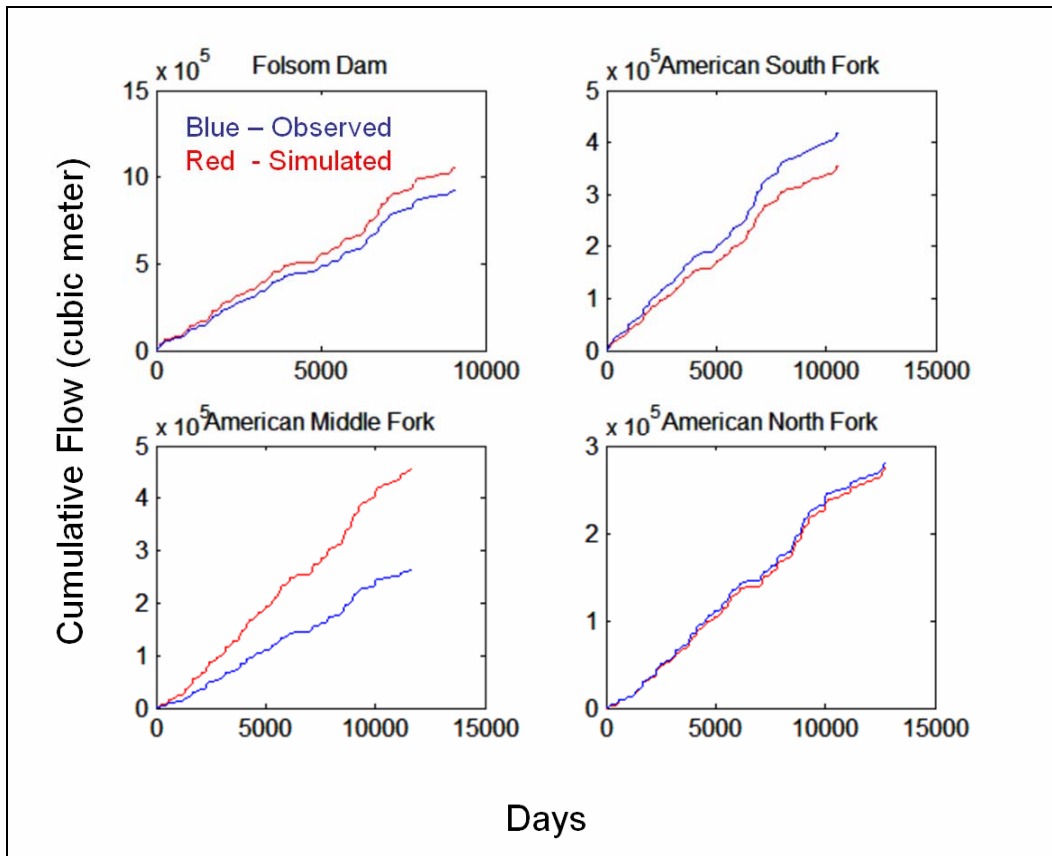


Figure 55. Cumulative distribution of the observed (blue) and simulated (red) flows over the length of the simulation for the American River catchments and for the operational hydrologic model

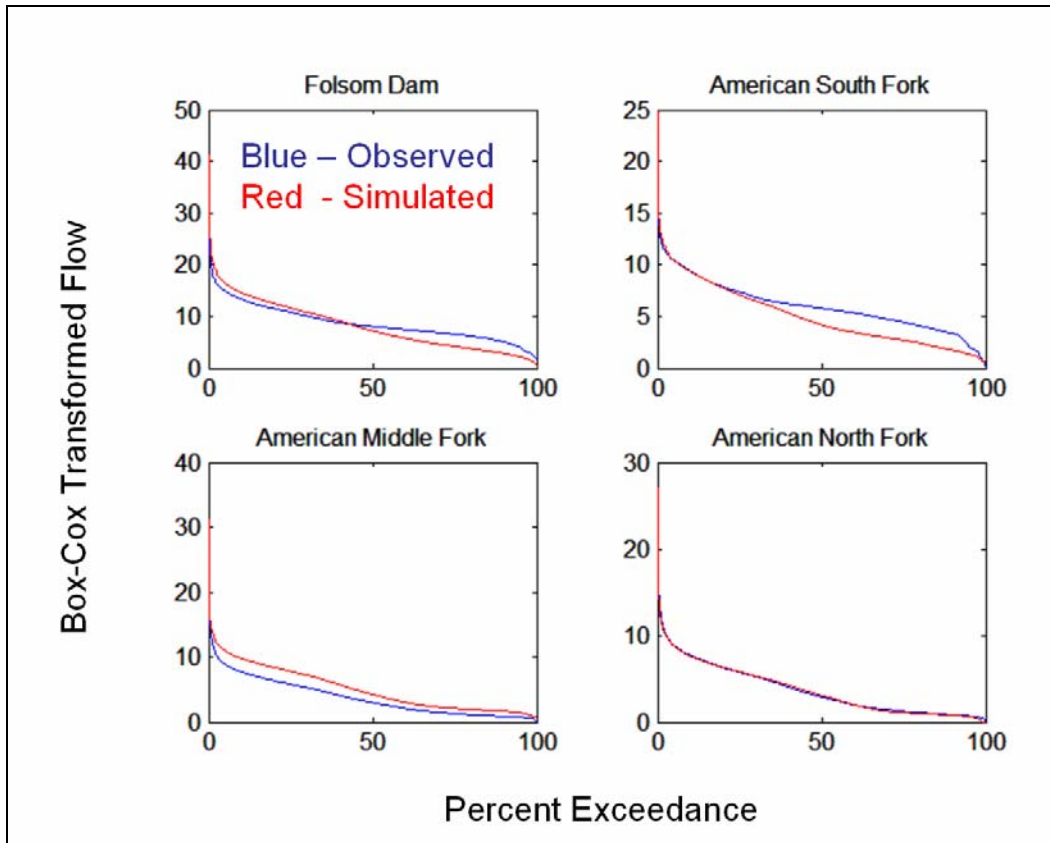


Figure 56. Observed (blue) and simulated (red) duration curves of Box-Cox transformed flow for the American River and for the operational hydrologic model

Likewise, Figure 58 presents the monthly contribution to the annual for the American River. For each month the mean and the standard deviation of the annual volume fraction are plotted for the simulated and observed flows. The model fails to reproduce the August through September (summer) flow well for most catchments. Poor simulation of the summer month flows is observed even in catchments for which the model has a good overall performance (e.g., North Fork of the American River).

An important aspect in the model representation of the natural flows is the timing of the spring melt onset pulse. The method used herein to identify the spring pulse is the cumulative departure method (Aguado et al. 1992; Cayan et al. 2001). This method identifies the time (day) at which the cumulative departure from that year's mean daily flow is most negative. This measure is equivalent to finding the day in which the flow magnitude shifts from less than average to greater than average. This method avoids early episodic melt events and captures the main shift of the spring melt. However, the indicated day is also related to basin physiographic characteristics and includes a basin lag time from snowmelt to flow at the basin outlet.

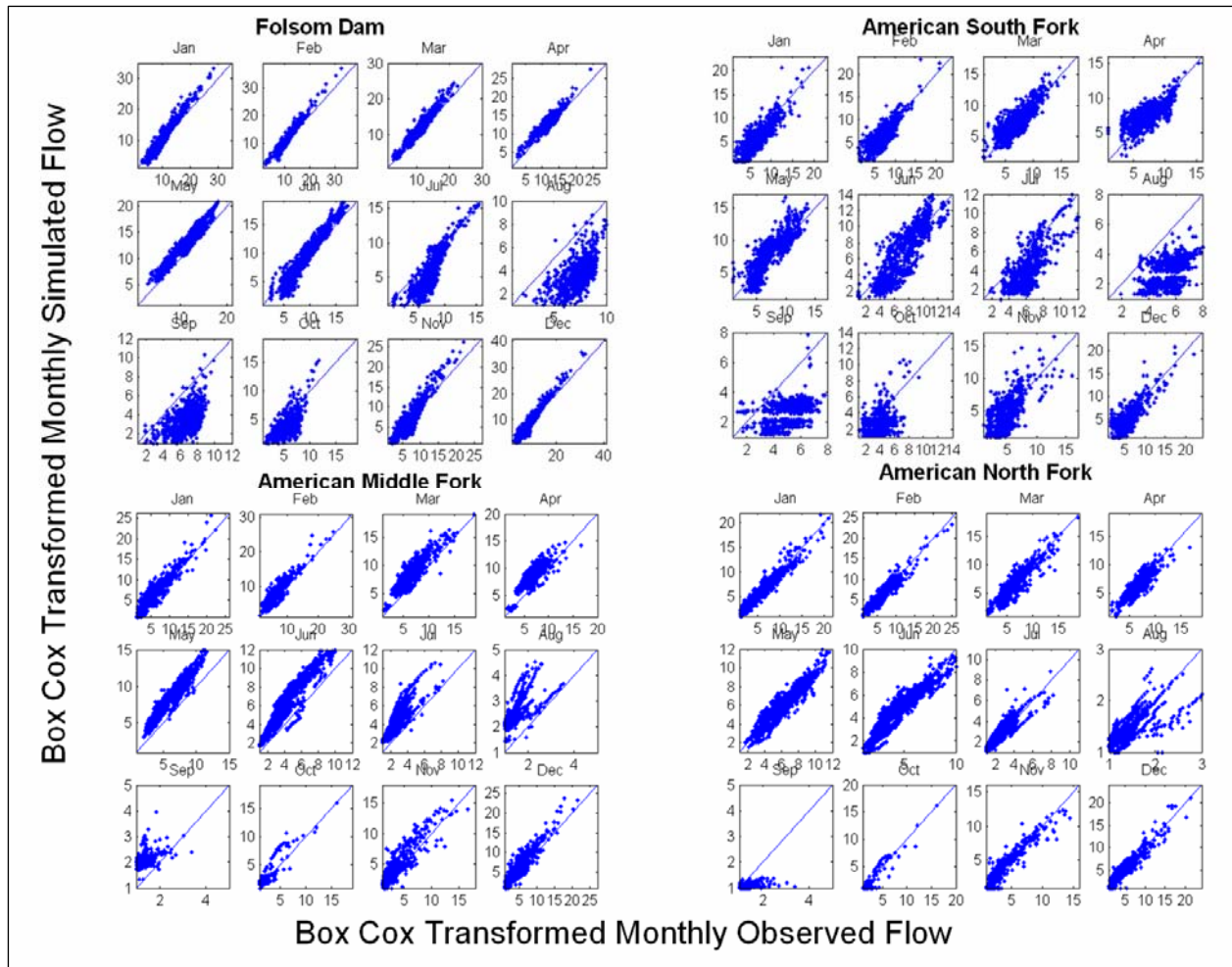


Figure 57. Scatter plots of the simulated versus observed flows at a monthly scale for the American River catchments

Figure 59 compares the simulated and observed annual spring pulse at the North Fork of the American River. Generally the timing of the spring pulse is quite good, within just a few days of the observed. Occasionally (e.g., 3 times in the 30-plus year simulation for the North Fork of the American River), large deviations of 30 or more days did occur.

4.6.2.2. Snow water equivalent evaluation

For an additional model performance assessment, the authors compared the SWE model simulation with snow sensor data located within the catchment under study. Figure 60 shows an example with four years of simulated SWE output compared with data within the South Fork of the American River catchment. Appendix E includes additional comparisons for other catchments within the INFORM region.

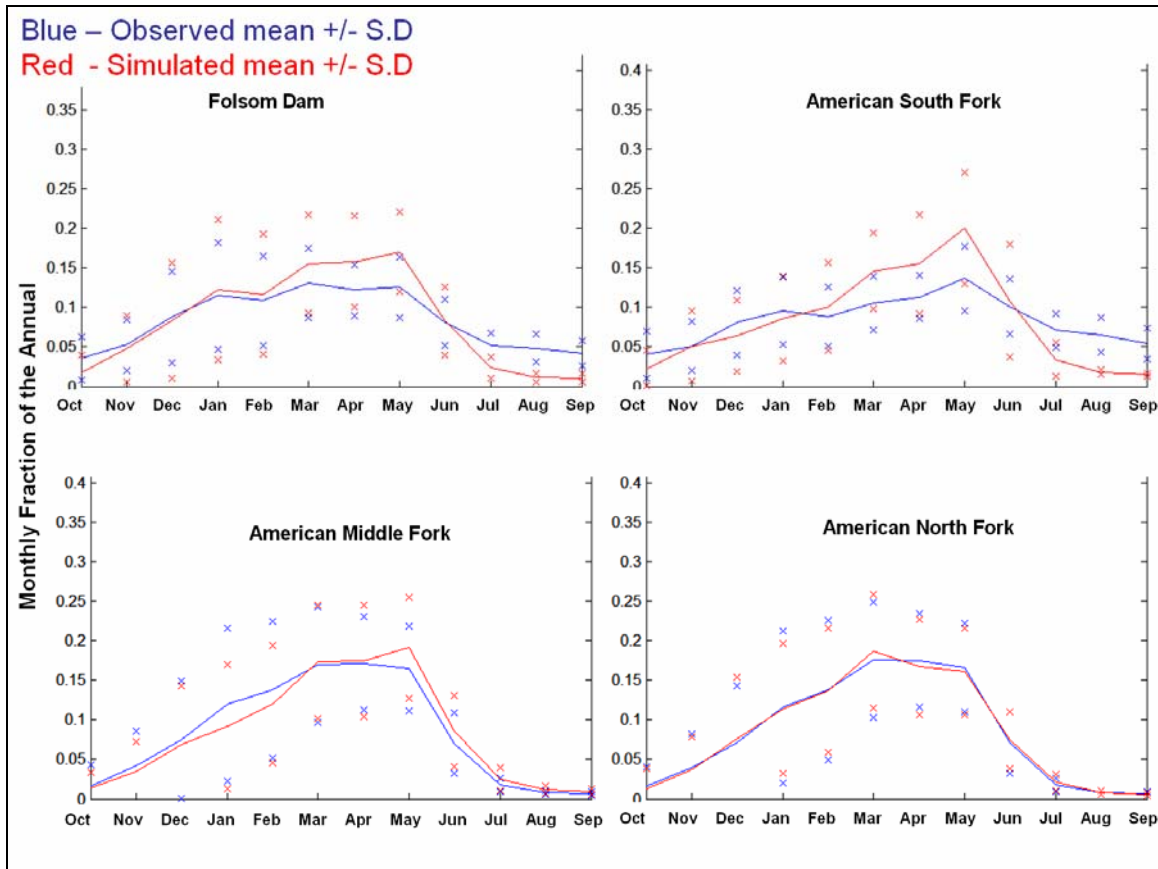


Figure 58. Observed and simulated monthly mean flows (+/- 1 standard deviation shown by “x”) expressed as a fraction of the annual flow volume for the American River catchments

In a qualitative sense, these plots point toward the conclusion that model performance is reasonable. The model-simulated SWE captures the shape of the observed SWE curve with appropriate snow accumulation and depletion periods, and accounts for most major snow storms. However, it is noted that snowmelt in the model occurs earlier than observed, and with a depletion slope that is not as steep as the observed data. The simulations also agree more with snow sensor data for locations that are at lower elevations than with higher elevation stations.

4.6.2.3. Summary of operational hydrologic model evaluation

In summary, the major findings from the evaluation of the operational hydrologic model include:

- The model simulations capture the overall hydrologic response. Poor performance during periods of medium to low flows at some catchments within the INFORM domain is often associated with regulation in upstream reservoirs, which alters the downstream natural flow.

- Model performance is poorest during summer months (August through September), even when overall performance is good. The natural discharge in these summer months is dominated by shallow groundwater flow and springs. Although this flow is of a low magnitude, it is about 5%–10% of the annual flow. This may have a cumulative effect on the overall water budget. The performance of the model during the summer months can be attributed to one or more of the following: (1) streamflow regulation in any existent upstream reservoirs; (2) errors in model parameters that represent the generation of baseflow in the model; and (3) errors in basin evapotranspiration during the summer months. Of course this might also be an effect FNF estimation errors and lack of knowledge about the operational activity during the summer months. However, it might also be an indication that the model components that control the very low seasonal flow are not well calibrated.

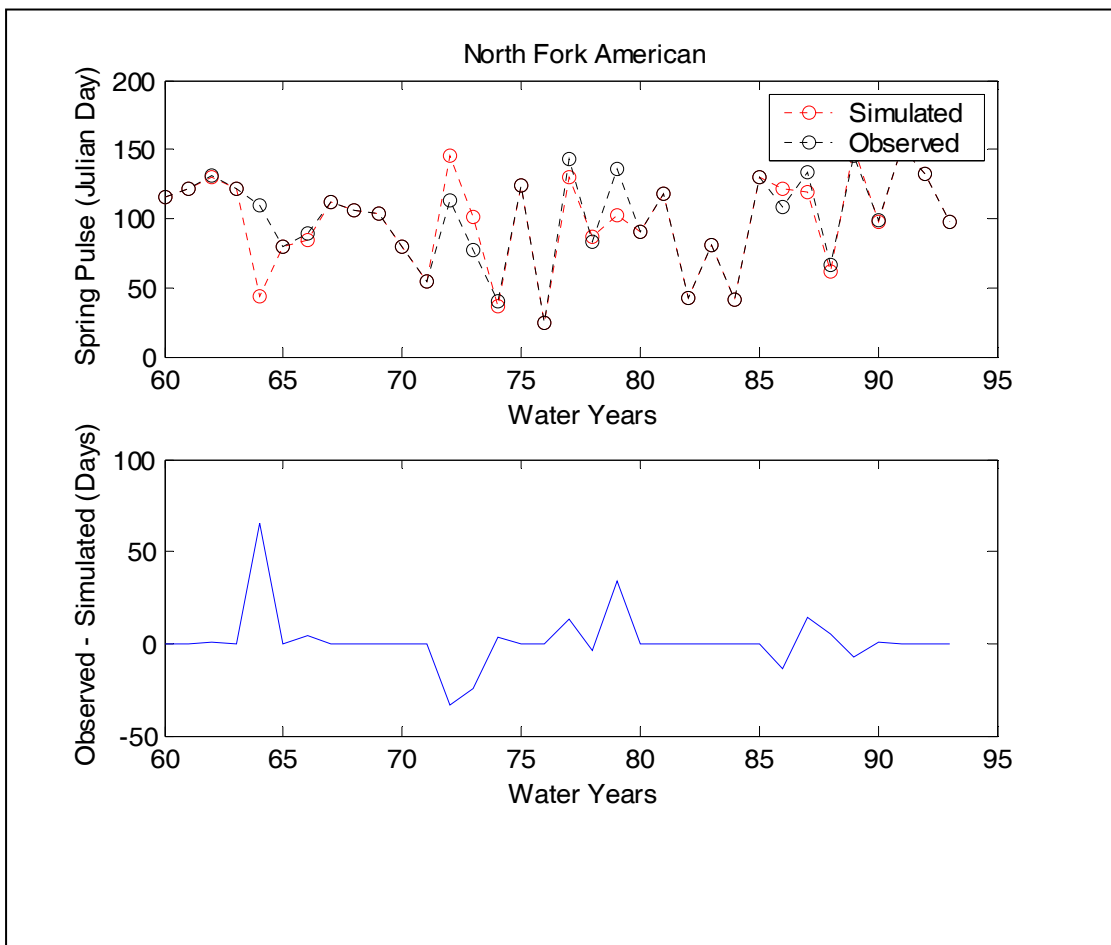


Figure 59. (a) Observed (black) and simulated (red) time trace of the spring pulse. (b) Annual differences between the observed and simulated spring pulse timing (given in days).

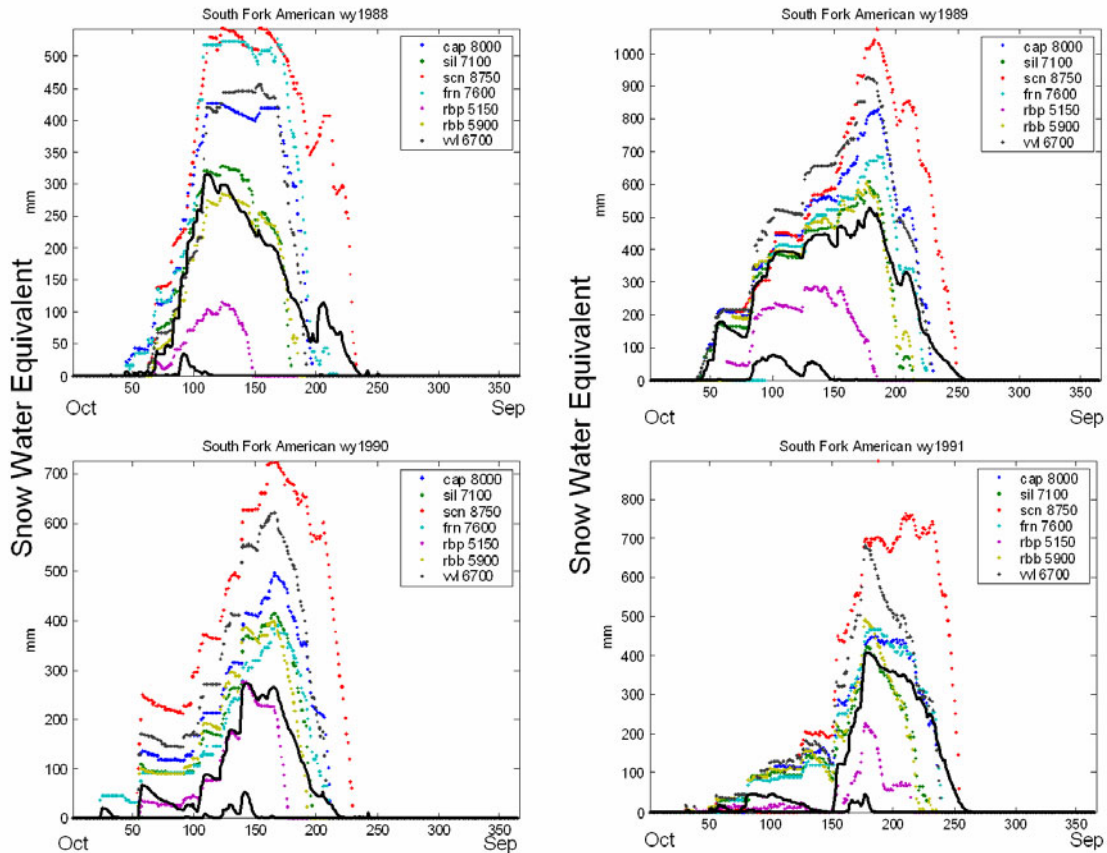


Figure 60. Daily snow water equivalent from snow sensors (dots) compared with simulated snow water equivalent from the operational model (solid line) for four different Water Years (1988–1991) and for the South Fork of the American River sub-watershed

- The simulation of the onset of the spring melt pulse is well simulated for most basins. Generally, the simulated onset is within a few days at most of the observed spring onset. Occasionally there are years in which a large deviation exists from the observed onset. Some of these cases are influenced by upstream streamflow regulation which alters the onset signal.
- The monthly flow behavior is captured well by the model, particularly for the North Fork of the American River and the Middle Fork of the Feather River. In some other catchments, the late winter and early spring transitions of the monthly volume fraction are not well captured. It is conjectured that this monthly behavior is dominated by the model snowpack development, and, thus, can be better captured by improving the simulation of the snowpack evolution. Performance is consistently better in early winter, compared to late winter and spring.

- Based on a qualitative comparison of the model-produced SWE with daily observations from point sensors, the general conclusion is that the model performs well with respect to SWE. The shape of the SWE curve captures the snow accumulation period and major snow storms. There is a tendency for the model to produce melt earlier than observed, with slopes of the depletion curves in the simulation being less steep than the observed snow depletion slope. This may be related to the fact that the slope of the depletion curve is a function of the spatial distribution of the catchment properties rather than the properties of any particular point. Satellite remote sensing data may be a better ground truth against which to measure the depletion curve properties. Finally, simulations agree well with the sensors that are located in lower elevations compared to the sensors at higher elevations. This may indicate that the model is, in fact, underestimating the actual catchment snow water equivalent.

4.6.2.4. Recommendations for operational model improvements

Reservoir operations and water diversions in the upper stream of the basins are a major difficulty, especially for low and medium flows, when using a model that attempts to represent the natural system. Although the day-to-day operational decisions pertaining to upstream reservoirs are difficult to predict for hydrologic modeling purposes, an effort should be made to incorporate this upstream flow regulation into the model. This will improve the continuous simulations of the model states and the water balance. Efforts along these lines have been initiated at the CNRFC for the Folsom Lake drainage.

Attention should be given to the parameters of the lower zone in the SAC-SMA model. Some adjustment will probably improve the performance of the model in the summer months. The summer flow regime (August through September) constitutes 3%–5% of the annual flow yield. Improving the prediction of the summer flow will also improve model representation of the baseflow process and will contribute to a better representation in the wet periods. Activities at the CNRFC target the improvement of the summer flow predictions for the American River basins.

The snow model component should be studied. Major issues that need attention are: understanding the uncertainty associated with the use of mean areal temperature in the mountainous area of Sierra Nevada, better representation of the snow spatial distribution, and improvement of the snow depletion curve representation. Shamir and Georgakakos (2006a, 2006b) provide first steps in this direction.

4.6.3. Evaluation of the Stand-Alone Hydrologic Model

4.6.3.1. Model calibration

Because the stand-alone distributed model uses the same forcing input of the snow and soil water components as the CNRFC operational hydrologic model, estimates of parameter values for these models were set equal to the calibrated CNRFC parameters. Some minor adjustments were made to the snow model component parameters to

reduce seasonal bias in flow volume. Tables 21 through 24 list the snow and soil water model parameters used for the stand-alone model (Folsom, Trinity, Shasta, and Oroville drainage areas, respectively).

Calibration of the stand-alone INFORM distributed hydrologic model focused on the routing model components, where the higher spatial resolution necessitated the estimation of routing parameters for more channel reaches than represented in the CNRFC operational hydrologic model. Although the model streamflow simulations are evaluated only at the reservoir inflow sites, the calibration utilized additional observed and reconstructed streamflow at various locations. Observed streamflow records are available through the U.S. Geological Survey (USGS) National Water Information System for various locations throughout the reservoir drainage basins and with varying record length (see Appendix D for a listing of collected USGS streamflow data). Calibration of the routing parameters (n_c and α , as given in Table 15) aimed to capture both the timing and the magnitude of the streamflow at the locations with observed records. Recall that these parameters are directly related to the travel time in the channel reach. The parameter estimates for gauged sub-basins were then regionalized for each reservoir drainage area based on relationships with channel reach characteristics, such as contributing drainage area, stream length, and channel slope.

4.6.3.2. Streamflow evaluation

Table 25 presents the scores of the three statistical performance measures (see Equations 51 to 53) for inflows into the four large reservoirs. The statistical criteria were computed with a daily time step for the entire available record with a total of n time steps. The table shows that the performance of the model is comparable for all the basins for the correlation coefficient and the *PDAE*. For the RMSE, it appears that the Trinity simulation outperforms the other basins, although in all cases the model performance is excellent. The research team speculates that these differences in RMSE among the basins are partially due to differences in magnitude of flow. Since the uncertainty in the simulation is relative to the flow magnitude, it implies that the RMSE criterion tends to have higher values in time series with larger magnitudes.

Table 21. Parameters of the snow and soil model components used for the Folsom Reservoir stand-alone distributed model simulation

SNOW PARAMETERS							
	NF-up	NF-lo	MF- up	MF-lo	SF- up	SF-lo	Fol-Lcl
SCA	1.0	1.0	1.35	1.0	1.2	1.0	1.0
MFMAX	0.86	0.85	0.69	0.5	0.75	0.85	0.8
MFMIN	0.2	0.3	0.12	0.16	0.2	0.25	0.25
NMF	0.15	0.15	0.15	0.15	0.15	0.15	0.15
PLWHC	0.04	0.04	0.04	0.04	0.04	0.04	0.04
TIPM	0.25	0.25	0.25	0.25	0.25	0.25	0.25
MBASE	1.0	1.0	1.0	1.0	1.0	1.0	0.0
UADJ	0.04	0.04	0.04	0.04	0.08	0.06	0.04
DAYGM	0.1	0.1	0.1	0.1	0.1	0.1	0.1
PXTEMP	2.0	2.0	2.0	2.0	2.0	2.0	1.0
SI	900.	300.	1200.	600.	1100.	500.	200.
ELEV	18.96	9.60	17.49	11.66	19.29	8.19	3.88
LAPSEMX	0.80	0.80	0.80	0.80	0.80	0.80	0.60
LAPSEMN	0.35	0.35	0.35	0.35	0.35	0.35	0.45
ELEV-TS	19.81	8.29	19.81	13.72	19.81	5.90	4.57
PADJ	1.0	1.0	1.0	1.0	1.1	1.05	0.97
SACRAMENTO MODEL PARAMETERS							
UZTWM	142.000	161.000	90.000	140.000	100.000	175.000	75.000
UZFWM	55.000	35.000	35.000	45.000	65.000	90.000	15.000
LZTWM	312.000	360.000	270.000	280.000	250.000	600.000	180.000
LZFPM	72.000	72.000	96.000	110.000	125.000	350.000	100.000
LZFSM	110.000	85.000	120.000	110.000	20.000	60.000	80.000
DU	0.300	0.280	0.420	0.460	0.160	0.200	0.250
DLPR	0.005	0.006	0.005	0.007	0.005	0.004	0.003
DL DPR	0.070	0.120	0.090	0.060	0.030	0.030	0.070
EPS	20.000	20.000	48.000	43.000	30.000	100.000	12.000
THSM	1.400	1.400	1.300	1.500	2.100	1.100	1.200
PF	0.250	0.350	0.150	0.300	0.250	0.250	0.250
XMIOU	0.000	0.000	0.000	0.000	0.000	0.000	0.100
ADIMP	0.010	0.010	0.000	0.020	0.000	0.000	0.075
PCTIM	0.000	0.000	0.005	0.005	0.000	0.000	0.065
ETADJ	1.000	1.000	1.000	1.000	1.000	1.000	1.000

Table 22. As in Table 21, except for the Trinity Lake inflow simulation

SNOW PARAMETERS		
	CEG-up	CEG-lo
SCA	1.0	1.06
MFMAX	0.75	0.85
MFMIN	0.2	0.4
NMF	0.15	0.15
PLWHC	0.02	0.02
TIPM	0.25	0.25
MBASE	0.0	0.0
UADJ	0.09	0.10
DAYGM	0.3	0.3
PXTEMP	1.5	1.5
SI	675.	300.
ELEV	18.79	11.17
LAPSEMX	0.80	0.80
LAPSEMN	0.35	0.35
ELEV-TS	17.07	9.45
PADJ	1.10	0.99
SACRAMENTO MODEL PARAMETERS		
UZWWM	100.000	85.000
UZFWM	50.000	50.000
LZWWM	150.000	135.000
LZFPM	150.000	150.000
LZFSM	30.000	30.000
DU	0.300	0.300
DLPR	0.013	0.012
DL DPR	0.110	0.100
EPS	25.000	25.000
THSM	1.700	1.470
PF	0.300	0.300
XMIOU	0.000	0.000
ADIMP	0.005	0.015
PCTIM	0.020	0.020
ETADJ	1.000	1.000

Table 23. As in Table 21, except for the Shasta Reservoir inflow simulation

SNOW PARAMETERS										
	CNB-up	CNB-lo	PIT-up	PIT-lo	DLT-up	DLT-lo	MSS-up	MSS-lo	IRON C	SHD-lo
SCA	0.90	0.85	0.95	0.95	1.40	0.95	0.95	1.00	0.95	1.0
MFMAX	0.70	0.80	0.80	0.95	0.95	1.05	0.75	0.80	0.95	0.90
MFMIN	0.2	0.3	0.3	0.5	0.25	0.15	0.1	0.15	0.5	0.45
NMF	0.15	0.15	0.15	0.15	0.15	0.15	0.15	0.15	0.15	0.15
PLWHC	0.03	0.03	0.02	0.02	0.02	0.25	0.02	0.02	0.02	0.02
TIPM	0.25	0.25	0.25	0.25	0.25	0.25	0.25	0.25	0.25	0.25
MBASE	0.0	0.0	0.0	1.0	0.0	0.0	0.0	0.0	0.0	0.0
UADJ	0.10	0.10	0.12	0.07	0.18	0.07	0.12	0.07	0.07	0.07
DAYGM	0.3	0.3	0.3	0.3	0.3	0.3	0.3	0.3	0.3	0.3
PXTEMP	1.0	1.0	1.5	1.5	1.5	1.5	1.5	1.5	1.5	1.5
SI	200.	75.	500.	500.	2000.	350.	1300.	500.	500.	500.
ELEV	16.36	12.46	18.04	13.23	17.28	10.06	18.00	11.58	13.23	5.79
LAPSEMX	0.80	0.80	0.80	0.80	0.80	0.80	0.70	0.70	0.80	0.80
LAPSEMN	0.35	0.35	0.35	0.35	0.35	0.35	0.45	0.45	0.35	0.35
ELEV-TS	18.86	14.96	18.04	13.23	17.98	10.36	16.46	11.58	13.23	5.79
PADJ	0.85	0.85	0.95	0.90	1.17	0.94	0.88	0.80	1.10	1.20
SACRAMENTO MODEL PARAMETERS										
UZTWM	90.000	80.000	185.000	135.000	70.000	130.000	270.000	100.000	185.000	50.000
UZFWM	75.000	55.000	100.000	100.000	40.000	32.000	60.000	30.000	100.000	20.000
LZTWM	250.000	150.000	150.000	100.000	280.000	140.000	400.000	230.000	150.000	25.000
LZFPM	30.000	30.000	1600.000	1450.000	1050.000	90.000	2500.000	300.000	4500.000	175.000
LZFSM	70.000	20.000	85.000	85.000	80.000	80.000	295.000	100.000	65.000	50.000
DU	0.060	0.170	0.150	0.350	0.400	0.600	0.400	0.400	0.010	0.200
DLPR	0.003	0.002	0.001	0.001	0.003	0.002	0.002	0.001	0.001	0.018
DL DPR	0.120	0.080	0.140	0.140	0.200	0.070	0.150	0.150	0.050	0.160
EPS	28.000	25.000	30.000	30.000	25.000	30.000	12.000	35.000	45.000	20.000
THSM	1.100	1.100	1.100	1.100	1.100	1.100	1.100	1.100	1.600	1.800
PF	0.250	0.250	0.500	0.500	0.150	0.200	0.800	0.300	0.300	0.300
XMIOU	0.000	0.000	0.000	0.000	0.000	0.000	0.000	0.950	0.000	0.000
ADIMP	0.060	0.050	0.080	0.050	0.150	0.000	0.001	0.120	0.000	0.050
PCTIM	0.000	0.000	0.005	0.005	0.010	0.010	0.008	0.010	0.005	0.005
ETADJ	1.000	1.000	1.000	1.000	1.000	1.000	1.000	1.000	1.000	1.000

Table 24. As in Table 21, except for the Oroville Reservoir inflow simulation

SNOW PARAMETERS												
	PLL-up	PLL-lo	IIF-up	IIF-lo	PLG-up	PLG-lo	FTC-up	FTC-lo	MRM-up	MRM-lo	ORD-up	ORD-lo
SCA	1.10	1.01	1.35	1.0	1.40	0.85	1.25	1.00	1.2	1.00	1.38	1.0
MFMAX	0.55	0.65	0.85	1.3	1.15	1.30	0.90	1.10	1.0	1.05	0.95	1.1
MFMIN	0.008	0.016	0.1	0.15	0.15	0.20	0.55	0.55	0.1	0.15	0.10	0.15
NMF	0.15	0.15	0.15	0.15	0.15	0.15	0.15	0.15	0.15	0.15	0.15	0.15
PLWHC	0.05	0.05	0.02	0.25	0.02	0.05	0.02	0.25	0.02	0.05	0.02	0.25
TIPM	0.10	0.10	0.25	0.25	0.25	0.25	0.25	0.25	0.25	0.25	0.25	0.25
MBASE	2.0	0.0	0.0	0.0	0.0	0.0	0.0	0.0	0.0	0.0	0.0	0.0
UADJ	0.0	0.01	0.09	0.05	0.04	0.15	0.16	0.07	0.06	0.03	0.16	0.07
DAYGM	0.3	0.3	0.3	0.3	0.3	0.3	0.3	0.3	0.3	0.3	0.3	0.3
PXTEMP	1.15	1.15	1.5	1.5	1.5	1.5	1.5	1.5	1.5	1.5	1.5	1.5
SI	2000.	1249.	2000.	1250.	2000.	500.	2000.	1250.	2000.	500.	2000.	1250.
ELEV	17.03	14.27	19.10	12.00	17.23	12.92	18.77	15.94	17.05	130.7	16.76	8.15
LAPSEMX	0.60	0.60	0.60	0.60	0.60	0.60	0.60	0.60	0.60	0.60	0.60	0.60
LAPSEMN	0.45	0.45	0.45	0.45	0.45	0.45	0.45	0.45	0.45	0.45	0.45	0.45
ELEV-TS	18.90	10.36	18.90	10.36	17.37	12.80	18.90	10.36	17.37	10.36	18.90	10.36
PADJ	1.02	1.08	0.98	0.95	1.10	0.98	0.98	1.0	1.06	1.04	1.14	0.97
SACRAMENTO MODEL PARAMETERS												
UZTWM	155.000	55.000	150.000	85.000	60.000	125.000	180.000	235.000	90.000	50.000	60.000	145.000
UZFWM	80.000	80.000	36.000	48.000	80.000	50.000	45.000	51.000	50.000	30.000	20.000	28.000
LZTWM	20.000	35.000	300.000	230.000	325.000	175.000	200.000	200.000	150.000	100.000	390.000	360.000
LZFPM	710.000	610.000	120.000	160.000	550.000	350.000	200.000	200.000	230.000	115.000	210.000	210.000
LZFSM	60.000	80.000	52.000	50.000	100.000	35.000	100.000	65.000	150.000	85.000	145.000	65.000
DU	0.100	0.100	0.300	0.300	0.150	0.300	0.400	0.300	0.200	0.500	0.500	0.500
DLPR	0.002	0.002	0.014	0.003	0.002	0.005	0.010	0.010	0.003	0.006	0.009	0.007
DL DPR	0.040	0.030	0.140	0.070	0.040	0.090	0.400	0.400	0.040	0.140	0.140	0.140
EPS	15.000	35.000	12.000	17.000	30.000	30.000	15.000	15.000	50.000	50.000	25.000	25.000
THSM	1.100	1.100	1.150	1.250	1.100	1.100	1.100	1.100	1.200	1.200	1.100	1.100
PF	0.800	0.800	0.350	0.650	0.550	0.450	0.400	0.400	0.350	0.300	0.250	0.250
XMIOU	0.000	0.000	0.000	0.000	0.000	0.000	0.000	0.000	0.000	0.000	0.000	0.000
ADIMP	0.060	0.040	0.000	0.000	0.100	0.100	0.050	0.050	0.100	0.200	0.050	0.090
PCTIM	0.000	0.240	0.002	0.001	0.010	0.025	0.001	0.015	0.005	0.008	0.003	0.080
ETADJ	1.000	1.000	1.000	1.000	3.000	3.000	1.000	1.000	1.000	1.000	1.000	1.000

Table 25. Performance statistics for the historical simulation of the INFORM distributed hydrologic model

	<i>R</i>	<i>RMSE</i>	<i>PDAE</i>	<i>Water Years</i>
Folsom	0.94	74.3	0.3	10/1/1960–9/30/1999
Oroville	0.92	117.9	0.32	10/1/1960–9/30/1997
Trinity	0.93	31.2	0.32	10/1/1963–9/30/1999
Shasta	0.94	105.2	0.25	10/1/1960–9/30/1992

Although these results appear very encouraging, further evaluation was conducted by comparing the simulated natural flows into the lakes at the basin outlets to CNRFC FNF estimates. For the stand-alone distributed model, this evaluation focused only on reservoir inflow simulations at the four reservoir locations. In a similar fashion to what was presented for the CNRFC operational hydrologic model evaluation, different types of plots were used during this process that highlight different performance aspects of the inflow simulations. In this section, example plots are included for the Folsom reservoir inflow simulations, with plots for the remaining reservoirs (Trinity, Shasta and Oroville) included in Appendix F.

Figure 61 shows a comparison of the simulated and observed FNF hydrographs of daily flow for Water Years 1961 to 1970 and for the Folsom inflows. These plots show that the simulated response captures well the unimpaired inflow over a range of flow magnitude. Water Year 1965 is a year of particularly high flows (peak near 5,000 m³/s), while Water Years 1961 and 1966 are low-flow years (peak flow less than 200 m³/s). The model simulates both high and low flows well. The analogous plots in Appendix F for Trinity, Shasta, and Oroville reservoirs lead to the same conclusion.

This result is corroborated by the scatter plot of observed versus simulated inflows over the period of record as shown in Figure 62 for Folsom (and similar plots in Appendix F for other reservoirs). In this plot, the straight line signifies the 45° line of perfect correspondence. These scatter plots allow for the assessment of overall functional relationship and performance with respect to extreme events, which are distinct from the cloud of points at lower flows. The plot shows good agreement over a wide range of flows, with a tendency toward underestimation for the highest flows.

Figure 63 presents the cumulative-flow curves for Folsom. Discrepancies in the long-term water yield in the simulation are signified by a deviation in the cumulative frequency curve from the observed. For Folsom, the deviation becomes noticeable after approximately 5000 days of simulation. Such deviation is similar for Shasta, but it is significantly smaller for Trinity and Oroville.

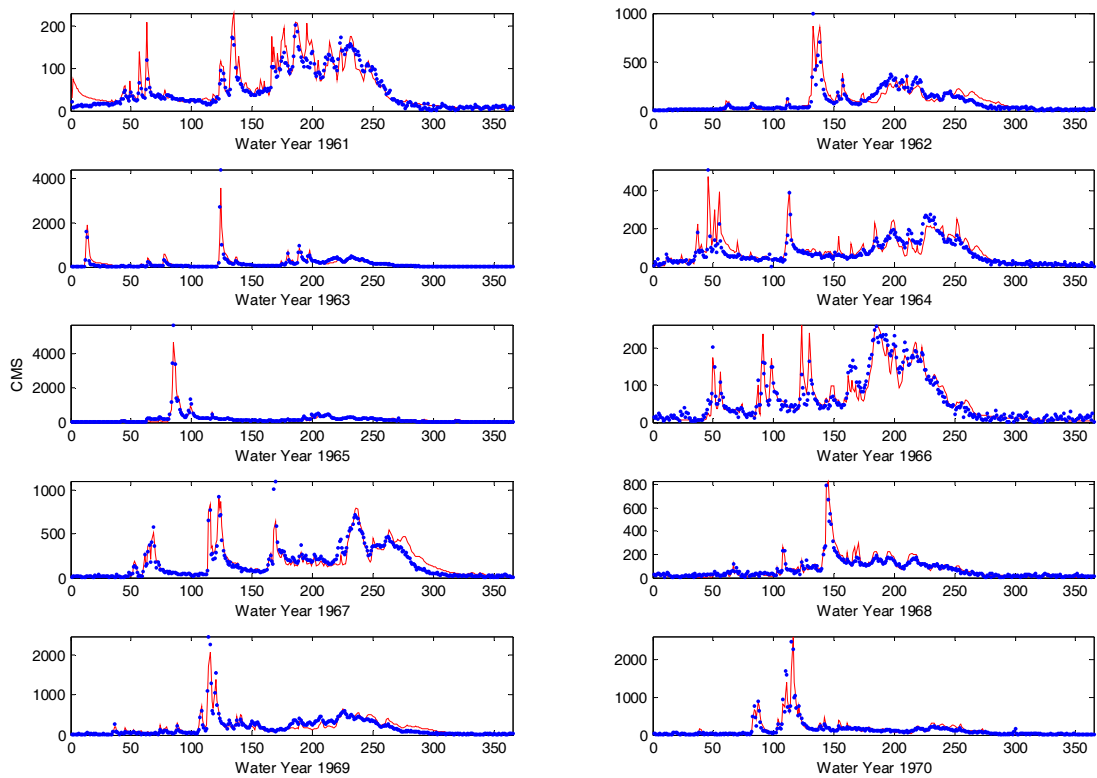


Figure 61. Comparison of observed (FNF, in blue) and simulated (red) inflows to Folsom Reservoir for the INFORM stand-alone distributed hydrologic model

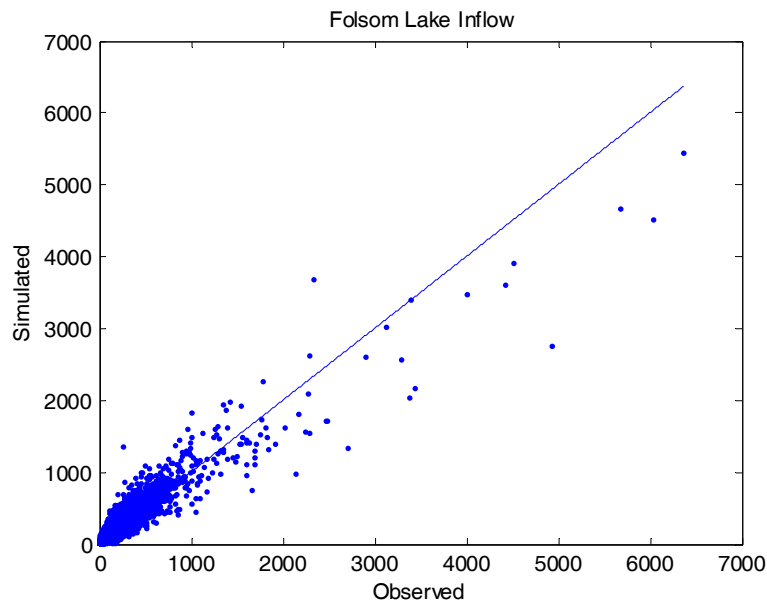


Figure 62. Mean daily observed (FNF) versus simulated inflows to Folsom Reservoir for the stand-alone distributed hydrologic model

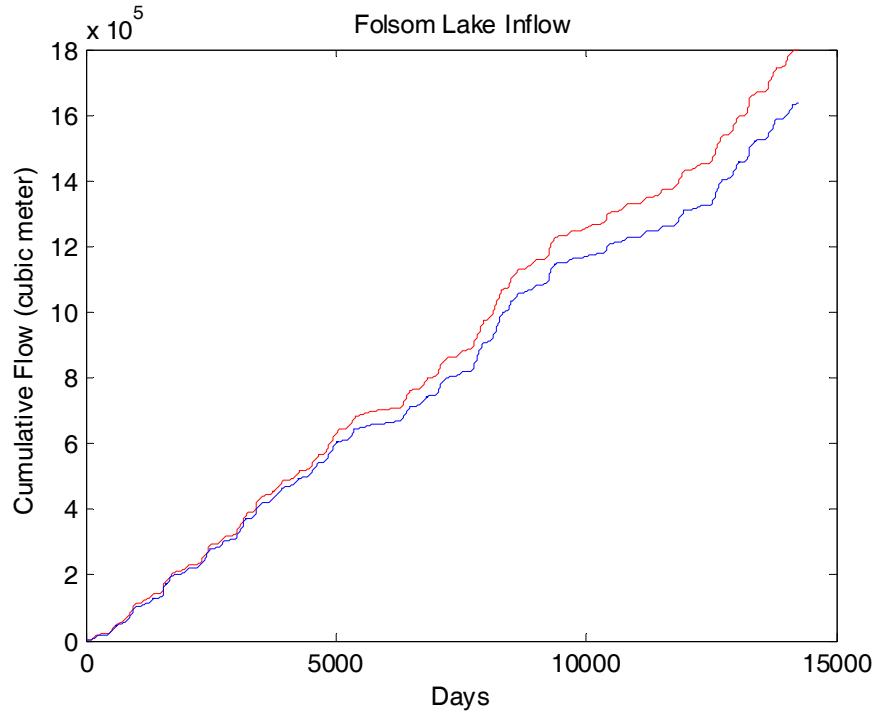


Figure 63. Observed (FNF, blue) and simulated (red) cumulative inflows to Folsom Reservoir for Water Years 1961–1999

As noted previously, the seasonal transition of inflows is an important hydrologic dynamic of the Sierra Nevada watersheds. Figure 64 presents the daily-flow scatter plot of Box-Cox transformed flows on a monthly scale (Equation 54). Again, the 45° line of perfect correspondence is indicated for each month. Good model performance and correspondence is observed for all months except the summer months of July, August and September. This relatively poor performance during summer months is also observed for the other reservoirs (shown in Appendix F). It is apparent that the stand-alone distributed model performs similarly to the CNRFC operational model with somewhat of a wider scatter of the points for certain months and with a lower bias exhibited in summer months

Lastly, the monthly cycle of the simulated and observed long-term averaged inflows to Folsom Lake is shown in Figure 65 for the INFORM stand-alone distributed model. This results may be compared to the analogous results obtained for the operational model shown in Figure 58 (upper left panel). The behavior of the INFORM model is similar to that of the operational model, with less-pronounced volume biases during the early snowmelt season (March–April) but with more pronounced biases during the late snowmelt season and in early summer (May–June).

4.6.3.3. Summary of stand-alone hydrologic model evaluation

The following summarize the major findings from the stand-alone distributed hydrologic model evaluation.

- Overall the model performed well and captured the hydrologic response with respect to timing and magnitude. In general, most of the conclusions drawn regarding the model performance were found to be relevant to all four basins.
- The stand-alone model tends to underestimate larger events. However it appears that over all it does not have a consistent bias.
- The cumulative flow plots show good agreement, especially for Oroville and Trinity. In Folsom and Shasta, there is slight overestimation of the total flow over the long term. This is an encouraging result and implies that the model performs well in long-term simulations and can be useful for long-term prediction of reservoir inflows when forced with good input data.
- At the monthly flow level, summer flows (June–September) have the weakest agreement with the FNF estimates. The summer flow at these basins is thought to be controlled by: (1) potential evapotranspiration; (2) groundwater discharge to the stream (baseflow); and (3) operational regulation of upstream reservoir releases. Therefore the poorer agreement in the summer flow might be due to errors in the model forcing of potential evapotranspiration, model errors in baseflow simulation, or inability of the FNF estimates to capture correctly upstream operational activities for low flows.

The INFORM stand-alone distributed hydrologic model captures the hydrologic response of the reservoir drainage basins. It also has comparable performance to the CNRFC operation hydrologic model.

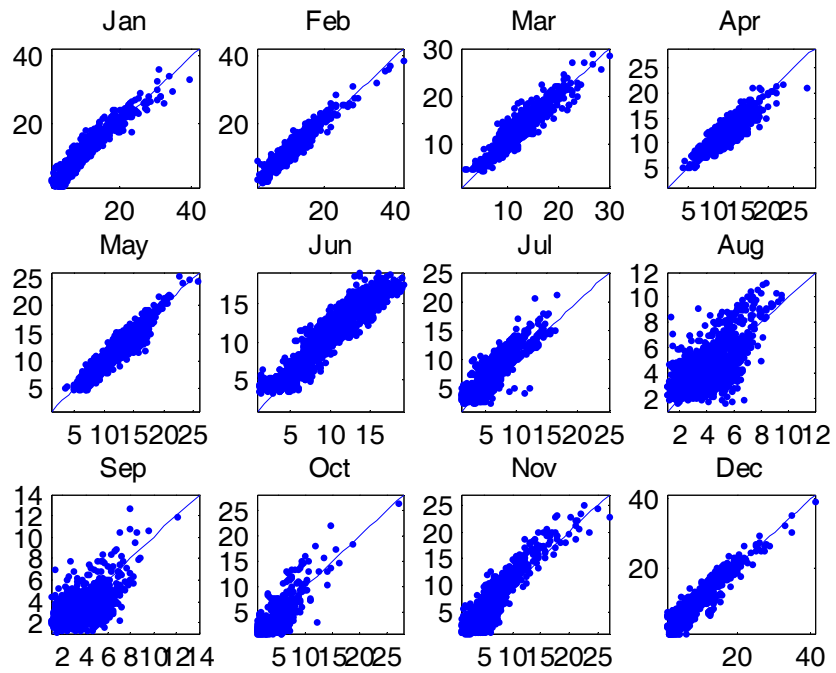


Figure 64. Monthly scatter plots of simulated inflows versus FNF flow for Folsom Reservoir in Box Cox transformed units for the stand-alone distributed hydrologic model

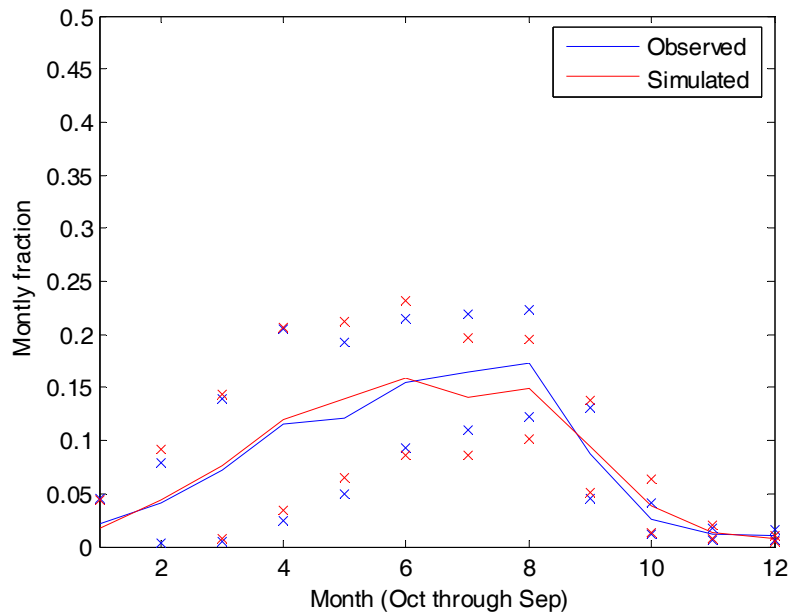


Figure 65. Observed (FNF) and simulated monthly mean inflows (+/- 1 standard deviation) for Folsom Reservoir, expressed as a fraction of annual flow volume. Presented is the simulation with the stand-alone distributed hydrologic model.

5.0 Decision Support System

5.1. Background and Overview

The INFORM DSS is a planning and management tool for the Northern California river and reservoir system described in Chapter 2 (and Figure 10). The system encompasses five rivers (Trinity, Sacramento, Feather, American, and San Joaquin), five major reservoirs (Clair Engle Lake, Shasta, Oroville, Folsom, and New Melones), 10 hydro power plants, the Sacramento-San Joaquin (Bay) Delta, and the water export system to southern California, including the San Luis reservoir. Water uses include water supply (to domestic, agricultural, and industrial sites), energy generation, minimum instream flow targets, and delta environmental and ecosystem requirements. Appendix G includes various project and demand data.

A 1986 agreement between the U.S. Department of the Interior, Bureau of Reclamation, and the California Department of Water Resources provides for the coordinated operation of the state (State Water Project, SWP) and federal (Central Valley Project, CVP) facilities. This Agreement of Coordinated Operation (COA) aims to ensure that each project obtains its share of water from the Delta and protects other beneficial uses in the Delta and the Sacramento Valley. The coordination is structured around the necessity to meet the in-basin use requirements in the Sacramento Valley and the Delta, including Delta outflow and water quality requirements.

The INFORM DSS modeling framework has been described in Chapter 2 (Figure 11). The DSS includes multiple interconnected modeling layers designed to support decisions associated with four temporal scales, several objectives, and a number of federal and state decision-making agencies. More specifically, the INFORM DSS includes models for long-range planning (monthly resolution/one-two year horizon), mid-range management (daily resolution/several months horizon), short-range management (hourly resolution/one day horizon), and near-real-time operation (hourly dispatching of each hydropower turbine and hydraulic outlet). The INFORM DSS also includes an assessment model which replicates the system response under various inflow scenarios, system configurations, and policy options. This chapter describes the DSS models in detail, and includes typical case studies. The models are discussed in the order they were developed, starting with the near-real-time operational models (highest resolution/shortest horizon), continuing with the short- and mid-range management models (intermediate resolution/horizon), and ending with the long-range planning models (lowest resolution/longest horizon). This model development order is necessary because each model in the DSS structure is built upon information generated by the preceding model.

5.2. Near-Real-Time Operations: Turbine Load Dispatching Model

In hydropower plants with many turbines, the turbine load dispatching problem for an individual plant can be expressed as follows: Given a total outflow discharge Q^* and a certain reservoir storage S , determine the discharge q_j through each turbine j and the

spillway flow rate s such that $\sum q_j + s = Q^*$ and total power P is maximized. Namely, the problem calls for allocating the total discharge among the turbines in a way that maximizes power generation. This mode of operation is also attractive from a water management standpoint because it implies that a given power generation level is achieved at the least possible outflow (water conservation).

The following material presents the mathematical formulation of this problem and outlines the solution method implemented in the INFORM DSS.

The formulation uses the following notation:

q_j	discharge of turbine j , $j=1, \dots, n$;
$[q_j^{\min}, q_j^{\max}]$	discharge operational range for turbine j ;
p_j	power load of turbine j ;
$[p_j^{\min}, p_j^{\max}]$	power operational range of turbine j ;
Q^*	total discharge target for the entire hydropower plant, including spillway outflow, if any;
s	spillway (or other outlet) discharge;
$p_j = g_j(H_n, q_j)$	turbine power generation function relating power generation (p_j) to discharge (q_j) and net hydraulic head (H_n);
$H = f(S)$	reservoir forebay elevation (H) versus storage (S) relationship;
$H_{ls}(Q)$	hydraulic loss function;
$t = r(Q)$	tailwater elevation (t) versus total outflow (Q) curve;
H_n	net hydraulic head.

The objective of the load dispatching problem is to find $\{q_j$ and $p_j, j = 1, \dots, n\}$ that

$$\text{maximize } P = \sum_{j=1}^n p_j$$

subject to

$$Q^* = \sum_{j=1}^n q_j + s$$

$$H_n = f(S) - r(Q) - H_{ls}(Q),$$

$$p_j = g_j(H_n, q_j),$$

$$p_j^{\min} \leq p_j \leq p_j^{\max} \quad \text{or} \quad p_j = 0,$$

$$q_j^{\min} \leq q_j \leq q_j^{\max} \quad \text{or} \quad q_j = 0.$$

An efficient way to handle the various nonlinearities and discontinuities of the above-stated problem is to reformulate it in multistage form and solve it via dynamic programming. The multistage formulation is as follows:

$$\text{Maximize } J = \sum_{j=1}^n p_j(q_j, H_n)$$

subject to

$$X_{j+1} = X_j + q_j, \quad j = 1, \dots, n,$$

$$X_1 = 0, \quad X_{n+1} = Q^*$$

$$H_n = f(S) - r(Q^*) - H_{ls}(Q^*),$$

$$p_j^{\min} \leq p_j \leq p_j^{\max} \quad \text{or} \quad p_j = 0,$$

$$q_j^{\min} \leq q_j \leq q_j^{\max} \quad \text{or} \quad q_j = 0.$$

Clearly, if the discharge target Q^* is higher than Σq_j^{\max} , the problem is trivial, and the optimal solution would be to load the turbines at full capacity and pass the excess flow through the spillway or some other outlet structure.

In the previous formulation, the individual turbine discharges (q_j) constitute the control variables and the cumulative discharges (X_j) constitute the state variables. Each stage j represents a different turbine, and the performance index maximizes the total plant power. This problem is in a typical, one-dimensional, dynamic programming form, and can be solved by the traditional backward DP procedure (Bellman and Dreyfus 1962).

An equivalent formulation that also maximizes plant operational efficiency would be to minimize the total plant discharge Q for a given plant power generation P^* . This problem can also be formulated in the same way and solved using dynamic programming.

The load dispatching problem can be solved for various combinations of plant discharge (Q) and reservoir level (H) to define the best efficiency plant power function $P(Q,H)$. This function determines the maximum possible power that can be produced by outflow Q and head H and is used by the short-range reservoir management model to represent the power generation function in the reservoir management process. The computations to obtain $P(Q,H)$ are performed only once in an off-line mode. Updating of $P(Q,H)$ is necessary only if turbine characteristics change.

Various reservoir and hydropower plant data used by the turbine load dispatching model are included in Appendix G. Specifically, the appendix contains tables and figures with storage versus elevation data, discharge versus tail water level data, and turbine characteristic curves (i.e., power versus discharge versus net hydraulic head relationships) for Trinity, Shasta, Oroville, and Folsom.

Model results are presented in Figure 66. This figure depicts the plant generation curves derived by the optimization procedure described in this section. The curves provide the maximum power output that a plant can generate for a particular combination of reservoir level and total discharge.

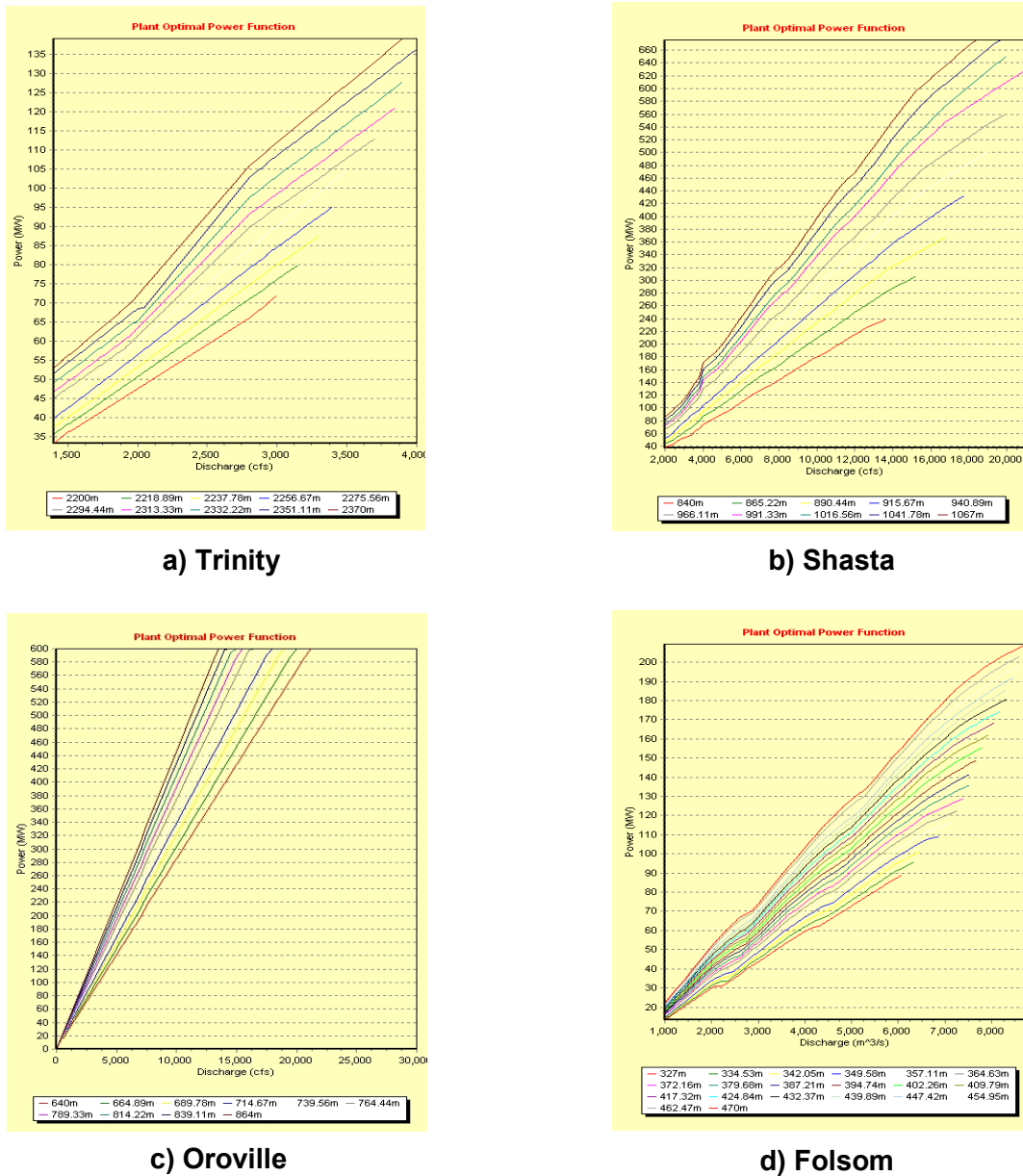


Figure 66. Plant power generation as function of hourly discharge and reservoir level for a) Trinity, b) Shasta, c) Oroville, and d) Folsom

5.3. Short-Range Reservoir Management

The purpose of this model is to find the most suitable hourly release schedule within a particular day. The short-range model uses the power functions generated by the turbine load dispatching model for each power plant, and must satisfy the daily release target decided by the mid-range control model (discussed next). The short-range model incorporates all release requirements (pertaining to water supply, flood control, environmental protection, etc.) as well as all power requirements, such as dependable capacity commitments. In addition to generating optimal schedules, the model is used in an off-line mode to generate the relationship between daily release, reservoir level, and energy generation to be used by the mid-range management model.

Denoting R the total daily release volume specified by the mid-range reservoir management model, the objective of the short-range model is to determine the hourly discharges $\{u(t), t = 0, \dots, 23\}$ for each reservoir that

$$\text{minimize } J_s[R, H(s(0))] = \sum_{t=0}^{23} F[u(t)] - P[u(t), H(S(t))]$$

subject to

$$S(t+1) = S(t) - u(t) + w(t) - L(t), \quad t = 0, \dots, 23, \quad S(0) = \text{known},$$

$$R = \sum_{t=0}^{23} u(t),$$

$$u(t) - \Delta u^{\min} \leq u(t+1) \leq u(t) + \Delta u^{\max}, \quad t = 0, \dots, 23,$$

$$P^{\min}(t) \leq P[u(t), H(S(t))] \leq P^{\max}(t), \quad t = 0, \dots, 23,$$

$$u^{\min}(t) \leq u(t) \leq u^{\max}(t), \quad t = 0, \dots, 23,$$

$$S^{\min}(t) \leq S(t) \leq S^{\max}(t), \quad t = 0, \dots, 23,$$

where t is the time index (in hours); $F[u(t)]$ is the flood damage or cost associated with hourly discharge $u(t)$ including both turbine and spillway outflow; $P[u(t), H(S(t))]$ is the best efficiency plant power function discussed earlier; $H(S(t))$ is the elevation versus storage relationship; $S(t)$ is reservoir storage at the beginning of hour t ; $w(t)$ is the inflow (characterized by ensemble forecasts); $L(t)$ is reservoir loss or gain due to water diversions and surface precipitation and evaporation, if the latter are significant; P^{\min}/P^{\max} are power generation constraints; u^{\min}/u^{\max} are hourly release constraints reflecting water supply, environmental, ecological, flood control, and other operational requirements; S^{\min}/S^{\max} are storage constraints; and Δu^{\min} and Δu^{\max} are operational limits on release decreases and increases from hour to hour.

The previous formulation accounts for different reservoir management objectives through various means. These are discussed in the following comments:

1. The objective function (or performance index) J aims to minimize flood damage and maximize energy generation. Although both terms are present in J , they are usually active during different hydrologic events. Specifically, during low, normal or moderate flows, flooding is not a concern, and the model aims to maximize energy generation (or, equivalently, minimize the negative of P []). During such times, low flow, water supply, and other operational requirements (such as dependable capacity constraints) are enforced through the release and power constraints (u^{\min}/u^{\max} , $\Delta u^{\min}/\Delta u^{\max}$, and P^{\min}/P^{\max}). On the other hand, during high floods, when significantly higher volumes R must be released, all available hydro turbines run at full gate, and the model is concerned with regulating spillway outflows to mitigate flood damage (F []).
2. If the inflow forecast over the next 24 hours is probabilistic, the storage constraints in the above formulation must also be converted in a probabilistic form, reflecting the requirement that the storage bounds S^{\min}/S^{\max} should not be exceeded by more than a certain tolerance level. Furthermore, in this case, the performance index aims to optimize a statistic of J such as the mean value or a certain percentile of its distribution. However, inflow forecast uncertainty over 24 hours may not translate to considerable uncertainty of reservoir storage, and the previous probabilistic considerations may not be necessary.
3. If hourly power sale prices are available, this model can be used to optimize total economic gains or losses by replacing function $P[u(t), H(S(t))]$ in the performance index by function $G[P[u(t), H(S(t)), t]$, which represents the economic gain associated with power generation $P[u(t), H(S(t))]$ in hour t . Alternatively (but not equivalently), one could determine the hourly power generation which minimizes the sum of square deviations from an hourly target power demand sequence $\{P^*(t), t = 0, 1, \dots, 23\}$. Namely, in this case, the objective would be to

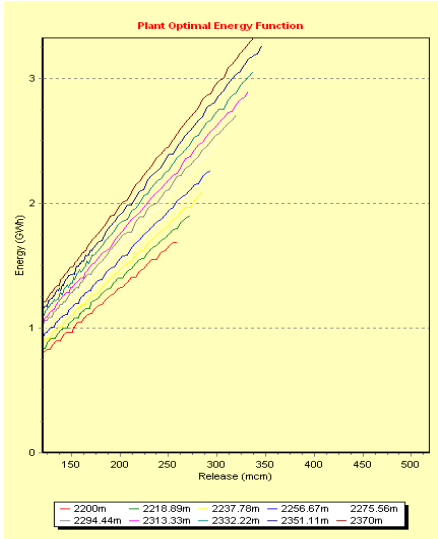
$$\text{minimize } J_s[R, H(s(0))] = \sum_{t=0}^{23} F[u(t)] - (P^*(t) - P[u(t), H(S(t))])^2 .$$

This procedure recognizes the need to generate more power during the peak generation period, but does not explicitly maximize economic gains.

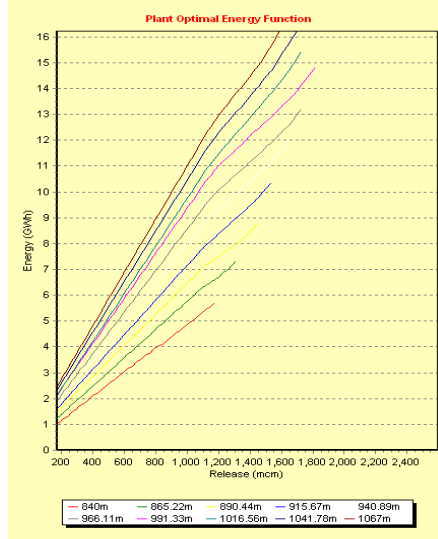
4. The above-formulated problem is solved by the Extended Linear Quadratic Gaussian (ELQG) control method to be discussed in Section 5.5. However, in cases where daily inflow and outflow is a small fraction of reservoir storage, the problem can be considerably simplified, assuming that reservoir level remains constant. This problem does not include the storage dynamical equation and associated constraints (S^{\min}/S^{\max}) and is solved via a one-dimensional dynamic programming scheme.
5. Repeated solution of the short-range problem for various combinations of initial reservoir levels $H(S(0))$ and $(R-I)$ yields the daily energy generation (or energy revenue) function $E[H(S(0), R-I]$, the daily flood damage function $F_1[H(S(0)), R-I]$,

and the daily spillage function $S_p[H(s(0)), R-I]$, where $(R-I)$ is the daily release minus the daily inflow. These functions are computed once, in an off-line mode, and are used by the mid-range control model to represent the benefits and costs associated with particular combinations of reservoir levels, daily releases, and inflow forecasts. If the daily inflow is not appreciable relative to reservoir storage and release, the previous functions are derived in terms of the daily release R , not the difference $R-I$.

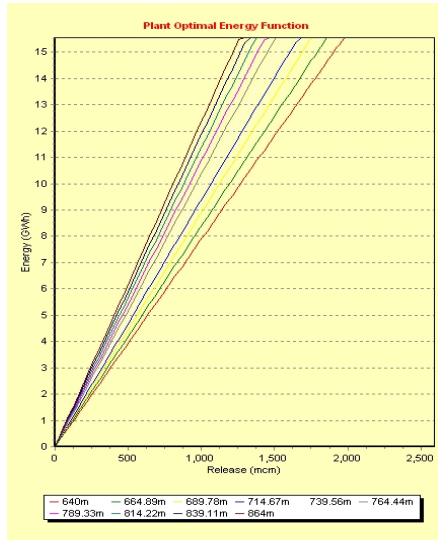
Results from the short-range management model for Trinity, Shasta, Oroville, and Folsom are presented in Figures 67 and 68. Figure 67 shows the daily energy generation functions obtained through the optimization process described earlier. These functions are used by the mid-range management model to translate daily release volumes into daily energy generation. Figure 68 depicts typical examples of 24-hour power generation sequences that correspond to each point of the daily generation functions.



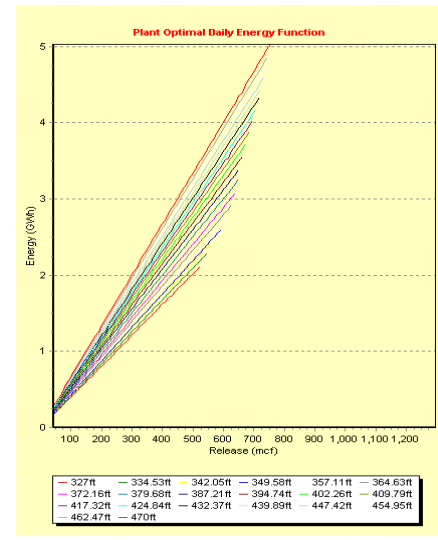
a) Trinity



b) Shasta

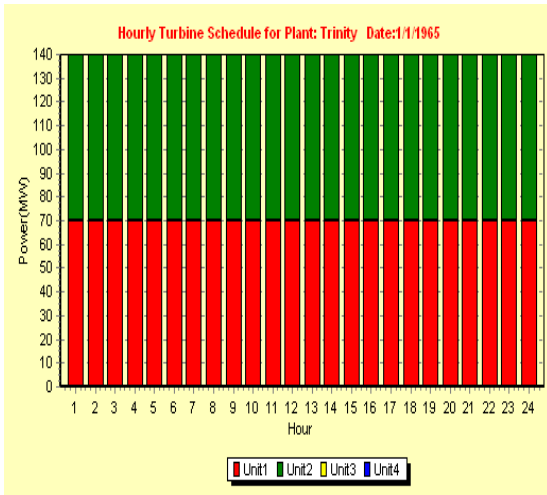


c) Oroville

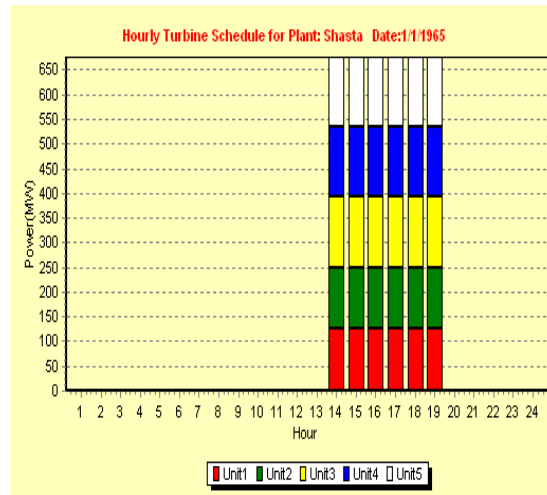


d) Folsom

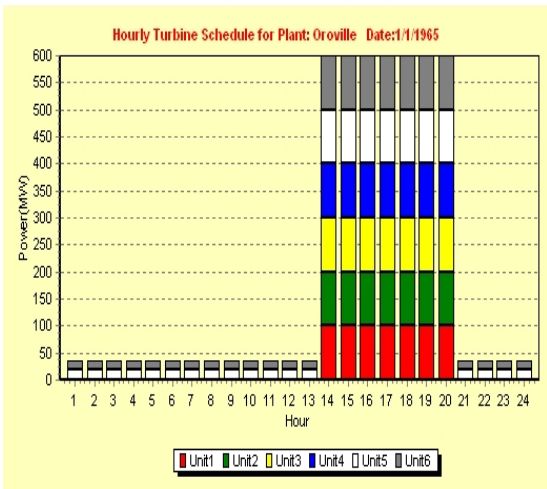
Figure 67. Plant daily generation as function of daily release and reservoir level for a) Trinity, b) Shasta, c) Oroville, and d) Folsom



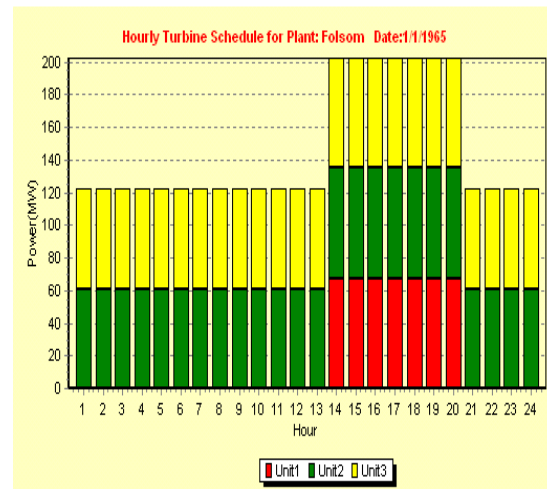
a) Trinity



b) Shasta



c) Oroville



d) Folsom

Figure 68. Typical hourly power generation schedules for a) Trinity, b) Shasta, c) Oroville, and d) Folsom

5.4. Mid-Range Reservoir Management

The mid-range management model has a time resolution of one day and a time horizon of several months. The links with the short-range control model are the daily energy generation, flood damage, and spillage functions, which ensure that the benefits and consequences associated with daily decisions are realizable in an hourly sense. The mid-range model also uses the seasonal forecasts provided by the forecasting component. The purpose of the model is to (1) assess the relevant operational tradeoffs, and (2) determine the reservoir releases associated with the tradeoff regions that might interest the management authorities.

The mathematical formulation of the mid-range management problem is similar to that of the short-range model, except that it applies to daily quantities and has a control horizon that extends over several months. The objective is to determine the daily release sequences $\{u(t), t = 0, \dots, N-1\}$ that

$$\begin{aligned} \text{minimize } J_M[H(S(0))] = & \left\{ \sum_{t=0}^{N-1} F_1[H(S(t)), u(t) - w(t)] - E[H(S(t)), u(t) - w(t)] \right. \\ & \left. + S_p[H(S(t)), u(t) - w(t)] + c(t) [S(t) - S^{\max}(t)]^2 \right\} + c(N) [S(N) - S^{\max}(N)]^2 \end{aligned}$$

subject to

$$S(t+1) = S(t) - u(t) + w(t) - L(t), \quad t = 0, \dots, N-1, \quad S(0) = \text{known},$$

$$E^{\min}(t) \leq E[H(S(t)), u(t) - w(t)] \leq E^{\max}(t), \quad t = 0, \dots, N-1,$$

$$u^{\min}(t) \leq u(t) \leq u^{\max}(t), \quad t = 0, \dots, N-1,$$

$$S^{\min}(t) \leq S(t) \leq S^{\max}(t), \quad t = 0, \dots, N,$$

where t is the time index (in days); N is the length of the control (and forecast) horizon; $F_1[\]$ is the daily flood damage or cost function associated with initial reservoir level $H(S(t))$, daily release $u(t)$, and inflow forecast $w(t)$; $E[\]$ is the daily energy generation function; $S_p[\]$ is the daily spillage function; $S(t)$ is reservoir storage at the beginning of day t ; $L(t)$ is reservoir loss or gain due to water diversions and surface precipitation and evaporation if the latter are significant; E^{\min}/E^{\max} are energy generation requirements based on energy contracts; u^{\min}/u^{\max} are daily release constraints reflecting water supply, environmental, ecological, flood control, and other operational requirements; S^{\min}/S^{\max} are storage constraints reflecting flood control and recreational requirements, and $\{c(t), t = 0, 1, \dots, N\}$ are coefficients penalizing storage deviations away from its maximum levels $S^{\max}(t)$. The following comments clarify various aspects of the mid-range reservoir management model formulation.

1. The daily inflow process $\{w(t), t=0, 1, \dots, N-1\}$ is characterized by forecast ensembles and is thus probabilistic. This inflow characterization is necessary in

the mid-range model in light of the significant magnitude and uncertainty associated with seasonal inflows. In view of this, the performance index is a random variable, and the objective of the optimization is to minimize its mean or a certain percentile. Furthermore, the storage constraints are understood in a probabilistic sense,

$$\text{Prob}[S^{\min}(t) \leq S(t)] \geq \pi^{\min}(t), \quad t = 0, \dots, N,$$

$$\text{Prob}[S(t) \leq S^{\max}(t)] \geq \pi^{\max}(t), \quad t = 0, \dots, N,$$

where π^{\min} and π^{\max} are user-defined probabilistic levels for keeping the reservoir storage respectively higher and lower than S^{\min} and S^{\max} at prescribed reliabilities.

2. The mid-range objective function aims to minimize flood damage and spillage (i.e., spillway releases in excess of turbine capacity), maximize energy generation, and maintain reservoir levels as high as possible while meeting water supply and environmental flow requirements. Clearly, these objectives cannot be fully met *all* at the same time. For this reason, the model is intended first to assess the tradeoffs among the various water uses. Tradeoffs are important information that management authorities can use to select management options in a dynamic fashion. For example, in any given season, a key decision is the portion of reservoir storage that should be reserved for flood control versus energy generation and other purposes. Clearly, more flood control storage would reduce the risk of flood damage. However, it would also draw reservoir levels down and could potentially compromise energy generation and other water uses (e.g., water supply and low flow augmentation) in the ensuing dry season. On the other hand, if the inflow forecast reliably indicates a drier than normal climate, the risks of reducing flood control storage would be small, and the impact to the other water uses less significant. Similar considerations apply to generating more energy versus keeping reservoir levels higher for use in future seasons. Thus, deriving and studying tradeoffs provides an insightful appreciation of the interrelations among water uses and establishes a holistic perspective of water management.

In the INFORM DSS, tradeoffs are quantified by gradually increasing the reliability parameters and the coefficients $c(t)$. The relationships of various quantities (e.g., flood risk, energy generation, terminals storage, risk of not meeting water supply and low flow requirements) are then examined and compared. After reviewing this information, the management authorities can decide on an acceptable compromise between benefits and risks. Once a decision is made, the INFORM DSS determines the associated release and storage sequences and is ready to activate the short-range management model to refine the daily release volumes into consistent hourly decisions. This process is intended to be sequential and be reevaluated adaptively as time progresses and

as more accurate information is collected on the state of the system, the hydrology, and the demands.

3. The above-stated problem is solved by the extended linear quadratic Gaussian control method developed by A. Georgakakos and associates (described in the next section and the cited references), a method suitable for multidimensional and uncertain reservoir systems. The mid-range management problem is formulated and solved for each *individual* reservoir, and it could thus be solved using a one-dimensional dynamic programming algorithm. However, for consistency with the basin-wide reservoir coordination that is carried out at the long-range planning model, the mid-range reservoir management problem is solved using ELQG, a dynamic optimization algorithm suitable for multi-reservoir uncertain systems. ELQG is an explicitly stochastic optimization method, determining releases that optimize with respect to the entire forecast ensemble, not with respect to individual traces. ELQG is described in detail in the following section, long-range planning, where it is more generally and uniquely applicable.

Results from the mid-range control model for Folsom and Oroville are included in Figures 69, 70, 71, and 72. These figures present example model runs with a 90-day forecast and management horizons. The reservoir management purpose for these runs is to determine releases that meet the minimum and maximum release requirements while maintaining (1) reservoir levels as high as possible, and (2) the probability of spillage less or equal to 10%. The graphs indicate that the model accomplishes this objective by keeping reservoir levels near the top of the conservation storage with 90% of the traces being within the pre-specified storage limits. The INFORM DSS can be used to generate operational tradeoffs by varying the reliability levels and other parameters (e.g., minimum and maximum release levels and storages) and running the model to explore the impacts that these changes might have on the system's performance relative to its various objectives (e.g., the reliability of meeting water supply and environmental flow targets, energy generation, and flood protection requirements).

5.5. Long-range Planning

The long-range planning model has a time resolution of one month and a time horizon of one to two years. In contrast to the preceding DSS models, the long-range planning model represents the entire Northern California river and reservoir system and aims to assess applicable planning tradeoffs and develop coordinated planning strategies.

The long-range planning model includes comprehensive simulation and optimization routines described next.

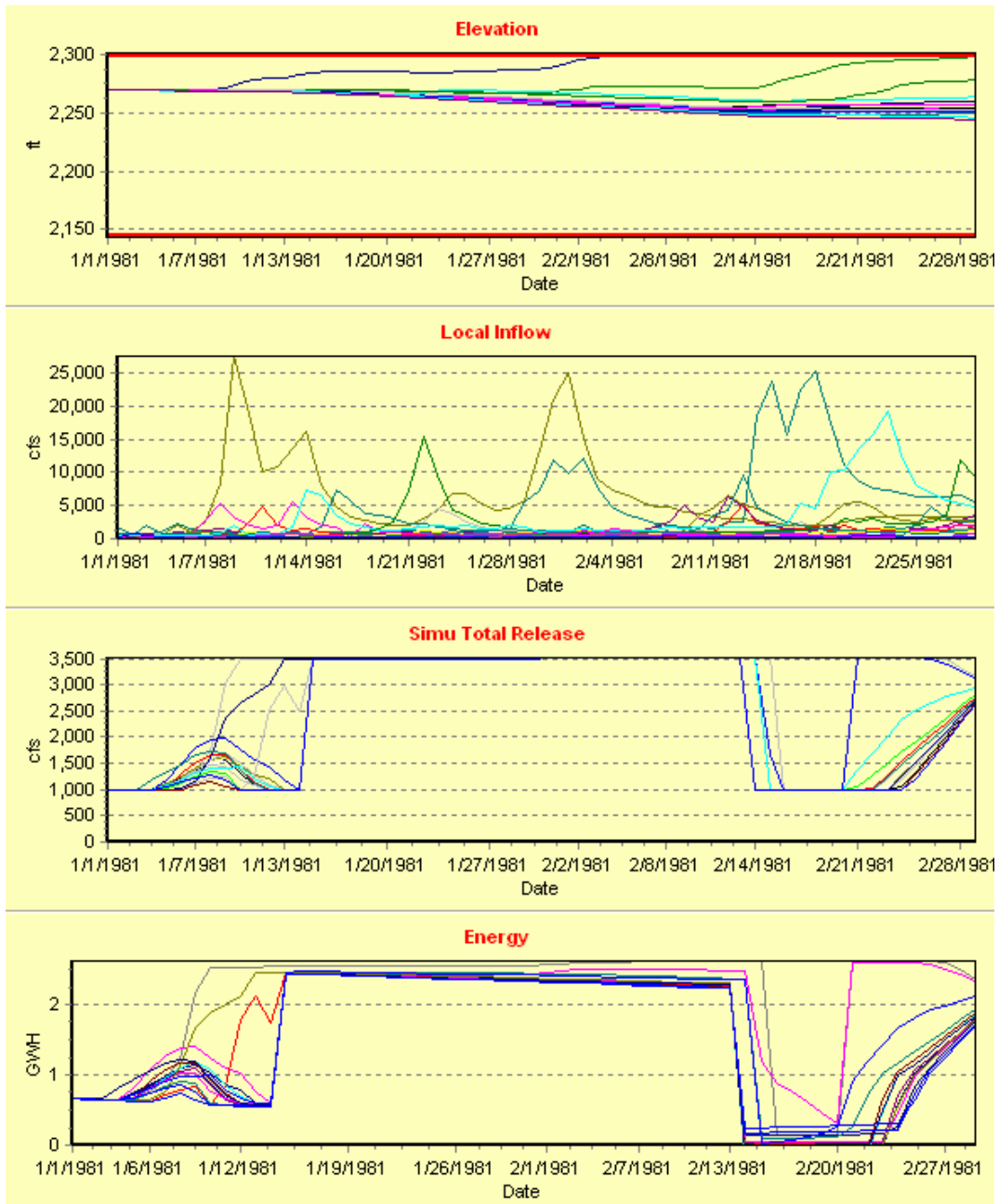


Figure 69. Mid-range model example run for Trinity. A 3-month forecast horizon from 1/1/1981.

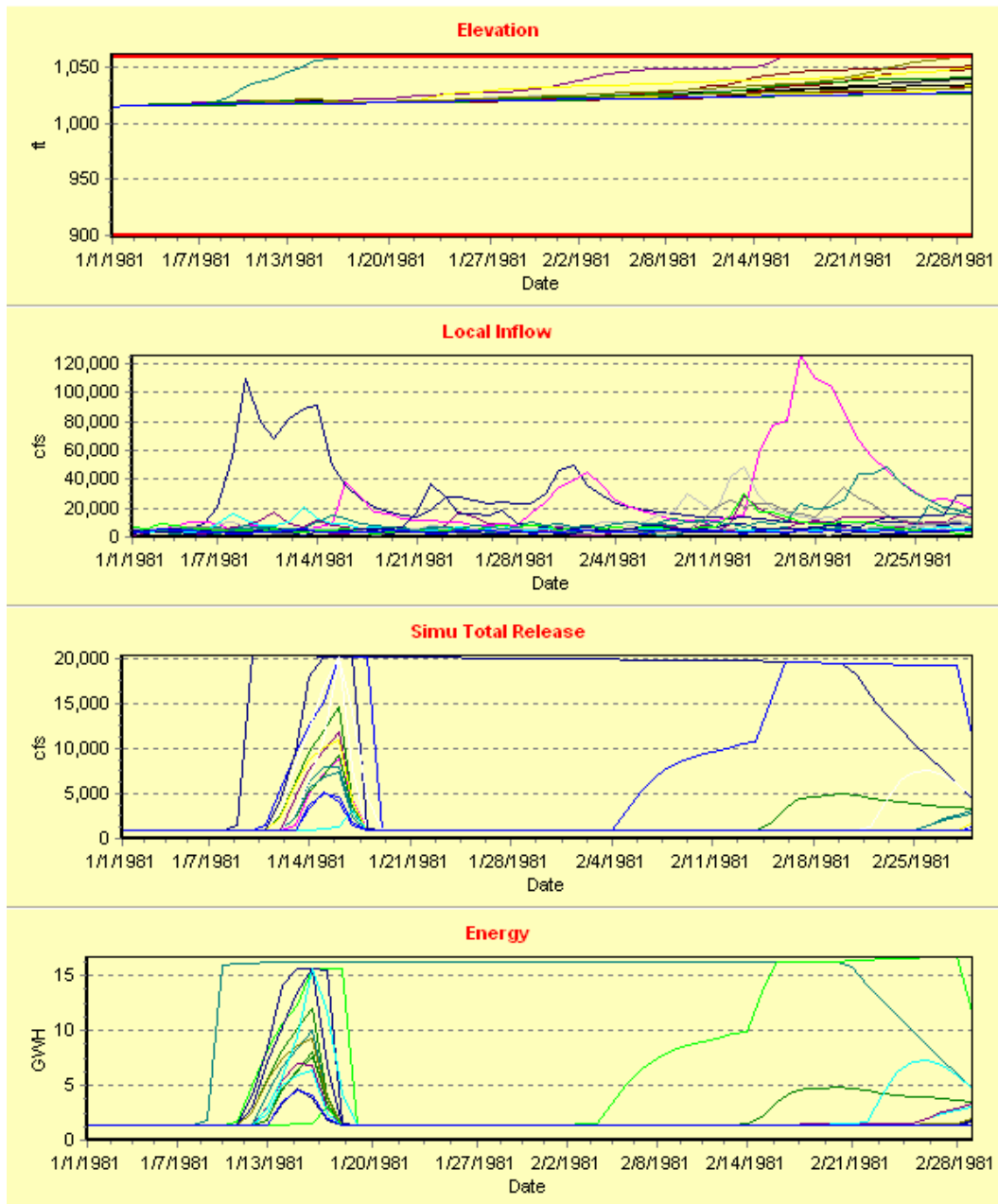


Figure 70. Mid-range model example run for Shasta. A 3-month forecast horizon from 1/1/1981.

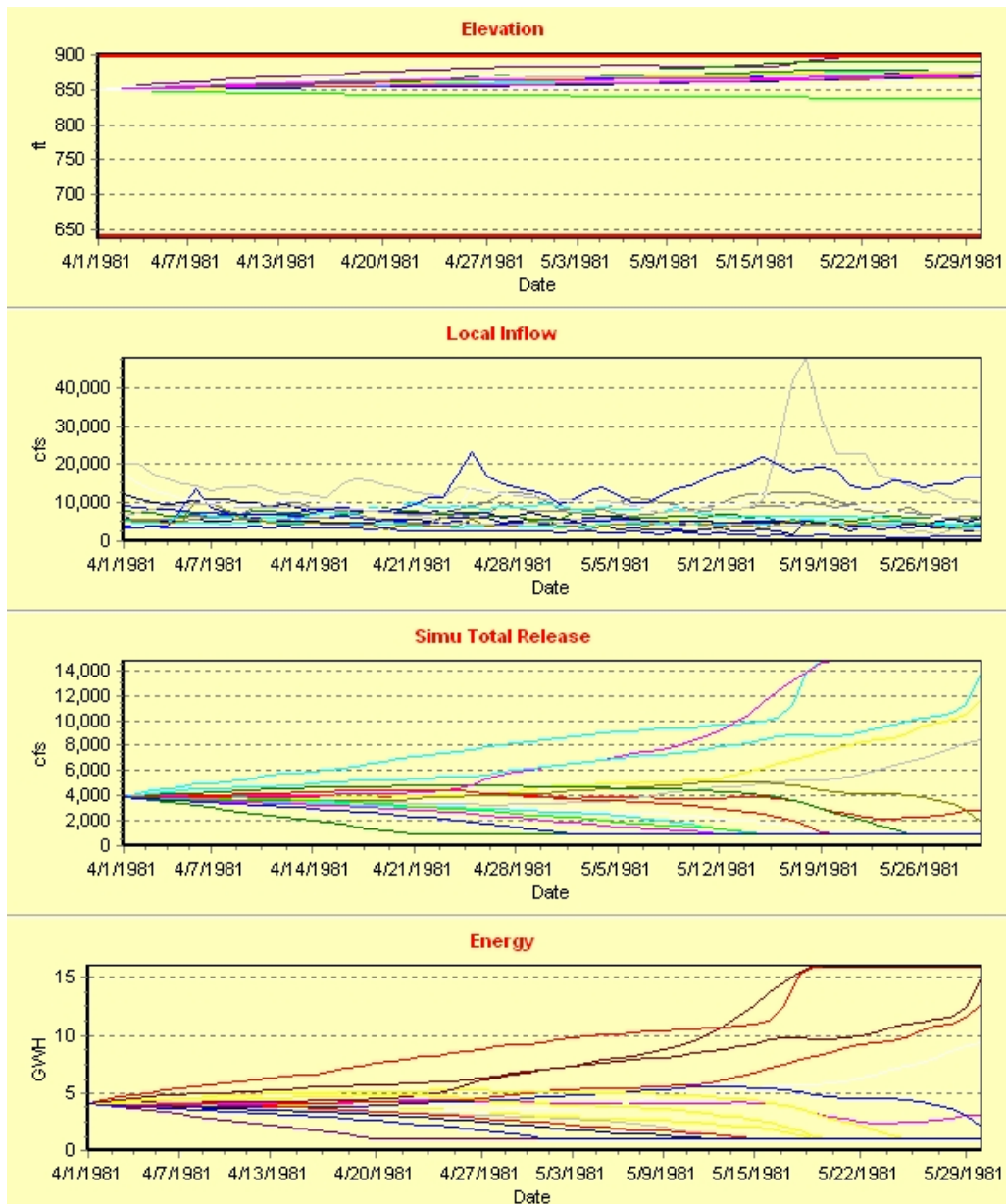


Figure 71. Mid-range model example run for Oroville. A 3-month forecast horizon from 4/1/1981.

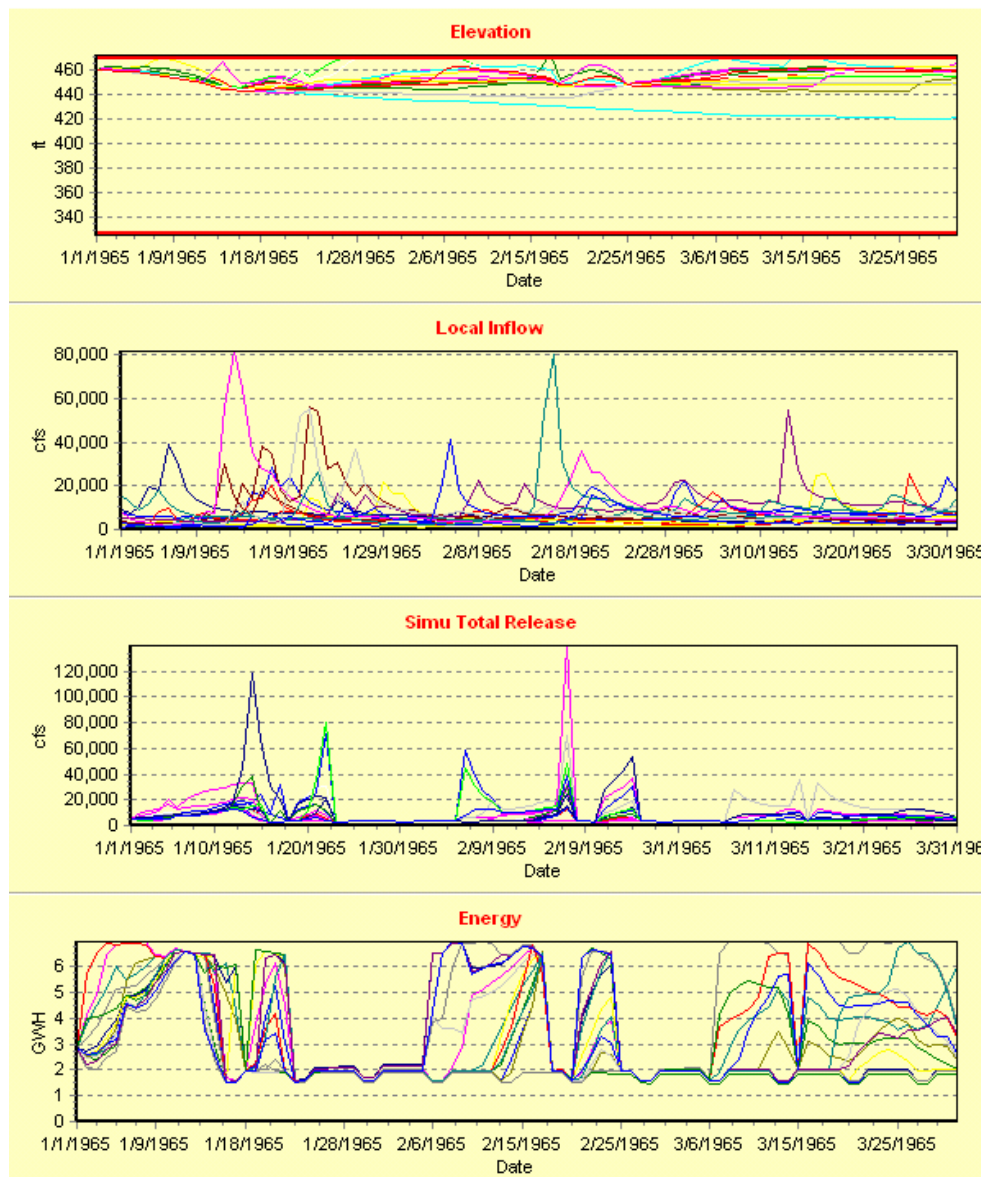


Figure 72. Mid-range model example run for Folsom. A 3-month forecast horizon from 1/1/1965.

5.5.1. System Simulation Model

The simulation model for the Northern California river and reservoir system was developed based on input received by DWR, the U.S. Bureau of Reclamation, and the USACE in the form of personal discussions, email communications, water balance and demand spreadsheets, and internal agency technical reports. The entire system is divided into 6 subsystems, based on hydrological network location and functionality. These subsystems are as follows (also see Figure 10):

- Trinity River System (Clair Engle Lake, Trinity Power Plant, Lewiston Lake, Lewiston Plant, JF Carr Plant, Whiskeytown, Clear Creek, and Spring Creek Plant).
- Shasta Lake System (Shasta Lake, Shasta Power Plant, Keswick Lake, Keswick Plant, and the river reach from Keswick to Wilkins).
- Feather River System (Lake Oroville, Oroville Power Plants, Thermalito Diversion Pond, Yuba River, and Bear River).
- American River System (Folsom Lake, Folsom Plant, Natoma Lake, Nimbus Plant, Natoma Plant, and Natoma diversions).
- San Joaquin River System (New Melones Lake, New Melones Power Plant, Tulloch Lake, Demands from Goodwin, and Inflows from the main San Joaquin River).
- Bay Delta (Delta Inflows, Delta Exports, Coordinated Operation Agreement (COA), and Delta Environmental Requirements).

The model formulation and associated assumptions for each subsystem are fully described in the next sections.

5.5.1.1. Trinity subsystem

The Trinity River System includes Clair Engle (or Trinity) Lake, Trinity Power Plant, Lewiston Lake, Lewiston Plant, JF Carr Plant, Whiskeytown, Clear Creek, and Spring Creek Plant. The Clair Engle Lake is operated to meet the minimum and target flows in the Trinity River, and the monthly target storage for Whiskeytown reservoir. This system is described by the following water balance equations:

Whiskeytown:

$$S_{WH}(k+1) = S_{WH}(k) + I_{WH}(k) - EVP_{WH}(S_{WH}(k), k) + R_{JF}(k) - R_{CC}(k) - R_{SC}(k);$$

Clair Engle Lake (Trinity):

$$S_{CL}(k+1) = S_{CL}(k) + I_{CL}(k) - EVP_{CL}(S_{CL}(k), k) - R_{CL}(k);$$

$$R_{CL}(k) = R_{LE}(k) + R_{JF}(k);$$

where

k is the time step in months;

S_{WH} , I_{WH} , and EVP_{WH} are respectively the storage, inflow, and evaporation loss of Whiskeytown;

R_{CC} is the minimum river flow requirement for Clear Creek;

R_{SC} is the target flow for Spring Creek plant;

R_{LE} is the minimum river flow requirement for Trinity River;

R_{JF} is the flow through JF Carr plant; and

S_{CL} , I_{CL} , EVP_{CL} , R_{CL} are respectively the storage, inflow, evaporation loss, and release of Clair Engle Lake.

5.5.1.2. Shasta Lake subsystem

The Shasta Lake System includes Shasta Lake, Shasta Power Plant, Keswick Lake, Keswick Plant, and the river reach from Keswick to Wilkins. The Shasta Lake is operated to meet the minimum and the target flow at Wilkins on the Sacramento River and share (if specified) the water supply in the Delta. The dynamical response of Shasta Lake and flow at Wilkins are described by the following equations:

Shasta Lake:

$$S_{SH}(k+1) = S_{SH}(k) + I_{SH}(k) - EVP_{SH}(S_{SH}(k), k) - R_{SH}(k);$$

$$R_{SH}(k) = R_{KE}(k) - R_{SC}(k) + Q_{DISH};$$

$$R_{KE}(k) = \max[R_{KE}^{\min}(k), Q_{Wil}^{\min}(k) - R_{CC}(k) - I_{Wil}(k)];$$

Flow at Wilkins:

$$Q_{Wil}(k) = R_{CC}(k) + R_{KE}(k) + I_{Wil}(k);$$

where

S_{SH} , I_{SH} , EVP_{SH} , and R_{SH} are respectively the storage, inflow, evaporation loss, and release of Shasta Lake;

R_{KE} is the release of Keswick reservoir;

R_{KE}^{\min} is the minimum Keswick release requirement;

Q_{Wil}^{\min} is the minimum river flow requirement at Wilkins;

I_{Wil} is the local inflow between Keswick and Wilkins; and

Q_{DISH} is Shasta's share of the Delta demand.

5.5.1.3. Feather River subsystem

The Feather River System includes Lake Oroville and power plants, Thermalito Diversion Pond, Yuba River, and Bear River. The inflows from Yuba and Bear are combined in the simulation model. The flow contributions to the Delta from both rivers are lumped into an aggregate quantity called *Sacramento Accretion*. Lake Oroville is operated to meet the demand associated with Thermalito and the Feather River minimum and target flow requirements, and share (if specified) the water demand of the Bay Delta. The system dynamics of Lake Oroville and flow downstream of Thermalito on the Feather River are described by the following equations:

Lake Oroville:

$$S_{OR}(k+1) = S_{OR}(k) + I_{OR}(k) - EVP_{OR}(S_{FO}(k), k) - R_{OR}(k);$$

$$R_{OR}(k) = D_{TH}(k) + \max(Q_{TH}^{\min}(k), Q_{TH}^{\text{TGT}}(k)) + Q_{DIIOR};$$

Flow at Thermalito:

$$Q_{TH}(k) = R_{OR}(k) - D_{TH}(k);$$

where

S_{OR} , I_{OR} , EVP_{OR} , R_{OR} are respectively the storage, inflow, evaporation loss, and release of Lake Oroville;

D_{TH} is the demand from Thermalito;

Q_{TH}^{\min} and Q_{TH}^{TGT} are the minimum and target flow requirement downstream of Thermalito; and

Q_{DIIOR} is the Oroville share of the Delta demand.

5.5.1.4. American River subsystem

The American River System includes the Folsom Lake, Folsom Plant, Natoma Lake, Nimbus Plant, Natoma Plant, and Natoma diversions. The Folsom Lake is operated to meet the demands of the Natoma reservoir and the minimum and the target flow requirements on the American River, and share (if specified) the water demands of the Delta. The dynamics of Folsom Lake and the flow downstream of Nimbus are described by the following equations:

Folsom Lake:

$$S_{FO}(k+1) = S_{FO}(k) + I_{FO}(k) - EVP_{FO}(S_{FO}(k), k) - R_{FO}(k);$$

$$R_{FO}(k) = \max(Q_{NI}^{\min}(k), Q_{NI}^{\text{TGT}}(k)) + DPM_{FO}(k) + D_{FS}(k) + Q_{DIIFO};$$

where

S_{FO} , I_{FO} , EVP_{FO} , R_{FO} are respectively the storage, inflow, evaporation loss, and release of Folsom Lake;

Q_{NI}^{\min} and Q_{NI}^{TGT} are the minimum and target flows downstream of Nimbus;

DPM_{FO} is the demand for Folsom pumping;

D_{FS} is the demand for Folsom South Canal; and

Q_{DIHFO} is Folsom's share of the Delta demand.

5.5.1.5. San Joaquin River subsystem

The San Joaquin System includes New Melones Lake, New Melones Power Plant, Tulloch Lake, Demands from Goodwin, and the inflows from the main San Joaquin River. The New Melones is operated to meet the demands at Goodwin and the minimum and the target flow requirement downstream. The system dynamics of New Melones Lake, Tulloch Lake, and the river flow at Vernalis are described by the following equations:

New Melones:

$$S_{NM}(k+1) = S_{NM}(k) + I_{NM}(k) - EVP_{NM}(S_{NM}(k), k) - R_{NM}(k);$$

Tulloch:

$$S_{TU}(k+1) = S_{TU}(k) + R_{NM}(k) - R_{TU}(k);$$

$$R_{TU}(k) = D_{CUP}(k) + D_{OID/SSJD}(k) + \max(Q_{GO}^{\min}(k), Q_{GO}^{TGT}(k));$$

$$R_{NM}(k) = R_{TU}(k) + (S_{TU}^{TGT}(k+1) - S_{TU}(k));$$

Flow at Vernalis:

$$Q_{VE}(k) = \max(Q_{GO}^{\min}(k), Q_{GO}^{TGT}(k)) + I_{SJR}(k);$$

where

S_{NM} , I_{NM} , EVP_{NM} , R_{NM} are respectively the storage, inflow, evaporation loss, and release of the New Melones Lake;

S_{TU} and R_{TU} are the storage and release of Tulloch;

D_{CUP} and $D_{OID/SSJD}$ are the demands at Goodwin;

Q_{GO}^{\min} and Q_{GO}^{TGT} are the minimum and target flows downstream of Goodwin;

S_{TU}^{TGT} is the target storage of Tulloch Lake;

Q_{VE} is the river flow at Vernalis; and

I_{SJR} is the inflow from Jan Joaquin above the Stanislaus junction.

5.5.1.6. Bay Delta

The Delta receives inflows from the Sacramento River, San Joaquin River, and several local streams. In addition to the consumptive use inside the Delta and the environmental constraints, the Delta provides storage for exporting water to the south part of California through pumping. Under normal hydrological conditions, the Delta inflows can meet the Delta demands and the water export targets. However, during dry water years, extra water has to be released from the upper major reservoirs to meet the Delta demands. The required extra water is shared by the large reservoirs in the Sacramento River basin (Clair Engle Lake, Shasta, Oroville, and Folsom). The shared percentage and operation rules in the simulation follow the COA but can also be modified by the program user.

Delta Inflows

The local Delta inflows include:

- Sacramento Valley Accretion: $I_{SV}(k)$;
- Freeport Treatment Plant: $I_{FT}(k)$;
- Eastside Stream: $I_{ES}(k)$;
- Miscellaneous Creeks Inflow: $I_{MC}(k)$;
- Yolo bypass: $I_{YB}(k)$; and
- Transfer Inflow: $I_{TI}(l)$.

Freeport Flow

$$Q_{FP}(k) = Q_{CC}(k) + Q_{KE}(k) + Q_{NI}(k) + Q_{TH}(k) + I_{SV}(k) + I_{FT}(k).$$

Total Delta Inflow:

$$I_{DE}(k) = Q_{FP}(k) + Q_{VE}(k) + I_{ES}(k) + I_{YB}(k) + I_{TI}(k) + I_{MC}(k).$$

Delta Exports

The Delta water exports are determined jointly by the US Bureau of Reclamation (USBR) and the State Department of Water Resources (DWR). Federal exports include:

- Contra Costa Water District Diversion, D_{CCWD} ;
- Barker Slough, D_{BS} ;
- Federal Tracy Pumping, D_{FTPP} ;
- Federal Banks on-peak, D_{FBON} ;
- Federal Banks off-peak, D_{FBOFF} ;

- Federal Banks Pumping total, D_{FPPTOT} ;
- Federal Banks PP CVC, $D_{FBPPCVC}$;
- Federal Banks PP Joint, $D_{FBPPJNT}$; and
- Federal Banks PP Transfer, D_{FBPPTR} ;

The total federal pumped water is estimated as follows:

$$D_{FPPTOT}(k) = D_{FPPP}(k) + D_{DFBON}(k) + D_{DFBOFF}(k) + D_{FBPP}(k) + D_{FBPPCVC}(k) + D_{FBPPJNT}(k) + D_{FBPPTR}(k)$$

The total federal planned export is the sum of the federal pumped water and the CCWD diversion:

$$D_{FEXTOT}(k) = D_{FPPTOT}(k) + D_{CCWD}(k)$$

State water exports include:

- NBA Diversion, D_{NBA} ;
- State Banks PP, D_{SBPP} ; and
- State Tracy PP, D_{STPP} .

The total state export is computed as the sum of the previous components:

$$D_{SEXTOT}(k) = D_{NBA}(k) + D_{SBPP}(k) + D_{STPP}(k).$$

The total planned export from both federal and state is computed as follows:

$$D_{EXTOT}(k) = D_{SEXTOT}(k) + D_{FEXTOT}(k) + D_{BS}(k).$$

Delta Coordinated Operation Agreement (COA)

The Delta COA is described using the following notation:

- Required Delta Outflow, Q_{minDlt} ;
- Delta Consumptive Use, D_{Dlt} ;
- Combined required reservoir release, QRES:

$$QRES(k) = \max(0, D_{Dlt}(k) + D_{EXTOT}(k) + Q_{Dlt}^{min}(k) - I_{SV}(k) - Q_{VE}(k) - I_{FT}(k) - I_{ES}(k) - I_{MC}(k) - I_{YB}(k))$$

- Total Federal Storage Withdrawal, DS_{FTOT} :

$$DS_{FTOT}(k) = (R_{CC}(k) - I_{WH}(k)) + (R_{KE}(k) - I_{SH}(k)) + (R_{FO}(k) - I_{FO}(k));$$

- Total State Storage Withdrawal, DS_{STOT} :

$$DS_{STOT}(k) = (R_{OR}(k) - I_{OR}(k));$$

- Computed Delta Outflow, Q_{Dlt} :

$$Q_{Dlt}(k) = Q_{FP}(k) + I_{YB}(k) + Q_{VE}(k) + D_{Dlt}(k) - D_{EXTOT}(k) + I_{ES}(k) + I_{MC}(k);$$

- Estimated Excess Outflow, Q_{ESTOT} :

$$Q_{ESTOT}(k) = (Q_{Dlt}(k) - Q_{Dlt}^{min}(k));$$

- Un-stored Flow for Export, Q_{UFE} :

$$Q_{UFE}(k) = \begin{cases} D_{EXTOT}(k) + Q_{ESTOT}(k) - (DS_{FTOT}(k) + DS_{STOT}(k)), & \text{if } DS_{FTOT}(k) + DS_{STOT}(k) < D_{EXTOT}(k) \\ 0, & \text{otherwise} \end{cases}$$

- Estimated in-basin use of storage withdrawal, Q_{INBSN} :

$$Q_{INBSN}(k) = \max(0, DS_{FTOT}(k) + DS_{STOT}(k) - D_{EXTOT}(k))$$

- USBR Allowable Export, D_{FEXTOT}^{max}

$$D_{FEXTOT}^{max}(k) = \begin{cases} D_{FEXTOT}(k), & \text{if } Q_{Dlt}(k) > Q_{Dlt}^{min}(k), \\ \begin{cases} 0.55Q_{UFE}(k) + DS_{FTOT}(k), & \text{if } Q_{UFE}(k) > 0 \\ DS_{FTOT}(k) - 0.75Q_{INBSN}(k) \end{cases} \end{cases}$$

- USBR Monthly COA Account, Q_{FCOA} :

$$Q_{FCOA}(k) = \begin{cases} 0, & \text{if } Q_{Dlt}(k) > Q_{Dlt}^{min}(k), \\ D_{FEXTOT}^{max} - D_{FEXTOT}(k), & \text{otherwise} \end{cases}$$

- Accumulated COA(k), S_{SCOA} :

$$S_{SCOA}(k+1) = S_{SCOA}(k) + Q_{FCOA}(k)$$

- Adjusted Delta Outflow, Q_{Dlta} :

$$Q_{Dlta}(k) = Q_{FP}(k) + I_{YB}(k) + Q_{VE}(k) + D_{Dlt}(k) - D_{FEXTOT}^{max}(k) + I_{ES}(k) + I_{MC}(k) + I_{YB}(k)$$

- Adjusted Excess Outflow, Q_{ESTOTA} :

$$Q_{ESTOTA}(k) = (Q_{Dlta}(k) - Q_{Dlt}^{min}(k))$$

- Rio Vista Flow, Q_{RV} :

$$Q_{RV}(k) = \begin{cases} 0.87Q_{FP}(k) - 0.333 * 2632 - 1000, & \text{if } X_{ChannelGate} = 1, \\ 0.7Q_{FP}(k) - 0.333 * 2632 - 2050, & \text{if } X_{ChannelGate} = 0, \\ 0.5(0.87Q_{FP}(k) - 0.333 * 2632 - 1000 + 0.7Q_{FP}(k) - 0.333 * 2632 - 2050), & \text{otherwise} \end{cases}$$

Bay Delta Environment

The Delta environmental conditions are simulated based on the following notation and relationships:

- X Channel Gates, XGopt;
- Cross Delta Flow, Q_{XDLT}:

$$Q_{XDLT}(k) = \begin{cases} 0.133Q_{FP}(k) + 829, & \text{if } X_{ChannelGate} = 1, \\ 0.293Q_{FP}(k) + 2090, & \text{if } X_{ChannelGate} = 0, \\ 0.213Q_{FP}(k) + 1460, & \text{otherwise} \end{cases}$$

- Antioch Flow, Q_{AN}:

$$Q_{AN}(k) = 0.8(Q_{VE}(k) + 2/3D_{DLT}(k) - D_{EXTOT}(k) + Q_{XDLT}(k))$$

- Q_{WEST}:

$$Q_{WEST}(k) = Q_{AN}(k)/0.8 + I_{ES}(k)$$

- Computed Delta/Inflow Ratio (%), DI%:

$$DI\%(k) = (Q_{EXTOT}(k) - CCWD)/I_{DE}(k)$$

- X2 Location (km from GG), X2:

$$X2(k) = 122.2 + 0.3287X2(k-1) - 17.65\text{Log}(Q_{DLT}(k))$$

- Supplemental project water, Q_{Sup}:

$$Q_{Sup}(k) = DS_{FTOT}(k) + DS_{STOT}(k) - D_{EXTOT}(k)$$

South Delta Formulation

The exports south of the Delta are simulated based on the following notation and relationships:

- Delta Mendota Canal, D_{DM};
- Federal Dos Amigos, D_{FDA};
- Federal ONeil to Dos Amigos, D_{FODA};
- San Felip Demands, D_{SE};
- Cross Valley Demands, D_{CV};
- Federal South Exports in ONeil, D_{FEXO};

- Federal South Exports in San Luis, DFEXSL;
- Federal San Luis Pumping, Q_{FSL}:

$$Q_{FSL}(k) = D_{DM}(k) + D_{FDA}(k) + D_{FODA}(k) + D_{FPPTOT}(k) - D_{FEXO}(k) - 0.47Evp_{ONeil}$$

- Federal Storage in San Luis, S_{SLF}:

$$S_{SLF}(k+1) = S_{SLF}(k) + Q_{FSL}(k) - D_{SF}(k) - 0.47EVP_{ONeil}$$

- South Bay Demand, D_{SB};
- State Dos Amigos Demand, D_{SDA};
- State San Luis Pumping, Q_{SSL}:

$$Q_{SSL}(k) = D_{SEXTOT}(k) - D_{SB}(k) - D_{SDA}(k) - .53Evp_{ONeil}$$

- State Storage in San Luis, S_{SLS}:

$$S_{SLS}(k) = S_{SLS}(k) + D_{SSL}(k) - 0.53Evp_{ONeil}$$

The previous relationships provide the means to simulate the month-by-month response of the Northern California system to a particular set of inflows, demands, and operational policies.

5.5.2. Simulation Model Validation

To determine the validity of the INFORM DSS system simulation model described in the previous section and to demonstrate its utility in relation to other commonly used models, a comprehensive comparison with the CALSIM water resources simulation model (Draper et al. 2004) was performed. CALSIM is also a monthly model but includes considerable detail with respect to withdrawals occurring at the various reaches of the Trinity, Sacramento, Feather, American, Yuba, and San Joaquin Rivers. The INFORM DSS simulation model includes a more aggregate system representation but is the basis for a more advanced system optimization model, to be described in the next section. The purpose of the comparison presented herein is to investigate whether the two simulation models yield consistent results under the same hydrologic and demand conditions and reservoir release policies.

5.5.2.1. Comparison set-up

The model comparison included the following steps:

1. CALSIM and its necessary computational accessories (databases and auxiliary programs) were acquired (reference site) and rendered operational at the Georgia Water Resources Institute computer facility;
2. CALSIM was run using data from the CALSIM 2001 Level-of-Development Benchmark Study;

3. The CALSIM hydrologic (e.g., inflows, evaporation coefficients) and demand sequences were aggregated to the spatial aggregation level used by INFORM DSS;
4. INFORM DSS was run using the previous sequences and the CALSIM reservoir releases;
5. CALSIM and INFORM DSS simulation results were finally compared to assess consistency with respect to major reservoir storages, river node flows, and the X2 location.

An example of the spatial aggregation performed on the CALSIM sequences for use by the INFORM DSS is provided in Figure 73, depicting a section of the American River. Specifically, the figure shows that INFORM represents inflows to the Folsom reservoir and demands taken out of Natoma, while CALSIM includes a more detailed representation of inflows and demands. The aggregation process is described in the figure. Similar spatial aggregations were performed for all other reaches of the northern California reservoir system.

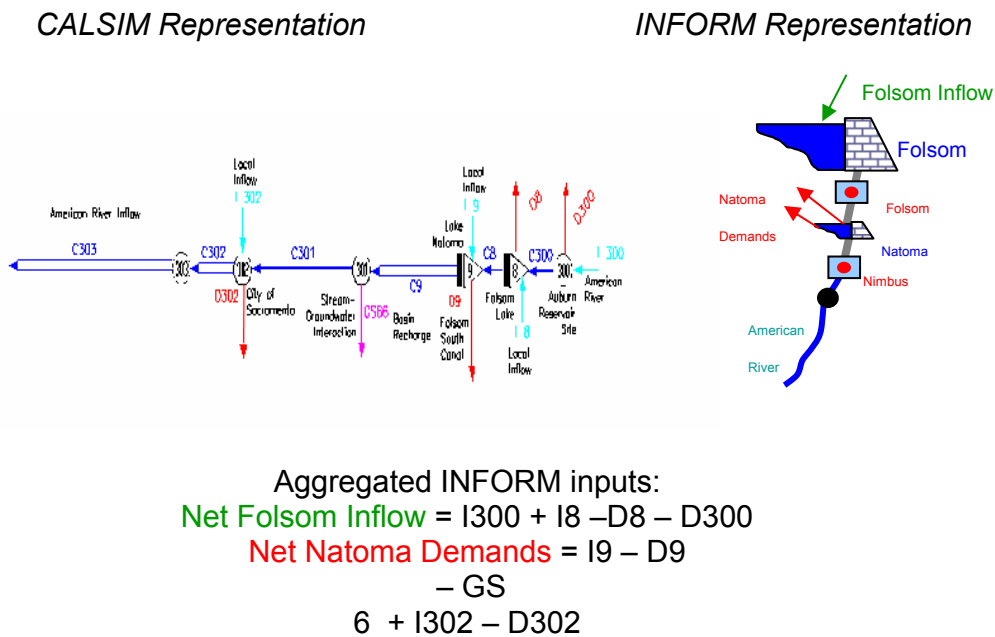


Figure 73. American River spatial aggregation

5.5.2.2. Model comparison

CALSIM and the INFORM DSS simulation model were compared with respect to river node flows, the X2 location (interface of saline and fresh water), and major reservoir storages. These quantities are compared in the following series of figures showing the two model sequences. Figures 74, 75, and 76 depict model results for the Delta outflow, Delta X2 location, and major reservoir storages, respectively. CALSIM and INFORM results for the first two quantities are identical. Furthermore, with the exception of

Oroville, all CALSIM and INFORM storage sequences also coincide. The discrepancy for the Oroville storage was traced to an error in the CALSIM code. During certain months in the sequence (primarily Septembers), CALSIM adds random quantities in the Oroville water balance equation. The end-of-period reservoir storage calculated by the model in these months differs from the value that would be obtained by adding/subtracting the net inflows/outflows from the beginning-of-period storage.

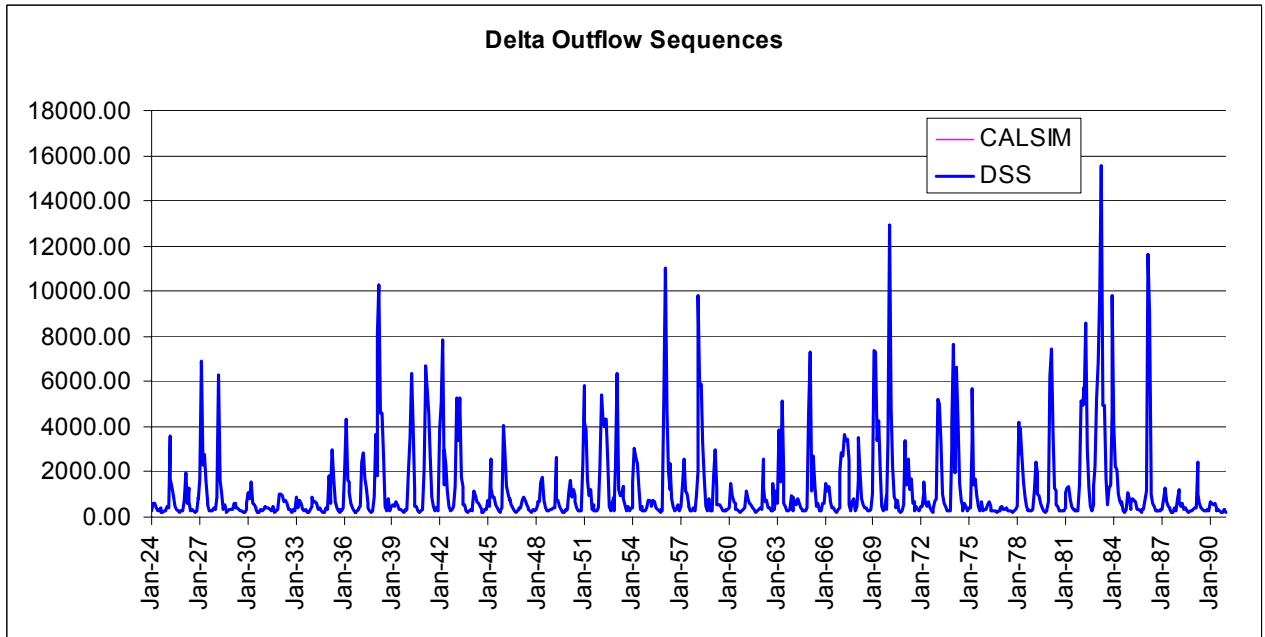


Figure 74. Delta outflow comparisons

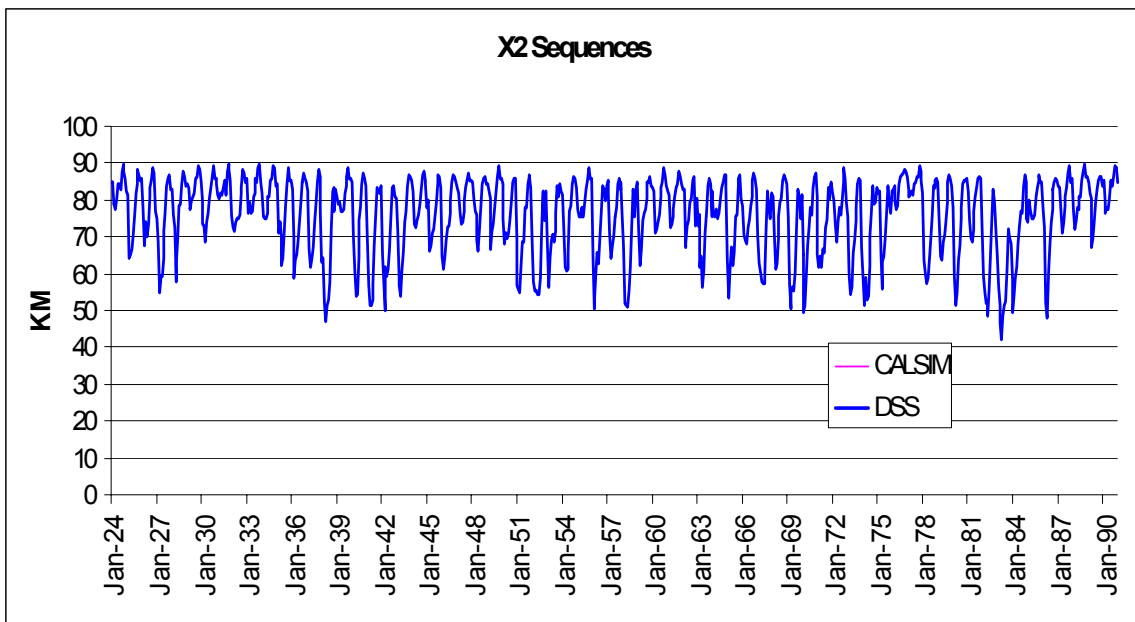
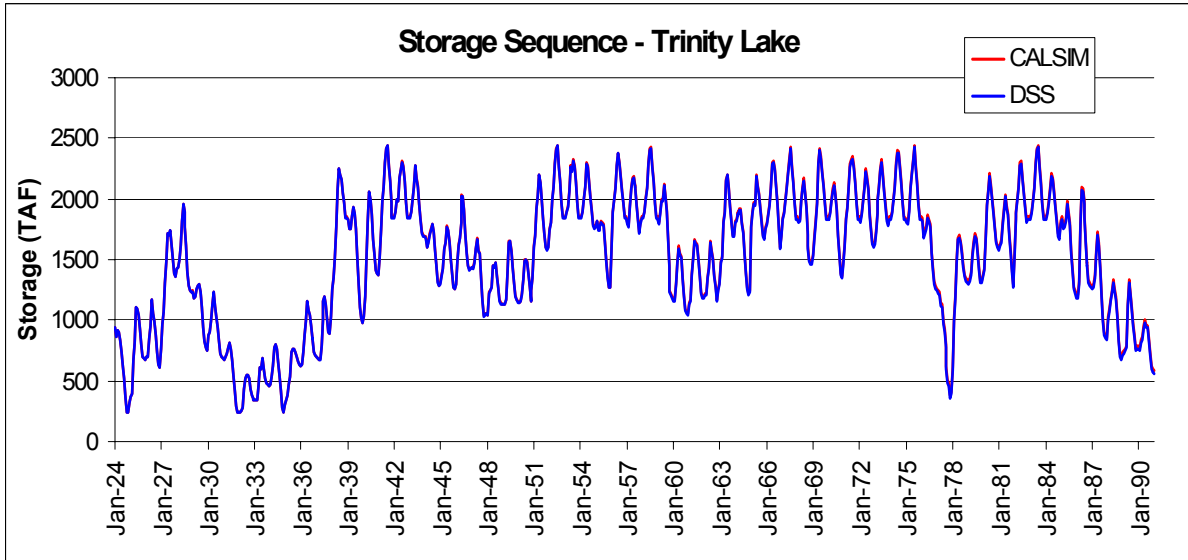
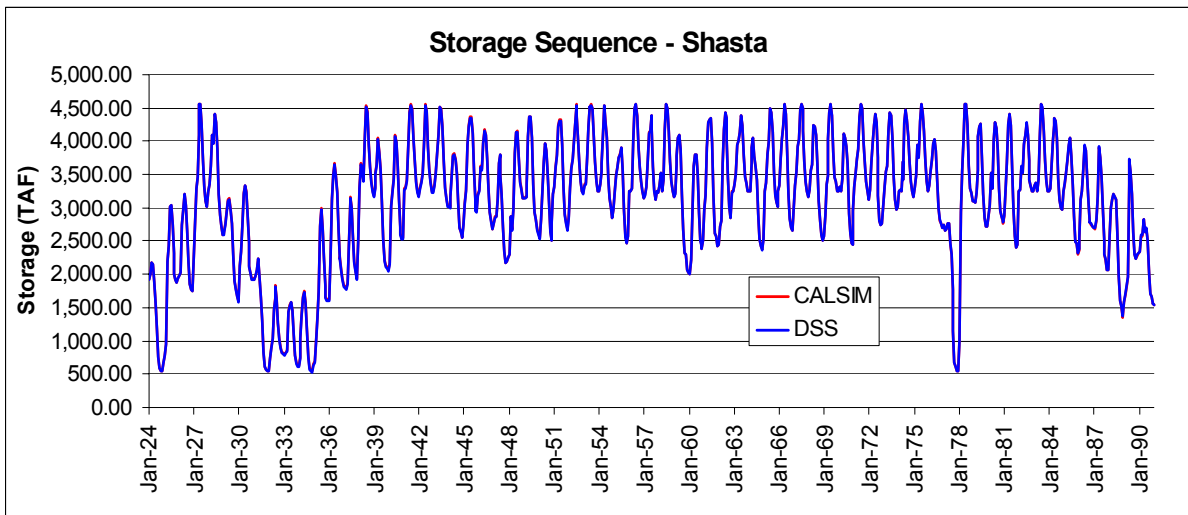


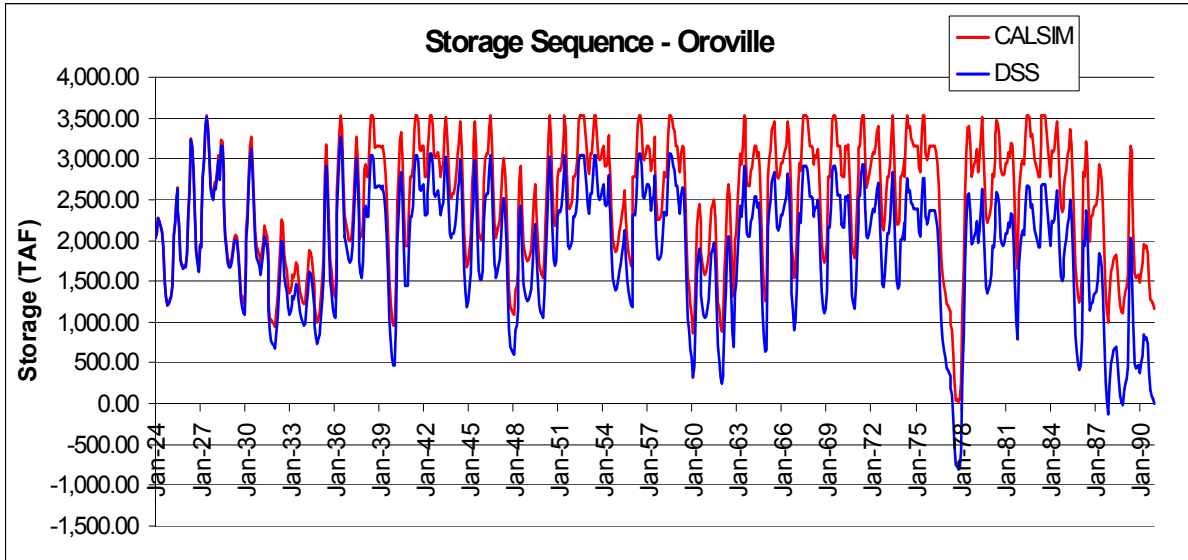
Figure 75. X2 Location comparisons



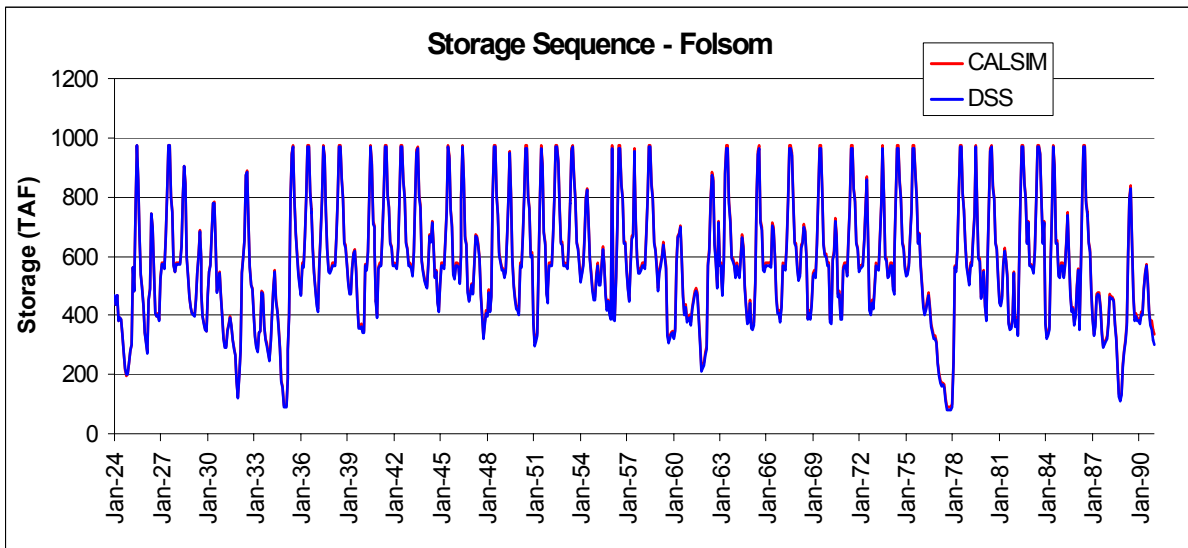
(a) Trinity



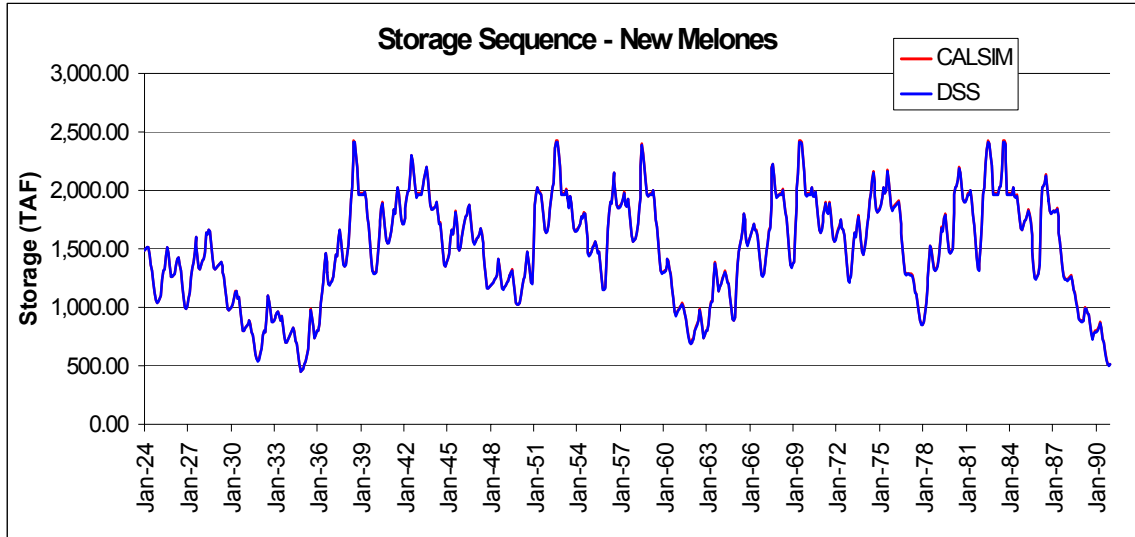
(b) Shasta



(c) Oroville



(d) Folsom



(e) New Melones

Figure 76. Reservoir Storage Comparisons: (a) Trinity, (b) Shasta, (c) Oroville, (d) Folsom, and (e) New Melones

Notwithstanding this discrepancy, which will hopefully be corrected in future CALSIM versions, the comparison results confirm that the INFORM simulation model is consistent with CALSIM and can be used to represent the response of the Northern California system at the same accuracy level.

In view of the above conclusion, it is recommended that CALSIM and INFORM DSS be used in a manner that re-enforces their individual utility. Namely, the planning process can benefit as follows: First, the INFORM DSS can be employed to generate long-range planning tradeoffs and associated reservoir release policies based on seasonal hydro-climatic forecasts. Second, the INFORM DSS policies and forecasts can be used by CALSIM to develop a more detailed spatial representation of the system processes (inflows, withdrawals, returns) that are more meaningful to individual stakeholders.

5.5.3. System Optimization Model

The optimization model is described by the system dynamics, various constraints, performance index, and optimization method.

5.5.3.1. System dynamics

System dynamics refers to the system simulation model described in Section 5.5.1. However, the optimization algorithm requires expressing the simulation model equations in state space form. This can be accomplished by assembling the water balance relationships for the major system reservoirs and the equation for the X2 location as follows:

$$\begin{aligned}
S_{CL}(k+1) &= S_{CL}(k) + I_{CL}(k) - EVP_{CL}(S_{CL}(k), k) - R_{CL}(k); \\
S_{OR}(k+1) &= S_{OR}(k) + I_{OR}(k) - EVP_{OR}(S_{OR}(k), k) - R_{OR}(k); \\
S_{SH}(k+1) &= S_{SH}(k) + I_{SH}(k) - EVP_{SH}(S_{SH}(k), k) - R_{SH}(k); \\
S_{FO}(k+1) &= S_{FO}(k) + I_{FO}(k) - EVP_{FO}(S_{FO}(k), k) - R_{FO}(k); \\
S_{NM}(k+1) &= S_{NM}(k) + I_{NM}(k) - EVP_{NM}(S_{NM}(k), k) - R_{NM}(k); \\
X2(k) &= 122.2 + 0.3287 X2(k-1) - 17.65 \text{ Log}(Q_{Dlt}(k));
\end{aligned}$$

where

$$\begin{aligned}
Q_{Dlt}(k) &= Q_{FP}(k) + I_{YB}(k) + Q_{VE}(k) + D_{Dlt}(k) - D_{EXTOT}(k) + I_{ES}(k) + I_{MC}(k); \\
Q_{FP}(k) &= R_{CL}(k) + R_{SH}(k) + R_{OR}(k) + R_{FO}(k) - D_{TH}(k) + I_{SV}(k) + I_{FT}(k); \\
Q_{VE}(k) &= R_{NM}(k) - D_{CUP}(k) - D_{OID/SSJID}(k) + I_{SJR}(k).
\end{aligned}$$

In the previous equations, the two-letter subscript includes the first two letters of the reservoir name; k is the discretization time interval corresponding to one month; $S(k)$ is reservoir storage at the beginning of the month; $EVP_i(S_i(k))$ is the net evaporation loss which is a function of reservoir surface area and therefore storage; $R(k)$ is the release volume during period k ; $I(k)$ is the local inflow volume; $X2(k)$ is the $X2$ location at time k ; and Q_{Dlt} is the delta outflow computed as a function of the flow at Freeport, flow at Yolo Bypass, flow at Vernalis, total Delta demand, total exports from Delta, East Side streams inflow, and inflow from miscellaneous creeks. The terms in the expressions for Q_{FP} and Q_{VE} have been defined in the description of the simulation model (Section 5.5.1 and subsections therein).

These equations can be compiled into one vector equation as follows:

$$\begin{aligned}
\mathbf{S}(k+1) &= \mathbf{f}(\mathbf{S}(k), \mathbf{u}(k), \boldsymbol{\xi}(k), k), \\
k &= 0, 1, \dots, N-1,
\end{aligned}$$

where $\mathbf{S}(k)$ is the state vector, $\mathbf{u}(k)$ is the vector of controllable releases, $\boldsymbol{\xi}(k)$ is the vector of uncertain inputs, $\mathbf{f}[\]$ is the state transition (vector) function relating the previous quantities, and N is the simulation horizon. An important feature of the above equation is that the quantities of its right side pertain only to time period k . Namely, there are no time-lagged quantities involved. This represents the *system state equation* and is a standard form necessary for the application of dynamic optimization (decision) methods.

The state and control vectors are defined as follows:

$$\mathbf{S}(k) = \begin{bmatrix} S_1(k) \\ S_2(k) \\ S_3(k) \\ S_4(k) \\ S_5(k) \\ S_6(k) \end{bmatrix} = \begin{bmatrix} S_{CL}(k) \\ S_{SH}(k) \\ S_{OR}(k) \\ S_{FO}(k) \\ S_{NM}(k) \\ X_6(k-1) \end{bmatrix}, \quad \mathbf{u}(k) = \begin{bmatrix} u_1(k) \\ u_2(k) \\ u_3(k) \\ u_4(k) \\ u_5(k) \end{bmatrix} = \begin{bmatrix} R_{CL}(k) \\ R_{SH}(k) \\ R_{OR}(k) \\ R_{FO}(k) \\ R_{NM}(k) \end{bmatrix},$$

where the initial state vector $\mathbf{S}(0)$ is presumed known. The state transition vector function is defined as shown below:

$$\mathbf{f}(k) = \begin{bmatrix} f_1(k) \\ f_2(k) \\ f_3(k) \\ f_4(k) \\ f_5(k) \\ f_6(k) \end{bmatrix} = \begin{bmatrix} S_{CL}(k) + I_{CL}(k) - EVP_{CL}(S_{CL}(k), k) - R_{CL}(k) \\ S_{SH}(k) + I_{SH}(k) - EVP_{SH}(S_{SH}(k), k) - R_{SH}(k) \\ S_{OR}(k) + I_{OR}(k) - EVP_{OR}(S_{FO}(k), k) - R_{OR}(k) \\ S_{FO}(k) + I_{FO}(k) - EVP_{FO}(S_{FO}(k), k) - R_{FO}(k) \\ S_{NM}(k) + I_{NM}(k) - EVP_{NM}(S_{NM}(k), k) - R_{NM}(k) \\ 122.2 + 0.3287 X_2(k-1) - 17.65 \text{Log}(Q_{Dlt}(k)) \end{bmatrix}.$$

Finally, the uncertain inputs associated with each transition equation comprise the input vector $\xi(k)$:

$$\xi(k) = \begin{bmatrix} f_1(k) : \{I_{CL}(k)\} \\ f_2(k) : \{I_{SH}(k)\} \\ f_3(k) : \{I_{OR}(k)\} \\ f_4(k) : \{I_{FO}(k)\} \\ f_5(k) : \{I_{NM}(k)\} \\ f_6(k) : \{I_{Dlt}(k)\} \end{bmatrix},$$

where $I_{Dlt}(k)$ represents all uncertain inflows to the Bay Delta.

The previous equations summarize the system dynamics. In decision systems terminology, S is the state vector, u is the control vector, and ξ is the input vector. As discussed next, these quantities are subject to various constraints imposed by physical or operational requirements.

5.5.3.2. Constraints

Generally, the storage and release variables for all reservoirs are constrained to be within certain feasible ranges:

$$S^{\min}(k) \leq S(k) \leq S^{\max}(k), \quad k = 1, 2, \dots, N,$$

$$R^{\min}(k) \leq R(k) \leq R^{\max}(k), \quad k = 0, 1, \dots, N-1.$$

In these relationships, the upper and lower storage limits delineate the extent of reservoir conservation storage and can vary seasonally. The lower release limits represent existing environmental and water supply requirements, aggregated along the river reaches downstream of each reservoir. The upper release limits are determined based on hydro generation and spillway capacities.

In view of the system uncertainties, however, the reservoir storage constraints are more properly expressed in a probabilistic form:

$$\text{Prob}[S_i^{\min}(k) \leq S_i(k)] \geq \pi_i^{\min}(k) ,$$

$$\text{Prob}[S_i(k) \leq S_i^{\max}(k)] \geq \pi_i^{\max}(k) ,$$

$$i \in \text{reservoirs} , k = 1, \dots, N ,$$

where π^{\min} and π^{\max} are user-specifiable reliability levels. These levels, similar to the upper and lower storage and release limits, can vary seasonally but are usually constant.

The goal of the optimization algorithm is to identify release sequences for all reservoirs $\{u_i^*(k), i = 1, 2, \dots, 5; k = 0, 1, \dots, N-1\}$ such that system objectives and constraints are met successfully. The element of the optimization formulation that brings this to bear and also measures the success of the various operational alternatives is the performance index discussed next.

5.5.3.3. Performance index

The optimization procedure aims to maximize systemwide benefits, while meeting all environmental and water supply demands. A performance index, J , that can achieve this objective is as follows:

$$J = E \left\{ \sum_{k=0}^{N-1} [P_h(\mathbf{S}(k)) + P_{\text{htrg}}(\mathbf{S}(k)) + P_{\text{utrg}}(\mathbf{u}(k)) + P_{\text{spl}}(\mathbf{u}(k), \mathbf{S}(k)) + P_{\text{hp}}(\mathbf{S}(k))] \right. \\ \left. + P_h(\mathbf{S}(N)) + P_{\text{hp}}(\mathbf{S}(N)) \right\} ,$$

where

$$P_H(\mathbf{S}(k)) = \sum_{i \in \text{Reservoirs}} \alpha_{1i} \left[\frac{[H_i^{\max} - H_i(S_i(k))]^2}{1 + e^{\frac{H_i^{\max} - H_i(S_i(k))}{T_H}}} + \frac{[H_i^{\min} - H_i(S_i(k))]^2}{1 + e^{\frac{H_i^{\min} - H_i(S_i(k))}{T_H}}} \right] ,$$

$$P_{\text{htrg}}(\mathbf{S}(k)) = \sum_{i \in \text{Reservoirs}} \alpha_{2i} \left[\frac{H_i(S_i(k)) - H_i^{\text{trg}}(k)}{H_i^{\max} - H_i^{\min}} \right]^2 ,$$

$$P_{\text{utrg}}(\mathbf{u}(\mathbf{k})) = \sum_{i \in \text{Reservoirs}} \alpha_{3i} \left[\frac{[u_i(\mathbf{k}) - u_i^{\text{trg}}(\mathbf{k})]^2}{[u_i^{\text{max}}(\mathbf{k}) - u_i^{\text{min}}(\mathbf{k})]^2} \right] ,$$

$$P_{\text{spl}}(\mathbf{u}(\mathbf{k}), \mathbf{S}(\mathbf{k})) = \sum_{i \in \text{Reservoirs}} \alpha_{4i} \text{SPL}_i(u_i(\mathbf{k}), S_i(\mathbf{k})) ,$$

$$P_{\text{HP}}(\mathbf{S}(\mathbf{k})) = \sum_{i,j \in \text{Reservoirs}} \alpha_{5ij} \left[\frac{H_i(S_i(\mathbf{k})) - H_i^{\text{min}}(\mathbf{k})}{H_i^{\text{max}} - H_i^{\text{min}}} - \frac{H_j(S_j(\mathbf{k})) - H_j^{\text{min}}(\mathbf{k})}{H_j^{\text{max}} - H_j^{\text{min}}} \right]^2 .$$

In the above, $E\{ \}$ denotes expectation of the quantity in the brackets with respect to the joint probability distribution of the reservoir inflows.

There are five penalty terms in the performance index to be minimized through the optimization algorithm. The first term— $P_{\text{H}}(\mathbf{S}(\mathbf{k}))$ —uses barrier functions (one for each reservoir) to enforce elevation (or equivalently) storage constraints. In this term, $H_i^{\text{min}}(\mathbf{k})$ and $H_i^{\text{max}}(\mathbf{k})$ are the lower and upper elevation limits for the i th reservoir, $H_i(S_i(\mathbf{k}))$ is the elevation versus storage function, and T_{H} is a barrier function parameter. Their most important feature is that they are everywhere analytical (with continuous first and second derivatives) and yet delimit with desirable accuracy the conservation storage regions. Namely, inside the $[H_i^{\text{min}}(\mathbf{k}), H_i^{\text{max}}(\mathbf{k})]$ range, they vanish; while outside of it, they impose a quadratic penalty the severity of which is controlled by the weighing coefficients α_{5ij} . The value of α_{5ij} should be high enough to ensure that these constraints have priority over other performance index terms. Parameter T_{H} controls the smoothness of the transition over $H_i^{\text{min}}(\mathbf{k})$ and $H_i^{\text{max}}(\mathbf{k})$, and requires some experimentation. (A value of $T_{\text{H}} = 0.002$ has been found to work well.)

The second term— $P_{\text{htrg}}(\mathbf{S}(\mathbf{k}))$ —penalizes departures from a target level. In this case, the target level is the top of the conservation storage zone. This choice promotes water conservation as well as hydropower generation efficiency. In addition, purely quadratic state and control terms improve the convergence speed of the optimization algorithm to be discussed later.

Similar to the second term, the third term— $P_{\text{utrg}}(\mathbf{u}(\mathbf{k}))$ —penalizes releases away from some target value. This term is useful if a certain release target pattern is provided. An example is provided in the case studies.

The fourth term— $P_{\text{spl}}(\mathbf{u}(\mathbf{k}), \mathbf{S}(\mathbf{k}))$ —aims at minimizing spillage. *Spillage* is defined as the portion of the release which is larger than the turbine capacity. Minimizing spillage is

consistent with the long-term goal of maximizing energy generation and conserving water.

The last term— $P_{HP}(\mathbf{S}(k))$ —aims to operate the system reservoirs in a fairly uniform manner and avoid extreme level fluctuations where some system reservoirs are fully depleted while others remain full.

Penalty parameters α are used to introduce priorities in the performance index terms. These parameters should be determined such that the first term of the performance index is dominant. The rest of the terms are adjusted based on the priority of the operating objective. The logic is to determine feasible sequences guaranteed to minimize the other terms.

It is noted that energy generation terms can also be included in the performance index. However, optimizing long-term energy generation is consistent with maintaining high reservoir levels (water conservation) and minimizing spillage, which are also achieved by the previous index terms. To be sure, energy generation terms will have to be included in the short-range models for hydropower operations scheduling.

5.5.3.4 Optimization method

The optimization problem formulated in the previous section is solved using the Extended Linear Quadratic Gaussian (ELQG) control method which was originally introduced by Georgakakos and Marks (1987) and further developed by Georgakakos (1989a, 1989b, 1989c), 1991, 1993), Georgakakos et al. (1997a, 1997b, 1997c), Yao and Georgakakos (2001), and Hooper et al. (1991). ELQG is an iterative optimization procedure starting from an initial control sequence $\{\mathbf{u}(k); k = 0, 1, 2, \dots, N-1\}$ and subsequently generating increasingly better sequences until convergence. Convergence is achieved when the value of the performance index cannot be reduced any further. ELQG is reliable, computationally efficient, and especially suited for uncertain, multi-reservoir systems. A more detailed account of the ELQG optimization algorithm and features is provided next.

The elements of the optimization problem (system dynamics, constraints, and performance index) are summarized below:

- System Dynamics

$$\mathbf{S}(k+1) = \mathbf{f}[\mathbf{S}(k), \mathbf{u}(k), \xi(k), k], \quad k = 0, 1, \dots, N-1,$$

- Constraints

$$\begin{aligned} \text{Prob}[H_i^{\min}(k) \leq H_i(S_i(k))] &\geq \pi_i^{\min}(k), \\ \text{Prob}[H_i(S_i(k)) \leq H_i^{\max}(k)] &\geq \pi_i^{\max}(k), \\ \mathbf{u}_i^{\min}(k) \leq \mathbf{u}_i(k) \leq \mathbf{u}_i^{\max}(k), \\ i &= 1, 2, \dots, 6; \quad k = 0, 1, \dots, N. \end{aligned}$$

These are associated with the system reservoirs and are expressed in a probabilistic form due to the uncertain inputs.

- Performance Index

$$\text{Minimize}_{\mathbf{u}(k), k=0,1,\dots,N-1} J = E \left\{ \sum_{k=0}^{N-1} g_k [\mathbf{S}(k), \mathbf{u}(k)] + g_N[\mathbf{S}(N)] \right\},$$

where $\mathbf{S}(k)$, $\mathbf{u}(k)$, and $\xi(k)$ are the state, control, and uncertain input vectors defined in the previous section, π_i^{\min} and π_i^{\max} are reliability parameters, g_k is a function including all performance index terms associated with period k , and g_N is a function including terms associated with the terminal time N . (As before, bold type indicates vector or matrix quantities.)

The ELQG optimization procedure starts with an initial control sequence $\{\mathbf{u}^0(k), k=0, 1, \dots, N-1\}$ and the corresponding mean state vector sequence $\{\bar{\mathbf{S}}^0(k), k=0, 1, \dots, N\}$:

$$\begin{aligned} \bar{\mathbf{S}}^0(k+1) &= \mathbf{f}[\bar{\mathbf{S}}^0(k), \mathbf{u}^0(k), \bar{\xi}(k), k], \\ \bar{\mathbf{S}}^0(0) &= \mathbf{S}(0) = \text{known}, \\ k &= 0, 1, \dots, N-1, \end{aligned}$$

where $\bar{\xi}(k)$ represents the mean vector of the uncertain input $\xi(k)$. The next step is to define a perturbation system model valid in the neighborhood of the nominal state and control sequences:

$$\begin{aligned} \Delta \mathbf{S}(k) &= \mathbf{S}(k) - \bar{\mathbf{S}}^0(k), \quad k = 0, 1, \dots, N, \\ \Delta \mathbf{u}(k) &= \mathbf{u}(k) - \mathbf{u}^0(k), \quad k = 0, 1, \dots, N-1, \\ \Delta \xi(k) &= \xi(k) - \bar{\xi}(k), \quad k = 0, 1, \dots, N-1. \end{aligned}$$

This model describes the dynamic relationship of the state, control, and input vector perturbations, and, to a first order approximation, it has the following form:

$$\begin{aligned} \Delta \mathbf{S}(k+1) &= \mathbf{A}(k) \Delta \mathbf{S}(k) + \mathbf{B}(k) \Delta \mathbf{u}(k) + \mathbf{C}(k) \Delta \xi(k), \\ \Delta \mathbf{S}(0) &= 0, \\ k &= 0, 1, \dots, N-1, \end{aligned}$$

where the matrices $\mathbf{A}(k)$, $\mathbf{B}(k)$, and $\mathbf{C}(k)$ represent the gradient matrices of the state transition function with respect to the state, control, and input vectors respectively:

$$\mathbf{A}(k) = \nabla_{\mathbf{S}(k)} \mathbf{f}(k) = \begin{bmatrix} \frac{df_1(k)}{d\mathbf{S}(k)} \\ \frac{df_2(k)}{d\mathbf{S}(k)} \\ \vdots \\ \frac{df_6(k)}{d\mathbf{S}(k)} \end{bmatrix}, \quad \mathbf{B}(k) = \nabla_{\mathbf{u}(k)} \mathbf{f}(k) = \begin{bmatrix} \frac{df_1(k)}{d\mathbf{u}(k)} \\ \frac{df_2(k)}{d\mathbf{u}(k)} \\ \vdots \\ \frac{df_6(k)}{d\mathbf{u}(k)} \end{bmatrix}, \quad \mathbf{C}(k) = \nabla_{\xi(k)} \mathbf{f}(k) = \begin{bmatrix} \frac{df_1(k)}{d\xi(k)} \\ \frac{df_2(k)}{d\xi(k)} \\ \vdots \\ \frac{df_6(k)}{d\xi(k)} \end{bmatrix}.$$

The performance index can also be expressed in terms of the perturbation variables as follows:

$$\begin{aligned} J = E \left\{ \sum_{k=0}^{N-1} \left[\frac{1}{2} \Delta \mathbf{S}^T(k) \mathbf{Q}_{ss}(k) \Delta \mathbf{S}(k) + \mathbf{q}_s^T(k) \Delta \mathbf{S}(k) + \frac{1}{2} \Delta \mathbf{u}^T(k) \mathbf{R}_{uu}(k) \Delta \mathbf{u}(k) \right. \right. \\ \left. \left. + \mathbf{r}_u^T(k) \Delta \mathbf{u}(k) + \Delta \mathbf{u}^T(k) \mathbf{Q}_{us}(k) \Delta \mathbf{S}(k) \right] \right. \\ \left. + \frac{1}{2} \Delta \mathbf{S}^T(N) \mathbf{Q}_{ss}(N) \Delta \mathbf{S}(N) + \mathbf{q}_s^T(N) \Delta \mathbf{S}(N) \right\}, \end{aligned}$$

where $\mathbf{Q}_{ss}(k)$, $\mathbf{q}_s(k)$, $\mathbf{R}_{uu}(k)$, $\mathbf{r}_u(k)$, $\mathbf{Q}_{us}(k)$ are coefficient matrices defining a quadratic approximation of the original performance index. These matrices include the first and second partial derivatives of the $g_k[\]$ and $g_N[\]$ functions with respect to the state and control variables evaluated at the nominal sequences.

The perturbation control problem defined above is next solved to generate an optimal control sequence $\{\Delta \mathbf{u}^*(k), k = 0, 1, \dots, N-1\}$. This constitutes the optimization direction which defines a new nominal control sequence according to the following relationship:

$$\begin{aligned} \mathbf{u}^{\text{new}}(k) &= \mathbf{u}^0(k) + \alpha \Delta \mathbf{u}^*(k), \\ k &= 0, 1, \dots, N-1, \end{aligned}$$

where α is the optimization step size. Some important features of the ELQG solution process are summarized below:

- The ELQG iterations are (1) analytically based (the optimization directions are obtained by Riccati-like equations), (2) reliable (the iteration process is guaranteed to converge if the problem has a feasible solution), and (3) computationally efficient (convergence is fast). In fact, in the neighborhood of the optimum, it can be theoretically shown that the method converges at a quadratic rate.
- Control constraints are not included in the performance index as penalty terms but are handled *explicitly* through a Projected-Newton procedure. This has important computational efficiency implications as it allows for many constraints to enter or exit the binding control set at the same iteration. The optimization direction is then obtained in the space of the binding constraints.

- State (or, equivalently, elevation) constraints are handled through the barrier penalty functions discussed in the previous section. This approach has proven to be reliable and computationally efficient. Handling of the state constraints requires the characterization of the state probability density. This is accomplished by developing a linear approximation of the true feedback laws as a by-product of the analytical computation of the optimization direction. These feedback law approximations are used within the state dynamical equation and to generate state variable traces corresponding to each member of the inflow forecast ensemble. The state variable traces characterize fully the joint probability density of the state vector and are used to convert the state probabilistic constraints into deterministic equivalents.

The ELQG iterations continue until the value of the performance index cannot be reduced any further. At this point the process terminates, and the current nominal control sequence becomes the solution of the optimization problem. Under convexity conditions (which are usually valid), this solution is globally optimal. (Convexity can be tested by starting the optimization process from different initial control sequences and verifying that the process converges at the same optimal sequence.)

As indicated earlier, the optimization model is applied sequentially, where only the first element of the control sequence is actually implemented. The system is then monitored, new values for the state variables are recorded, new forecast ensembles are generated, and the optimization cycle is repeated at the beginning of the next time period (i.e., at the beginning of the next month). In this way, the model always uses the most recent system information and continually updates its policies to the current demands, storage availability, and hydrologic conditions (adaptive management).

ELQG is unique in that it is the only optimization method that can handle large reservoir systems with an explicit account of uncertainty. More details on this method can be found in the above-cited and in forthcoming references.

5.5.3.4. Long-range planning case study

The case study was performed in March 2006 using real forecasts with a nine-month forecast and management horizon. More specifically,

- Inflow forecast ensembles (112 traces) were generated by the procedures described in Sections 3 and 4 at five locations (Clair Engle Lake, Shasta, Oroville, Folsom, and Yuba) from March 1, 2006, through November 30, 2006 (a 9 month forecast horizon);
- Historical monthly average values are used for locations where forecasted inflows are not available (Appendix G; Table G-3);
- Monthly reservoir parameters and constraints (max, min, and target storages, and evaporation rates) are recorded in Appendix G, Table G-4;

- Minimum river flow requirements are shown in Appendix G, Table G-5; and
- Monthly base demands at all locations are as reported in Appendix G, Table G-6.

The forecasted inflow sequences are shown on Figure 77. Figure 78 presents comparisons of the forecasted inflow means versus the corresponding historical means for Trinity, Shasta, Oroville, and Folsom. The Figure shows that the forecasted means for March, April, and May are higher than the historical means for all locations, indicating a wet spring season. (It is noted that these results preceded the spring 2006 flooding of the Sacramento River.)

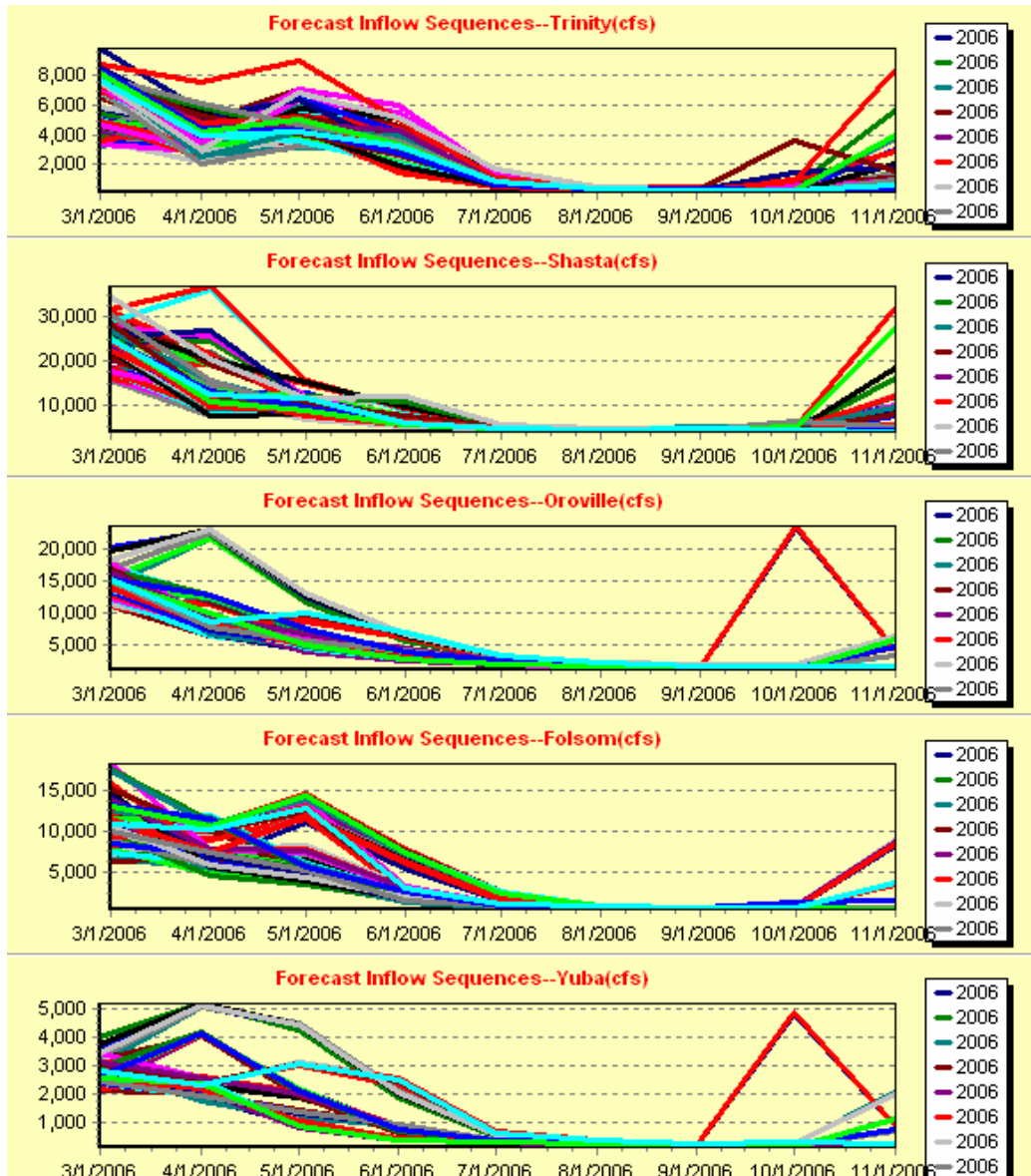


Figure 77. Long-range inflow forecasts from March 1, 2006

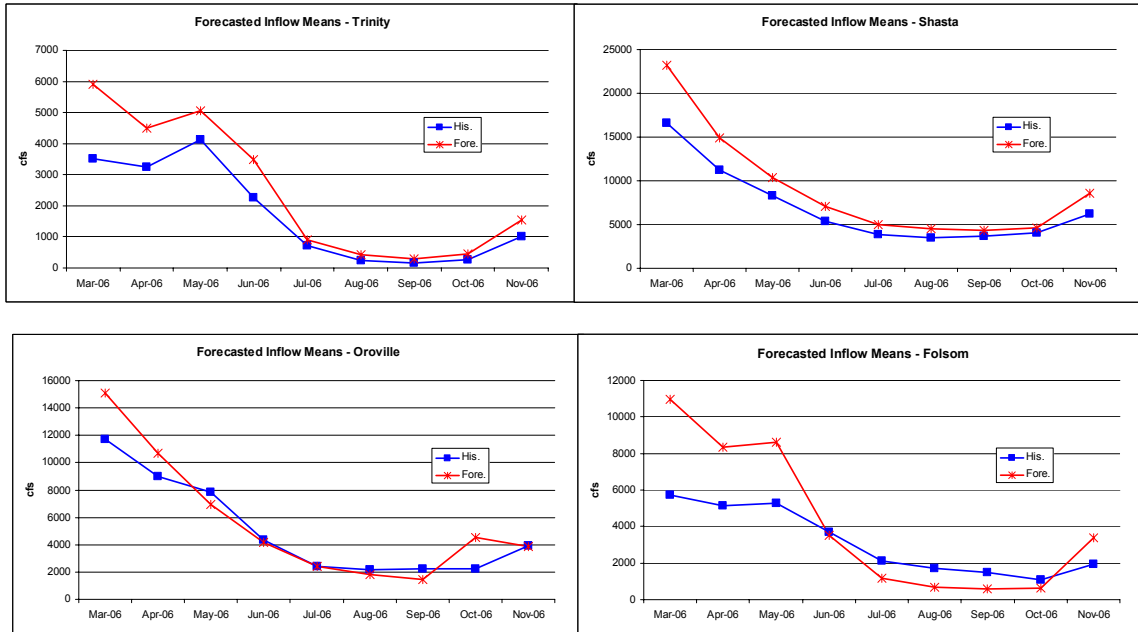
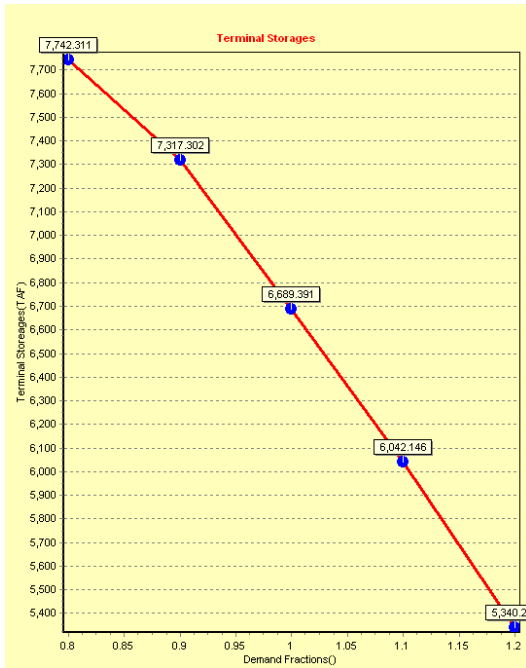


Figure 78. Long-range inflow forecast vs. historical means

Using the forecasted inflows, tradeoffs are generated by the long-range planning model by gradually varying the demand targets at all locations from 80% to 120% of the base demands. Figure 79 depicts the tradeoffs between (1) reservoir carry over storage versus demand target level, and (2) energy generation versus demand target level. As expected, reservoir carryover storage decreases with increasing demands. Depending on the risk level that the management authorities are willing to assume in the next year, this tradeoff can be used to determine water allocations for this year. The energy generation versus demand tradeoff shows that, initially, energy generation increases with increasing demand targets. However, as reservoir releases increase to meet downstream demands, reservoir levels fall, generation efficiency decreases, and energy generation eventually falls (tradeoff point 5; 120% of base demand targets). Overall, these results imply that, under the forecasted inflows and current storage levels, the system could meet up to 10%–15% more than the base demand targets. Demands beyond this level would result in reservoir drawdowns, water supply deficits, and energy generation losses.

a) Carry-over Storage vs. Demand



b) Energy Generation vs. Demand

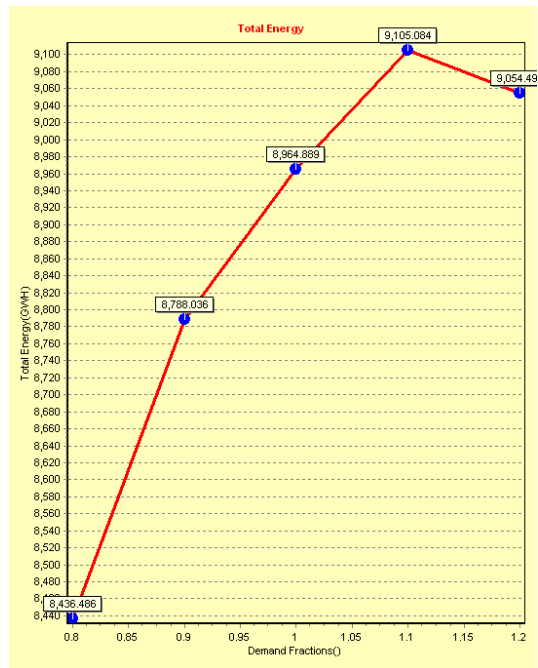


Figure 79. Planning tradeoffs: a) Carry-over storage vs. demand; b) Energy generation vs. demand

The reservoir and other system sequences corresponding to all tradeoff points are saved in the DSS database. Selected reservoir elevation, release, and energy generation sequences are shown in Figures 80 and 81.

a) Storage Sequences

b) Release Sequences

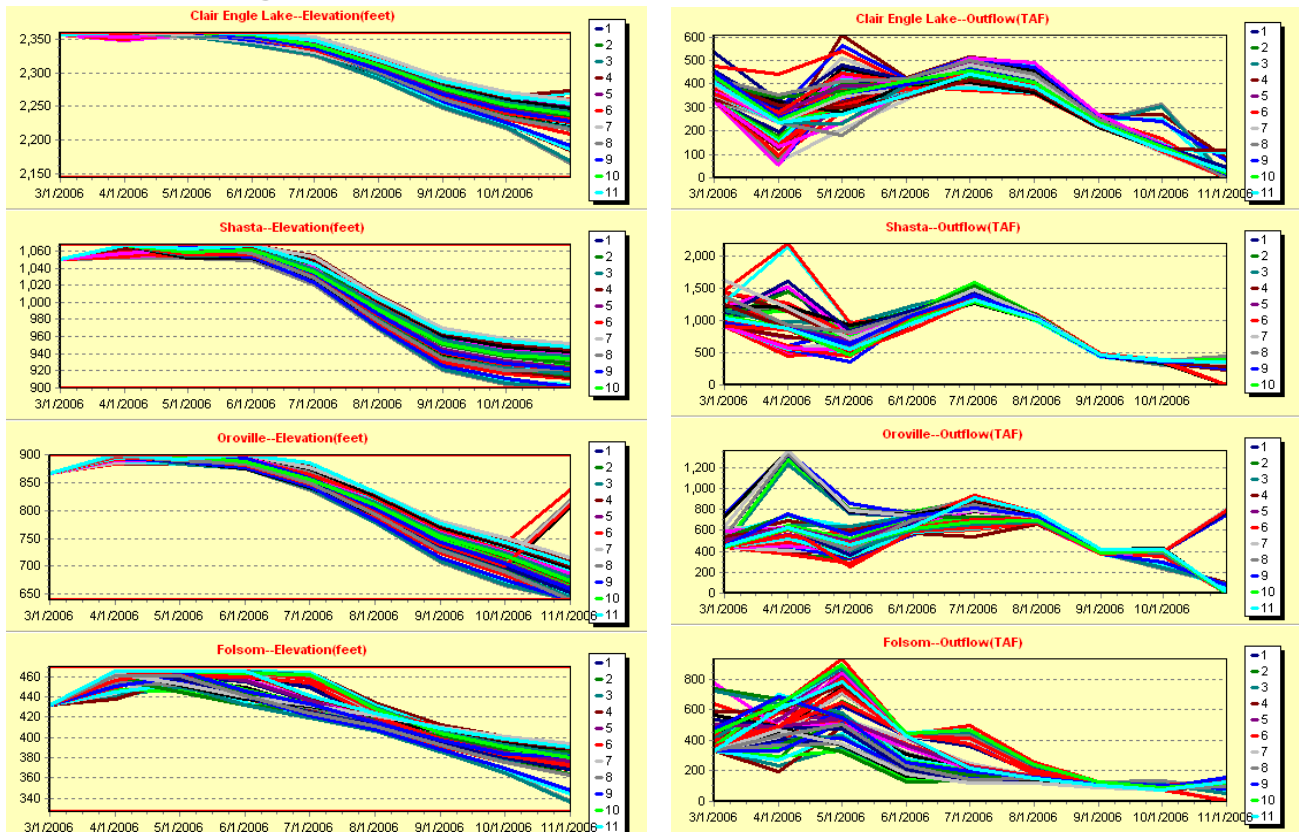


Figure 80. Reservoir storage and release sequences associated with tradeoff point 3

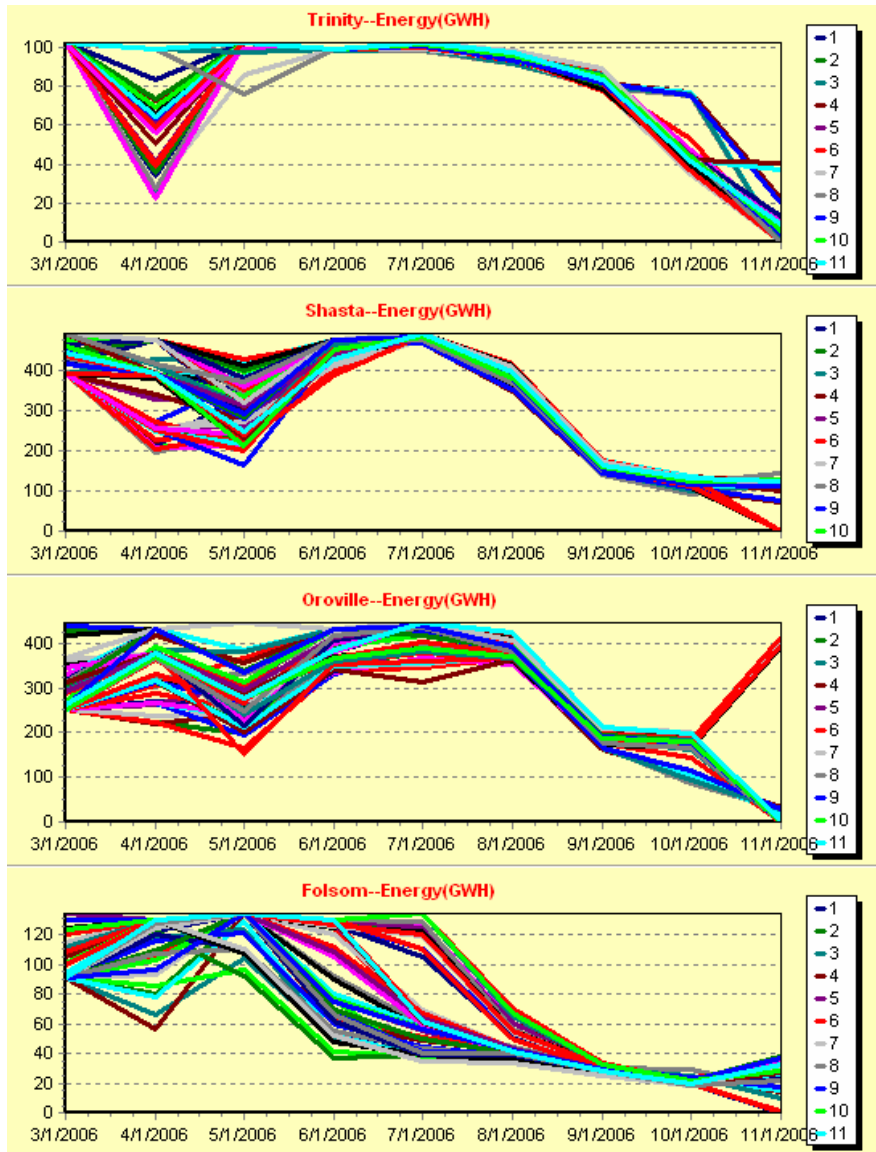
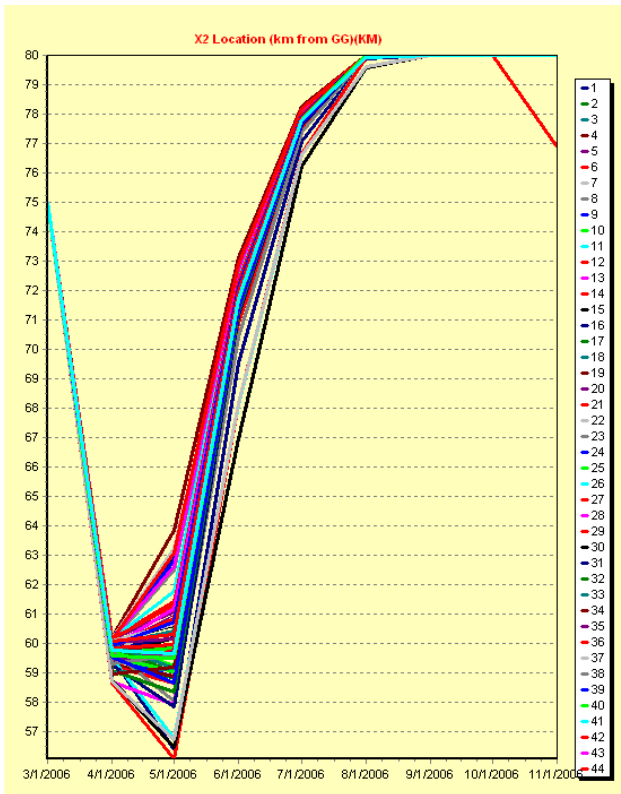


Figure 81. Energy generation sequences associated with tradeoff point 3

Figure 82 shows the X2 location sequences for tradeoff points 3 (100% of base demand targets) and 5 (120% of base demand targets). At tradeoff point 3, due to wetter than normal forecasts, the X2 is located less than 80 km from the Golden Gate Bridge in all scenarios. (The distance of 80 km was used as an upper limit for this state variable.) At tradeoff point 5, however, the X2 location begins to exceed 80 km at the end of November, 2006, for some scenarios. The probability that this might happen can be estimated by the proportion of the traces exceeding 80 km in each month. Finally, Delta outflow sequences are plotted on Figure 83, indicating that the low flow period extends from June to October.

a) Tradeoff Point #3



b) Tradeoff Point #5

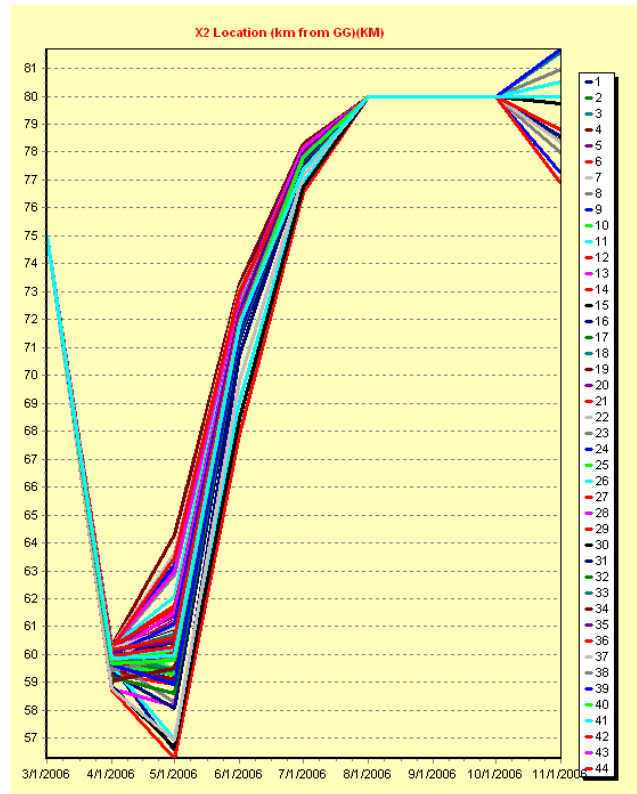


Figure 82. X2 location sequences associated with tradeoff points 3 and 5

It is noted that the INFORM long-range planning model can additionally derive other types of tradeoffs. For example, by establishing a range of minimum Delta outflows or maximum X2 distance limits, one can assess the impacts on other system variables and outputs such as reservoir storages, water supply allocations, and energy generation. Tradeoff information is an important DSS output and can be useful in planning water allocations and reservoir releases with quantitative appreciation of the associated risks.

Once the management authorities decide on the most preferable policy, the INFORM DSS determines the associated reservoir releases and water allocation targets and passes them to the mid-range model for operational implementation.

5.6. Scenario and Policy Assessment Models

The scenario and policy assessment models are part of the INFORM decision support system, their main purpose being to provide a quantitative and consistent procedure to assess the benefits and risks associated with particular hydrologic scenarios, demand levels, forecasting schemes, and management policies. The assessment process operates in a sequential fashion simulating the system response as it would have occurred under the conditions specified.

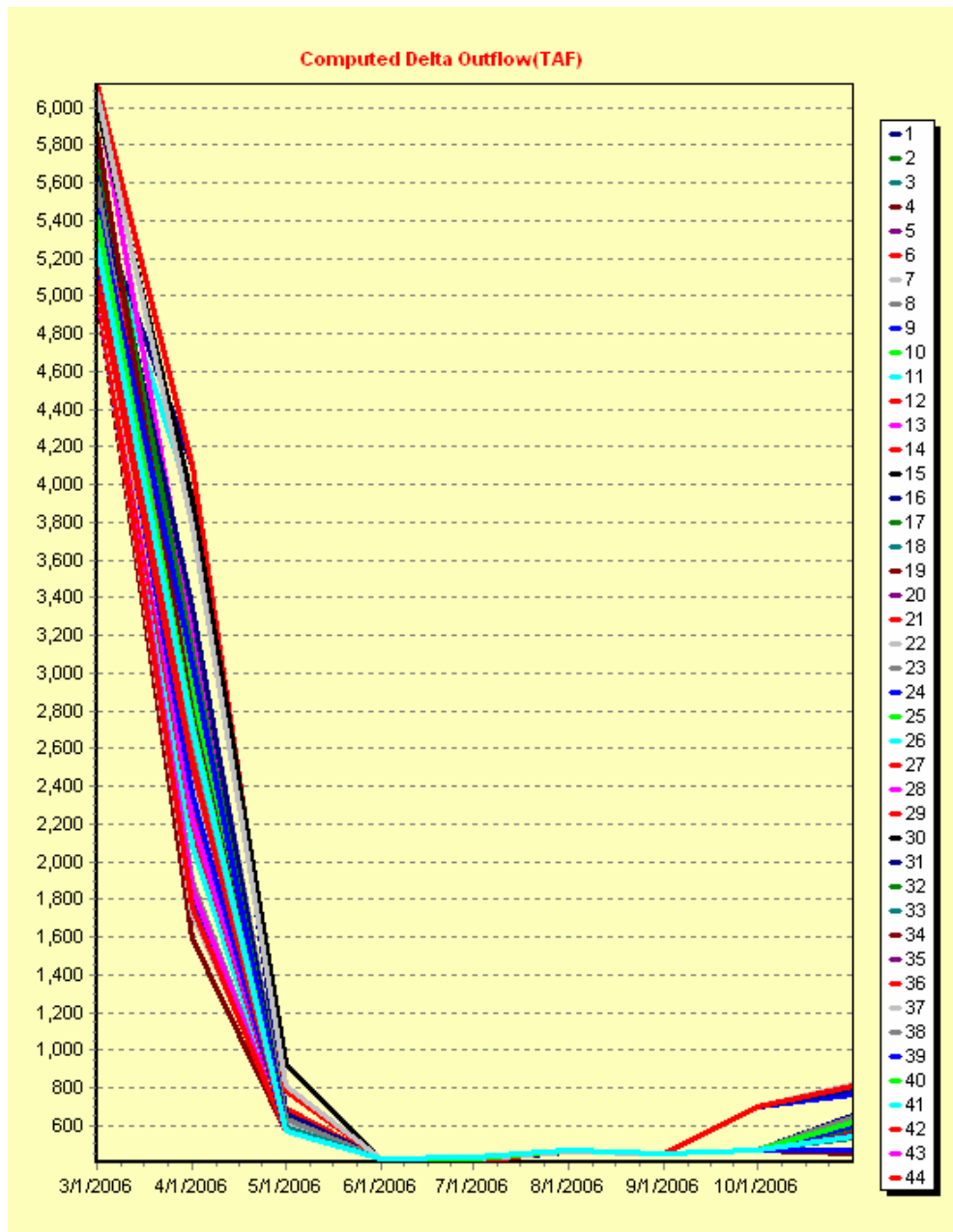


Figure 83. Delta outflow associated with tradeoff point 3

The scenario and policy assessment process is depicted on Figure 84 and consists of the sequential, day-by-day, or month-by-month, application of the mid-range management or long-range planning model over a pre-specified simulation horizon. Each assessment first requires selecting the

1. hydrologic scenario, assessment horizon, and time resolution (i.e., daily or monthly) over which the assessment will be carried out,
2. demand target levels (i.e., water supply and low flow requirements, energy commitments, and flood management risk thresholds) and management policies, including COA terms, water year characterization rules, and reservoir regulation

attributes (i.e., heuristic or adaptive; focused on individual reservoirs or system-wide), and

- the inflow forecasting model and forecast horizon (i.e., deterministic or ensemble based; statistical, hydrologic, or hydro-climatic).

After selecting these parameters, the assessment is carried out as follows: First, future inflows are forecasted based on the scheme selected. Next, the mid-range management (or the long-range planning) model is activated to develop release and generation schedules for all system reservoirs and hydropower plants. The releases for the first day (or the first month) of the control horizon and the daily (or monthly) inflows (unknown up to this time) are applied, and the system response (reservoir levels, releases, spillage, water supply deficits, energy generation and shortages, flood damage if any, and Delta conditions) is simulated and recorded. This process is repeated for the next day (or month) until the end of the assessment horizon. At the conclusion of the assessment process, several criteria are used to measure system performance, including statistics of water supply deficits, energy generation, flood damage, violation of low flow requirements, reservoir draw downs, Delta X2 location, Delta outflow, and other quantities relevant to system management.

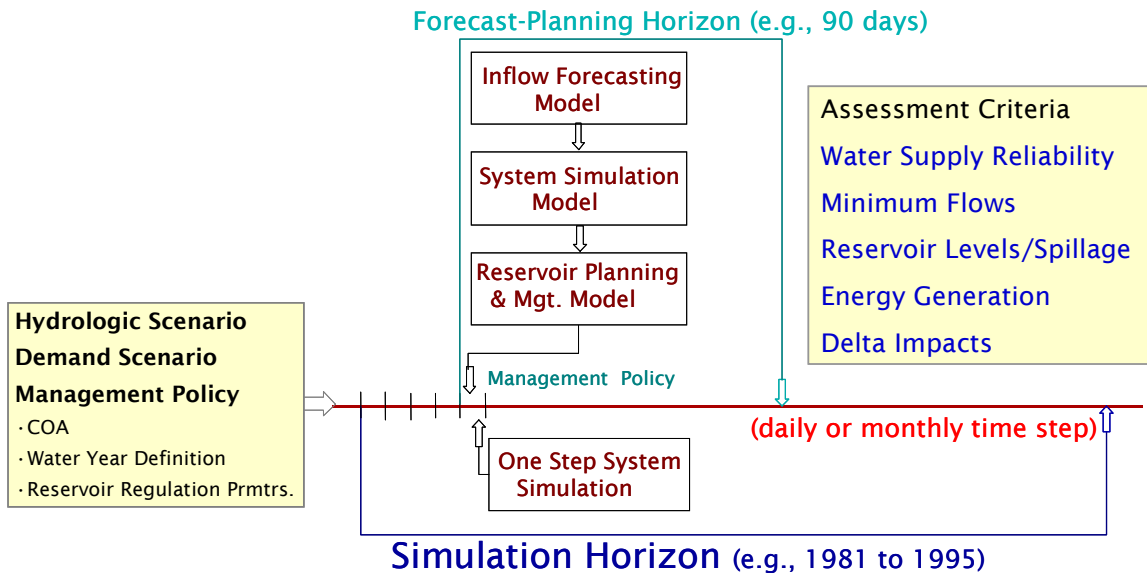


Figure 84. Scenario and policy assessment models

The following sections present assessments pertaining to mid-range management and long-range planning.

5.6.1. Mid-range Scenario and Policy Assessment Examples

This section describes three assessments with the following attributes and scope:

- The assessments aim to evaluate the response of Trinity, Shasta, Oroville, and Folsom over a 15-year horizon in daily time steps.
- The assessments are carried out over the historical reservoir inflows from 1981 to 1995.
- The mid-range management model is run sequentially for each day of the assessment horizon.
- The management objectives are to (1) avoid flooding, (2) pass as much of the release as possible through the plant turbines and avoid spillage (energy generation), (3) meet the applicable minimum flow requirements (water supply and environmental/ecological flows), and (4) maintain high reservoir levels (water conservation and energy generation).
- Inflow forecasts have a forecast horizon of 90 days and are generated by either a Perfect Forecast scheme, which assumes that the upcoming 3-month inflows are perfectly known, or a Historical Analog (HA) scheme. The historical analog approach, described in Appendix H, identifies historical periods where inflows exhibited similarity with recently observed inflows and develops a forecast ensemble with the inflow sequences that materialized following these historical periods. These forecasting schemes are used here to establish benchmarks for the more elaborate forecasting schemes to be used in the following chapter (integrated assessments).
- The assessments differ by the forecasting scheme and the way forecasts are used by the mid-range management model. More specifically, the first assessment uses perfect forecasts (one 90-day sequence identical to the forthcoming inflows); the second assessment employs the historical analog forecast scheme with 10 ensemble members but only uses the mean ensemble sequence (i.e., one 90-day sequence representing the conditional ensemble mean) to drive the mid-range management model; and lastly, the third assessment also generates historical analog forecasts but uses the full forecast ensemble to drive the mid-range management model. In the third case, storage constraints are expected to be met at 90% reliability, whereas the first and second cases are essentially deterministic.

The results of these assessments are summarized in Figures 85, 86, 87, and 88, and Table 26. Figure 85 displays the Trinity elevation and release sequences associated with the three assessment runs. Figures 86, 87, and 88 show the same information for Shasta, Oroville, and Folsom respectively. These Figures illustrate that reservoir levels and releases differ significantly for each assessment, underscoring the importance of forecast information in the management process.

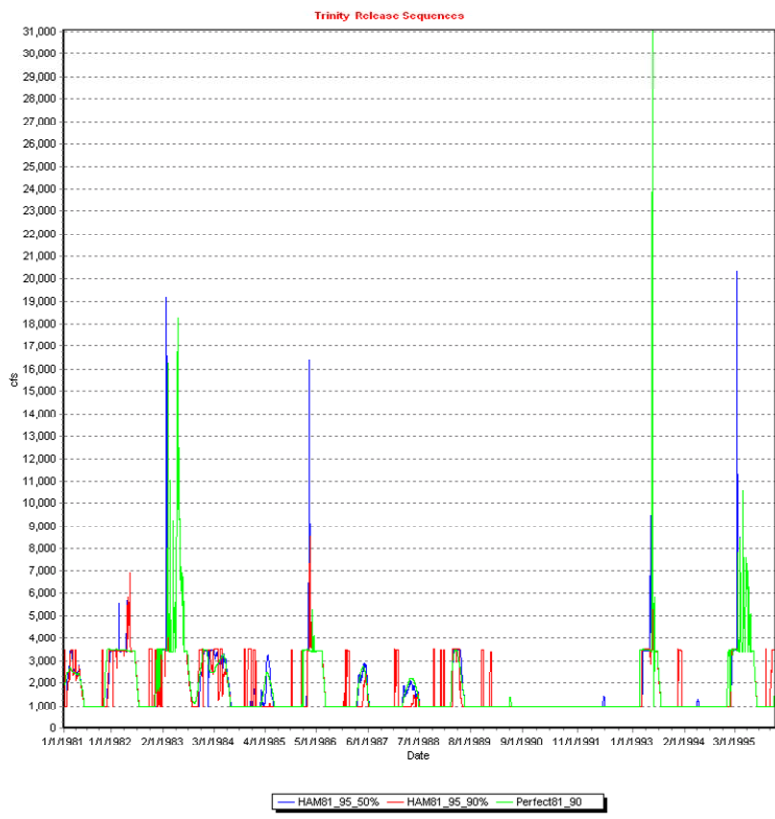
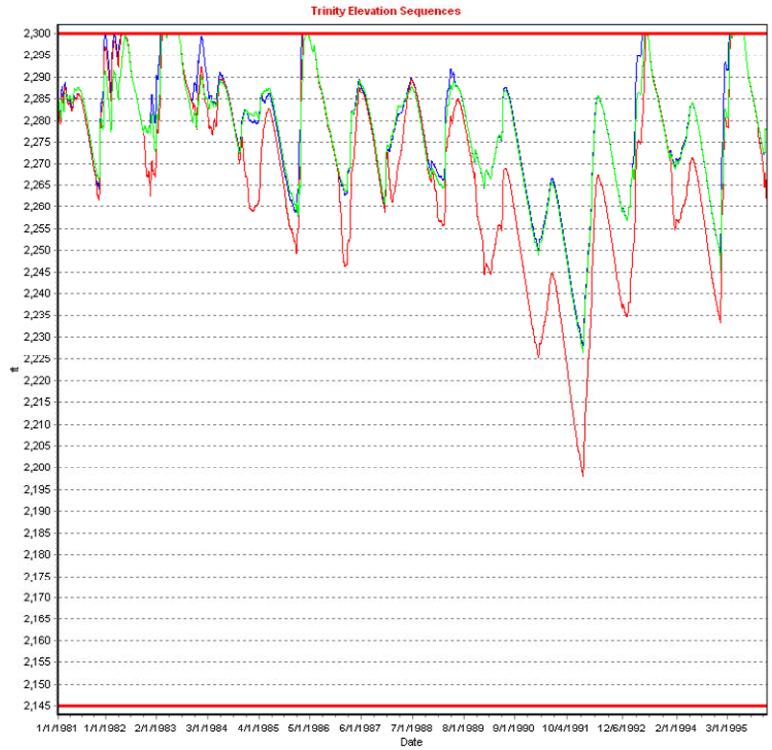


Figure 85. Mid-range assessments: Trinity elevation and release sequences

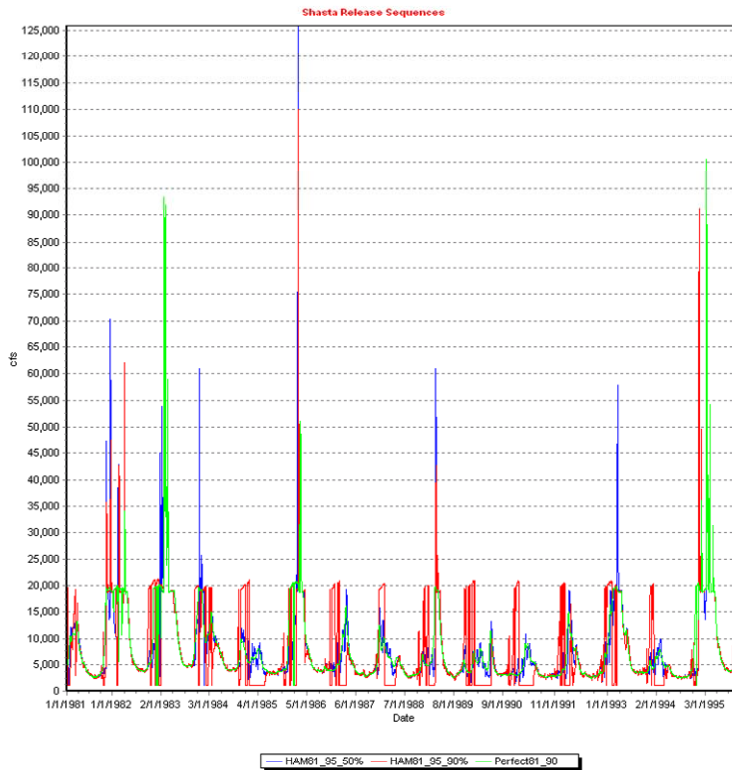
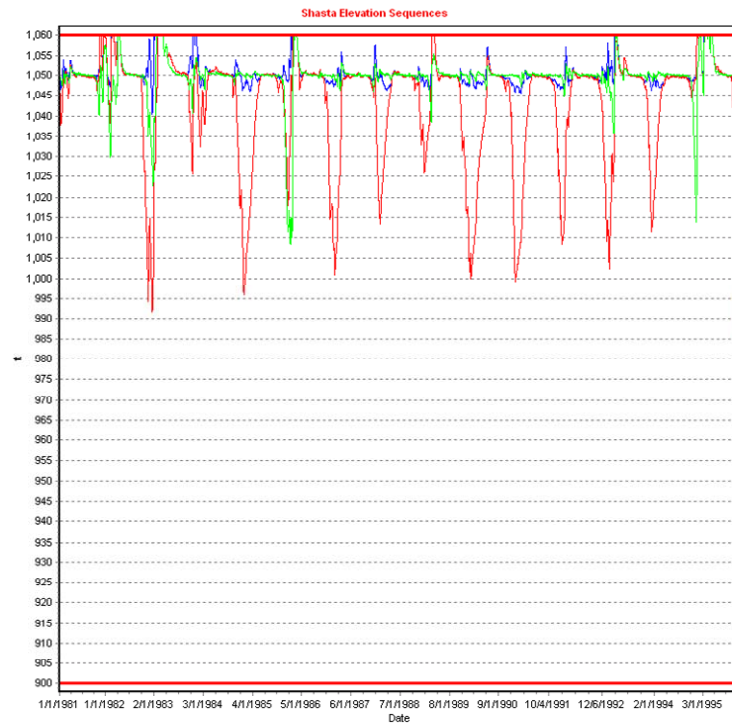


Figure 86. Mid-range assessments: Shasta elevation and release sequences

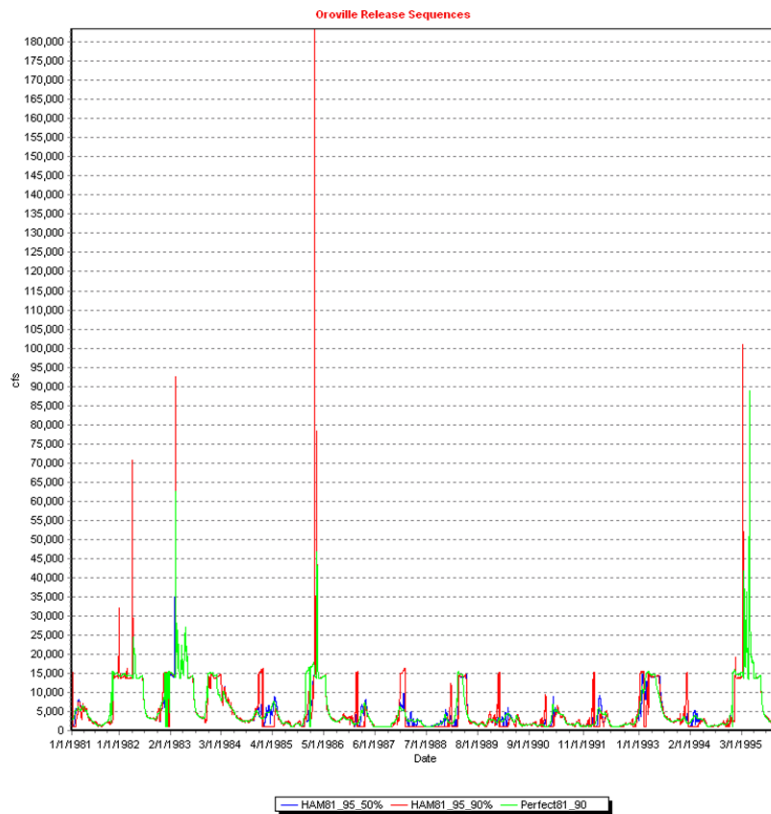
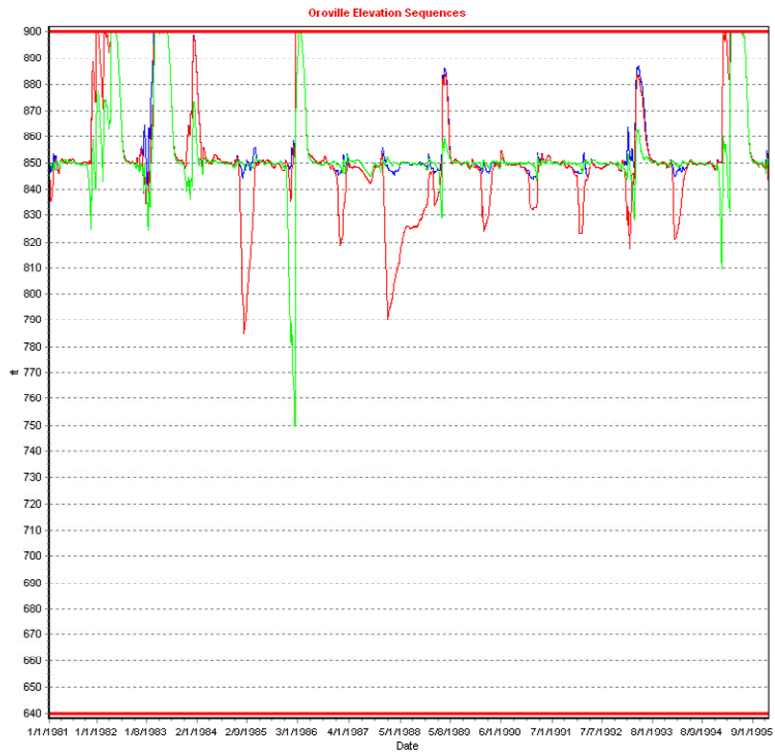


Figure 87. Mid-range assessments: Oroville elevation and release sequences

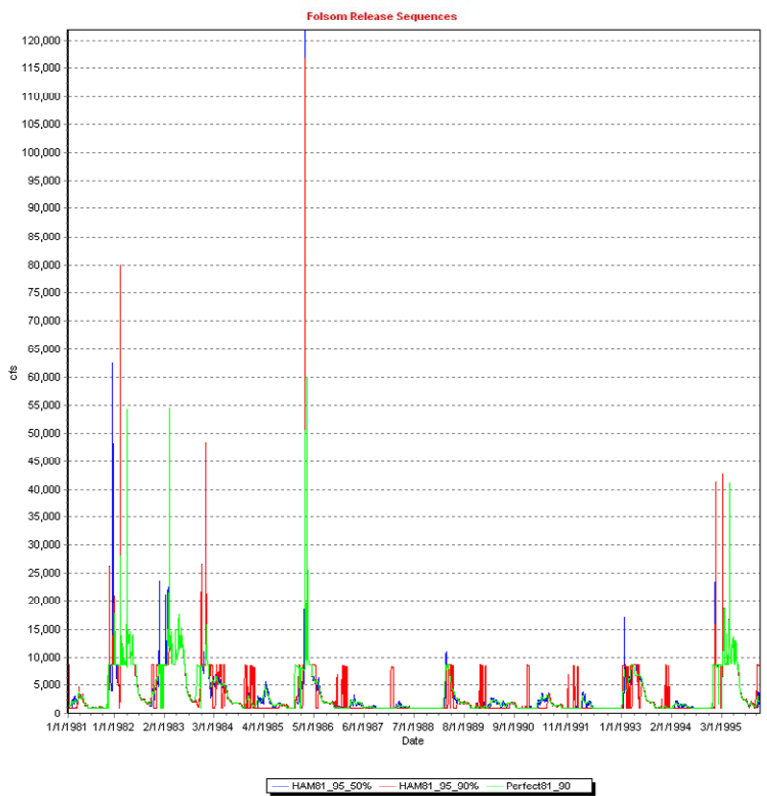
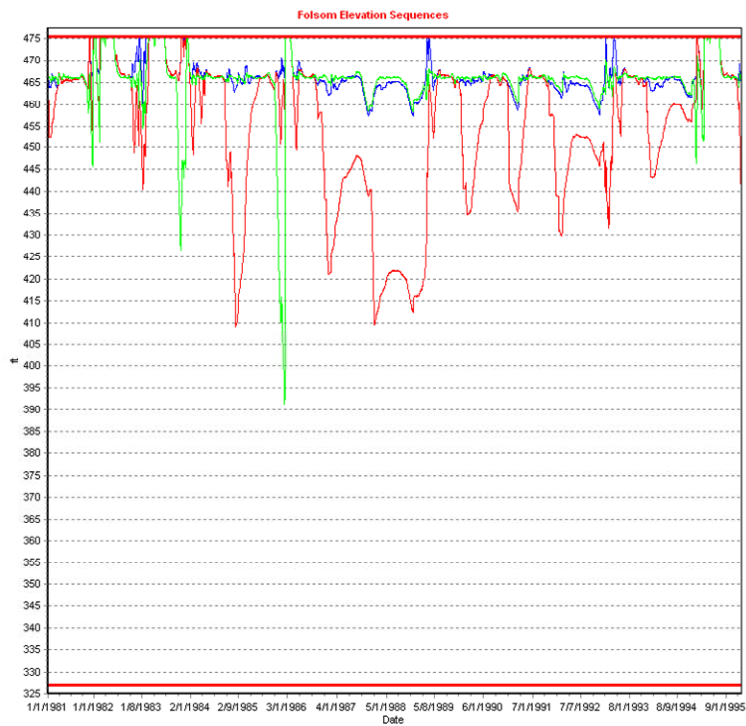


Figure 88. Mid-range assessments: Folsom elevation and release sequences

Table 26. Mid-range assessment statistics

Reservoirs	Comparison Criteria	HA Forecasts		Perfect Forecasts
		Stochastic	Deterministic	
Folsom	Inflow (cfs)	3382	3382	3382
	Spillage (cfs)	406	456	270
	Energy (GWh)	1.74	1.75	1.84
	Max. Release (cfs)	116791	121841	59968
	Max. Damage (\$)	220,400,000	842,000,000	0
Oroville	Inflow (cfs)	5634	5634	5634
	Spillage (cfs)	562	585	310
	Energy (GWh)	5.45	5.45	5.62
	Max. Release (cfs)	183476	183476	88773
	Max. Damage (\$)	0	0	0
Shasta	Inflow (cfs)	7800	7800	7800
	Spillage (cfs)	554	759	329
	Energy (GWh)	6.66	6.63	6.92
	Max. Release (cfs)	109937	125837	100590
	Max. Damage (\$)	0	0	0
Trinity	Inflow (cfs)	1779	1779	1779
	Spillage (cfs)	108	161	114
	Energy (GWh)	1.07	1.09	1.12
	Max. Release (cfs)	18260	31081	31081
	Max. Damage (\$)	0	0	0

cfs=cubic feet per second; GWh=gigawatthours

More specifically, comparing first the deterministic and stochastic historical analog forecast cases (corresponding respectively to the blue and red lines in the figures), one observes that the deterministic case maintains consistently higher reservoir levels but also causes more frequent and more severe spills. This holds true for all reservoirs and occurs because the deterministic HA forecast model communicates (to the management model) information only on the ensemble mean and not the possible extremes. In view of this, the management model cannot anticipate potentially high flows and maintains high reservoir levels, causing more frequent and more severe spills. This is illustrated in Table 26 which shows that the spillage, maximum release, and flood damage associated with the deterministic historical analog model are always higher than (or equal to) those of the stochastic model. Thus, ignoring forecast uncertainty in the management process leads to increased flood risks and, eventually, higher flood damage.

Second, comparing the perfect forecast case with the other two, one can appreciate the value of forecast information for reservoir management. When forthcoming inflows are predicted with good precision, the management model guides the reservoir to meet all objectives more effectively. Thus, high reservoir levels are maintained throughout the assessment horizon, more hydropower is generated, while spillage and flood damage are minimized. When forecast information is imperfect (as in all real world applications), system performance depends critically on forecast precision and reliability. In this regard, narrower and more reliable forecast ensembles lead to better performance. A third desirable forecast attribute is long lead time. In the case of the perfect forecast assessment, system performance would improve further if the forecast lead time extended longer than three months.

Although forecast precision, reliability, and long lead time are all necessary attributes for good system performance, they are not also sufficient. The second critical factor for good system performance is the implementation of an adaptive management system that can fully utilize the forecast information and derive dynamic, risk-based management policies. Yao and Georgakakos (2001) illustrate this aspect, demonstrating that even the best possible forecasts lead to inferior performance if they are coupled with static and heuristic regulation schemes. More specifically, they show that static regulation rules cannot take full advantage of inflow forecasts, leading to less energy generation and inability to balance reservoir management objectives during wet and dry climatic periods.

In Chapter 6, assessments will also be performed with the forecast schemes described in Chapters 3 and 4, and the results will be compared with the baseline results presented in this section.

5.6.2. Long-range Scenario and Policy Assessment Examples

This section discusses four long-range assessments with the following attributes and scope:

- The assessments aim to evaluate the response of the entire Northern California system described in Section 5.5.1.
- The assessments are carried out over the historical hydrology from 1970 to 1995 (26 years), in monthly time steps.
- The long-range planning model is run sequentially for each month of the assessment horizon.
- The management objectives are to (1) meet water demands and the minimum required flows, (2) meet the Delta requirements associated with the X2 location and the Delta outflow, (3) generate as much energy as possible, and (4) maintain high reservoir levels.
- The objectives of the assessments are to (1) quantify the capacity of the system to meet increasing demands, (2) assess the potential impacts on other water uses, and (3) evaluate the effectiveness of adaptive forecast-management schemes as a means to mitigate the adverse impacts of increasing stresses.
- Inflow forecasts have a forecast horizon of three months and are generated by either a Perfect Forecast scheme, or a Historical Analog scheme forecasting the mean of a 10-member ensemble. These two forecast schemes are selected to provide a range of system performance—the expectation being that most other forecast schemes of interest should yield intermediate performance.
- The assessments differ by the forecasting scheme (previous two options) and by two water-demand target levels. The demand targets are determined as a function of the base demands reported in Table G-6 (Appendix G) and as a function of the river index. More specifically, the forecasted inflows, along with the observed inflows up to the current month, are used to compute the river index as stipulated by the COA (Appendix I). Based on the river index, the water demands and minimum flow requirements reported in Table G-6 are adjusted according to agreed-upon rules. The adjusted demands and minimum flows are subsequently multiplied by 0.5 or 0.6 (two options) and used as targets in the simulations.

The results of these assessments are summarized on Figures 89 through 94 and Tables 27, 28, 29, and 30. More specifically, Figure 89 shows the simulated reservoir level sequences of Trinity, Shasta, Oroville, Folsom, and New Melones for all four scenarios. Figures 90 and 91 display the release and energy generation sequences for the same five reservoirs. Figure 92 presents the target south exports sequences, the south exports sequences that were actually met, and the deficits incurred, if any. Finally, Figures 93 and 94 depict the simulated sequences of the X2 location and Delta outflow. The tables include statistics on (a) reservoir levels, releases, net evaporation, and inflows (Table 27), (b) energy generation and spillage (Table 28), (c) water demands and associated deficits

(Table 29), and (d) maximum X2 location distance (Table 30). The results support the following observations:

System Capacity to Meet Water Demand Targets: The 0.5 water demand scenario can be fully met throughout the assessment horizon, without causing violation of any other system requirement (such as minimum flows, Delta environmental conditions, or other factors). To meet this water demand scenario, however, reservoir levels fluctuate markedly on seasonal and interannual basis. The 0.6 water demand scenario, on the other hand, begins to experience water supply deficits (Delta demand and south exports) and fails to keep the Delta X2 location less than 80 km from the Golden Gate Bridge during the 1991–1992 dry years. This scenario also leads to greater reservoir fluctuations, including five to six years of full conservation storage depletion. On average, reservoir levels are 10 to 20 feet lower than those of the 0.5 demand scenario. Scenarios of higher water demands would lead to more frequent and more severe water shortages and failures to meet other system requirements. Thus, the water stress that uses up the system capacity to meet its objectives is estimated to be between 50% and 60% of the base demands (Tables G-5 and G-6).

Value of Forecast Information: The results associated with the two forecasting schemes (Perfect Forecasts and Deterministic Historical Analog) show that better forecast information improves system performance and mitigates the impacts of increasing water stress. More specifically, the Perfect Forecast scenario (three months lead time) leads to higher reservoir levels, more energy generation, and increased capacity to meet water demands and the Delta environmental requirements. This is particularly evident at the 0.6 water demand scenario where the Perfect Forecast case practically avoids water supply deficits and maintains the Delta X2 location less than 80 km from the Golden Gate Bridge in all years.

Need for Reservoir Coordination in Planning and Management: An interesting observation can be made by comparing the results of the long-range planning and the mid-range management assessments. The two assessments share a common simulation period, from 1981 to 1995. The main difference between the assessments is that the mid-range assessment manages the reservoirs *individually* and does not include potential interactions that might arise as part of the need to meet Delta demands and environmental conditions. To a certain extent, this approach reflects current practices, which during flood periods focus on individual reservoir management (daily or sub-daily operations), while for purposes of long-range planning consider the entire system (monthly operations). The assessments show that this incompatibility between planning and management may compromise system performance and lead to potential failures. This can be seen by the different reservoir level sequences generated by the two assessments. More specifically, mid-range management objectives and the need to fully use forecast information, occasionally cause significant reservoir draw downs. From the mid-range management model standpoint, this is an appropriate operational strategy. Long-range planning, on the other hand, concerned with interannual droughts and systemwide demands, imposes additional reservoir storage requirements and results in

different interannual storage sequences. Thus, from a long-range planning standpoint, significant reservoir drawdowns imply increased drought risks. This incompatibility between mid-range management and long-range planning can be addressed by expanding the mid-range management scope to include a systemwide, rather than an individual reservoir, perspective.

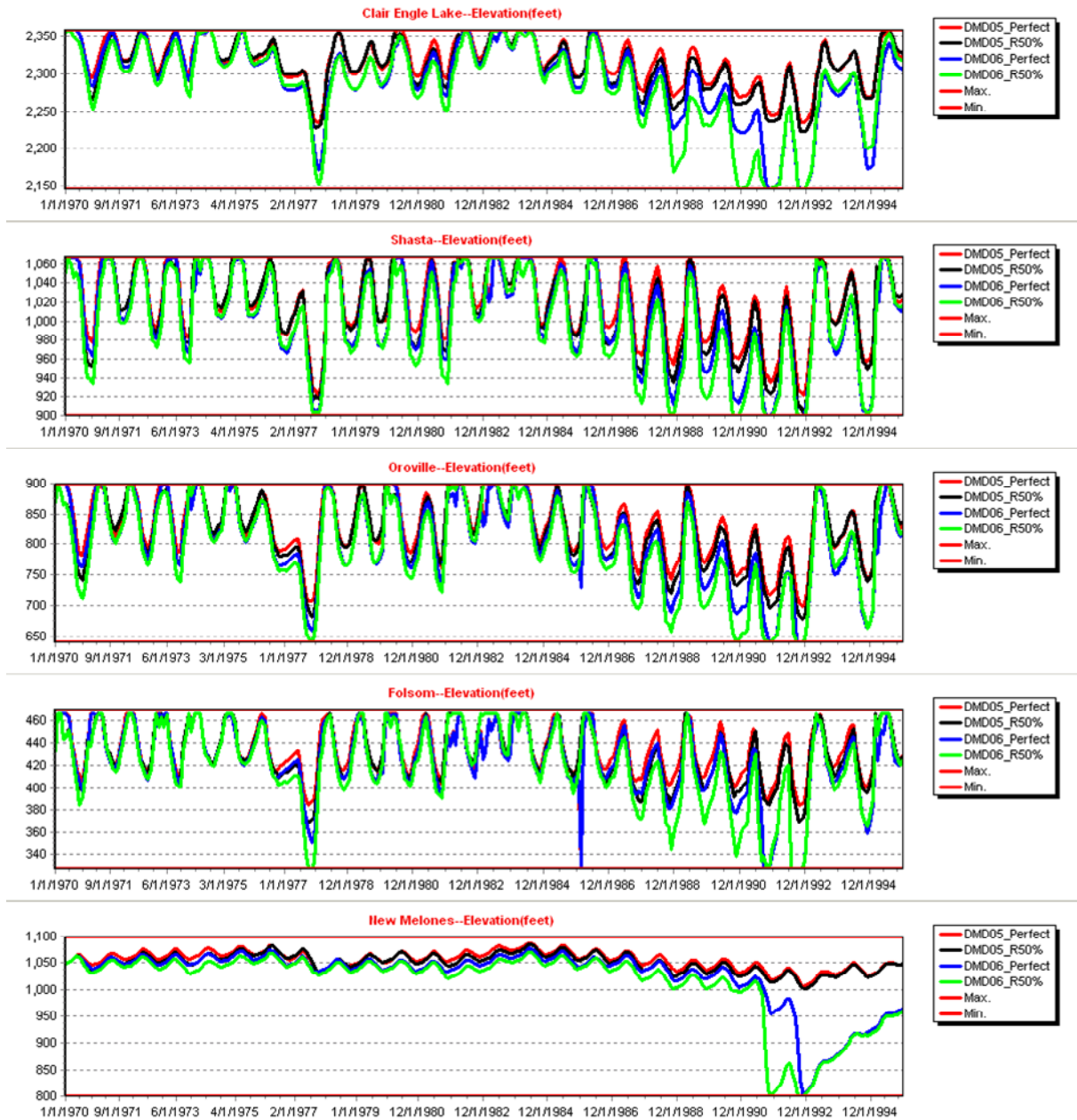


Figure 89. Long-range assessments: Reservoir elevation sequences



Figure 90. Long-range assessments: Reservoir release sequences

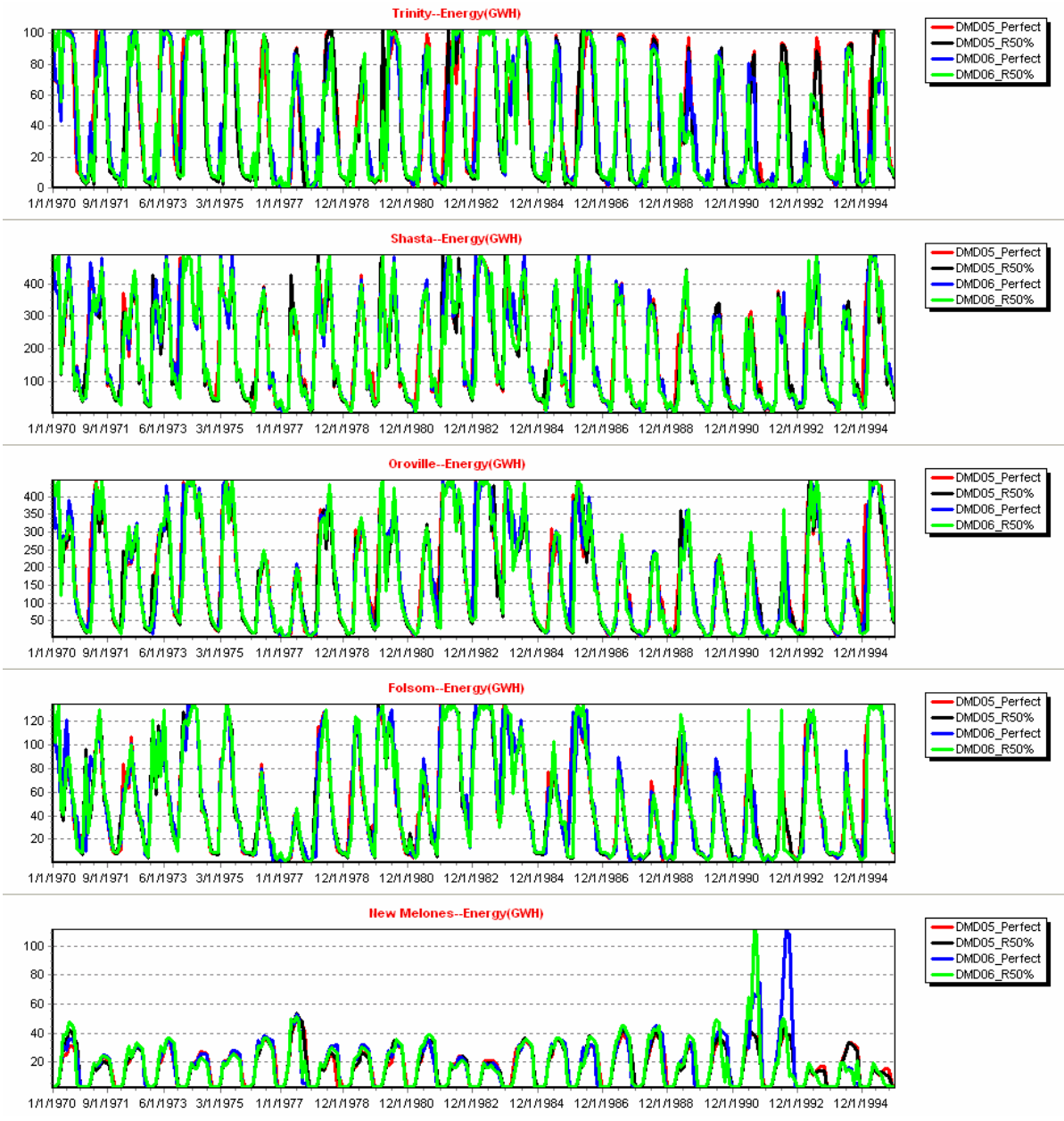


Figure 91. Long-range assessments: Energy generation sequences

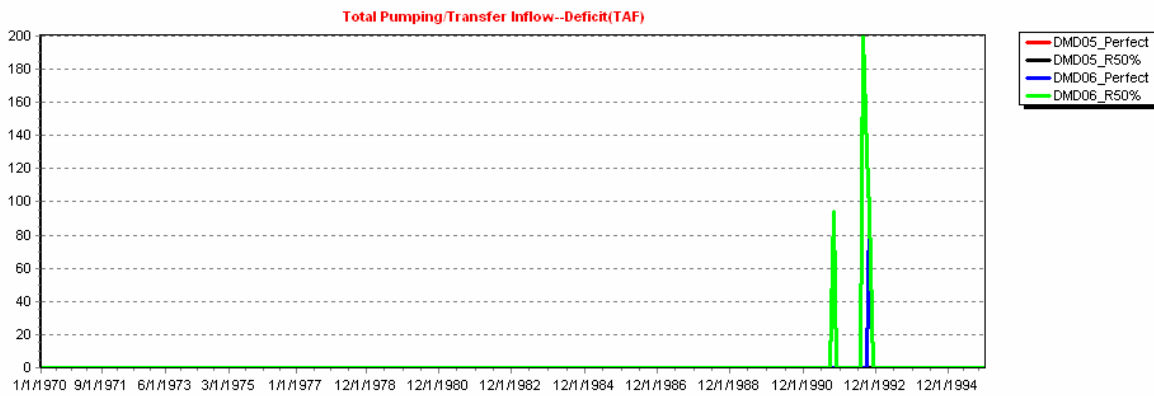
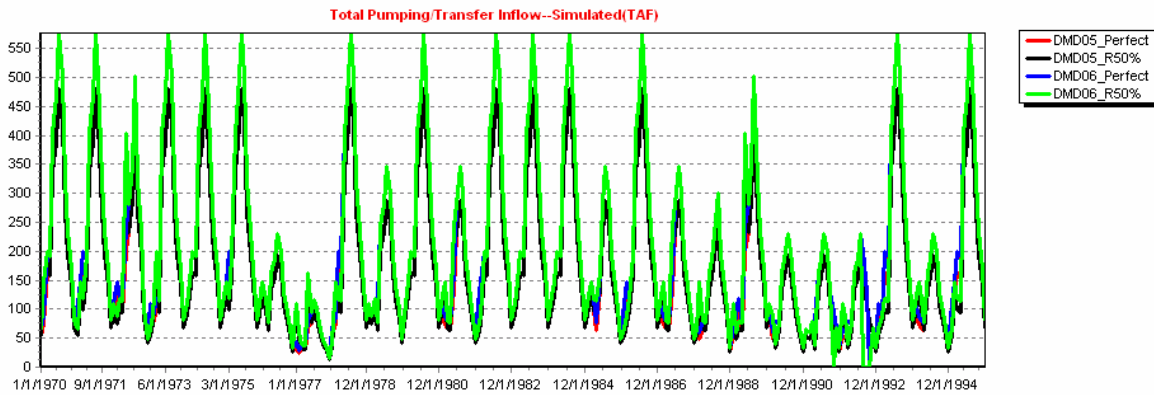
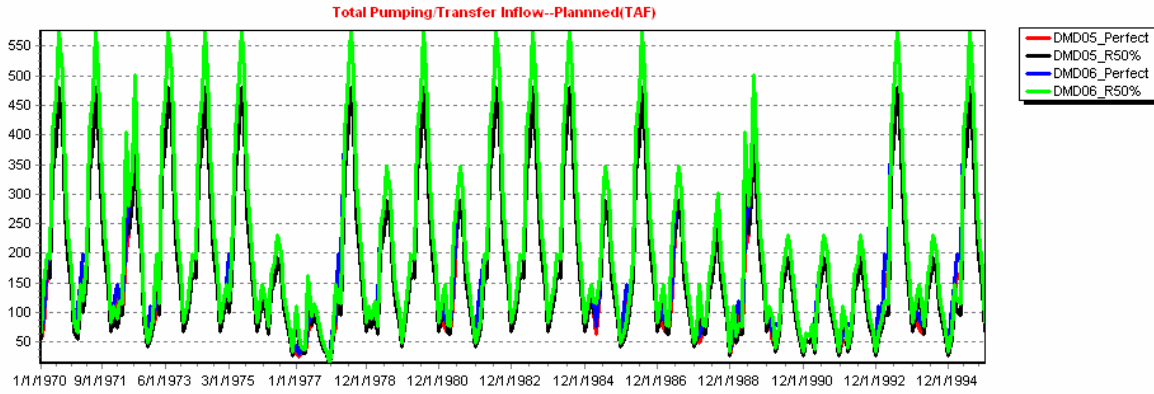


Figure 92. South export and deficit sequences

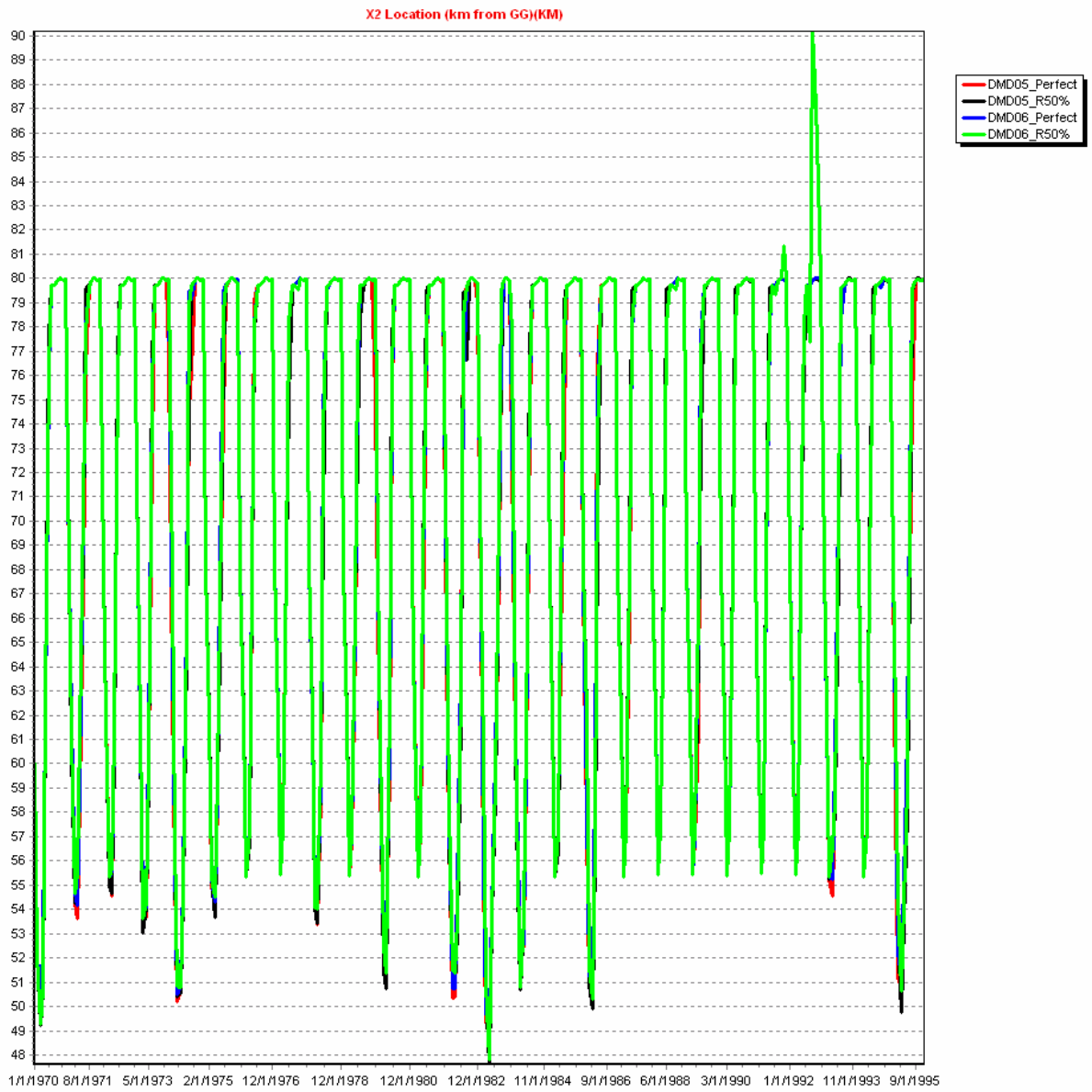


Figure 93. X2 location sequences

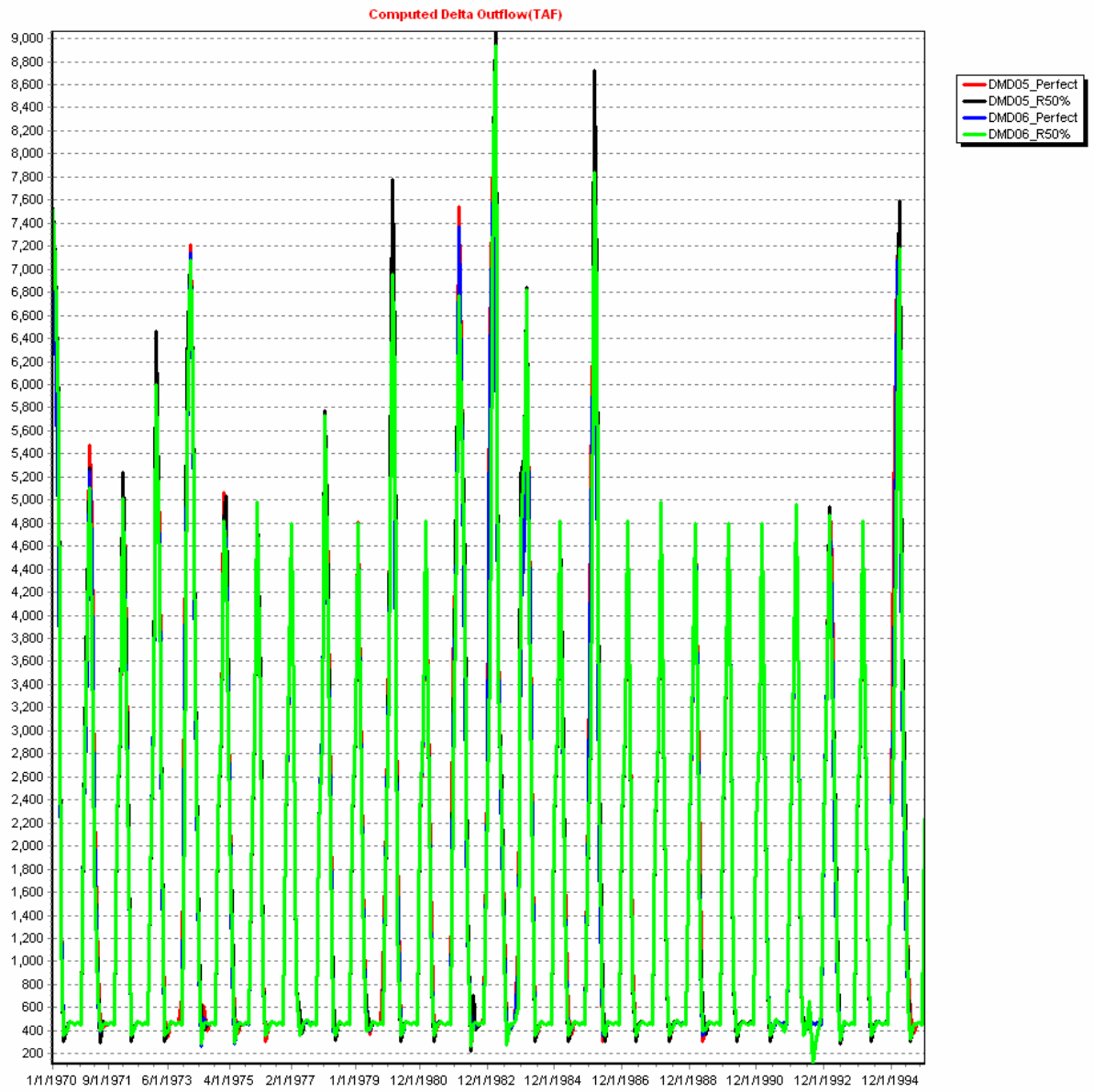


Figure 94. Delta outflow sequences

Table 27. Long-range assessment: Reservoir statistics

Scenarios	Parameters	Units	Trinity	Shasta	Oroville	Folsom	New Melones	San Luis
50%DMND PerFor	Elevation	FEET	2317.42	1020.62	830.72	434.45	1056.22	454.43
	Storage	TAF	1707.13	3384.04	2613.38	671.76	2048.92	1083.98
	Local Inflow	TAF	110.10	488.03	333.45	199.72	46.44	0.00
	Net Evaporation	TAF	5.12	9.51	5.03	3.58	4.34	3.77
	Outflow	TAF	106.18	479.54	329.29	195.85	42.02	0.00
50%DMND HA50%	Elevation	FEET	2312.63	1015.60	824.40	431.84	1051.44	454.43
	Storage	TAF	1652.30	3280.99	2547.34	651.77	1995.87	1083.98
	Local Inflow	TAF	110.10	488.03	333.45	199.72	46.44	0.00
	Net Evaporation	TAF	5.00	9.29	4.92	3.51	4.27	3.77
	Outflow	TAF	106.03	479.21	329.15	195.94	42.05	0.00
60%DMND PerFor	Elevation	FEET	2294.15	1005.56	807.70	425.17	1026.13	454.43
	Storage	TAF	1473.00	3078.30	2374.05	608.63	1777.44	1083.98
	Local Inflow	TAF	110.10	488.03	333.45	199.72	46.44	0.00
	Net Evaporation	TAF	4.63	8.94	4.72	3.36	3.95	3.77
	Outflow	TAF	107.35	480.95	330.23	196.23	44.96	0.00
60%DMND HA50%	Elevation	FEET	2286.31	999.82	799.41	421.29	1013.08	454.43
	Storage	TAF	1403.11	2966.97	2296.30	585.43	1667.63	1083.98
	Local Inflow	TAF	110.10	488.03	333.45	199.72	46.44	0.00
	Net Evaporation	TAF	4.47	8.70	4.59	3.25	3.78	3.77
	Outflow	TAF	107.03	480.82	330.22	196.32	45.26	0.00

TAF=thousand acre feet

Table 28. Long-range assessment: Hydropower and spillage statistics

Scenarios	Parameters	Units	Trinity	Shasta	Oroville	Folsom	New Melones
50%DMND_PerFor	Energy	GWh	41.38	198.11	175.87	52.74	17.01
	Spillage	TAF	3.31	11.35	19.68	8.13	0.00
50%DMND_HA50%	Energy	GWh	40.36	191.05	168.51	51.20	17.02
	Spillage	TAF	5.14	23.91	31.32	14.40	0.00
60%DMND_PerFor	Energy	GWh	40.12	194.43	174.19	52.19	18.03
	Spillage	TAF	3.58	10.47	17.41	8.15	0.43
60%DMND_HA50%	Energy	GWh	39.34	188.57	167.22	50.53	17.58
	Spillage	TAF	4.32	19.87	28.02	13.88	1.83

GWh=gigawatthours; TAF=thousand acre feet

Table 29. Long-range assessment: Water supply statistics

Scenarios	Parameters	Units	Thermalito	Folsom Pumping	Folsom South Canal	OID/SSJID	Delta Use	South Water Export
50%DMND PerFor	Planned	TAF	37.70	2.82	0.75	4.43	37.36	177.05
	Simulated	TAF	37.70	2.82	0.75	4.43	37.36	177.05
	Deficit	TAF	0.00	0.00	0.00	0.00	0.00	0.00
50%DMND HA50%	Planned	TAF	37.87	2.81	0.75	4.43	37.51	177.15
	Simulated	TAF	37.87	2.81	0.75	4.43	37.51	177.15
	Deficit	TAF	0.00	0.00	0.00	0.00	0.00	0.00
60%DMND PerFor	Planned	TAF	45.24	3.38	0.90	5.32	44.83	212.46
	Simulated	TAF	45.24	3.38	0.90	5.32	44.83	212.16
	Deficit	TAF	0.00	0.00	0.00	0.00	0.00	0.30
60%DMND HA50%	Planned	TAF	45.45	3.38	0.90	5.32	45.01	212.58
	Simulated	TAF	45.45	3.38	0.90	5.32	44.48	210.92
	Deficit	TAF	0.00	0.00	0.00	0.00	0.52	1.66

TAF=thousand acre feet

Table 30. Long-range assessment: Maximum X2 location statistics

Scenarios	Unit	Max. X2 Location
50%DMND_PerFor	km	80.00
50%DMND_HA50%	km	80.00
60%DMND_PerFor	km	80.00
60%DMND_HA50%	km	90.19

6.0 Assessments

6.1. Introduction

The first phase of INFORM (the first three years) allowed for the development of three components: (1) the Global Forecast System (GFS)-driven near-real-time forecast component (featuring a synoptic time scale with lead times out to 16 days), (2) the off-line Climate Forecast System (CFS)-driven forecast component (featuring a seasonal time scale with lead times out to 9 months), and (3) the off-line decision component (featuring long-range/planning and medium-short-range modules)—all within the context of the integrated system as discussed in Chapter 2. In addition, the project first phase included initial assessments of system performance during the latter part of the wet season 2005–2006.

In the present chapter, the authors discuss the experiments conducted and results obtained during this wet season, as well as additional retrospective studies of the decision component performed with the unconditional ESP and CFS-conditioned ESP. This discussion includes assessments of INFORM system forecast performance, as well as corresponding decision component assessments.

The discussion also includes assessments for short-range forecast and risk-based management (0–16 days forecast horizon) and for long-range management (1–9 months of decision horizon). Chapter 3 contains a discussion of long-range forecasts both for unconditioned ESP and CFS-conditioned ESP in the context of probabilistic downscaling. This discussion will not be repeated here. It is notable that the GFS-driven near-real-time forecast component of INFORM ran with no bias adjustments in any of the model output it uses and/or produces. To highlight the need for such adjustments, the authors conducted numerical retrospective experiments after the wet season to produce a preliminary quantitative assessment of the influence of simple adjustment methods on the ensemble forecast output of the INFORM system. This chapter includes a summary of these results as well.

The GFS-driven INFORM forecast simulations involve real-time links to NCEP and CNRFC, both under the U. S. National Weather Service. The link to NCEP provides the GFS three-dimensional ensemble forecast fields that feed the downscaling models of the INFORM system, while the link to CNRFC provides MAP and MAT estimates based on observed precipitation data and initial model state fields for the snow and soil water models of the INFORM system. (Figure 6 of Chapter 2 and relevant discussion therein highlight these real-time links.) During the beginning of the 2005–2006 wet season, especially, and at other times later, these links were broken occasionally due to intentional changes in INFORM system configuration toward a more robust real-time system performance, so the short-range results to follow should be considered as initial results, rather than definitive results for the INFORM system. The authors believe that real-time runs for two to three additional wet seasons will be necessary to reliably measure system performance and effect relatively simple physics-based adjustments for the real-time component of INFORM. Nevertheless, these initial results are presented

herein as an indication of the INFORM system capabilities under a “dry run” scenario. Lastly, to note a present limitation of the INFORM forecast component, with the available hardware at the HRC, only 8 of available 15 ensemble GFS forecasts are currently used to produce real-time ensemble reservoir inflow forecasts (four times daily). Increasing the GFS ensemble size to 15 (with the prerequisite increase of CPU processors to 16–20 as well) would provide more reliable estimates of reservoir inflow forecast uncertainty by virtue of increased sample size.

The next section discusses the INFORM forecast component simulations using CNRFC estimated MAP and MAT data for the wet season 2005–2006 for comparison and to indicate the level of maximum accuracy feasible using the present configuration of the INFORM forecast models. Section 6.3 presents the INFORM MAP and MAT forecasts for various lead times and catchments within the application area. Section 6.4 presents and discusses the ensemble reservoir inflow forecasts for the large reservoirs of the INFORM region at various forecast lead times. A summary assessment section, Section 6.5, includes overall assessments of INFORM real-time short-range forecast performance. It also provides evidence that substantial improvement can be realized in reservoir inflow forecasts through bias adjustment of the MAP forecasts. The chapter concludes with an integrated forecast-decision assessment in Section 6.6. The assessment is similar to those described in Section 5.6.1 and aims to quantify the value of unconditional ESP, climate-conditioned ESP, and other forecast schemes in mid-range reservoir management.

6.2. Reservoir Inflow Simulations

To assess the best possible level of accuracy achievable for the 2005–2006 wet season with the present models of the reservoir inflow component, the INFORM snow-soil-channel models (see formulation and tests with historical data in Chapter 4) ran off-line with CNRFC estimates of MAP and MAT obtained using station observations. Thus, referring back to Figure 6 of Chapter 2, the hydrologic snow accumulation and ablation model, the soil water accounting model and the channel routing model of INFORM ran off-line with MAP and MAT data in simulation mode (that is, decoupled from the rest of the GFS data ingest and downscaling INFORM models of Figure 6). The reader is reminded that these models are adaptations of the CNRFC analogous operational models, and that their parameter values are essentially those estimated by CNRFC (only minor fine-tuning was performed, as discussed in Chapter 4). The main difference between the INFORM hydrologic models and the CNRFC models is that the channel routing model of INFORM is a cascade of linear reservoirs while CNRFC routing for the catchments under study is done using unit hydrograph models. It is noted though that there is direct correspondence between the parameters of the cascade of linear reservoirs and the unit hydrographs (e.g., Sperflage et al. 1996). During the simulation runs of the INFORM hydrologic models there was no link to CNRFC model states, as indicated in Figure 6 for the real-time INFORM forecast component. Thus, some deviation of the stand-alone INFORM hydrologic model from the CNRFC stand-alone model simulation is possible, even when the model input consists of the same MAP and MAT data.

Figures 95 through 99 present the six-hourly simulation results for all five major reservoirs in the INFORM application area: Folsom, New Bullards Bar, Oroville, Shasta, and Trinity, respectively. All the figures show the simulations (blue dashed line) together with the corresponding observations (red line). For each reservoir the observations consist of the CNRFC six-hourly estimates of full natural flow (FNF) or “unimpaired flow” obtained using standard operational procedure. Direct streamflow observations are lacking at reservoir sites because often the reservoirs integrate the flows of more than one river, there is significant upstream regulation, and the reservoir presence substantially modifies natural flows. It is important to note that the INFORM forecast component provides ensemble forecasts or simulations of unimpaired flows.

The results shown in Figures 95 to 99 indicate good reproduction of the FNF estimates by the INFORM hydrologic simulation models for the 2005–2006 wet season. Some evidence of overestimation of high unimpaired flows exists for the Trinity and New Bullards Bar reservoir inflows, while some delay in the recession curves of the unimpaired flow hydrographs for the Folsom and Oroville reservoir inflow is also evident. Given the short duration of the simulations, however, these should be considered preliminary assessments and simulations for additional wet seasons should be performed to arrive at more definitive assessments of model performance. Nevertheless, the level of reproduction is good overall in all cases, and the authors consider such performance to be a good target for the INFORM forecasts (rather than the simulations as in this case). The INFORM forecast for the same wet season are discussed next.

6.3. Precipitation and Temperature Forecasts for INFORM Catchments

As described in Chapter 4, for each reservoir drainage area, the INFORM hydrologic models simulate snow, soil, and channel processes in the tributary catchments. Most of these catchments are subdivided into upper and lower areas to allow for a better definition of snow accumulation and melt. The nominal terrain elevation for the subdivision of catchments into upper and lower areas is 1,500 m. To emulate the CNRFC hydrologic forecast operations, the INFORM hydrologic models receive MAP and MAT input for both upper and lower areas of each catchment. Thus, the INFORM downscaling models described in Chapter 3 of this report are designed to provide ensemble MAP and MAT forecasts for upper and lower areas within the tributary catchments of each reservoir drainage area. The reader should keep in mind that for the 10 x 10-km² resolution of the INFORM gridded precipitation forecasts, there may be only a few grid points used for producing MAPs and MATs for several of these areas (a few hundred square kilometers).

This section presents characteristic MAP and MAT forecast results from the real-time operation of the INFORM system during the 2005–2006 wet season. Forecasts are based on eight forecast ensembles of three-dimensional forcing fields from the GFS operational model of NCEP.

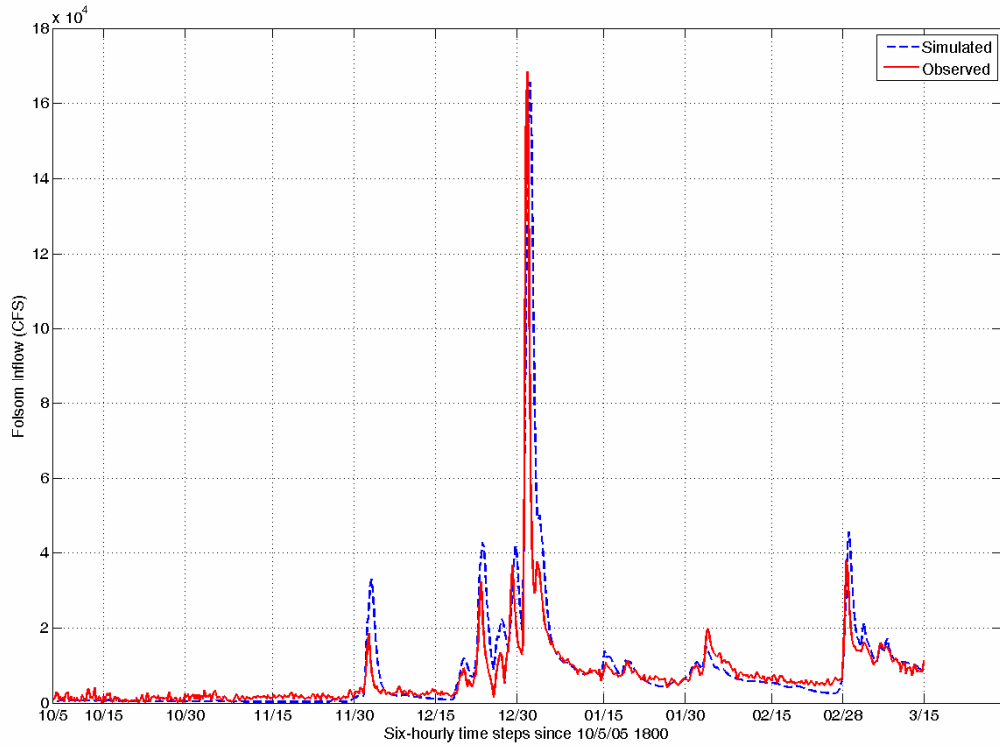


Figure 95. INFORM hydrologic model 6-hour simulations of Folsom reservoir inflow using CNRFC-estimated MAP and MAT time series for the period 10/5/2005–3/15/2006 (blue dashed line). The red line signifies the corresponding CNRFC full natural flow (FNF) estimates (observations).

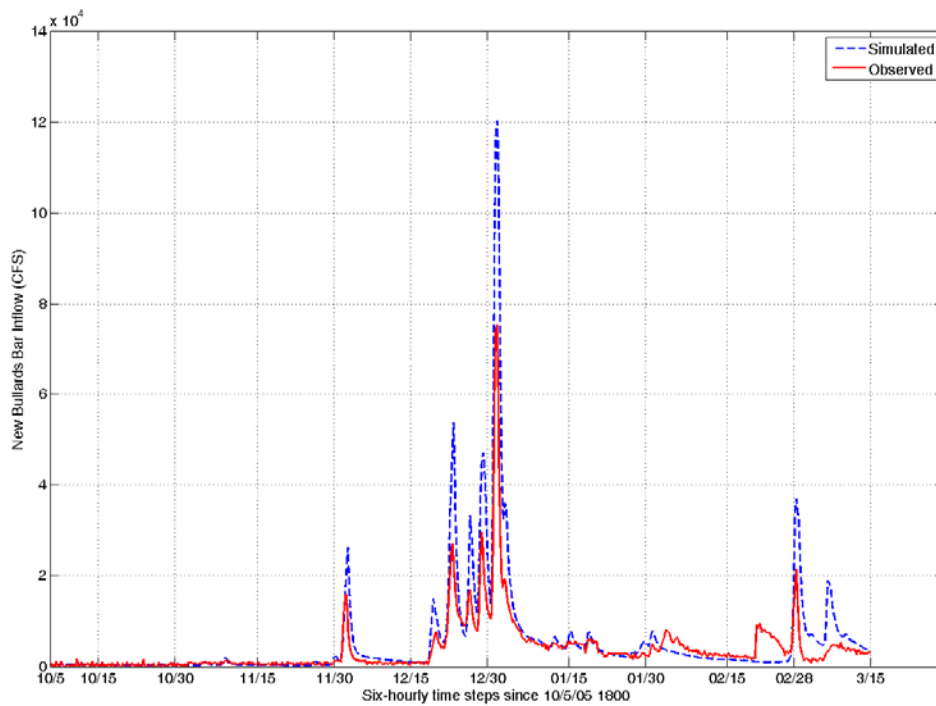


Figure 96. As in Figure 95, but for the New Bullards Bar reservoir inflow on the Yuba River

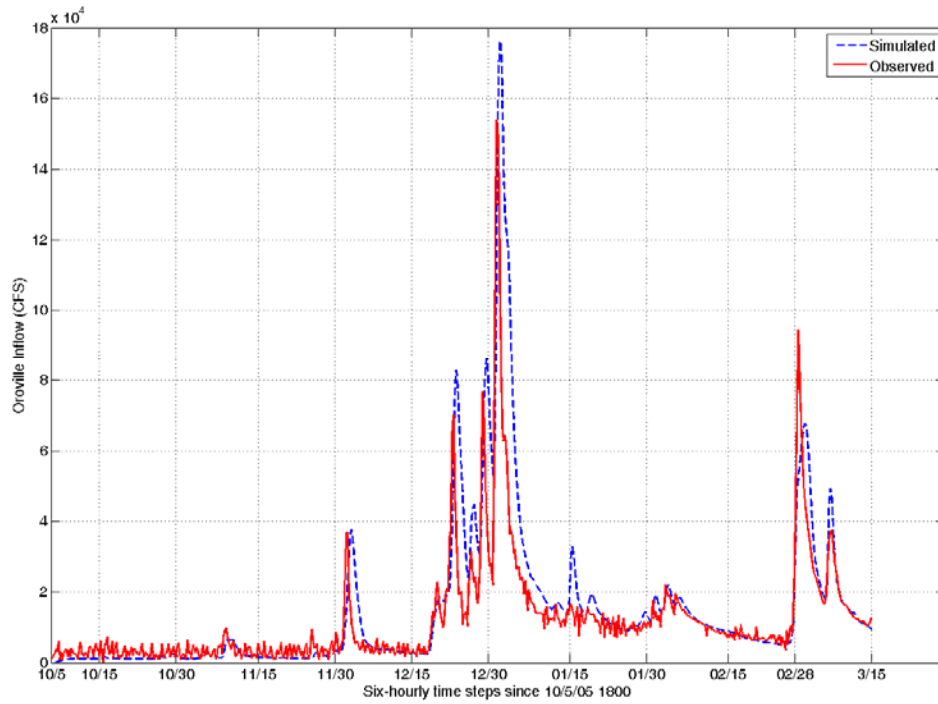


Figure 97. As in Figure 95, but for the Oroville reservoir inflow

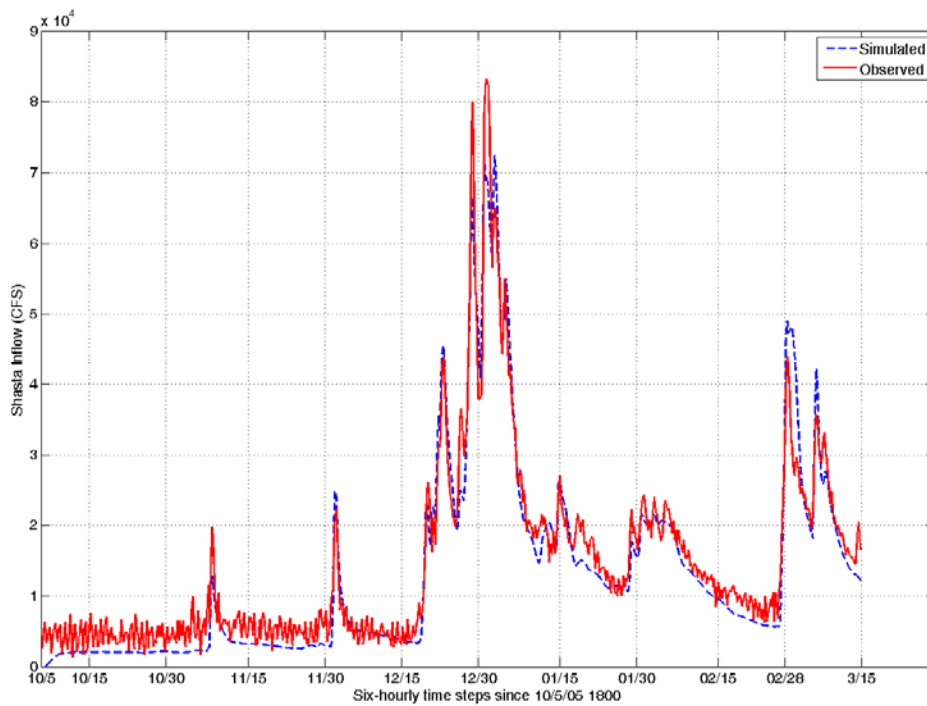


Figure 98. As in Figure 95, but for the Shasta reservoir inflow

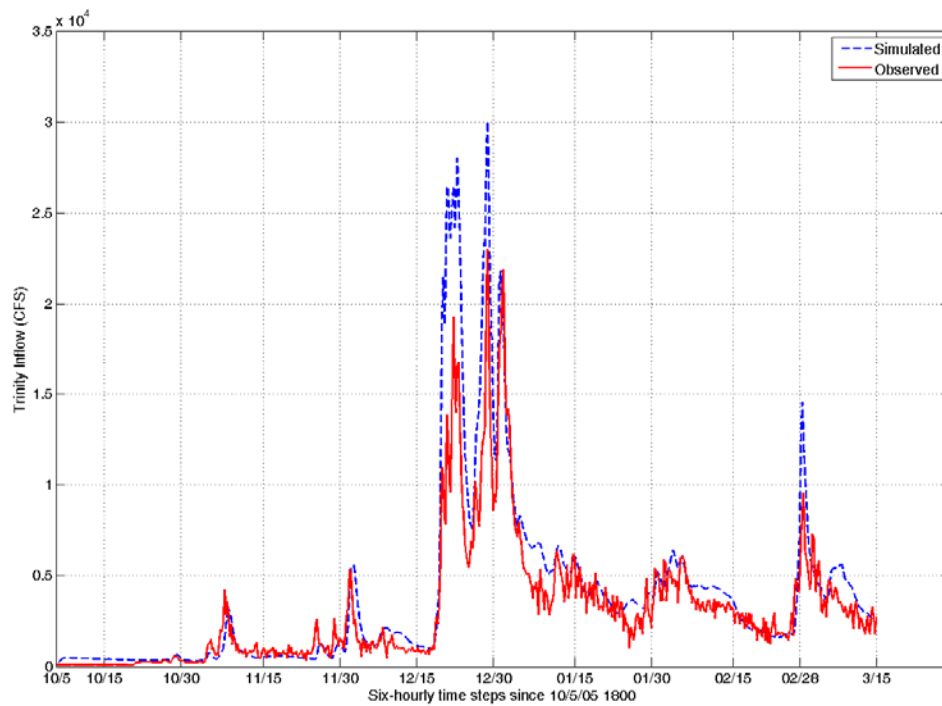


Figure 99. As in Figure 95, but for the Trinity reservoir inflow

6.3.1. MAP Ensemble Forecasts

The INFORM system uses ensemble gridded forecast fields of downscaled surface precipitation to produce MAP ensemble forecasts for each of the tributary catchments within each INFORM reservoir drainage area. The discussion here uses selected cases that the authors consider representative of the range of performance obtained by the real-time INFORM system operations. Figures 100 through 103 present these results. To illustrate performance, each figure includes several panels that contain results corresponding to several forecast lead times (from 12 hours to 5 days). For a certain lead time with a given number of time steps (six-hourly periods), the average forecast over the lead-time period was computed for each ensemble member, and the panels display the highest and lowest averages among the ensemble members (blue dashed lines) at each validation time. In addition, the panels show the corresponding averages of the observations for the same validation time (red lines). These observations are the operational CNRFC MAP estimates for each area (generated using station precipitation data). The science literature documents well the significant errors of estimating MAP in mountainous terrain from sparse observations (e.g., see Tsintikidis et al. 2002 for a discussion concerning the American River catchment with outlet at Folsom). Although the CNRFC MAP estimates used for the evaluation undoubtedly contain errors, the authors expect that these errors are substantially smaller than the expected forecast errors over the several-hundred square-kilometer areas used for the evaluation.

Figure 100 presents the results for the upper area of the North Fork of the American River. During the period of analysis shown (11/18/2005–3/15/2006) there were six significant precipitation periods. The first period was early December 2005, the second period was during the second half of December 2005 and the beginning of January 2006, the third was around the middle of January 2006, the fourth was around the beginning of February 2006, the fifth period was near the middle of February 2006 (with a smaller precipitation), and the sixth period was in the first half of March 2006. The most significant precipitation event occurred at the beginning of 2006, with 12-hourly averaged MAP rates estimated to be over 50 mm/6 hrs by CNRFC.

Examination of the forecast results displayed in the various panels of Figure 100 leads to the conclusion that the INFORM precipitation downscaling component, when run in real time as part of the INFORM system, produced ensemble forecasts that encompassed the observations in most cases, for at least the first three major precipitation periods—even for forecast lead times out to 5 days. The INFORM precipitation downscaling model overestimates the MAP averages for the fourth and sixth precipitation periods, when even the lowest ensemble member average is in several cases above the observed MAP average for the given lead time. This situation is clearly shown for the longer lead times and the last precipitation period of March 2006. With the small number of ensemble members used (8) and the small number of observed events it is difficult to assign the cause of this overestimation to persistent model bias for certain events, ensemble size, or GFS input errors. For the rest of the cases and for lead times out to

three days the model shows remarkably good reproduction of the observations, including the timing of precipitation events.

Figure 101 presents analogous results for the lower area of the Middle Fork of the American River. The CNRFC estimated MAP average precipitation over a 12-hour period is still near 50mm/6hrs for the 1 January 2006 event, while even the high ensemble member average is substantially lower. Apart from this underestimation of the end of 2005/beginning 2006 precipitation period, the remaining precipitation periods show reasonable results for all forecast lead times. Compared to those of Figure 100 (similar to those obtained for the upper area of the Middle Fork, not shown for brevity), the results suggest a tendency of the INFORM precipitation downscaling component to produce higher ensemble forecasts for upper areas (elevations above 1,500 m) than for low areas in the application domain. This behavior is observed for other reservoir drainage area catchments as exemplified by the results from the upper and lower area of the Pit River catchment within the Shasta drainage shown in Figure 102. In this northern catchment in the INFORM domain, the most significant precipitation period occurred in the first half of March 2006 and in most cases the ensemble forecasts encompass the observations for all forecast lead times. The last precipitation event is also forecasted within the high and low ensemble members for all lead times. This holds true for both upper and lower areas of the Pit River catchment. Underestimation of the first of the year (2006) event, especially for the lower area of the Pit River catchment, is evident for all lead times. Similar underestimation may be observed in Figure 103, which shows the forecast and observations for the upper area of the neighboring Sacramento River catchment (outlet at Delta, California). In this case as well, the INFORM precipitation downscaling component produced ensemble forecasts that encompass the majority of the remaining periods at most lead times. Even the last significant event was predicted reasonably well for a five-day forecast average. It is notable that there were several periods of missing INFORM ensemble forecast information for the northern catchments during the beginning of the evaluation period. In several cases, this is the result of missing initial moisture fields from prior time steps during real-time operation, and this may have had some effect on the production of precipitation forecasts.

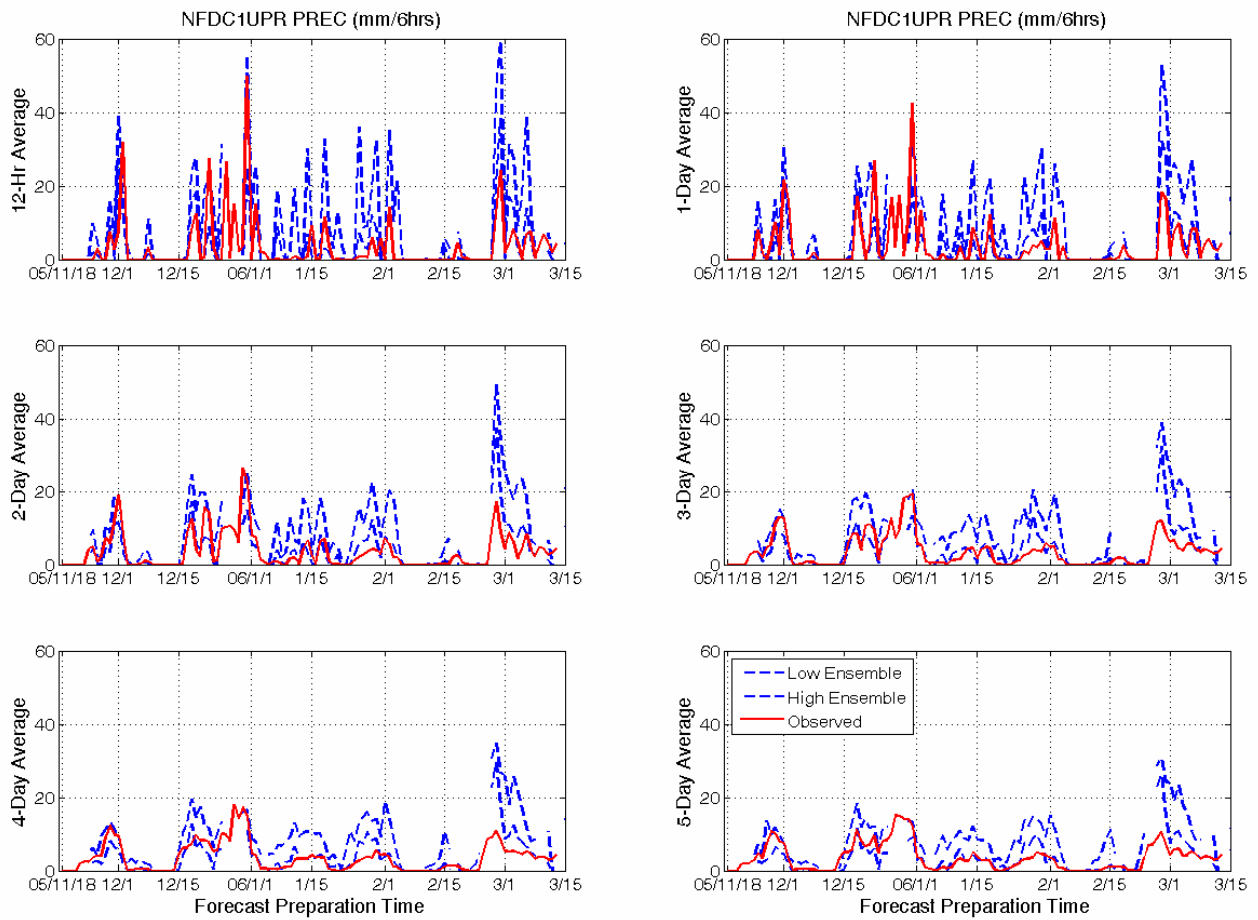


Figure 100. Highest and lowest averages of ensemble members over the indicated forecast lead time period at each valid time (blue dashed lines). The INFORM downscaling component produced these forecasts in real time for the upper modeling area of the American River North Fork. The panels also show the corresponding observed averages estimated by CNRFC (red lines). Forecast lead times range from 12 hours to 5 days.

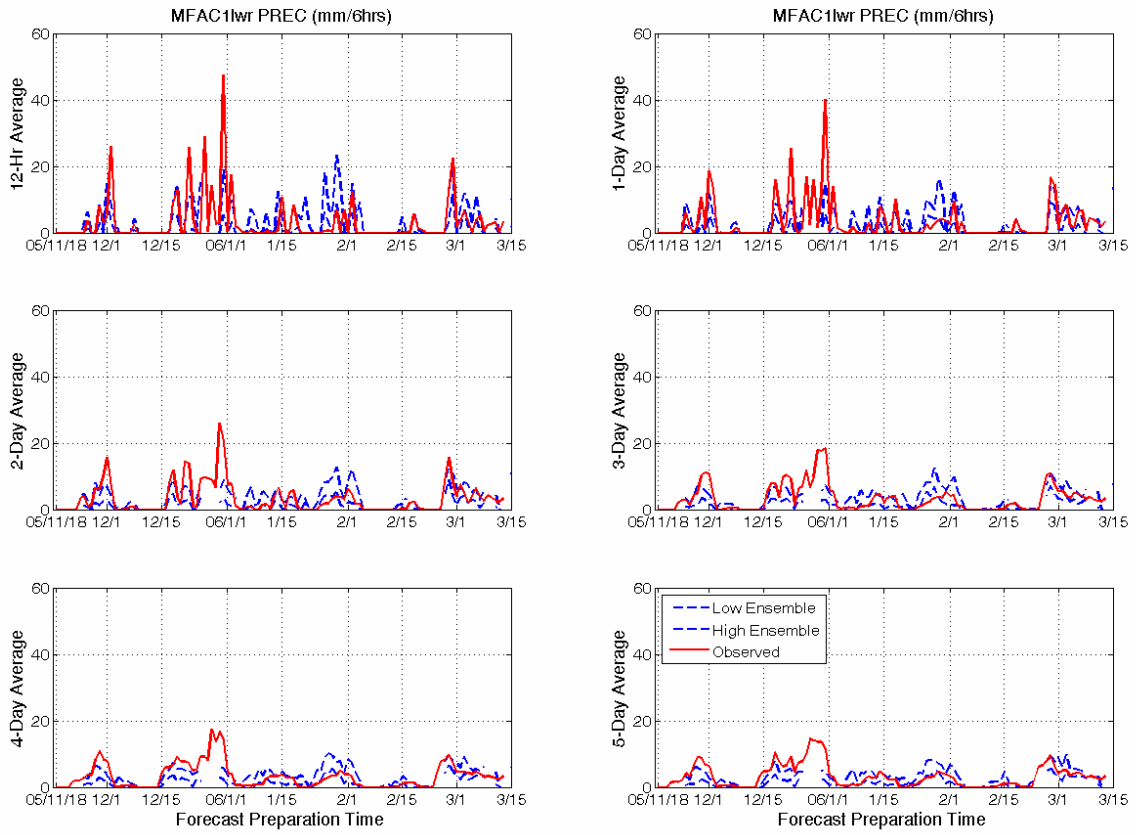


Figure 101. As in Figure 100, but for the Middle Fork of the American River

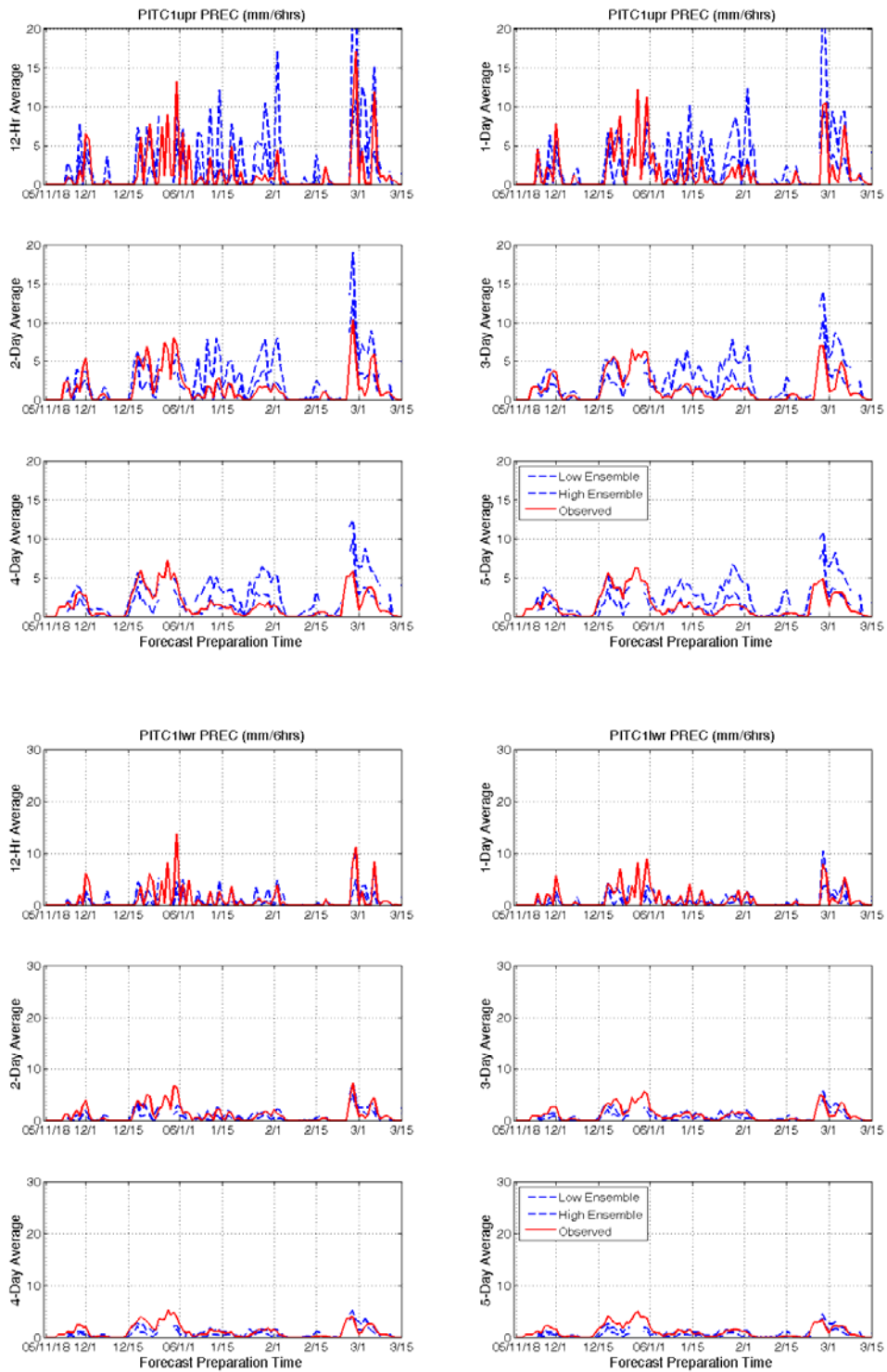


Figure 102. (Upper six panels) As in Figure 100, but for the upper area of the Pit River catchment within the Shasta reservoir drainage area. (Lower six panels) as in Figure 100, but for the lower area of the Pit River catchment.

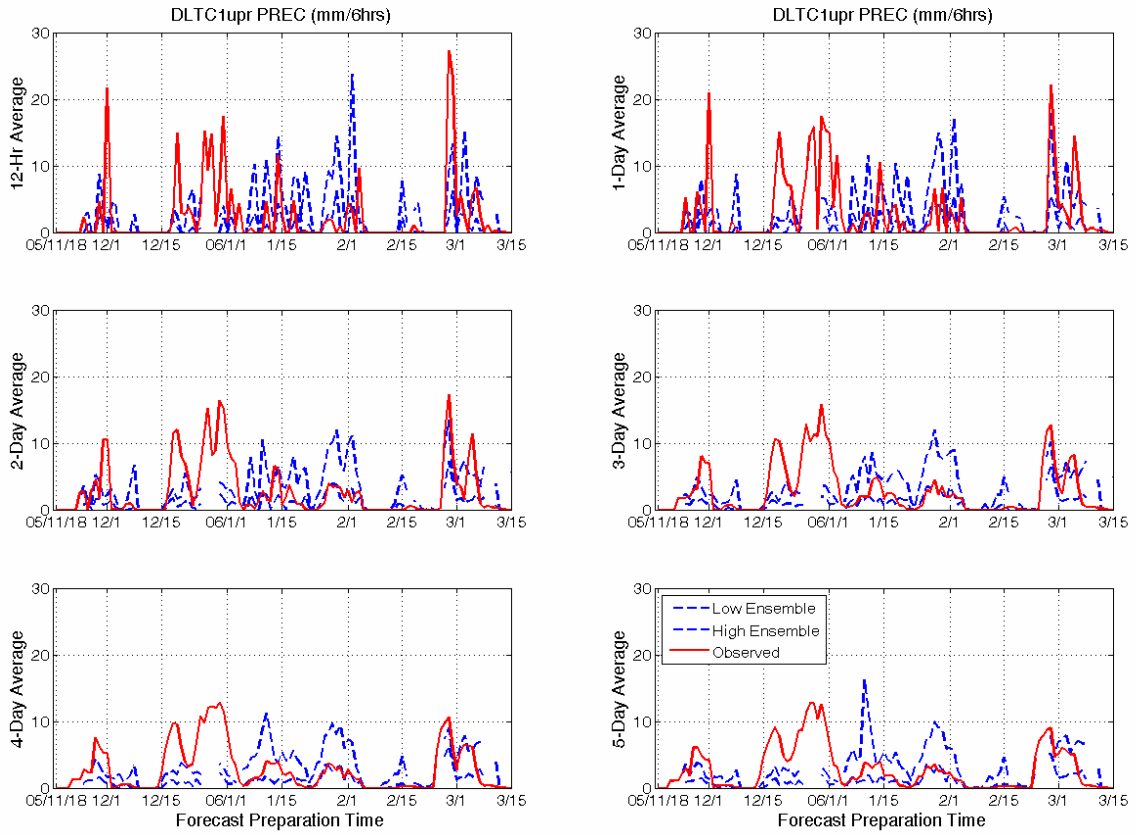


Figure 103. As in Figure 100, but for the upper area of the Sacramento River catchment with outlet at Delta, California

6.3.2. MAT Ensemble Forecasts

The spatially distributed INFORM system temperature forecasts are important during the California winter because they control the generation of snowmelt from the upper and lower areas of the reservoir drainage area catchments. Their influence is most pronounced in the northern regions of Northern California and in the higher elevations. Even in the lower latitude catchments of the American and Yuba Rivers within the INFORM area, they provide significant information that affects the location of the snow line and contributes to the definition of the regional separation of the precipitation phases. For these reasons, this section presents an evaluation of the ensemble surface air temperature forecasts of the INFORM downscaling models. As with precipitation forecasts, INFORM first generates gridded surface temperature ensemble forecasts with a 10 x 10-km² resolution. The reader is reminded that the temperature downscaling model uses estimates of snow cover and soil water from the hydrologic component of INFORM. It then uses the gridded temperature forecasts to produce MATs for the upper and lower areas of each tributary catchment within the reservoir drainage areas that comprise the application region. These MAT ensemble forecasts are evaluated by comparison to CNRFC estimated MATs from surface station temperature data. In this case too, estimation of MATs from point observations contains significant errors in mountainous terrain. The evaluation is done with the expectation that such errors are smaller than the corresponding forecast errors.

Selected representative results are shown in Figures 104 through 107. The figures share the same format as the MAP figures in the previous section. Inspection of these figures suggests that the INFORM downscaling component performed well in real time, providing ensemble forecasts of MAT that are close to the CNRFC MAT estimates obtained from station data for all lead times out to 5 days, even in periods with significant MAT excursions from the period average. It is also evident that for the Shasta drainage area catchments (northern part of the INFORM domain with results in Figures 104 and 105) there is a tendency of the ensemble forecasts to occasionally overestimate the temperature in the upper elevations and underestimate the temperature in the lower elevations. Overestimation and underestimation is up to 2°C–3°C in some cases. For the Oroville drainage (Figures 106 and 107) there is some underestimation present for the lower area of the North Fork Feather River with outlet at Pulga (see the lower six panels of Figure 106), but no other significant error trends are evident. Additional data from periods of real-time operation and evaluation are required to determine whether such underestimations or overestimations are the result of (1) model errors, (2) ensemble size, or (3) boundary and initial condition errors, or whether there is a systematic pattern of such errors across the catchments. The authors consider the performance of the temperature downscaling component during this first wet season of INFORM real-time operation to be satisfactory, but they also recommend that additional real-time tests be performed to allow a more thorough evaluation.

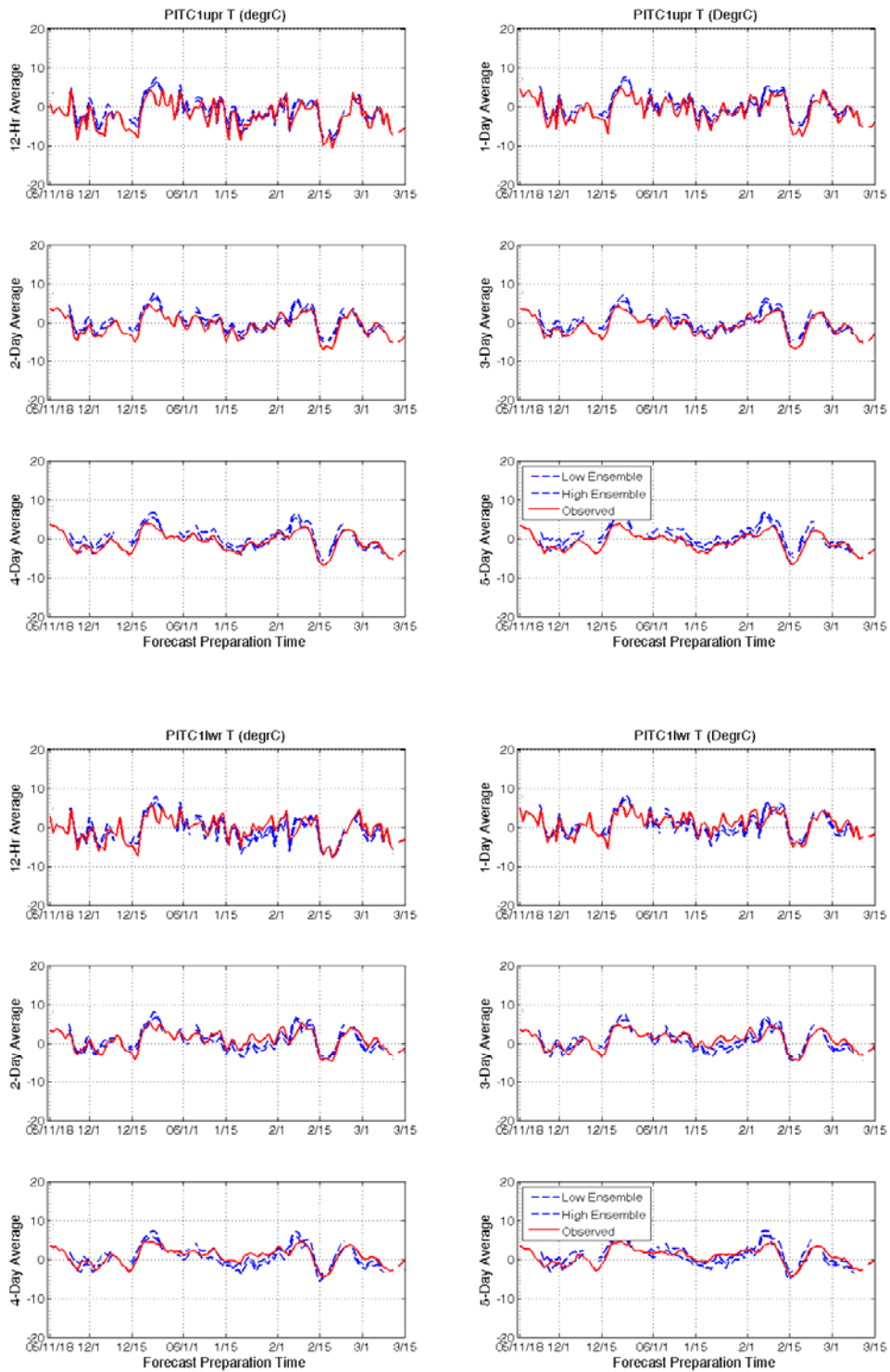


Figure 104. (Upper six panels) As in Figure 100, but for MAT over the upper area of the Pit River catchment within the Shasta reservoir drainage area. (Lower six panels) as in Figure 100, but for MAT over the lower area of the Pit River catchment.

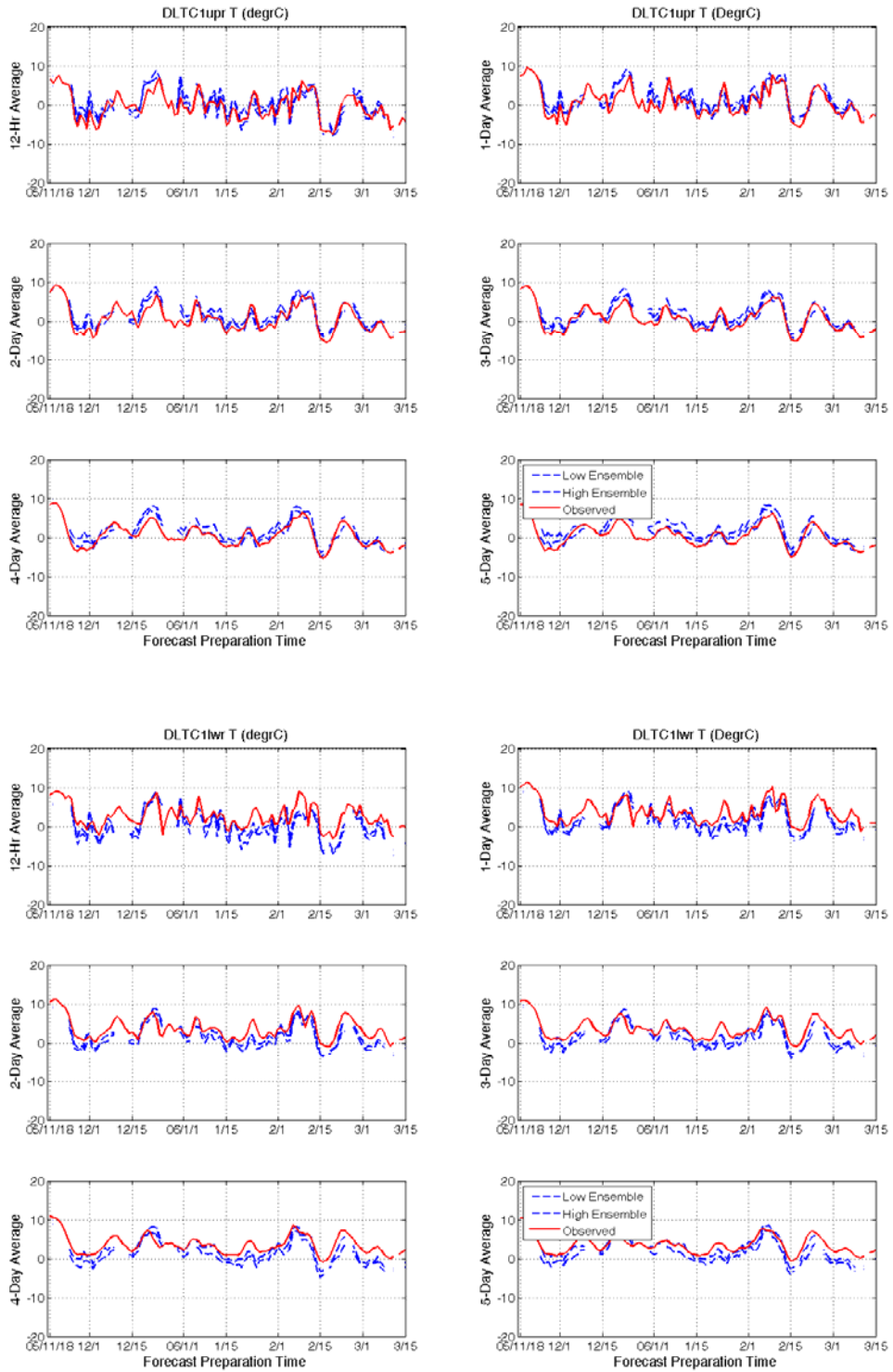


Figure 105. As in Figure 104, but for the upper and lower areas of the Sacramento River with outlet at Delta, California

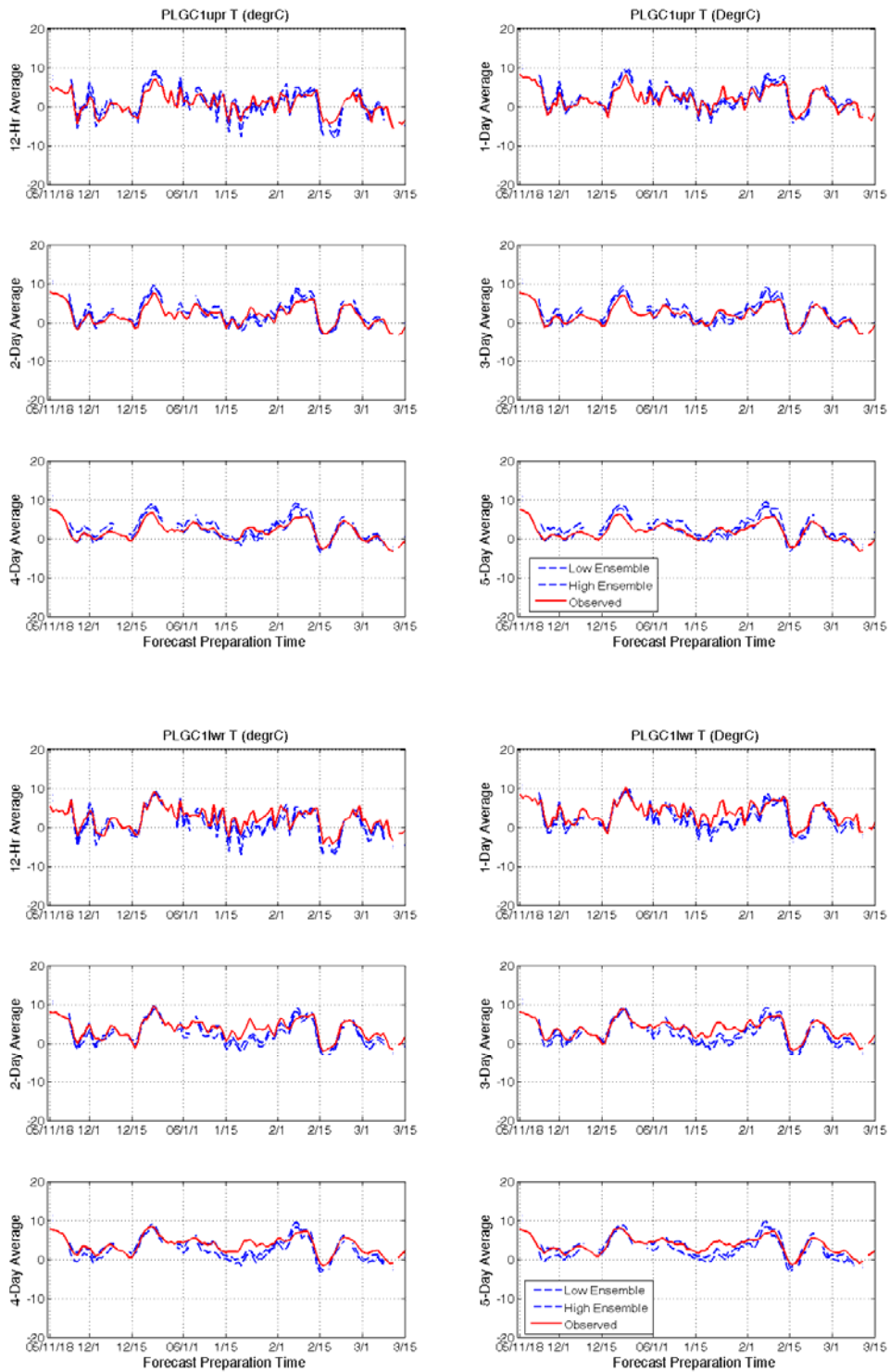


Figure 106. As in Figure 104, but for the North Fork Feather River with outlet at Pulga in the Oroville reservoir drainage

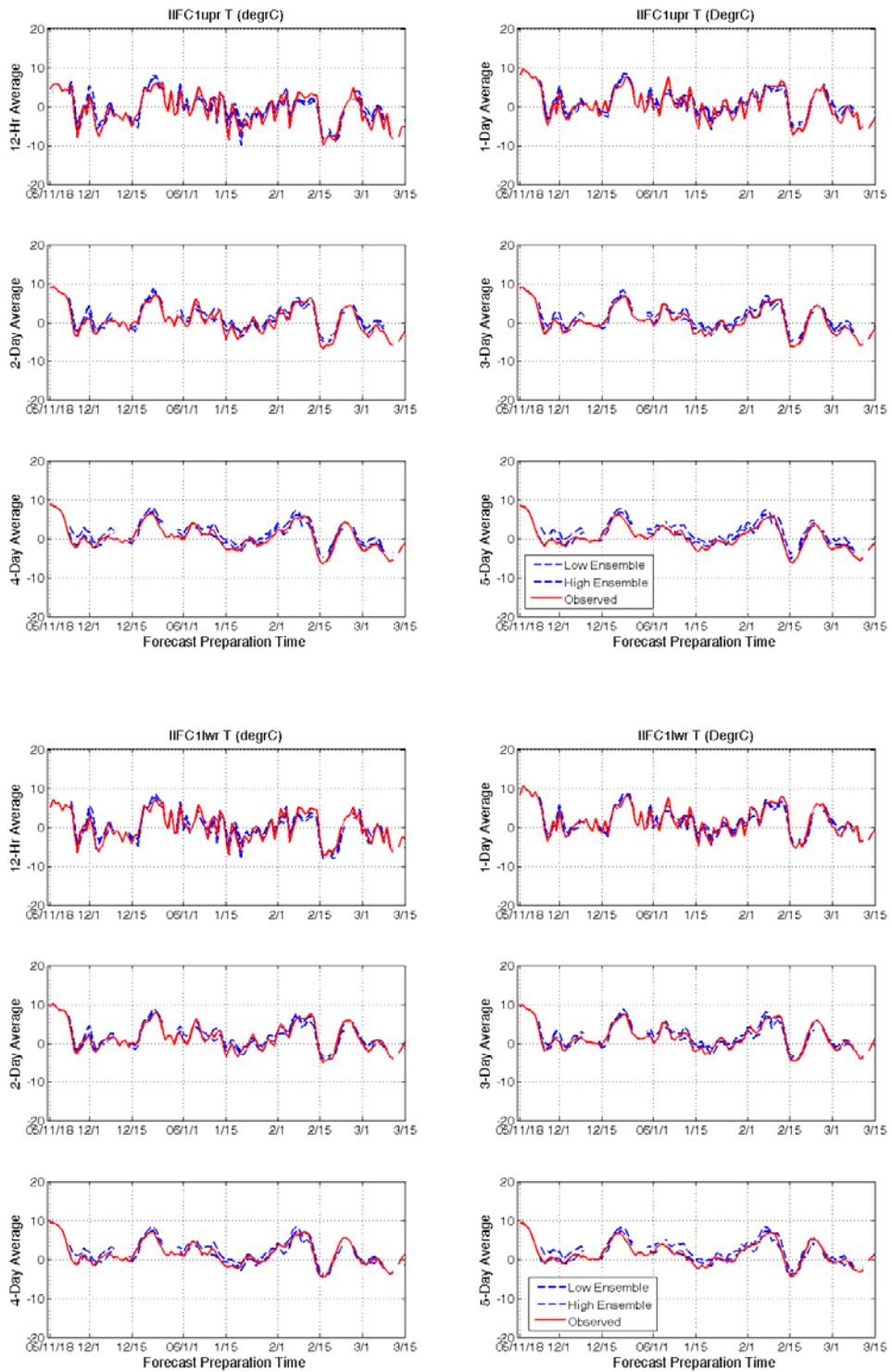


Figure 107. As in Figure 104, but for the Indian Creek in the Oroville reservoir drainage

6.4. Reservoir Inflow Forecasts

Figures 108 through 112 present the INFORM real-time ensemble forecast bounds (high and low), together with corresponding FNF estimates for various forecast lead times and for the large INFORM reservoirs: Folsom, New Bullards Bar, Oroville, Shasta and Trinity. The period of record is the part of the wet season of 2005–2006 for which real-time ensemble forecasts were issued by the INFORM system. In this case too the forecasts and corresponding FNFs are presented in the figures as flow averages over the 12-hour to 5-day forecast horizon.

The bounds of the flow forecast averages shown in Figure 108 encompass the CNRFC FNFs for most of the events of the test period and for most of the forecast lead times (Figure 108). Notable exceptions are the forecasts for the flow event of the March 1, 2006, for which the INFORM ensemble forecasts overestimated the FNFs significantly for lead times up to 3 days. Longer lead time (i.e., 4 and 5 days) ensemble forecasts contain the FNFs for most validation times but they do tend to have large ensemble member spread, especially for February and March 2006. The most significant flow event of the record (January 1, 2006) was reasonably well predicted by the forecasts, albeit with late timing with a 1-day lead time and with better timing with a 2-day lead time. Undoubtedly, missing CNRFC data (hydrologic model initial conditions) during the early real-time operations of INFORM in this wet season—and particularly right before the onset of this event—contributed to the late timing. Further real-time evaluations during periods that include additional significant flow events are necessary for more reliable assessments of performance and underlying causes of errors.

Figure 109 shows the INFORM real-time reservoir inflow forecasts for the New Bullards Bar reservoir on the Yuba (northern neighbor of Folsom drainage) and corresponding observations for a forecast lead time of 12 hours. Comments similar to those made for Folsom inflows may be stated for this reservoir inflow as well. Timing is better in this case, but lack of data during the first large event affected timing and magnitude of subsequent forecasts for the larger peak of January 1, 2006. Underestimation of the first peak on December 1, 2005, and overestimation of the event of March 1, 2006, by all the ensemble members are also evident. The rest of the record is well reproduced by the range of the ensembles.

The results pertaining to the Oroville reservoir inflows (Figure 110) show analogous behavior as that discussed for the American and Yuba River reservoirs to the south of Oroville. In this case there is better reproduction of the March 1, 2006, event by the forecasts for all lead times out to 5 days. Again, the authors attribute the late timing and underestimation of the January 1, 2006, event to the lack of reliable and continuous model initial conditions in real time. Here too, for longer lead times the ensemble spread is significant but contains the CNRFC FNF. A larger number of ensemble members would allow more refined estimates of the reliability of the ensemble forecasts. This is a recommendation that is realizable with the present system configuration by increasing computational power.

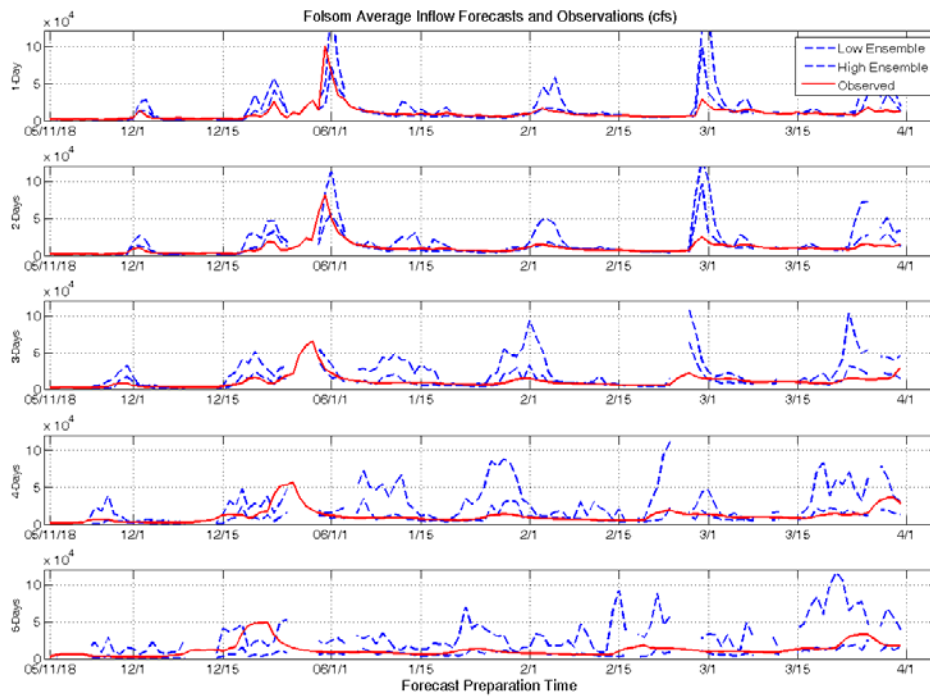


Figure 108. Folsom highest and lowest ensemble member average reservoir inflow forecasts (blue dashed lines) for forecast lead times from 1 day (upper panel) to 5 days (lower panel). Corresponding CNRFC FNF estimates are shown in each case (red line).

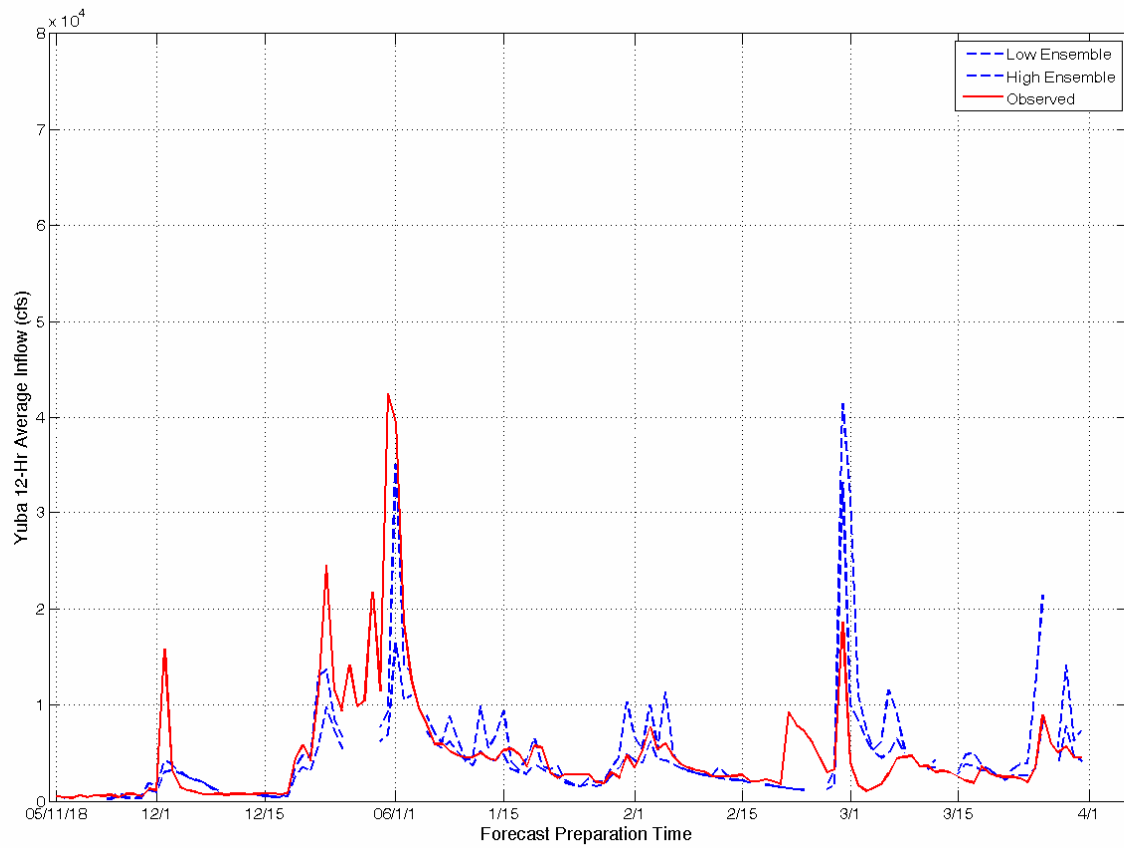


Figure 109. As in Figure 108, but for the New Bullards Bar reservoir inflow on the Yuba River and for a forecast lead time of 12 hours

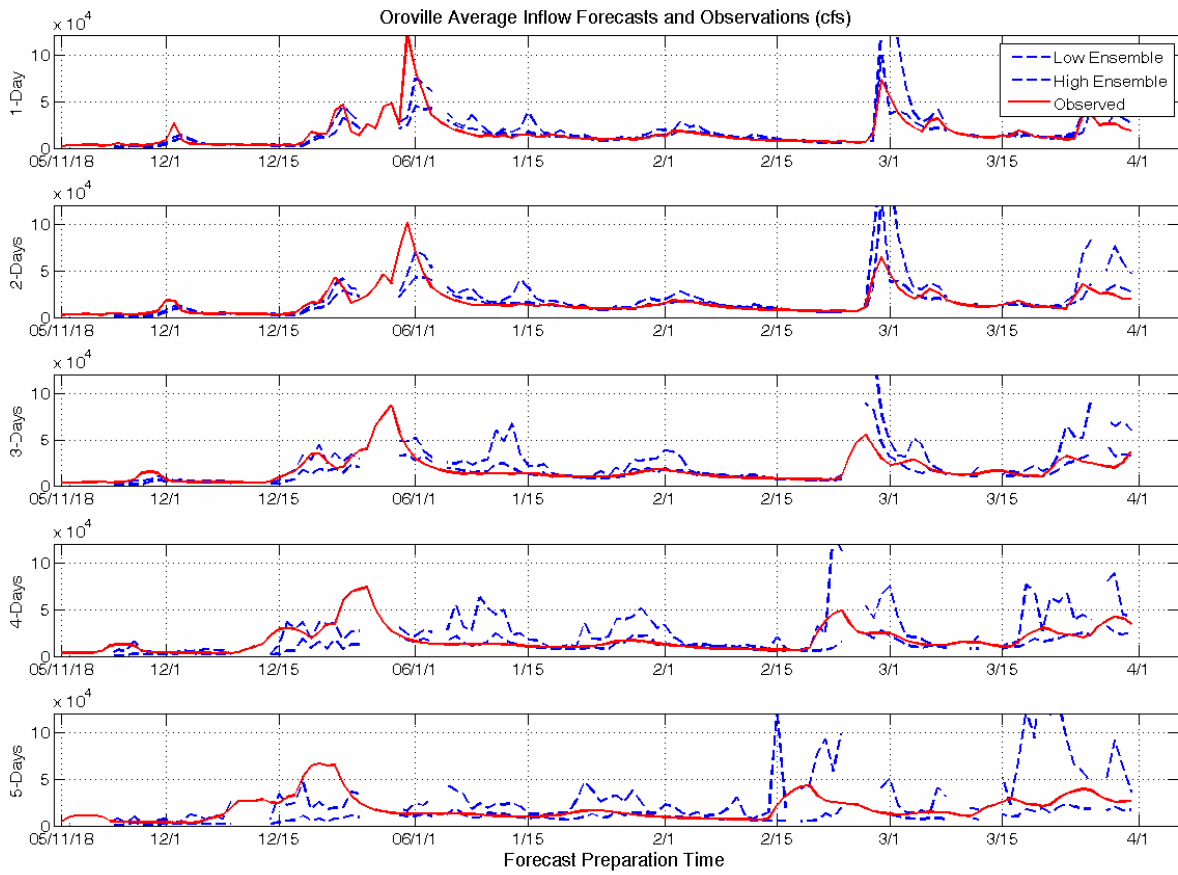


Figure 110. As in Figure 108, but for the Oroville reservoir inflow

The results for Shasta inflows (Figure 111) show good reproduction at all lead times of the FNFs in all but the January 1, 2006, event. Interruption of CNRFC links at the early phases of this latter event probably contributed to the underestimation of the forecast flows. Other peaks are reasonably well reproduced, with a notable small range of ensemble member forecasts for lead times out to three days in this drainage area. The results for the smaller drainage area of the Trinity reservoir inflows (Figure 112) in the northwestern-most part of the INFORM region show good timing of the ensemble forecasts with a tendency of overestimation of significant peaks for lead times up to two hours. The FNFs are within the forecast bounds for most cases for lead times from three to five days.

6.5. Overall Assessment of INFORM Real-Time Short-Range Forecasts

The previous three sections discussed a number of attributes of the performance of the INFORM forecast component under the conditions of the first performance evaluation. In this section the authors discuss their overall assessment of system real-time performance and suggest fruitful ways to move forward. The authors emphasize that these evaluations represent an initial effort toward performance assessment, and that real-time experiments in two to three additional wet seasons in Northern California are necessary for more definitive evaluations.

The first assessment that is evident from the previous discussions is that for the validation and lead times considered and for all the reservoir drainage basins of interest, the MAP and MAT ensemble forecasts contain the MAP and MAT estimates derived from point observations. Although not evident in all cases, the authors also assess that there is some overestimation of precipitation and temperature exists for high-elevation areas and some underestimation for low-elevation areas. These may be caused by forecast ensemble size and/or systematic biases in the INFORM downscaling models. The latter in turn are due to either systematic bias in the GFS ensemble forecasts (effecting biases in initial and boundary conditions), systematic biases in snow and soil water boundary conditions (for the downscaling temperature model), or downscaling model structure errors. Determination of the causes requires a longer INFORM demonstration period allowing better statistical characterization of model behavior and sensitivity analyses.

It is important to note that in order to successfully produce real-time ensemble forecasts, the structure of the precipitation downscaling model of INFORM has been considerably simplified to include only orographic precipitation production. Therefore, this model will not reproduce well precipitation from unrelated influences (such as large-scale lifting, convection in the valleys or coastal circulations). This lack of accurate reproduction will have an effect not only on low-elevation precipitation forecasts, but also on high-elevation precipitation forecasts due to the redistribution of the incoming available atmospheric moisture.

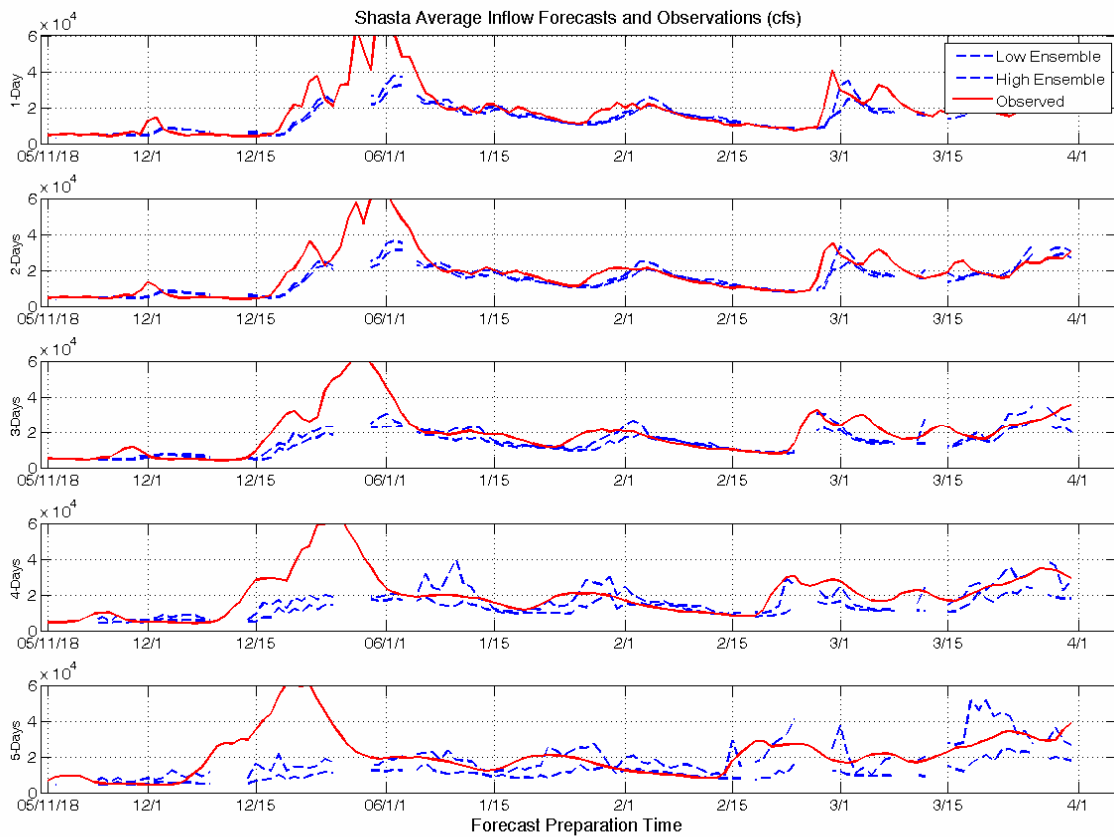


Figure 111. As in Figure 108, but for the Shasta reservoir inflow

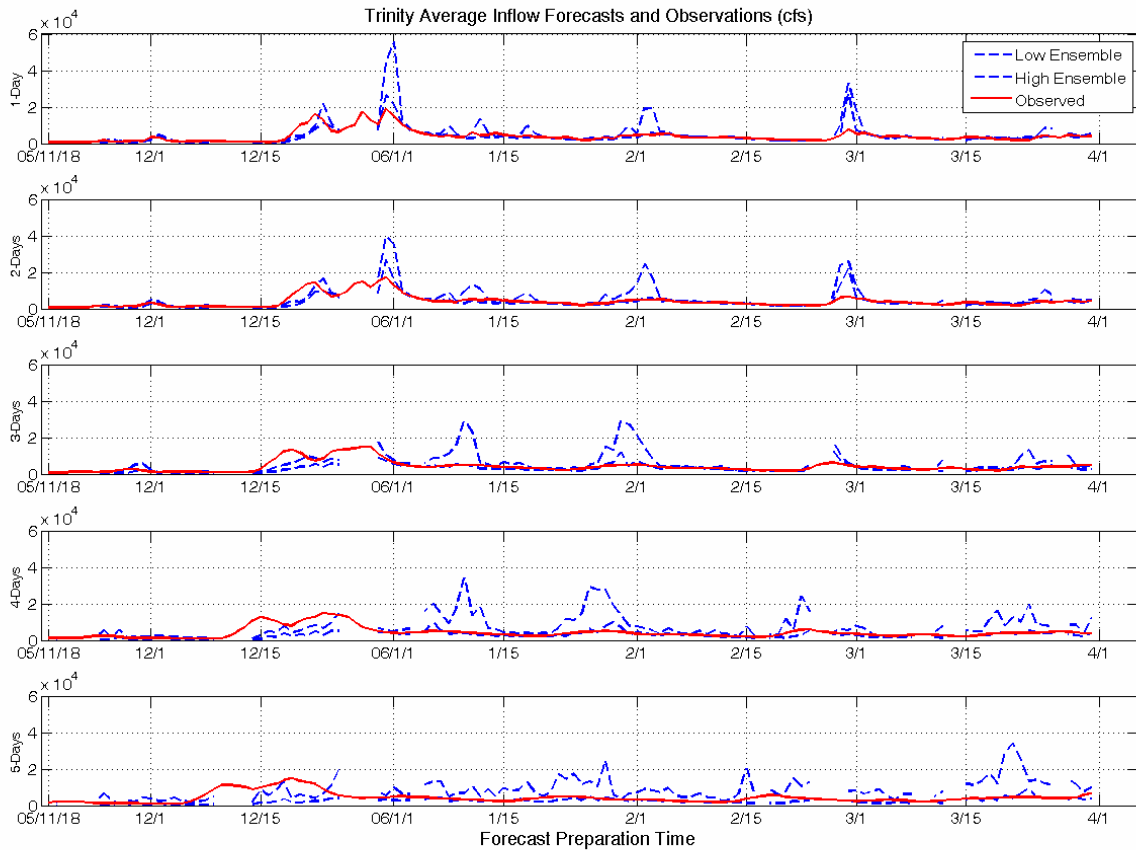


Figure 112. As in Figure 108, but for the Trinity reservoir inflow

A second important issue is associated with the accuracy of the CNRFC estimated MAPs and (especially) MATs from point observations within the INFORM region. For MAPs, Tsintikidis et al. (2002), in their analysis for the Folsom drainage area, show that the errors are functions of station numbers and locations, and they are very much dependent on the spatial scale of the area of the MAP estimates. In particular, they show that systematic errors are very small when the entire Folsom reservoir drainage is considered, but increase substantially when each individual tributary catchment is considered independently (i.e., the errors increase as the spatial scale diminishes). The authors do not know of analogous recent studies that have considered the errors of MAT estimates computed from point observations over catchments of the INFORM region. This is an area that requires further investigation to establish the error characteristics of the “ground truth” used to evaluate forecast performance.

The last issue the authors mention in association with the evaluation of MAPs and MATs pertains to bias adjustment strategies for these forecast quantities. Four options for adjustment are feasible:

1. A posteriori adjustments through the use of a set of statistically determined factors that adjust the ensemble forecasts.
2. A priori adjustments of the GFS boundary and initial conditions, and of the CNRFC snow and soil water conditions for the temperature downscaling model, all through statistical methods.
3. Downscaling model reformulation to include additional physics.
4. A combination of (1) through (3) above.

To determine the most profitable option, additional real-time INFORM forecast evaluations with data from future wet seasons are necessary. For options (1), (2), and (3) this is because the determination of statistically derived adjustments requires a substantial set of forecast-observation data to determine factor dependence on catchment elevation, latitude, month of the year, exposure to moisture influx, etc. For options (3) and (4), this is because the model enhancements would require a variety of forcing scenarios in real time to allow for an informed decision regarding the trade-off between the effectiveness of the enhancements and the additional CPU time requirements for real-time operation.

With respect to the INFORM real-time short-range ensemble forecasts of reservoir inflow, the results obtained lead to the assessment that there is evidence of forecast skill for a range of forecast lead times, from 12 hours to 5 days, and for all the large reservoirs of the INFORM region. Generally, underestimation of the early events of the 2005–2006 wet season is followed by overestimation of the late events in the season in some cases. As mentioned for MAPs and MATs, in the case of reservoir inflows too, reliable determination of the existence, character and causes of persistent errors requires additional real-time experiments with the INFORM forecast component and a longer demonstration period. Candidate actions to eliminate persistent errors in the ensemble forecasts are: increase of ensemble size, hydrologic model input bias adjustment, and fine-tuning of hydrologic model parameter values and, possibly, model structure. All require additional data for effective implementation once the causes have been determined.

An indication of the effect of input bias adjustment on INFORM short-range ensemble forecasts may be discerned from the results displayed in Figure 112. The upper panel of this figure is for the Shasta reservoir inflows (northernmost reservoir in INFORM region) while the lower panel of this figure is for the Folsom reservoir inflows (southernmost reservoir in the INFORM region). The format of the figure panels is the same as that of Figure 109. To obtain the results of this figure, the ensemble forecast MAPs throughout the domain and for all validation and forecast lead times were multiplied by a single factor. Improvement throughout the range of flows is evident by comparing the upper panel of Figure 113 with the second panel of Figure 111 and the

lower panel of Figure 113 with the second panel of Figure 108. In all cases of the forecasts obtained with bias-adjusted input the range of forecast ensembles contains the CNRFC estimated FNFs, even for the early large event of the season when the INFORM operation included several interruptions of the real-time links to NCEP and CNRFC. These encouraging results, obtained using an (admittedly) ad hoc correction scheme, are a first indication that simple adjustments may produce significant performance improvements at minimal computational cost. Again, additional demonstration periods are needed to obtain reliable proof of this assertion.

6.6. Integrated Forecast-Decision Assessments

The assessments described herein are performed using the mid-range assessment model of the INFORM DSS and are similar to those presented in Section 5.6.1. The assessment attributes and scope are as follows:

- The assessments aim to quantify the response of Trinity, Shasta, Oroville, and Folsom over the 1981 to 1995 historical hydrologic period.
- The management objectives are as in Section 5.6.1—namely, (1) avoid flooding, (2) pass as much of the release as possible through the plant turbines and avoid spillage (energy generation), (3) meet the applicable minimum flow requirements (water supply and environmental/ecological flows) associated with each reservoir, and (4) maintain high reservoir levels for water conservation and energy generation.
- The inflow forecasts have a forecast horizon of 90 days and are generated by the following forecast schemes:
 - Perfect Forecasts.
 - Historical Analog ensemble forecasts (streamflow based) used with a 50% and 90% management reliability level.
 - Extended Streamflow Prediction (ESP) ensemble forecasts (watershed hydrology based) used with a 50% and a 90% management reliability level.
 - Climate-Conditioned ESP ensemble forecasts (climate and hydrology based) used with a 50% and 90% management reliability level. (This forecast scheme is referred to as *CCF* in the assessment figures.)

The results of these assessments are summarized in Figures 114, 115, 116, 117, and Table 31. Figure 114 displays the Trinity elevation and release sequences associated with four assessment runs. The assessments not shown are associated with the HA, ESP, and CCF forecasts used with a 50% management reliability. Figures 115, 116, and 117 show the same sequences for Shasta, Oroville, and Folsom respectively. Table 31 includes statistics of spillage (15-year average), energy generation (15-year average),

release (15-year maximum), and flood damage (15-year maximum) for each project and all assessment runs (including those associated with a 50% management reliability).

The assessment results support several observations:

Value of Stochastic versus Deterministic Forecasts: Table 31 shows that using full forecast ensembles (as opposed to a single sequence) improves management performance for all forecast schemes and all projects. This can be seen by comparing the table results for average spillage, maximum release, and/or flood damage for any forecast scheme. As commented in Section 5.6.1, this occurs because deterministic (single-sequence) forecasts communicate information only on a particular ensemble statistic (usually the mean) and not other probable sequences, especially sequences associated with extreme events. In view of this, the management model cannot assess the risks of upcoming high flows and is frequently forced to spill, release at higher rates, and cause more costly flood damages. In the case of Folsom and the climate-conditioned ESP forecast model (CCF), stochastic management completely avoids flood damage, which in the case of deterministic forecasts amounts to 220 million dollars. Thus, the opportunity loss of ignoring forecast uncertainty in management models and processes can be rather costly. Unfortunately, nearly most analytical tools used for operational management in the world today are simple simulation type models lacking the ability to fully utilize probabilistic forecasts.

Value of Hydrologic and Hydro-climatic Forecasts: The value of the hydrologic ESP and climate-conditioned ESP models is assessed by comparing their performance with that of the historical analog and perfect forecast models. (This comparison focuses on the stochastic models.) To this end, Table 31 indicates a consistent performance ranking across all reported criteria and projects, with the perfect forecasts performing best, followed by the climate-conditioned ESP, the hydrologic ESP, and the historical analog forecasts. Relative performance differences are more pronounced for Folsom, where flood damage increases from 0 (perfect and climate-conditioned forecasts) to 220 million dollars (hydrologic ESP and historical analog forecasts), and Oroville, where maximum release increases from 88,773 cubic feet per second (cfs) (perfect forecasts) to 133,303 cfs (climate-conditioned ESP forecasts) to 169,254 cfs (hydrologic ESP and historical analog forecasts). The same relative performance is noted with respect to spillage and energy generation, albeit with less-pronounced differences. Thus, the assessments demonstrate that more comprehensive representations of the hydro-climatic processes underlying runoff can benefit mid-range reservoir management.

Forecast Attributes Important for Reservoir Management: The previous conclusion can be better understood by examining the assessment sequences depicted on Figures 114 through 117. Focusing on the Folsom elevation sequences, Figure 114, one notes that the climate-conditioned ESP forecasts cause the deepest reservoir drawdowns, followed by the historical analog, the hydrologic ESP, and the perfect forecasts. In light of the same reliability threshold used by all models, this result implies that, on the average, forecast ensemble bands are widest for the climate-conditioned ESP, becoming

progressively less wide for the historical analog, the hydrologic ESP, and the perfect forecasts. Thus, the climate-conditioned ESP performs better than the hydrologic ESP and the historical analog because it cautions the management model to expect a considerably larger range of probable inflows. In response, the management model draws the reservoirs down to create additional flood control storage pools and provide better flood protection. The only opportunity loss for mid-range management is slightly less energy generation. This favorable conclusion, however, is misleading because it does not consider the long-range risks of deep reservoir draw downs. If such risks were also assessed, the performance of the climate-conditioned ESP procedure would not have attained a high rank. This aspect has been discussed in Section 5.6.2, and it is an important reason to improve the skill of the climate-conditioned ESP forecast scheme, as recommended earlier in this chapter.

Thus, although forecast ensemble reliability is most important for reservoir management, the range of the forecast ensemble is also critical. Among the forecasts that exhibit the same reliability (of containing the true inflows), those with the narrowest ensemble range are most effective.

Using these criteria, one can conclude that hydrologic ESP forecasts are better than historical analog forecasts. This can first be seen by Figure 114 where hydrologic ESP forecasts lead to somewhat higher reservoir levels than those of the historical analog, indicating narrower forecast bands. Furthermore, judging by the statistics recorded in Table 31, the performance of the hydrologic ESP is better than the historical analog, indicating higher reliability. The hydrologic ESP is thus a better forecasting scheme for reservoir management because it exhibits narrower forecast ensembles and higher reliability than the historical analog.

As noted in Section 5.6.1, a third important forecast attribute is the forecast lead time. Generally, the value of forecasts exhibiting a certain reliability and precision (as measured by the ensemble range) is expected to increase with the length of the forecast horizon. However, there is a critical lead time where forecast uncertainty saturates the system storage capacity. Increasing the forecast lead time beyond this critical length (effective lead time) yields no additional improvements. The effective lead time of a particular forecasting scheme can be determined by assessing the system performance for different lead times. In summary, the value of forecasts in reservoir management increases with increasing reliability, precision, and effective lead time.

Lastly, an important aspect of adaptive management methods such as the ones implemented in the INFORM DSS is that they can increase the effective lead time of the forecasts by managing uncertainty systemwide. This attribute provides adaptive methods with a clear advantage over heuristic and static regulation schemes.

Table 31. Integrated, mid-range assessments statistics

Reservoirs	Assessment Criteria	ESP		CCF		Historical Analog		Perfect For.
		Stochastic	Deterministic	Stochastic	Deterministic	Stochastic	Deterministic	
Folsom	Inflow (cfs)	3382	3382	3382	3382	3382	3382	3382
	Spillage (cfs)	334	422	297	401	406	456	270
	Energy (GWh)	1.77	1.76	1.72	1.77	1.74	1.75	1.84
	Max. Release (cfs)	116791	121841	99905	116791	116791	121841	59968
	Max. Damage (\$)	220,400,000	842,000,000	0	220,400,000	220,400,000	842,000,000	0
Oroville	Inflow (cfs)	5634	5634	5634	5634	5634	5634	5634
	Spillage (cfs)	541	554	468	549	562	585	310
	Energy (GWh)	5.46	5.46	5.43	5.46	5.45	5.45	5.62
	Max. Release (cfs)	169254	169394	133303	146799	183476	183476	88773
	Max. Damage (\$)	0	0	0	0	0	0	0
Shasta	Inflow (cfs)	7800	7800	7800	7800	7800	7800	7800
	Spillage (cfs)	464	694	431	685	554	759	329
	Energy (GWh)	6.68	6.67	6.61	6.66	6.66	6.63	6.92
	Max. Release (cfs)	109937	125837	109937	125837	109937	125837	100590
	Max. Damage (\$)	0	0	0	0	0	0	0
Trinity	Inflow (cfs)	1779	1779	1779	1779	1779	1779	1779
	Spillage (cfs)	134	158	119	154	108	161	114
	Energy (GWh)	1.08	1.09	1.05	1.09	1.07	1.09	1.12
	Max. Release (cfs)	31081	31081	31081	31081	18260	31081	31081
	Max. Damage (\$)	0	0	0	0	0	0	0

cfs=cubic feet per second; GWh=gigawatt hours

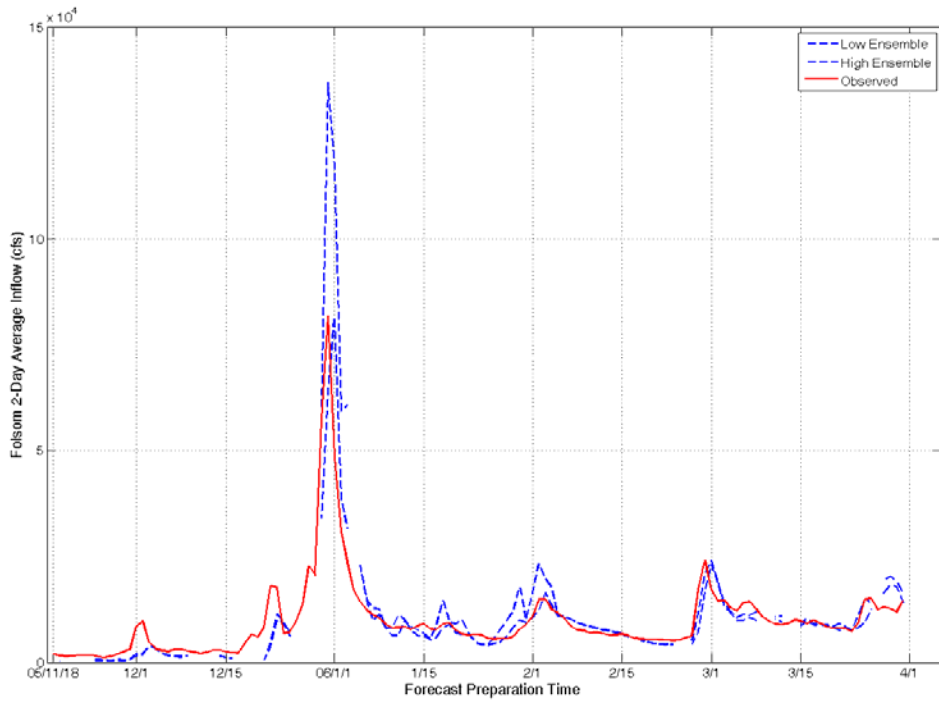
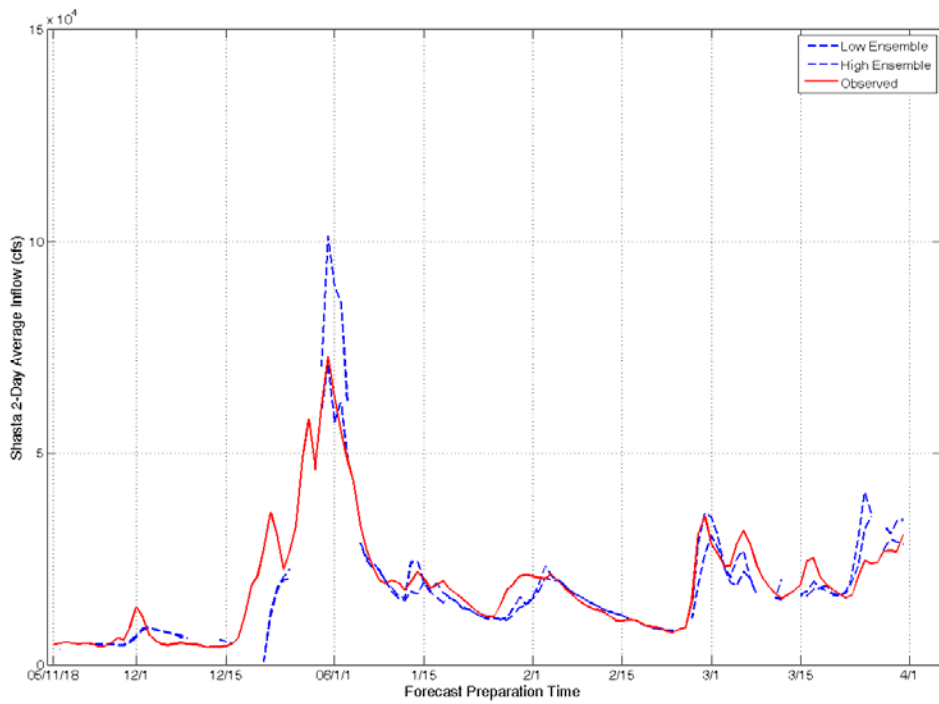


Figure 113. As in Figure 109, but for Shasta reservoir inflows (upper panel) and for Folsom reservoir inflows (lower panel) and for a 2-day forecast lead time. Input of bias adjusted MAPs through a single factor.

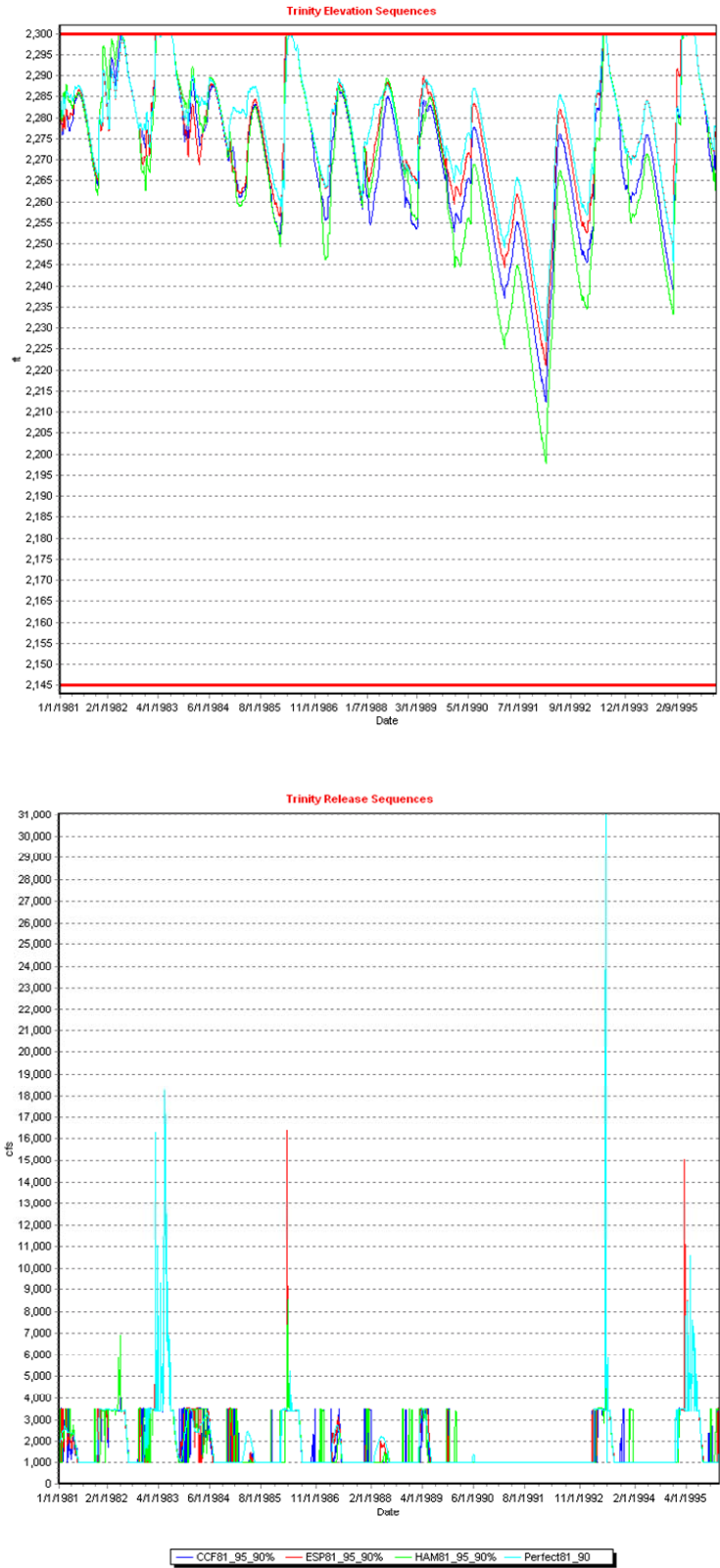


Figure 114. Integrated, mid-range assessments: Trinity elevation and release sequences

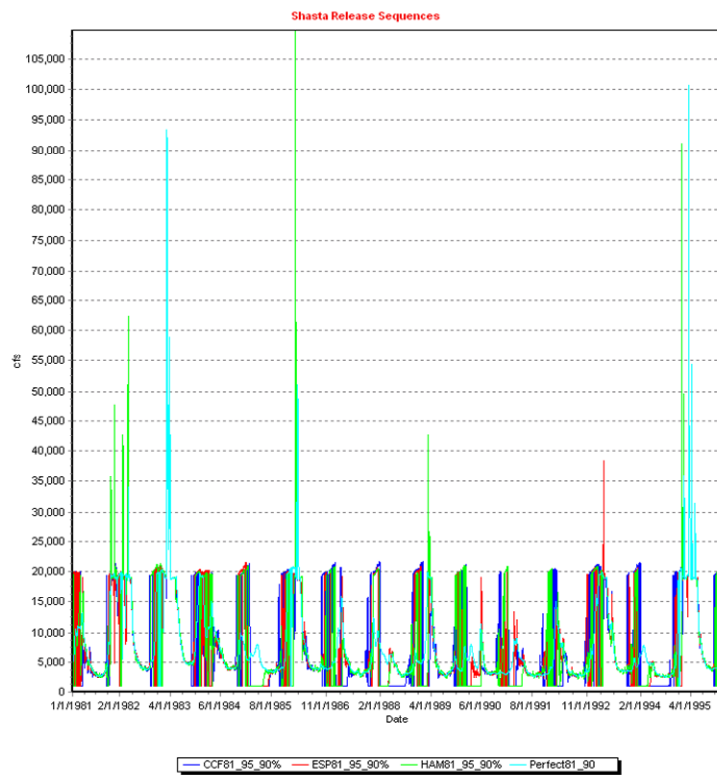
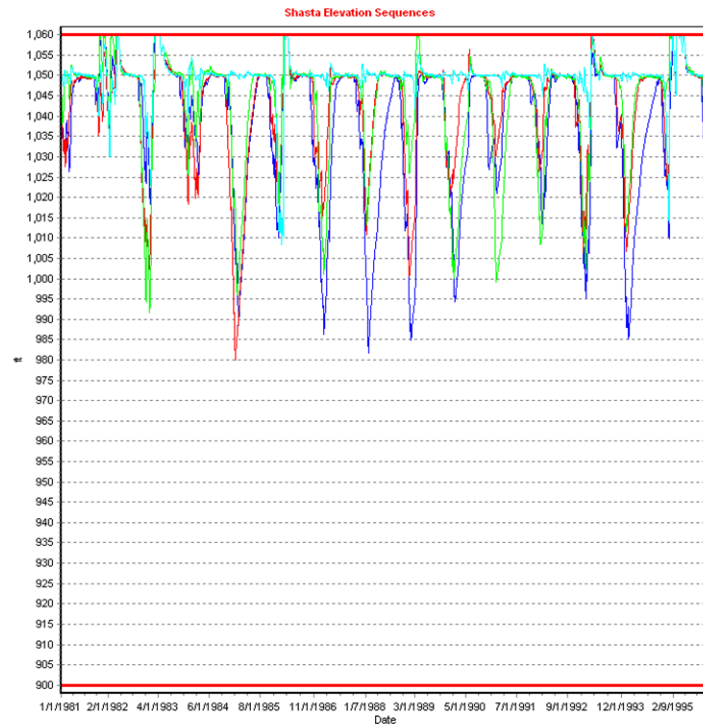


Figure 115. Integrated, mid-range assessments: Shasta elevation and release sequences

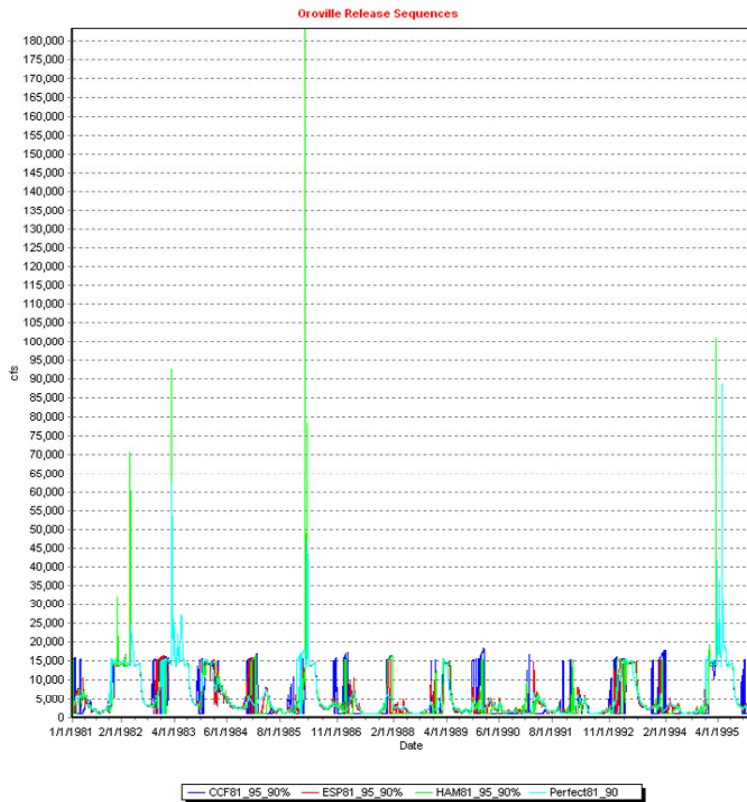
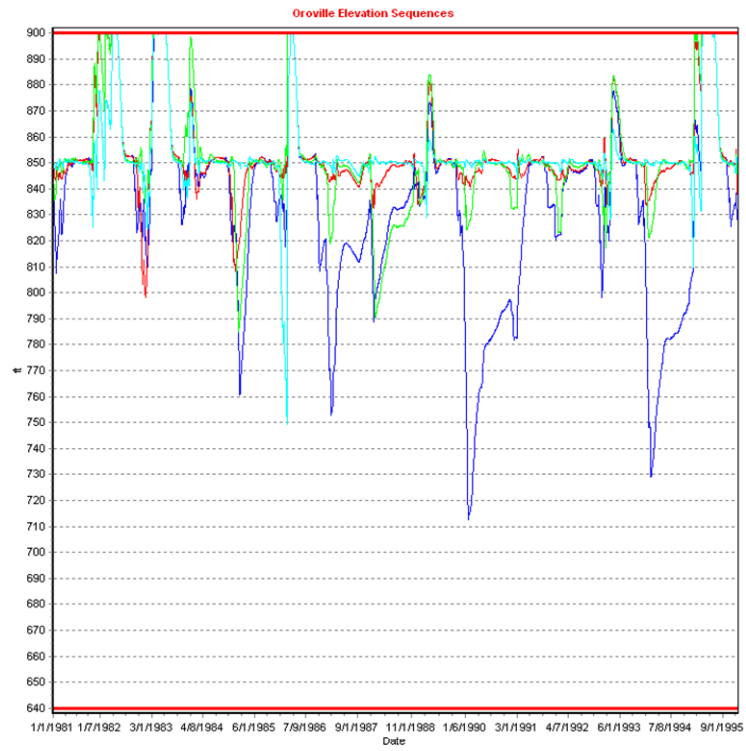


Figure 116. Integrated, mid-range assessments: Oroville elevation and release sequences

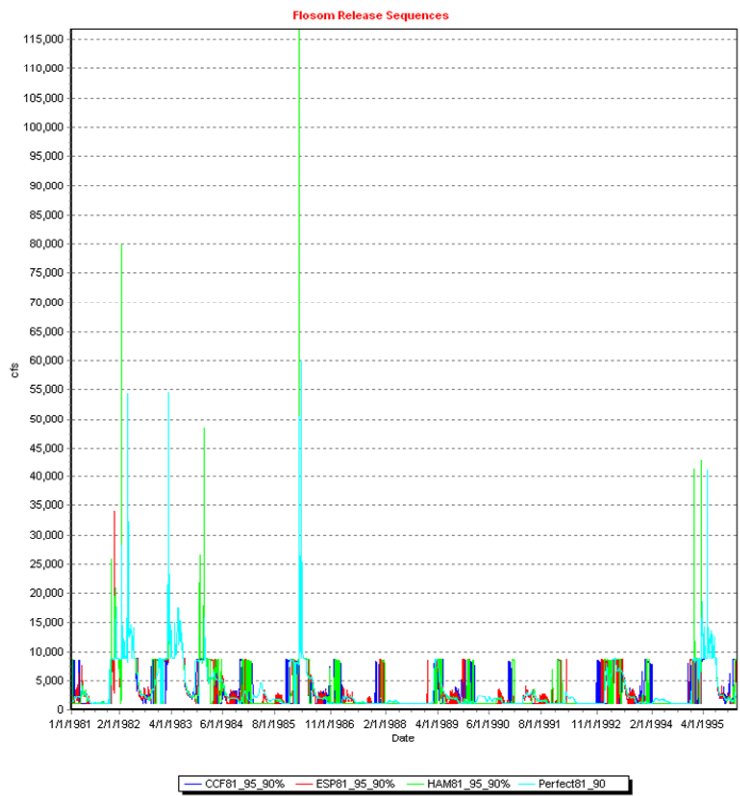
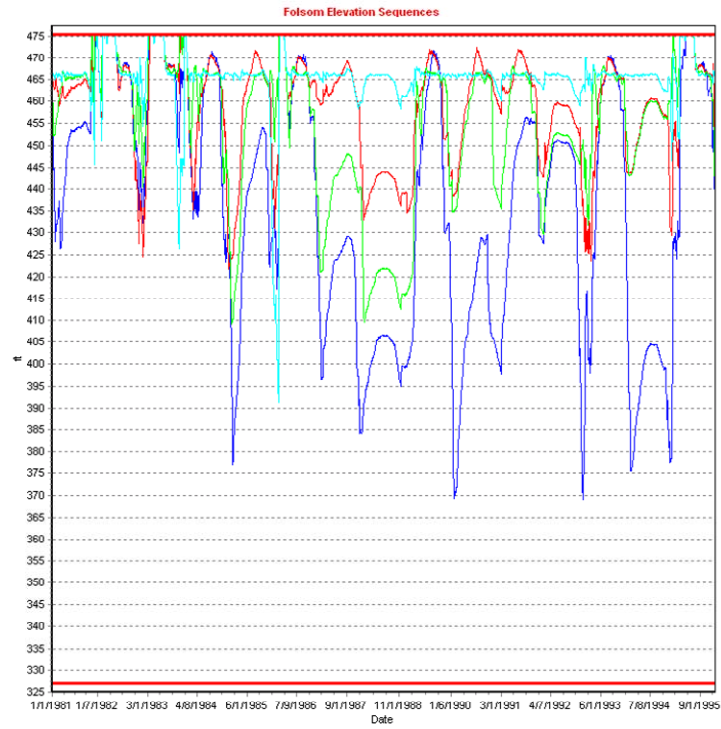


Figure 117. Integrated, mid-range assessments: Folsom elevation and release sequences

7.0 Conclusions and Recommendations

The vision of the Integrated Forecast and Reservoir Management (INFORM) project is to increase efficiency of water use in Northern California using meteorological/climate, hydrologic and decision science. The three primary project objectives of INFORM are to:

1. Implement an integrated forecast-management system for the Northern California reservoirs using real-time data.
2. Perform tests with actual data and with management input.
3. Demonstrate the utility of climate and hydrologic forecasts for water resources management in Northern California.

The first three-year phase of INFORM met the first two objectives by designing and implementing the INFORM forecast-decision system in close collaboration of forecast and management agencies in Northern California, and by testing all of its components with historical data. Chapter 2 of this report documents the design and implementation of the real-time and off-line components of the system. The critical input of forecast and management agencies of Northern California water supply contributed substantially to the final system configuration. Chapters 3, 4 and 5 document the model component formulations and extensive tests with historical data of the precipitation and temperature downscaling model, the hydrologic snow-soil-channel models, and the decision model, respectively.

The first phase of INFORM also provided an initial demonstration of the utility of the INFORM hydrometeorological forecasts for (1) the mid-range management of the large reservoirs in Northern California (Folsom, Oroville, Shasta, and Trinity) with real-time data from the 2005–2006 wet season, and (2) the long-range management of the entire Northern California river and reservoir system, including the Bay Delta. Chapter 6 of this report contains these initial assessments and suggests that operation of the INFORM forecast and decision system for two to three additional wet seasons is necessary to complete the demonstration. The present chapter discusses the overarching and detailed conclusions of the project, and puts forth recommendations for future development. Conclusions and recommendations are separated into those that concern the INFORM forecast component and those that concern the decision component of the system for easier reference by forecast and management agencies.

7.1. Overarching Conclusions

A first conclusion is that, with the present day real-time availability of forecast information from the National Centers for Environmental Prediction (NCEP) and with real-time observed precipitation and temperature as well as hydrologic model state values from the California Nevada River Forecast Center (CNRFC), integrated forecast-management systems are realizable as operational decision support tools for management and planning of California water resources. Such systems assist water managers to translate forecasts and their uncertainty into risk-based policies. They advance current operational practices by (1) incorporating forecast uncertainty in

decisions on a range of time scales, and (2) allowing for regional coordination of management decisions.

With respect to the INFORM forecast component, simulations and ensemble forecasts averaged over lead times from 6 hours to 5 days, when compared against historical and real-time observations, have skill for mean areal precipitation (MAP), mean areal surface air temperature (MAT), and reservoir inflows for a range of elevations and latitudes and for spatial scales ranging from a few hundred square kilometers to several thousand square kilometers.

The most significant contribution of the decision support system is to provide an integrated planning and management framework and tools that address three critical challenges:

1. Quantitative and explicit forecast utilization by the decision tools and processes.
2. Integration of planning, management, and operational decision-making tools and functions within each management agency.
3. Establishment of a common set of analytical tools that facilitate agency communication, cooperation, and coordination.

7.2. Specific Conclusions

7.2.1. Forecast Component

Several additional conclusions pertaining to the forecast component are supported by the INFORM work reported in this document. These are listed below:

1. MAP from the INFORM 10-km-resolution orographic precipitation model using boundary conditions from large scale ($2.5^{\circ} \times 2.5^{\circ}$) NCEP reanalysis explains 20%–40% of the historical (CNRFC estimated) six-hourly MAP variance for most Sierra Nevada catchments. The model generally tends to overestimate low MAP values. It produces higher scores for catchments with higher exposure to 700-mbar wind flow from the upstream boundary point. The exposure of the INFORM domain Sierra Nevada catchments is such that for the Oakland boundary point, southwesterly flow produces higher scores than northwesterly flow. The explained portion of observed precipitation variance increases substantially for forecast averaging times greater than 6 hours.
2. Gridded estimates of six-hourly surface air temperature from the INFORM surface temperature downscaling model using boundary conditions from large-scale ($2.5^{\circ} \times 2.5^{\circ}$) NCEP reanalysis compare well with corresponding historical station measurements in the INFORM domain during the wet season. A tendency for underestimation was noted for some northern catchments in the INFORM domain of Northern California.
3. The ESP methodology, when used with the hydrologic models of the INFORM system and with historical MAP and MAT data, generates ensemble flows that

are generally reliable and with good resolution in terms of predicting the 30- to 90-day wet-season flow volumes being in the upper or lower third (tercile) of their distribution. Notable exception is the case of Shasta inflow volumes being in the upper tercile of their distribution, for which the ensemble forecasts overestimate the observed frequencies. For all the application reservoirs, results for upper terciles are more reliable than those for lower terciles, and 30-day inflow volumes are associated with more reliable results than 60- and 90-day inflow volumes.

4. Improvement in reliability is limited when statistically downscaled climate forecast system (CFS) ensemble forecasts of monthly resolution are used to condition the ESP. This is also evident from the intercomparison of the decision model results corresponding to unconditional ESP and CFS-conditioned ESP (see Section 7.2.2).
5. Sensitivity analysis of the snow model of the INFORM hydrologic forecast component (also used by CNRFC for operational forecasting in the Sierras) resulted in the identification of the snow depletion curve as the most important parameterized curve for calibration. This curve influences significantly the evolution of snow accumulation and ablation during the wet season. This analysis also showed that systematic or random errors in surface air temperature input to the snow model result in significant perturbations of the snow water equivalent evolution.
6. Evaluation of the operational CNRFC hydrologic model simulations using historical data of unimpaired flows showed that the model simulations capture the overall hydrologic response well. Poor performance during periods of medium to low flows at some catchments within the INFORM domain is often associated with regulation in upstream reservoirs which alter the downstream natural flow. Model performance is poorest overall during summer months (August through September). Also, during the wet season, performance is generally better in early winter than in late winter and spring. Model snow water equivalent evolution is in agreement with that of daily observations from point sensors, with better agreement at lower elevations.
7. The INFORM hydrologic model simulations with historical data exhibit performance that is very similar to the analogous simulations of the CNRFC operational model. The INFORM model simulations capture the observed hydrologic response for all the watersheds well, with respect to timing and magnitude and without significant bias.
8. The initial evaluation of the real-time performance of the forecast component of the INFORM system with data from the wet season 2005–2006 (“dry run”) and with some interruptions of the real-time links to CNRFC and NCEP, showed that, over several catchments, for several periods, and for lead times out to 5

days, the MAP and MAT 8-member ensemble forecasts contained the observations. For northern catchments within the INFORM domain, there is a tendency for overestimation of MAP and MAT in higher elevations and a tendency for underestimation in lower elevations.

9. Real-time reservoir inflow ensemble (8-member) forecasts by the INFORM system showed skill for several important flow events, catchments and lead times out to 5 days, when compared to unimpaired flow estimates by CNRFC (treated as observations for these evaluations). In some cases interruption of real-time links to CNRFC and NCEP led to poor initial conditions for some forecast preparation times with biased resultant ensemble flows. The good performance of simulations with observed MAP and MAT corroborates this conclusion. Folsom and Oroville reservoir inflows are somewhat delayed with respect to CNRFC unimpaired flow estimates. Significant spread of the ensemble forecasts was observed in several cases. These results were obtained without any bias adjustments of the downscaling model output. A simple adjustment of the INFORM MAP ensemble forecasts yielded substantially improved ensemble reservoir inflow forecasts.

7.2.2. Decision Component

Specific conclusions related to the decision support system and its applications are noted below:

1. The INFORM DSS includes four planning and management decision layers aimed to address long-range system planning (monthly resolution/one to two years horizon), mid-range management (daily resolution/several months horizon), short-range management (hourly resolution/one day horizon), and near-real-time operations scheduling (hourly hydro power unit commitment and load dispatching). The INFORM DSS models are interlinked to ensure consistency across modeling layers, both with respect to physical system representations, as well as with respect to the flow of decisions.
2. The INFORM DSS is designed to support participatory decision-making processes in which stakeholder agencies evaluate the benefits and risks of possible management decisions and develop consensus on the way forward. To this end, the INFORM DSS first quantifies the associated benefits and risks by deriving applicable planning and management tradeoffs. Once the stakeholder agencies reach agreement on acceptable risks and equitable benefits, the INFORM DSS can be used to develop the planning and management policies that realize the agreements made.
3. *Value of Stochastic versus Deterministic Forecasts:* Extensive assessments described in Chapter 5 and 6 demonstrate that using full forecast ensembles (as opposed to a single sequence) improves management performance for all forecast schemes and all projects. In the case of Folsom and the climate-conditioned ESP forecast

model, stochastic management completely avoids flood damage, which in the case of deterministic forecasts amounts to 220 million dollars. Thus, the opportunity loss of ignoring forecast uncertainty in management models and processes can be rather costly.

4. The value of the hydrologic ESP and climate-conditioned ESP models is assessed by comparing their performance with that of the historical analog and perfect forecast models in retrospective simulations. These assessments (Chapter 6) indicate a consistent performance ranking across all reported criteria and projects, with the perfect forecasts performing best, followed by the climate-conditioned ESP, the hydrologic ESP, and the historical analog forecasts. Relative performance differences are more pronounced for Folsom, where flood damage increases from 0 (for perfect and climate-conditioned forecasts) to 220 million dollars (for hydrologic ESP and historical analog forecasts), and Oroville, where maximum release increases from 88,773 cfs (for perfect forecasts) to 133,303 cfs (for climate-conditioned ESP forecasts) to 169,254 cfs (hydrologic ESP and historical analog forecasts). The same relative performance is noted with respect to spillage and energy generation, albeit with less pronounced differences. Thus, the assessments demonstrate that hydro-climatic forecasting schemes can benefit reservoir management.
5. The retrospective assessments also show that climate-conditioned ESP forecasts cause the deepest reservoir drawdowns, followed by the historical analog, the hydrologic ESP, and the perfect forecasts. In light of the same reliability thresholds used by all management models, this result implies that, on the average, forecast ensembles exhibit the widest spread for the climate-conditioned ESP, becoming progressively less wide for the historical analog, the hydrologic ESP, and the perfect forecasts. Thus, the previous favorable conclusion regarding the climate-conditioned ESP forecasts should be reviewed further in light of the long-range drought risks that reservoir draw downs may pose. This aspect suggests that the value of climate-conditioned ESP forecasts for reservoir management can be improved.
6. Although forecast ensemble reliability is most important for reservoir management, the range (or spread) of the forecast ensemble is also critical. Among the forecasts that exhibit the same reliability (of containing the true inflows), those with the narrowest ensemble range are most effective. According to this criterion, the hydrologic ESP is shown to be a better forecasting scheme than the historical analog. A third important forecast attribute is the forecast lead time. In general, the value of forecasts in reservoir management increases with increasing reliability, precision (as measured by the ensemble spread), and effective lead time.
7. An important aspect of adaptive management methods such as the ones implemented in the INFORM DSS is that they can increase the effective lead time

of the forecasts by managing uncertainty systemwide. This attribute provides adaptive methods with a clear advantage over heuristic and static regulation schemes.

8. CALSIM and the INFORM DSS simulation model were compared with respect to river node flows, the X2 location (interface of saline and fresh water), and major reservoir storages. The comparison results confirm that the INFORM simulation model is consistent with CALSIM and can be used to represent the response of the Northern California system at the same accuracy level.
9. Long-range planning retrospective assessments demonstrate the ability of the INFORM DSS to determine the capacity of the system to meet increasing water stresses. It is shown that 50% of the base water demand scenario (defined by Tables G-5 and G-6) can be fully met throughout the assessment horizon, without causing violation of any other system requirement (e.g., minimum flows, Delta environmental conditions). By contrast, increasing water demand targets to 60% of the base water demands brings about water supply deficits (in the Delta demand and south exports) and fails to keep the Delta X2 location less than 80 km from the Golden Gate Bridge during the 1991–1992 dry years. This level of water stress also leads to greater reservoir fluctuations, including five to six years of full conservation storage depletion. On average, reservoir levels are 10 to 20 feet lower than those of the 50% base demand scenario. Scenarios of higher water demands would lead to more frequent and more severe water shortages and failures to meet other system requirements. Thus, the water stress that uses up the system capacity to meet its objectives is estimated to be between 50% and 60% of the base demands. The assessments also demonstrate that better forecast information improves system performance and mitigates the impacts of increasing water stress.
10. Comparing the results of long-range planning and mid-range management assessments reveals an incompatibility between the respective decision models and processes. The main difference between the assessments is that the mid-range assessment manages the reservoirs *individually* and does not include potential interactions that might arise as part of the need to meet Delta demands and environmental conditions. To a certain extent, this approach reflects current practices which during flood periods focus on individual reservoir management (daily or sub-daily operations), while for purposes of long-range planning consider the entire system (monthly operations). The assessments show that this incompatibility between planning and management may compromise system performance and lead to potential failures. This incompatibility between mid-range management and long-range planning can be addressed by expanding the mid-range management scope to include a systemwide, rather than an individual reservoir, perspective.

7.3. Overarching Recommendations

Perhaps the most important recommendation arising from this work is to continue the INFORM demonstration experiments for two or (more usefully) three additional operational seasons beyond the system “dry run” wet season of 2005–2006 in continued close collaboration with the forecast and management partner agencies in Northern California. These additional operational seasons are necessary for the reliable evaluation of the INFORM system performance and utility in specific situations, for the application of any system corrections and adjustments that appear necessary from system evaluation, for the establishment of a protocol for its operational use by the collaborating agencies; and for exploring alternative applications for the system that have been suggested by sponsor agencies.

A second overarching recommendation pertains to the use of the INFORM system in a stand-alone mode for climate change simulations. The INFORM system closely emulates several of the actual forecast and management procedures used in routine operations in Northern California. As such, it constitutes a realistic simulation system for impact analysis in this region using the output of state-of-the-science global climate models that predict climatic variability and change. Such impacts include potential future climatic influences on precipitation, temperature, and snowmelt and runoff patterns in the Sierra Nevada resolved on the scale of INFORM catchments (from hundreds to thousands of square kilometers), the effects of increased demand scenarios, and the effectiveness of alternative management scenarios for improved water-use efficiency.

7.4. Specific Recommendations

7.4.1. Forecast Component

As discussed in Chapter 6, one of the limitations of the present INFORM system implementation as regards the short-range forecast component is the ensemble size. At present, the INFORM system ingests eight NCEP global forecast system ensemble members to produce eight ensemble-member forecasts of MAP and MAT fields, and reservoir inflow. There are currently fifteen GFS ensemble members produced by NCEP; the reason INFORM uses only eight of these is the limited capability of the INFORM computational server, which is based on eight computational processing units (CPUs). A fifteen- or twenty-CPU multiprocessing configuration is recommended to allow ingest of all available GFS ensemble members resulting in improved ability to use the INFORM system-generated ensemble forecasts in a probabilistic context for validation and for decision support. Along this line of future work, the authors also recommend experimentation with statistical/probabilistic methods for effective ensemble size increases.

In contrast to the GFS INFORM system input (forecast lead time up to 16 days), NCEP climate forecast system input consists of surface precipitation and temperature fields with monthly resolution. Efforts during this first phase of INFORM to have NCEP make available in real time the CFS-computed three-dimensional fields with (at least)

twice-daily forecast preparation times have not been successful (due to NCEP resource limitations as discussed in Chapter 2). This is an important issue for INFORM for two reasons:

1. The decision component requires reliable ensemble forecast input that spans the scales from hours to months to accommodate the multiple objectives of reservoir management.
2. The current methods for downscaling and the resultant statistical characteristics of the short-range (GFS-based) and long-range (CFS-based) forecast are different yielding statistical discontinuities for the INFORM forecast ensembles at the transition times (from 16 days to 30 days of forecast lead time) and between the first and the rest of the forecast months.

Availability of three-dimensional forecasts from CFS twice daily would lead to a seamless downscaling component for INFORM resulting in physics-based downscaling methods throughout (rather than a mix of physics-based and statistical methods) and in improved performance through single adjustment strategies of downscaled precipitation and temperature for the entire forecast horizon. It is thus highly recommended that CFS input analogous to GFS input be made available. Should such ensemble forecast fields become available, it is recommended that the necessary changes to INFORM structure for real-time ingest and downscaling be made to use the new data.

As discussed in Chapter 3, Chapter 6, and in Section 7.2.1 above, during this first phase of the INFORM project, no adjustments in the GFS forecast input, downscaled forecast precipitation and temperature, and forecast reservoir inflow were effected in real time or for the historical validation. Simple adjustments, applied off line to the downscaled forecast precipitation fields for sensitivity testing, removed biases in the magnitude of ensemble forecast reservoir inflows, and promise significant improvements in real-time ensemble forecasts for real-time implementation. It is thus recommended that during the second phase of the INFORM project, adjustments are considered and implemented.

The main issues to be resolved in this regard concern whether adjustments of the physical structure of the precipitation and temperature downscaling models are adequate to correct for biases or whether statistical bias adjustment of various forecast fields is necessary. Candidate physical structure adjustments for the precipitation downscaling model are the incorporation of (1) surface friction effects, (2) temperature gradient effects, and (3) convection. Candidate physical structure adjustments for the temperature downscaling component are (1) improvement of initial temperature interpolation and (2) temperature advection. If statistical bias adjustment is necessary, regression relationships between corresponding forecast and observed quantities may be used.

7.4.2. Decision Component

As indicated in Section 7.2.2, there is a need to rectify the incompatibility between mid-range management and long-range planning by expanding the mid-range model scope

to include a systemwide, rather than an individual reservoir, perspective. This can be accomplished by incorporating river routing models for the reaches downstream of the major reservoirs and by representing the Delta and south water export operations with a daily resolution. In addition to *synchronizing* the long- and mid-range system representations, this modeling extension will enable the decision system to address fish-related flow requirements more explicitly.

A second useful modeling addition would be the inclusion of a monthly river temperature model to ensure that reservoir management is also responsive to fish requirements related to temperature.

Lastly, a more direct linkage between CALSIM and INFORM DSS can be established to leverage complementary model strengths. It is recommended that the planning process use both models in the following iterative manner: First, the INFORM DSS can be employed to generate long-range planning tradeoffs and associated reservoir release policies based on seasonal hydro-climatic forecasts. Second, the INFORM DSS policies and forecasts can be used by CALSIM to develop a more detailed spatial representation of the system processes (inflows, withdrawals, returns) that are more meaningful to individual stakeholders. It is recommended that this process be automated and become user friendly as part of the INFORM DSS.

7.5. Benefits to California

A significant benefit of this first phase of INFORM for Northern California is its contribution toward the integration of operational water supply forecast and management activities by federal and state agencies toward increased water use efficiency. The mutual technology transfer and science cooperation between research centers and operational agencies is another. Lastly, even in its current prototype form, the INFORM system provides a unique resource for operational and management agencies in Northern California. These agencies may benefit by using this system as a tool for evaluating potential decision policies pertaining to the use of Northern California's water supply during real-time operations and for seasonal planning, both for the present and future years.

8.0 References

- Aguado, E., D. R. Cayan, L. Riddle, and M. Ross, 1992: "Climatic Fluctuation and the Timing of the West Coast Streamflow." *J. Climate* 5: 1468–1483.
- Anderson, E. A., 1973: National Weather Service River Forecast System – Snow Accumulation and Ablation Model. NOAA Technical Memorandum NWS HYDRO-17, Office of Hydrology, National Weather Service, NOAA, Silver Spring, Maryland, 271pp.
- Anderson, E. A., 1976: *A Point Energy and Mass Balance Model of a Snow Cover*. NOAA Technical Report 19, National Weather Service, NOAA, Silver Spring, Maryland, 150 pp.
- Bellman, R. E., and S. E. Dreyfus, 1962: *Applied Dynamic Programming*. Princeton University Press, 363 pp.
- Benjamin, J. R., and C. A. Cornell, 1970: *Probability, Statistics, and Decision for Civil Engineers*. McGraw-Hill Co., New York, 684 pp.
- Bras, R. L., 1990. *Hydrology an Introduction to Hydrologic Science*. Addison-Wesley, Reading, Mass., 643 pp.
- Burnash, R. J. C., Ferral, R. L., and R. A. McGuire, 1973: *A Generalized Streamflow Simulation System: Conceptual Modeling for Digital Computers*. U.S. National Weather Service and California Department of Water Resources, Joint Federal-State River Forecast Center, Sacramento, California, 204pp.
- Carpenter, T. M., and K. P. Georgakakos, 2001: "Assessment of Folsom Lake Response to Historical and Potential Future Climate Scenarios: 1. Forecasting." *J. of Hydrology* 249: 148–175.
- Cayan, D. R., S. A. Kammerdiener, M. D. Dettinger, J. M. Caprio, and D. H. Peterson, 2001: "Changes in the Onset of Spring in the Western United States." *Bull. Amer. Meteo. Soc.* 82(3): 399–413.
- Dettinger, M. D., D. R. Cayan, M. K. Meyer, and A. E. Jeton, 2004: "Simulated hydrologic responses to climate variations and change in the Merced, Carson, and American River basins, Sierra Nevada, California, 1900–2099." *Clim. Change* 62: 283–317.
- Draper, A., A. Munevar, S. Arora, E. Reyes, N. Parker, F. Cheng, and L. Peterson, 2004: "CalSim: Generalized Model for Reservoir System Analysis." *ASCE J. of Water Res. Plann. and Mgt.* 130(6) 480–489, November/December.
- Georgakakos, A. P., 1989a: "Extended Linear Quadratic Gaussian (ELQG) Control: Further Extensions." *Water Resources Research* 25(2): 191–201.
- Georgakakos, A. P., 1989b: Extended Linear Quadratic Gaussian Control for the Real-Time Operation of Reservoir Systems. In *Dynamic Programming for Optimal Water*

- Resources Systems Analysis*, A. Esogbue, ed., Prentice Hall Publishing Company, New Jersey, 329–360.
- Georgakakos, A. P., 1989c: "The Value of Streamflow Forecasting in Reservoir Control." *Water Resources Bulletin* 25(4): 789–800.
- Georgakakos, A. P., 1991: Computer-Aided Management of the Southeastern U.S. Reservoir System. In *Decision Support Systems*, D. P. Loucks, ed., NATO ASI Series, Vol. G 26, pg. 407–428.
- Georgakakos, A. P., 1993: "Operational Tradeoffs in Reservoir Control." *Water Resources Research* 29(11): 3801–3819.
- Georgakakos, A. P., 2004: Decision Support Systems for integrated water resources management with an application to the Nile Basin. Proceedings, International Federation for Automatic Control Workshop on Modeling and Control for Participatory Planning and Managing Water Systems, Venice, Italy.
- Georgakakos, A. P., 2006: Decision Support Systems for Integrated Water Resources Management with an Application to the Nile Basin. Chapter 6 in *Topics on System Analysis and Integrated Water Resources Management*, eds. A. Castelletti and R. Soncini-Sessa, Elsevier.
- Georgakakos, A. P., and Marks, D. H., 1987: "A Stochastic Control Method for the Real-Time Operation of Reservoir Systems," *Water Resources Research* 23(7): 1376–1390, 1987.
- Georgakakos, A. P., Yao, H., and Y. Yu, 1997a: "A Control Model for Hydroelectric Energy Value Optimization." *ASCE J. for Wat. Res. Plan. and Mgt* 123(1): 30–38.
- Georgakakos, A. P., Yao, H., and Y. Yu, 1997b: "A Control Model for Dependable Hydropower Capacity Optimization." *Water Resources Research* 33(10): 2349–2365.
- Georgakakos, A. P., Yao, H., and Y. Yu, 1997c: "Control Models for Hydroelectric Energy Optimization." *Water Resources Research* 33(10): 2367–2379.
- Georgakakos, K. P., 1986: "A Generalized Stochastic Hydrometeorological Model for Flood and Flash-Flood Forecasting, 1. Formulation." *Water Resources Research* 22(13): 2083–2095.
- Georgakakos, K. P., 2002: "U.S. Corporate Technology Transfer in Hydrometeorology." *J. Hydroinformatics* 4(1): 3–13.
- Georgakakos, K. P., 2003: "Probabilistic Climate Model Diagnostics for Hydrologic and Water Resources Impacts Studies." *Journal of Hydrometeorology* 4: 92–105.
- Georgakakos, K. P., and R. L. Bras, 1982: "Real-time Statistically Linearized Adaptive Flood Routing." *Water Resources Research* 18(3): 513–524.

- Georgakakos, K. P., and D. E. Smith, 2001: "Soil Moisture Tendencies into the Next Century for the Conterminous United States." *Journal of Geophysical Research - Atmospheres* 106(D21): 27367–27382.
- Georgakakos, K. P., A. P. Georgakakos, and N. E. Graham, 1998: "Assessment of benefits of climate forecasts for reservoir management in the GCIP region." *GEWEX News* 8(3): 5–7.
- Georgakakos, K. P., J. A. Sperflage, D. Tsintikidis, T. M. Carpenter, with an Appendix by W. F. Krajewski and A. Kruger, 1999: *Design and Tests of an Integrated Hydrometeorological Forecast System for the Operational Estimation and Forecasting of Rainfall and Streamflow in the Mountainous Panama Canal Watershed*. HRC Technical Report No. 2, Hydrologic Research Center, San Diego, California, 143 pp.
- Georgakakos, K. P., E. Shamir, S. V. Taylor, T. M. Carpenter, and N. E. Graham, in collaboration with A. P. Georgakakos and H. Yao, 2004: *Integrated Forecast and Reservoir Management INFORM – A Demonstration for Northern California Phase 1 Progress Report*. HRC Limited Distribution Report No.17, Hydrologic Research Center, San Diego, California, 105 pp. + 10 Appendices.
- Georgakakos, K. P., N. E. Graham, T. M. Carpenter, A. P. Georgakakos, and H. Yao, 2005: "Integrating Climate-Hydrology Forecasts and Multi-Objective Reservoir Management for Northern California." *EOS* 86(12): 122, 127.
- Hooper, E. R., A. P. Georgakakos, and D. P. Lettenmaier, 1991: "Optimal Stochastic Operation of the Salt River Project, Arizona." *ASCE Journal of the Water Resources Planning and Management* 117(5): 566–587.
- Kanamitsu, M., J. C. Alpert, K. A. Campana, P. M. Caplan, D. G. Deaven, M. Iredell, B. Katz, H.-L. Pan, J. Sela, and G. H. White, 1991: "Recent changes implemented into the global forecast system at NMC." *Weather and Forecasting* 6: 425–435.
- Kessler, E., 1969: *On the Distribution and Continuity of Water Substance in Atmospheric Circulations*. Meteorological Monographs, 10, American Meteorological Society, Boston, 84 pp.
- Knowles, N., 2000: *Modeling the Hydroclimate of the San Francisco Bay-Delta Estuary and Watershed*. PhD Dissertation, University of California, San Diego, La Jolla, California, 291 pp.
- Mahrer, Y., and R. A. Pielke, 1978: "A Test of an Upstream Spline Interpolation Technique for the Advective Terms in a Numerical Mesoscale Model." *Monthly Weather Review* 106: 818–830.
- National Oceanic and Atmospheric Administration (NOAA), 1999: *Interactive Calibration of the Sacramento Soil Moisture Accounting Model*. VHS Training

- Video. Office of Hydrologic Development, National Weather Service, Silver Spring, Maryland, 5:15 hours.
- National Research Council (NRC), 2001: *Climate Change Science, An Analysis of Some Key Questions*. National Academies Press, Washington, D.C., 29 pp.
- National Research Council (NRC), 2004: *Confronting the Nation's Water Problems, The Role of Research*. National Academies Press, Washington, D.C., 310 pp.
- Pandey, G. R., D. R. Cayan, M. D. Dettinger, and K. P. Georgakakos, 2000: "A Hybrid Orographic plus Statistical Model for Downscaling Daily Precipitation in Northern California." *J. Hydrometeorology* 1: 491–506.
- Pielke, R. A., 1984: *Mesoscale Meteorological Modeling*. Academic Press, San Diego, California, 297–331.
- Reed, S., V. Koren, M. Smith, Z. Zhang., F. Moreda, D.-J. Seo, and DMIP Participants, 2004: "Overall Distributed Model Intercomparison Project Results." *J. Hydrology* 298(1–4): 27–60.
- Rhea, J. O., 1978: *Orographic Precipitation Model for Hydrometeorological Use*. Atmospheric Paper 278. Dept. Atmospheric Sciences, Colorado State University, Fort Collins, Colorado, 198 pp.
- Shamir, E., and K. P. Georgakakos, 2006a: "Distributed snow accumulation and ablation model in the American River basin." *Advances in Water Resources* (in press).
- Shamir, E., and K. P. Georgakakos, 2006b: "Estimating snow depletion curves for American River basins using distributed modeling." *Journal of Hydrology* (in press).
- Singh, V. P., 1992: *Elementary Hydrology*. Prentice Hall, 973 pp.
- Smith, J. A., G. N. Day, and M. D. Kane, 1991: *A nonparametric framework for long-range streamflow forecasting*. WMO/TD-428, World Meteorol. Organ., Geneva, Switzerland, 28 pp.
- Smith, M. B., D.-J. Seo, V. I. Koren, S. M. Reed, Z. Zhang., Q. Duan, F. Moreda, and S. Cong, 2004: "The Distributed Model Intercomparison Project (DMIP): Motivation and Experiment Design." *J. Hydrology* 298(1–4): 4–26.
- Sperflage, J. A., and K. P. Georgakakos, 1996: *Implementation and Testing of the HFS Operation as Part of the National Weather Service River Forecast System*. HRC Technical Report No, 1. Hydrologic Research Center, San Diego, Cal., 213 pp.
- Sperflage, J. A., K. P. Georgakakos, D. Tsintikidis, A. Kruger, and W. F. Krajewski, 1999: *PANMAP v.1.0.1. User's Guide*. HRC Limited Distribution Report No. 10, Hydrologic Research Center, San Diego, California, 50 pp.

- Tateya, K., M. Nakatsugawa, and T. Yamada, 1991: Observations and Simulation of Rainfall in Mountainous Areas. In *Hydrological Applications of Weather Radar*, I.D. Cluckie and C.G. Collier (editors), Ellis Horwood, New York, 279–295.
- Tsintikidis, D., and K. P. Georgakakos, 1999: “Microphysical and Large-Scale Dependencies of Temporal Rainfall Variability over a Tropical Ocean.” *J. Atmos. Sci.* 56, 724–748.
- Tsintikidis, D., K. P. Georgakakos, J. A. Sperflage, D. E. Smith, and T. M. Carpenter, 2002: “Precipitation Uncertainty and Raingauge Network Design within the Folsom Lake Watershed.” *J. Hydrologic Eng.* 7(2): 175–184.
- Wilks, D. S., 1995: *Statistical Methods in the Atmospheric Sciences*. Academic Press, New York, 467 pp.
- Xue, M., K. K. Droegemeier, and V. Wong, 2000: “The Advanced Regional Prediction System (ARPS) – A multiscale nonhydrostatic atmospheric simulation and prediction tool. Part I: Model dynamics and verification.” *Meteor. Atmos. Physics* 75: 161–193.
- Yao, H, and A. P. Georgakakos, 2001: “Assessment of Folsom Lake Response to Historical and Potential Future Climate Scenarios.” *Journal of Hydrology* 249: 176–196.

9.0 Glossary

ARPS	Advanced Regional Prediction System
CALFED	Consortium of California and Federal Agencies
CALSIM	A water resources simulation model for evaluating operational alternatives of large, complex river basins
CCWD	Contra Costa Water District
CDBE	California Bay-Delta Authority
CFS	Climate Forecast System
CMIS	Climate Model Information System
CNRFC	California Nevada River Forecast Center
COA	Coordinated Operation Agreement
CPO	Climate Program Office of NOAA
CPU	Computer Processing Unit
CVO	Central Valley Operations (USBR)
CVP	Central Valley Project
DMIP	Distributed Modeling Intercomparison Project
DSS	Decision Support System
DWR	California Department of Water Resources
ELQG	Extended Linear Quadratic Gaussian control algorithm
EMC	Environmental Modeling Center
ESP	Ensemble Streamflow Prediction
ETD	Evapotranspiration Demand
FNF	Full Natural Flow (also, unimpaired flow)
GCM	Global Climate Model
GFS	Global Forecast System
GIS	Geographic Information System
GWRI	Georgia Water Research Institute (Georgia Tech)
HA	Historical Analog

HRC	Hydrologic Research Center
INFORM	Integrated Forecast and Reservoir Management
MAP	Mean Areal Precipitation
MAT	Mean Areal Temperature
NCEP	National Centers for Environmental Prediction
NOAA	National Oceanic and Atmospheric Administration
NOMADS	NOAA Operational Model Archive Distribution System
NRC	National Research Council
NWP	Numerical Weather Prediction
NWS	National Weather Service
OIC	Oversight and Implementation Committee
OSST	Observed surface sea temperatures
PDAE	Percent Daily Absolute Error
PIER-EA	Public Interest Energy Research, Environmental Area
RMSE	Root Mean Square Error
SAC-SMA	Sacramento Soil Moisture Accounting Model
SCA	Snow Cover Area
SDC	Snow Depletion Curve
SIMOROP	Simplified Orographic Precipitation Model
SNOW 17	NWS Hydro-17 Model
SWE	Snow Water Equivalent
SWP	State Water Project
USACE	United States Army Corps of Engineers
USBR	United States Bureau of Reclamation
USGS	United States Geological Survey
UTC	Coordinated Universal Time (French Initials)
UTM	Universal Transverse Mercator (mapping coordinates)

Appendices

Appendix A. Summary of Proceedings for the INFORM Oversight and Implementation Committee Meetings

Appendix B. Validation Figures for the Application of the Downscaling Precipitation Model to the Folsom Lake Drainage

Appendix C. Reliability-Diagram tables for CFS-Conditioned and Unconditioned ESP for INFORM Reservoir Inflows

Appendix D. INFORM Project Hydrometeorological Database

Appendix E. Plots from the Evaluation of the CNRFC Operational Hydrologic Model

Appendix F. Plots from the Evaluation of the INFORM Stand-Alone Distributed Hydrologic Model

Appendix G. Selected Reservoir, Hydropower Facility, and Demand Data

Appendix H. Historical Analog Streamflow Forecasting Model

Appendix I. River Index Calculation and Water Year Characterization

These appendices are available in three separate volumes.